

IMPERIAL COLLEGE OF SCIENCE AND TECHNOLOGY
(University of London)

IDENTIFICATION OF STRUCTURAL DYNAMIC CHARACTERISTICS

by
Jimin He

A thesis submitted to the University of London for the degree of
Doctor of Philosophy, and for the Diploma of Imperial College.

Department of Mechanical Engineering
Imperial College, LONDON SW7

October 1987

ABSTRACT

Modal analysis is a rapidly growing field in vibration research. It has been used effectively in the identification of structural dynamic characteristics and has become a flourishing area of vibration research. There are some aspects of the modal analysis method which hinder the application of the method to practical cases. Among them are analytical model correction, damping properties investigation and nonlinearity study. This thesis seeks to present the newest development on these aspects.

The dynamic characteristics of a vibrating structure are usually predicted by analytical techniques such as the Finite Element (FE) method. It is believed that errors in the analytical model are inevitable, while the modal data extracted from measurement are usually accepted to be correct, albeit incomplete. Hence, the correlation of an FE model and corresponding measured data becomes a very important process for structural vibration research. In this thesis, a new technique is developed to locate the area(s) in an analytical model where the errors are concentrated by using the incomplete modal data obtained from tests. An iteration process is introduced for the correction of the analytical model after the errors are **localized** and the feasibility of these new techniques is assessed by both theoretical and practical cases.

Associated with the correction of analytical models, this thesis also investigates the damping properties of a vibrating structure. It is believed that the most significant damping often comes from the joints between the various components of a structure and a method is proposed to locate the spatial damping elements from measurements on the structure. It is also shown that the located damping could then be quantified using the iteration process.

Nonlinearity is encountered in many practical structures. However, currently available means for studying this effect are not fully developed. This thesis describes an advantageous method, based upon a new understanding of the FRF data measured on a nonlinear system, to identify more conclusively the nonlinearity and to offer much better chance for its quantification. This method has been shown to be effective and convenient in application and could be very useful for further investigation such as modelling the nonlinearity and/or predicting the vibration response of the nonlinear system.

ACKNOWLEDGEMENT

The author is most grateful to his supervisor Professor D J Ewins for his continuous help and guidance throughout the duration of this research, and for his sustained advice in the preparation of the manuscript.

Very special thanks are due to Mr D Robb in the Modal Testing Unit who was most helpful to the author in computing and conducting experiments. Thanks are also due to Dr P Cawley, Dr C F Beards and Dr M Imregun in the Dynamics Section for their useful discussions and help.

Finally, the author is indebted to the Government of the People's Republic of China for providing the financial support.

NOMENCLATURE

a	subscript for analytical model
A	modal constant
C_r	modal constant of the r^{th} mode
d	Euclidian norm
i	imaginary unit
k_{ij}	the 'ij' element in stiffness matrix
m	number of measured vibration modes
n	number of coordinates employed the experimental model
N	number of coordinates employed by the analytical model
x	subscript for experimental model
\hat{x}	response amplitude of a nonlinear system
$[C]$	symmetric viscous damping matrix (real)
$[\Delta K_c]$	stiffness error matrix, defined as $([K_c] - [K_a])$ (complex)
$[H]$	symmetric structural damping matrix (real)
$[I]$	unity matrix
$[K_a]$	symmetric analytical stiffness matrix (real)
$[K_a]_R$	Guyan-reduced symmetric analytical stiffness matrix (real)
$[K_x]$	symmetric experimental mass matrix (real)
$[K_c]$	symmetric experimental stiffness matrix, defined as $([K_x] + i[H])$ (complex)
$[M_a]$	symmetric analytical mass matrix (real)
$[M_a]_R$	Guyan-reduced symmetric analytical mass matrix (real)
$[M_x]$	symmetric experimental mass matrix (real)

ΔA	error on modal constant estimate A
$[\Delta K]$	stiffness error matrix, defined as $([K_x] - [K_a])$ (real)
$[\Delta M]$	mass error matrix, defined as $([M_x] - [M_a])$ (real)
$H(\omega), G(\omega)$	frequency response function of a dynamic system
$I(t)$	impulse response of a dynamic system
$S_{xf}(\omega)$	cross power spectrum
$S_{xx}(\omega)$	auto power spectrum
$H[f(x)]$	the Hilbert transform of $f(x)$
$F[f(x)]$	the Fourier transform of $f(x)$
$\text{sgn}(t)$	sign function (is equal to one when t is positive and zero when negative)
$k(\hat{x})$	harmonic response amplitude-dependent stiffness
$c(\hat{x})$	harmonic response amplitude-dependent viscous damping
$[]^T$	transpose of matrix $[]$
$[]^{-1}$	inverse of matrix $[]$
$\text{Re}()$	the real part of
$\text{Im}()$	the imaginary part of
α	receptance FRF data
a	receptance FRF data when the complexity is removed
$1/\alpha$	reciprocal of receptance data
$(\omega_a)_r$	the r th analytical radial natural frequency.
$(\omega_x)_r$	the r^{th} experimental radial natural frequency
ω_0	radial natural frequency
$\omega_0(x)$	harmonic response amplitude-dependent natural frequency
$\omega_p^{(r)}$	the natural frequency of the p^{th} mode of the updated model after ' r ' iterations

$[\omega_a^2]$	diagonal analytical natural frequency matrix (real)
$[\omega_x^2]$	diagonal experimental natural frequency matrix (real)
$[\phi_a]$	analytical mode shape matrix (real)
$[\phi_x]$	experimental mode shape matrix (complex or real)
$\{\phi_a\}_r$	the r^{th} analytical mode shape (real)
$\{\phi_x\}_r$	the r^{th} experimental mode shape (complex or real)
$ \phi_{pq} ^{(r)}$	the 'pq' element in the mode shape matrix of the updated model after 'r' iterations
η_r	damping coefficient of the r^{th} mode
ξ_r	damping loss factor of the r^{th} mode
$\xi(x)$	harmonic response amplitude dependent damping loss factor

- CONTENTS -

	<i>Page</i>
<i>ABSTRACT</i>	1
<i>ACKNOWLEDGEMENT</i>	2
<i>NOMENCLATURE</i>	3
<i>CHAPTER 1 INTRODUCTION</i>	
1-1 The Identification of Structural Dynamic Characteristics	12
1-2 Theoretical Prediction Approach	13
1-3 Experimental Measurement Approach	14
1-4 Correlation of FE Model and Modal Testing Results	17
1-5 Nonlinearity	19
1-6 Preview of Thesis	20
<i>CHAPTER 2 ANALYTICAL MODEL IMPROVEMENT - THEORETICAL BASIS</i>	
2-1 Preliminaries	23
2-2 Some Current Approaches for Model Improvement	26
2-2-1 Matrix Perturbation Theory for Model Improvement	26
2-2-2 Constraint Minimization Method (CMM)	28
2-3 The Error Matrix Method (EMM)	31
2-3-1 Principle and Essence of the Error Matrix Method	31
2-3-2 Validation of the Assumption Made by the EMM	34
2-4 Model Improvement Using Iteration	37
2-4-1 Strategy of the Iteration Process	38
2-4-2 Criteria for the Assessment of the Iteration Results	39
2-5 Numerical Study	40

2-6 Conclusions	44
<i>CHAPTER 3 LOCATION OF MISMODELLED REGION - NEW DEVELOPMENTS</i>	
3-1 Preliminaries	61
3-2 Structural Connectivity in an Analytical Model	62
3-3 Location of Mismodelled Regions in the Analytical Model	64
3-3-1 The Analytical Stiffness Case	64
3-3-2 The Analytical Mass Case	67
3-3-3 General Case	69
3-4 Direct Numerical Calculation of [AK]	70
3-5 Numerical Assessment of Location Technique and Refined Iteration Process	72
3-6 Conclusions	74
<i>CHAPTER 4 IDENTIFICATION OF DAMPING PROPERTIES OF VIBRATING STRUCTURES</i>	
4-1 Preliminaries	86
4-2 Current Approaches for Studying Damping Properties	87
4-3 Identification of Damping Type from Measured Data	90
4-3- 1 Methodology for Identification of Damping Types	90
4-3-2 Removal of Complexity from Measured Data	91
4-4 Location of Damping Elements from a Structure	92
4-4- 1 Usual Damping Condition of a Vibrating Structure	92
4-4-2 The Approach for Damping Element Location	93
4-5 Estimation of Damping Matrix	95
4-5-1 Extension of the EMM to Estimate Damping Matrix	95
4-5-2 Iterative Approach to Improve the Estimation of [H]	99
4-6 Numerical Assessment of Damping property Investigation	100
4-7 Conclusions	103

*CHAPTER 5 COMPATIBILITY OF MEASURED MODES AND ANALYTICAL
MODEL*

5-1 Preliminaries	117
5-2 Model Condensation by Guyan Reduction	118
5-3 Expansion of Measured Modes by Analytical Model	119
5-4 Comments of Different Approaches	121
5-4- 1 Guyan Reduction	121
5-4-2 Expansion of Measured Modes	123
5-5 Expansion of Measured Complex Modes	124
5-6 Assessment of Approaches for Compatibility	126
5-7 Conclusions	127

*CHAPTER 6 APPLICATION OF MODELLING ERROR LOCATION TO A
PRACTICAL STRUCTURE*

6- 1 Introduction	136
6-2 Analytical Modelling of the Structure	137
6-3 Modal Testing of the Structure and Comparison of the Modal Model and the FE Model	138
6-4 Location of the Mismatched Region in the Analytical Stiffness Matrix Using Measured Vibration Modes	140
6-4- 1 Expansion of the Measured Vibration Modes	140
6-4-2 Location of Mismatched Region in the Analytical Stiffness Matrix	140
6-5 Conclusions	141

CHAPTER 7 MEASUREMENT OF NONLINEARITY

7- 1 Introduction	153
7-2 Excitation Techniques	155
7-2- 1 Sinusoidal Excitation	155
7-2-2 Random Excitation	157

7-2-3 Transient Excitation	158
7-2-4 Comments on Different Excitation Techniques	160
7-3 Practical Considerations of Nonlinearity Measurements	161
7-4 Simulation for Nonlinearity Investigation	163
7-4-1 Significance of Simulation of Nonlinearity	163
7-4-2 Analogue Simulation of Nonlinearity	164
7-5 The Frequency Responses of the Nonlinear Systems	168
7-6 Conclusions	171

CHAPTER 8 MODAL ANALYSIS OF NONLINEAR SYSTEMS

8-1 Current Methods and Applications of Modal Analysis for Nonlinear Systems	187
8-1-1 Bode Plots	188
8-1-2 Reciprocal of Frequency Response Function	189
8-1-3 Modal Analysis and the Isometric Damping Plot	191
8-1-4 The Hilbert Transform	192
8-1-4-1 The Principle of the Hilbert Transform	193
8-1-4-2 Basis of its Application to Modal Analysis	194
8-2 Comments on Current Methods for the Modal Analysis of Nonlinearity	197
8-3 A New Interpretation of the Effect of Nonlinearity on FRF Data	198
8-3-1 Interpretation of FRF Data with Nonlinearity	198
8-3-2 Interpretation of the Reciprocal of Receptance Data with Nonlinearity	201
8-3-2-1 Stiffness Nonlinearity	201
8-3-2-2 Damping Nonlinearity	203
8-4 A New Method for the Modal Analysis of Nonlinear Systems	204
8-4-1 Modal Analysis of Stiffness Nonlinearity	204
8-4-1-1 Description of Methodology	205
8-4-1-2 Algorithm for Modal Analysis of Nonlinear Stiffness	206
8-4-2 Modal Analysis of Damping Nonlinearity	208
8-4-3 The Extraction of an Accurate Modal Constant Estimate	209

8-5 Application of the New Method for the Modal Analysis of Nonlinearity	211
8-5- 1 Analysis of Stiffness Nonlinearity	212
8-5-2 Analysis of Damping Nonlinearity	213
8-5-3 Practical Applications of the New Method	213
8-6 Conclusions	215
 <i>CHAPTER 9 CONCLUSIONS AND SUGGESTION FOR FURTHER STUDIES</i>	
9-1 Analytical Model Improvement Using Modal Testing Results	239
9-2 Damping properties of Practical Structures	241
9-3 Compatibility of Analytical Model and Measured Vibration Modes	242
9-4 Nonlinearity in Modal Testing	243
9-5 Suggestion for Further Studies	244
 <i>APPENDICES</i>	
APPENDIX 1: Matrix Perturbation Results	247
APPENDIX 2: Inverse of a Complex Matrix	250
APPENDIX 3: FE Analysis of a Beam Element	252
 <i>REFERENCES</i>	
	254

CHAPTER 1

CHAPTER 1

INTRODUCTION

1-1 THE IDENTIFICATION OF STRUCTURAL DYNAMIC CHARACTERISTICS

In many practical circumstances, the vibration characteristics of a dynamic structure require to be understood and, subsequently, an accurate mathematical model needs to be derived. Such a model is needed for response and load prediction, stability analysis, system design, structural coupling etc.

Since a dynamic structure is a continuous system rather than a discrete one, theoretically, an infinite number of coordinates are necessary to specify the position of every point on the structure and hence the structure can be said to have an infinite number of degrees of freedom. Its vibration characteristics should then include an infinite number of vibration modes and cover the active frequency range from zero to infinity. However, for most practical applications, only a certain frequency range is of major interest and only those vibration characteristics which fall in this range will be investigated. In this case, only a certain number of vibration modes are to be sought and it becomes feasible to represent the continuous system by an approximate, discrete, one.

For a discrete linear dynamic system with lumped masses and **massless** elastic components, theory has been well developed to study such vibration characteristics. This is because the differential equations of a discrete linear dynamic system are generally available, and hence mathematics can be introduced directly to solve the equations of motion and the vibration characteristics can then be defined accurately. For a truly continuous system, such as a practical structure, such advantages do not exist. However, like many other sciences to achieve good approximation by discretization, the strategy of investigating the vibration characteristics of a practical structure relies basically on the

hypothesis of discretizing the structure so that the theory for discrete systems can then apply and the mathematical model for the structure can then be built. It is evident that as the number of coordinates employed in the discretization approaches **infinity**, the discrete system will approach the continuous one.

Basically, there are two ways of achieving a mathematical model for a dynamic structure with the help of the discretization concept, they being by theoretical prediction and by experimental measurement respectively. Both approaches effectively assume that the vibration characteristics of a continuous system within certain frequency range can be described approximately by a limited number of coordinates. In the following, both approaches are reviewed briefly.

1-2 THEORETICAL PREDICTION APPROACH

Physics and mathematics have been so developed nowadays that for commonly encountered mechanical components, such as beams and plates, accurate analytical solutions are readily available to predict their vibration characteristics. For instance, the natural frequencies and mode shapes of a lengthy uniform beam could now be easily computed.

For a rather complicated practical structure, however, there is generally no analytical solution to predict its vibration characteristics. With the help of new computational technology, the Finite Element (FE) approach is now widely used in the study of the vibration characteristics of various practical structures. The fundamental principle of the FE method is to discretize a complicated structure into many small elements. For each such an element, known as a finite element, the mass and stiffness properties are assumed to obey a known and relatively simple linear pattern. Thus, the mass and stiffness matrices of an element can be constructed. The global mass and stiffness matrices of the structure can be assembled using these element matrices and also by considering the connectivity and the boundary conditions. These global mass and stiffness matrices,

which actually constitute the so-called FE (analytical) model for the structure, can then be used to derive the description of the vibration characteristics of the structure, namely, the natural frequencies and mode shapes.

The natural frequencies and mode shapes derived from the global mass and stiffness matrices from the FE model are often referred to as undamped natural frequencies and undamped mode shapes since the damping properties for a structure cannot be predicted in the same way as mass and stiffness and a FE model does not normally include a damping matrix. Although an approximation for the damping properties can be made by introducing a proportional damping matrix (i.e. to assume that damping matrix is proportional to a linear combination of the mass and stiffness matrices), the mode shapes obtained from such a FE model are still the same as the undamped ones. Besides, it has been generally accepted that damping properties thus predicted can be incorrect in most cases.

1-3 EXPERIMENTAL MEASUREMENT APPROACH

Apart from the approach of theoretical prediction to achieve an analytical model for the study of vibration characteristics of a dynamic system, another major approach is to establish an experimental model for the system by performing vibration tests and subsequent analysis on the measured data. This process, including the data acquisition and the subsequent analysis, is now known as 'Modal Testing'. In the last two decades, modal testing (it is believed that this name is much younger than its real practice) continues to develop, both in theory - new methodology, and in practice - new test techniques and modern instrumentations - because of continuous new challenges from real life and capabilities offered by powerful computer technology. It is not surprising that modal testing has penetrated into many branches of engineering.

In common with the approach of theoretical prediction, modal testing assumes that the vibration characteristics of any systems or structures, discrete or continuous, can be

described by a selected number of coordinates within a frequency range of interest. In reality, modal testing can serve many purposes according to different requirements. In vibration engineering, current modal testing practice has shown its application in various aspects and they can be **categorized** briefly as follows:

- (i) The most significant application of modal testing is perhaps to produce modal data (natural frequencies, damping loss factors and mode shapes) of a dynamic system so that they can be used to compare with the corresponding modal data produced by the system's analytical model, in order eventually to validate the analytical model itself. Further investigation involves using the experimental model consisting of the derived modal data to improve the analytical model - a practice known as model improvement or correlation of the experimental and analytical results - and this is substantially studied in this thesis;
- (ii) In the absence of an analytical model, the experimental modal data are used sometimes to construct a spatial mathematical model for a dynamic system which will then be used to predict the effects of modifications on the system and to conduct sensitivity analysis.
- (iii) For some practical structures consisting of various components, direct testing may present certain difficulties. If mathematical models can be obtained for each component, and boundary conditions are correctly assumed, then a global model can be constructed. This process, often referred to as 'substructuring' or 'modal synthesis', requires an accurate derivation of the modal data from modal testing for each component.
- (iv) In the absence of an analytical model, an experimental model consisting of the modal data is sometimes used to predict the system's vibration response under certain external excitation conditions. Alternatively, it can also be used to determine the dynamic loading if the vibration responses of the system are measured.

Modal testing practice involves two major aspects: measurement to acquire data (frequency response function or time domain response) and modal analysis to extract a modal, or experimental, model. Although the final goal of modal testing is produced by the *analysis*, the importance of measurement could never be overstressed.

Currently, there are two main excitation techniques in common use, they being of single point excitation and multi-point excitation. The single point excitation method excites a structure at one coordinate and measures the response at all the coordinates. Theoretically, such a test - one point excitation and multi-point responses - is sufficient for the subsequent analysis in order to extract the experimental model. However, it is often found that the single excitation point is not appropriate to expose all the vibration modes of interest. Thus, changing the excitation point and repeating the measurement for several points is essentially required. This single point excitation method involves less instrumentation, employs inexpensive computer software and is easy to master, but is obviously not suitable for exciting a large structure. Unlike the single point excitation method which excites a structure to vibrate in several modes simultaneously, the multi-point excitation method attempts to excite a structure in order to eliminate the unwanted modes so as to get a single pure mode. This brings about a significant advantage for the subsequent analysis. The price, however, is paid to require much more sophisticated instrumentation and the measurement operation could become very involved.

The data acquired from measurement are to be analysed in different ways, depending on the different requirements made of the data. It is believed that the direct requirement in most cases is to derive the natural frequencies, damping loss factors and mode shapes. Since the data acquired from measurement are normally in the form of frequency response functions, two methods are widely applied in the modal analysis process known as 'Single Degree-of-freedom (SDOF) Curve-Fit' and 'Multi-Degree-of-freedom (MDOF) Curve-Fit' respectively.

The SDOF curve-fit method assumes that, in the vicinity of a resonance, the frequency response function is dominated by this vibration mode and can therefore be approximated to that of a SDOF system plus a constant quantity, which is usually referred to as the 'residual'. Thus, by applying the nature of the Nyquist circle or its equivalent for a SDOF system, a curve-fit can be made for each mode to extract the natural frequency, modal constant and damping loss factor. Although the assumption itself restricts the condition of close modes, it is found in practice that using an iterative process for this SDOF curve-fit method even cases with close modes could often produce satisfactory results.

The MDOF curve-fit method seeks to derive a theoretical frequency response function which provides a "best fit" to the measured frequency response data. Since it operates for several modes simultaneously, it can be used directly for the case of close modes when the interactions among vibration modes are taken care of at the same time. Besides, when the damping in measured data is so small to cause difficulties on Nyquist circle-fit, the MDOF curve-fit method can still analyse the data^[1].

Among other methods being used in the analysis of measured data, Ibrahim Time Domain method (ITD) is one of the noticeable techniques. Unlike the previous descriptions, the ITD makes use of the measured data in time domain form (rather than frequency domain). The basic idea of ITD is to extract the modal data from the free decay response of a system. Once the free decay response is measured or computed from other forms of data, the modal data extraction can be made routine, requiring much less interactive effort. This characteristic accelerates the analysis process, while in the mean-time loses visual control of the modal data extraction and, as a result, could end up with unrealistic results in some circumstances.

1-4 CORRELATION OF FE MODEL AND MODAL TESTING RESULTS

Due to their own respective advantages, both the Finite Element approach and Modal

testing approach are widely used nowadays to study the vibration characteristics of dynamic systems and structures. The FE method predicts the vibration characteristics by theoretical studies so that no experimental facilities are needed. It can employ a large number of coordinates so that the vibration characteristics can be described in detail and can cover a comparatively wide frequency range. In addition, it can be used at the design stage to predict the vibration behaviour of a future structure and, possibly, to modify the blueprint. However, due to the crucial complexity of practical structures, especially the joints between the components in them, the modelling of the mass and stiffness properties could be inaccurate or even incorrect, and that of the damping properties is generally artificial or omitted altogether. Modal testing is supposed to identify the 'true' vibration characteristics of a structure, since it deals with the real object rather than an idealisation. Thus, the experimental model possesses the information of the 'correct' mass, stiffness and damping properties. However, due to the limited number of coordinates and incomplete number of modes - both are the consequences of various practical restrictions in measurement - the information thus obtained is available primarily as the modal parameters, rather than the **spacial** properties as provided by the FE model.

No doubt, differences will exist between the FE model and the experimental model.

The principle of correlating the models derived from these two different approaches is basically to make use of the advantages on both and to overcome their disadvantages. Since a representative spatial model is increasingly demanded in vibration practice, current efforts are mainly directed to using modal testing results to improve or to correct the FE model. This is nowadays often referred to as 'model improvement' or 'model correction'. In a model improvement study, the advantages of both modal testing results - containing correct information (albeit incomplete) of the vibration characteristics - and of the FE model - a complete model - are retained. The improved model is expected to be a better approximation of the correct but unavailable model.

1-5 NONLINEARITY

In the previous description, there is an important assumption for using the two main approaches to identify vibration characteristics, namely, that the dynamic system to be studied should behave linearly in vibration. In general, a dynamic system is said to be linear if: (i) doubling the input force will double the vibration response and (ii) the summation of the responses due to two independent inputs should be the same of the response due to the summation of these two inputs. Failure to obey these relationships implies the structure to be nonlinear. Thus, the measured frequency response function data of a linear dynamic system from different tests with different force levels should be the same.

It is believed that all real structures have a certain degree of nonlinearity. In many cases, they are regarded as linear structures because the degree of nonlinearity is small and therefore insignificant in the response range of interest. While in other cases, nonlinearity may have to be tolerated simply because of lack of effective means to cope with it.

Basically, the existence of nonlinearity has two consequences in the realm of identification of vibration characteristics. Firstly, the analytical model of a nonlinear system will be erroneous because, unless a real measurement is taken, the existence of nonlinearity usually cannot be foreseen merely by theoretical prediction and nor can it be quantified theoretically. Secondly, since the frequency response function data become input force-dependent, the significance of the modal parameters extracted by modal testing has to be considered much more carefully.

The theoretical study of known types of nonlinearity such as cubic stiffness can be dated back to the beginning of this century. Although the nonlinearity described by known differential equations has been thoroughly understood in textbooks, the difficulty faced by modal testing is to investigate unknown type(s) of nonlinearity from practical structures. Nevertheless, using modal testing techniques to study the theoretical or simulated data

with known type(s) of nonlinearity paves the way to an understanding of nonlinearity in practical structures. Once the types of nonlinearity most commonly encountered in practice have been categorised by their effects on modal data, the results can be referenced helpfully by the analysis of measured data from real structures.

Current efforts in modal testing practice are directed towards the detection and identification of nonlinearity in real structures, although the quantification of nonlinearity is still in its infancy. The detection of the existence of nonlinearity from measured data is believed to be relatively much easier, if the excitation method is properly selected and measurement is performed appropriately. However, it is its identification that has attracted most efforts in modal testing study. Despite the complexity of practical structures, the main difficulty for the identification is to be able to produce a conclusive answer from the analysis.

1-6 PREVIEW OF THE THESIS

Despite the rapid development in the identification of dynamic characteristics of structures in recent decades, there are still some aspects in modal analysis research with common interests, which hinder the vast application of modal analysis to practical cases. Among these aspects, damping properties of structures, analytical model correction using modal testing results and nonlinearity are three notable subjects. The research project presented in this thesis is intended to seek new improvements on these three subjects and, as a result, to pursue better understanding of the dynamic characteristics of structures.

Conventional methods to modify, or to correct, an FE model using modal testing results are discussed in Chapter 2, including the perturbation method, the constraint minimization method and the error matrix method. It is found that, when the number of measured vibration modes is insufficient, these methods could not successfully improve the FE model. In fact, the resultant model suggested by these methods could be mathematically optimal although physically unrealistic, Since it is generally accepted **that** errors existed in

an FE model are often small and isolated, efforts in this thesis are directed towards first enabling to locate the existent errors and then to correct them objectively rather than to modify the whole model. Chapter 3 presents the development of a new technique to locate the errors in an FE model using a very limited number of measured modes. It is then suggested that an FE model should be improved by only correcting the located errors using the measured modes. In Chapter 4, damping properties are studied in order to offer an existing FE model with a sensible damping model, rather than merely a proportional one or none at all.

One of the practical difficulties faced by the model correlation process is the incompatibility of the FE model and the modal testing results in the sense of the adopted coordinates. Chapter 5 concentrates on resolving this difficulty. Both undamped and damped conditions are investigated. The new development in this study is assessed by a practical application presented in Chapter 6.

For those cases where nonlinearity cannot realistically be ignored, Chapters 7 and 8 seek to investigate this phenomenon by modal testing techniques. The measurement of nonlinear systems is discussed in Chapter 7, including the excitation methods and the simulation of various commonly encountered types of nonlinearity. In Chapter 8, the present development of nonlinearity study is discussed and summarized. Based upon these present developments and a new interpretation of the effect of nonlinearity on modal data, a new method is proposed to identify the nonlinearity from measured data.

Finally, Chapter 9 reviews all the new developments presented in this thesis and exhibits the direction from which possible further studies can be cultivated.

CHAPTER 2

CHAPTER 2

ANALYTICAL MODEL IMPROVEMENT - THEORETICAL BASIS

2-1 PRELIMINARIES

When the identification of structural dynamic characteristics is undertaken by both of the two widely-used techniques, i.e. (1) theoretical analysis (normally by Finite Elements) and (2) modal testing and analysis, an inconsistency often exists between the vibration data predicted by the theoretical model and those identified experimentally. Although the argument of what causes this inconsistency has been **raised**^[4], it is nowadays often believed, that more confidence can be placed on the experimental modal data than on either the analytical mass or stiffness matrices and, as a consequence, the analytical model of a structure should be modified upon the basis of the experimental modal data, provided this modification is required in practice. In this Chapter, we shall deal mainly with systems with little damping so that all the vibration modes involved are real. Special interest is paid to the stiffness properties although it will be seen that the methodology can be similarly applied to the mass properties. The **damping** and complex mode case will be investigated in Chapter 4.

When both an analytical model of a structure and experimental modal data are available, the analytical model improvement can be cast into the following mathematical problem:

>>> for a linear and undamped system, the dynamic characteristics (natural frequencies and mode shapes) can be described by a set of second order differential equations:

$$[M_a]\{\ddot{x}\} + [K_a]\{x\} = \{0\} \quad (2-1)$$

where $[M_a]$ and $[K_a]$ are $N \times N$ approximate (due to modelling errors) mass and stiffness matrices, comprising the analytical model of the system

The “analytical” modal data (natural frequencies and mode shapes) can be derived by solving equation (2-1), yielding a set of solutions:

$$([K_a] - (\omega_a)_r^2 [M_a])\{\phi_a\}_r = \{0\} \quad (2-2)$$

where $(\omega_a)_r$ and $\{\phi_a\}_r$ ($r=1, \dots, N$) are the r^{th} mode analytical natural frequency and mode shape respectively. All the mode shape vectors are $N \times 1$ in dimension.

Meanwhile, the modal data from measurement provide the experimental natural frequencies $(\omega_x)_r$ and mode shapes $\{\phi_x\}_r$ ($r=1, \dots, m$), and have all the mode **shape vectors $\{\phi_x\}_r$ are** $n \times 1$ in dimension. They are incomplete (because not all coordinates are measured) and relate to an experimental model consisting the experimental mass matrix $[M_x]$ and stiffness matrix $[K_x]$ which are generally close to, but different from, their analytical counterparts $[M]$ and $[K_a]$. The difference between the analytical mass (or stiffness) matrix and the experimental mass (or stiffness) matrix can be represented by a mass error matrix $[AM]$ (or stiffness error matrix $[AK]$).

It is supposed that the analytical model ($[M_a]$ and $[K_a]$) needs to be updated using the experimental modal data $(\omega_x)_r$ and $\{\phi_x\}_r$, ($r=1, \dots, m$) so that it represents more accurately the dynamic characteristics of the modelled structure. <<<

In recent years, a number of methods have been published in the literature to deal with analytical model improvement by a variety of approaches. It is believed that the problem of model improvement was **first** addressed intuitively by Berman and **Flannelly**[5]. In the paper, they stress the incompleteness involved in model improvement and suggest that measured vibration modes are used to improve an analytical mass matrix and to identify an 'incomplete' stiffness matrix, although the stiffness matrix thus deduced is certainly not appropriate from today's point of view. Collins et al[6] employ a technique of statistical parameter estimation in an iterative procedure to adjust an analytical model. Instead of directly improving the constructed analytical mass and stiffness matrices, their technique seeks to modify the physical parameters (such as mass per unit length) of which the analytical model consists. Although the method preserves the connectivity of the original analytical model during the iterative procedure, the formulation of the method restricts its application for practical structures. Matrix perturbation theory was later introduced[7],[8] as an attempt to modify an analytical model using measured modes. On the other hand, Baruch and Bar **Itzhack**[9],[10] employed constraint minimization theory from control engineering in model improvement and developed formulations to modify the analytical stiffness and flexibility matrices after the measured vibration modes are optimized using analytical mass matrix, based upon orthogonality property. The resultant model thus modified has analytical modes identical to the corresponding measured modes used. Having considered that analytical mass matrix improvement could be the primary goal (rather than the stiffness case), **Berman**[11] applied the same constraint minimization theory and obtained a modified analytical mass matrix using measured modes. Later, **Caesar**[12] developed an algorithm to apply these formulations derived from constraint minimization theory. Some applications of model improvement are also found in the literature[14],[15]. Apart from the methods summarised above, the Error Matrix **Method**[16] is notably different from others. It aims at using the measured vibration modes to locate errors existing in an analytical model.

In the following, some of the methods which have been mentioned are summarised. Moreover, the Error Matrix Method (EMM) has been given special attention in this thesis and will be studied in detail later in this chapter.

2-2 SOME CURRENT APPROACHES FOR MODEL IMPROVEMENT

2-2-1 Matrix Perturbation Theory for Model Improvement

The essential objective of analytical model improvement can be stated as aiming to **find** the differences between the analytical model mass and stiffness matrices $[M_a]$ and $[K_a]$ and the experimental model mass and stiffness matrices $[M_x]$ and $[K_x]$, the former matrices being assumed erroneous and the latter ones to be correct. Since the difference between these two models is generally believed to be small compared with the analytical model itself, it is supposed (here) that $[AM]$ could be regarded as the perturbation of the analytical mass matrix $[M_a]$, which consequently leads $[M_a]$ to the perturbed mass matrix, $[M_x]$. The same argument can be made for the stiffness matrix case. Thus, matrix perturbation theory can be applied to develop a relationship between the perturbations $[AM]$ and $[AK]$ and the corresponding differences in the modal data, including natural frequencies and mode shapes.

Supposing the analytical model of a system ($[M_a]$ and $[K_a]$) differs from the assumed correct experimental model ($[M_x]$ and $[K_x]$) by $[AM]$ and $[AK]$, then

$$[M_x] = [M_a] + [\Delta M] \quad (2-3)$$

$$[K_x] = [K_a] + [\Delta K] \quad (2-4)$$

The consequence of introducing $[AM]$ and $[AK]$ on the predicted modal properties can be

written as:

$$[\phi_x] = [\phi_a] + [\Delta\phi] \quad (2-5)$$

$$[\omega_x^2] = [\omega_a^2] + [\Delta\omega^2] \quad (2-6)$$

If the two difference matrices $[AM]$ and $[AK]$ are small compared with $[M_a]$ and $[K_a]$, and hence can be regarded as a perturbation of the analytical model, then, according to matrix perturbation theory, the mode shape difference can be approximated by a linear combination of all the analytical mode shapes:

$$[\Delta\phi] = [\phi_a][\alpha] \quad (2-7)$$

where $[a]$ is a transformation matrix with zero diagonal elements. Thus, equation (2-5) becomes:

$$[\phi_x] = ([I] + [\alpha])[\phi_a] \quad (2-8)$$

The modal data $[\phi_x]$ and $[\omega_x^2]$ should satisfy the orthogonality conditions:

$$[\phi_x]^T[M_x][\phi_x] = [I] \quad (2-9)$$

$$[\phi_x]^T[K_x][\phi_x] = [\omega_x^2] \quad (2-10)$$

The substitution of equations (2-3) to (2-6) into equations (2-9) and (2-10) yields the following formulae:

$$[\Delta M] = [M_a][\phi_a] (2[I] - [\phi_a]^T[M_a][\phi_x] - [\phi_x]^T[M_a][\phi_a]) [\phi_a]^T[M_a] \quad (2-11)$$

$$[\Delta K] = [M_a][\phi_a] ([\omega_a^2] + [\omega_x^2] - [\phi_a]^T[K_a][\phi_x] - [\phi_x]^T[K_a][\phi_a]) [\phi_a]^T[M_a] \quad (2-12)$$

Equations (2- 11) and (2- 12) represent the relationship between the perturbation matrices [AM], [AK] and the modal data of the system before and after the perturbation. These equations give the correct [AM] and [ΔK] provided the complete modal data are available. However, in practice, the high-frequency modes which happen to dominate the estimation of [AM] and [AK] in the equations are not obtainable from measurement. This makes these equations less practical in reality.

2-2-2 Constraint **Minimization** Method (CMM)

The ideal model of a vibration system including mass and stiffness matrices is a model such that the modal data derived from it should not only satisfy the eigendynamics properties (see (i) below), but must also satisfy physical constraints such as symmetry and **orthogonality** of the model. Baruch and Bar Itzhack proposed a **method**^[9] by which the analytical stiffness matrix [K_a] can be improved using experimental modal data. The method assumes that the analytical mass matrix [M_a] is reliably accurate (and hence that [AM]=[O]) and applies the following physical constraints which the improved stiffness matrix [K_x] is required to satisfy:

- (i) $[K_x][\phi_x] = [M_x][\phi_x][\omega_x^2]$ eigendynamics and
- (ii) $[K_x]^T = [K_x]$ symmetry.

The difference between the analytical stiffness matrix [K_a] and the objective stiffness matrix [K_x] is evaluated by the following Euclidian norm, which is a physically sensible and mathematically convenient function:

$$d = \|[M_x]^{-1/2}([K_x]-[K_a])[M_x]^{-1/2}\|$$

The two physical constraints are incorporated by Lagrange multipliers into a Lagrange function which is to be minimized to derive the optimal stiffness matrix, $[K_x]$. The final stiffness matrix thus optimized is given by:

$$[K_x] = [K_a] - [K_a][\phi_x][\phi_x]^T[M_x] - [M_x][\phi_x][\phi_x]^T[K_a] + [M_x][\phi_x][\omega_x^2][\phi_x]^T[M_x] + [M_x][\phi_x][\phi_x]^T[K_a][\phi_x][\phi_x]^T[M_x] \quad (2-13)$$

Alternatively, it may be said that the difference between the optimized and analytical stiffness matrices is defined by the CMM as:

$$[AK] = -[K_a][\phi_x][\phi_x]^T[M_x] - [M_x][\phi_x][\phi_x]^T[K_a] + [M_x][\phi_x][\omega_x^2][\phi_x]^T[M_x] + [M_x][\phi_x][\phi_x]^T[K_a][\phi_x][\phi_x]^T[M_x] \quad (2-13b)$$

It can be seen from equation (2-13) that this method does not require the analytical modal data. Instead, it attempts to improve the stiffness distributions which are the physical parameters by using the experimental modal data directly. This simplifies the procedure of analytical model improvement. However, the basic assumption that the analytical mass matrix is reliable - which this method requires - does not hold in some practical cases and this limits the applicability of this method to improve the analytical stiffness matrix of practical structures.

It is found that because of the inevitable incompleteness of experimental modal data, the optimal stiffness matrix deduced by equation (2-13) will somehow dramatically change the structural connectivity of the system being modified. In this case, the analytical stiffness matrix is improved in such a way that the modified model will surely represent the incomplete modal data from measurement, but at the expense of the structural connectivity which is also an essential constraint on the model. Hence, it is desirable that the structural connectivity be imposed directly into this method as another necessary

constraint so that the stiffness matrix can be adjusted in a more convincing way. Unfortunately, this is mathematically difficult to achieve.

Berman has successfully applied a similar methodology to the case of analytical mass improvement^[11]. He imposed the orthogonality constraint during the correction procedure and derived an optimal mass matrix by minimizing the following Euclidian norm:

$$\mathbf{d} = \left\| [\mathbf{M}_a]^{-1/2}([\mathbf{M}_x] - [\mathbf{M}_a])[\mathbf{M}_a]^{-1/2} \right\|$$

and this yields an optimized mass matrix:

$$[\mathbf{M}_x] = [\mathbf{M}_a] + [\mathbf{M}_a][\phi_x][\mathbf{m}_a]^{-1}([\mathbf{I}] - [\mathbf{m}_a])[\mathbf{m}_a]^{-1}[\phi_x]^T[\mathbf{M}_a] \quad (2-14)$$

where matrix $[\mathbf{m}_a]$ is a modal mass matrix defined as:

$$[\mathbf{m}_a] = [\phi_x]^T[\mathbf{M}_a][\phi_x]$$

As has been seen above, that the main drawback for the Matrix Perturbation Method is its failure to estimate the dominant parts in matrices $[\mathbf{AM}]$ and $[\mathbf{AK}]$ due to the usual absence of high frequency modes from the measured data. On the other hand, the Constraint Minimization Method requires an accurate analytical mass matrix for analytical stiffness matrix improvement, and this requirement is not likely to be fulfilled in reality. Besides, the current methods concentrate on modifying the analytical model while few of them pay attention to locating the errors which exist in the model. Hence, the model improvement problem somehow needs a different approach and the Error Matrix Method described below is intended to fill this requirement.

2-3 THE ERROR MATRIX METHOD (EMM)

2-3-1 Principle and Essence of the Error Matrix Method (EMM)

The Error Matrix Method (EMM)^[16] is a different approach to the others in the analytical model improvement study. The EMM correlates the analytical modal data, which are generated by the analytical model, with the corresponding modal data from measurement in an attempt to identify and locate the cause of the differences between the analytical model and the experimental model. To begin with the stiffness case, the EMM first supposes that the complete experimental stiffness matrix $[K_x]$ is available as well as the analytical one $[K_a]$ and then defines the difference between the two stiffness matrices as the “stiffness error matrix”:

$$[\Delta K] = [K_x] - [K_a] \quad (2-15)$$

Equation (2-15) can be rearranged and inverted on both sides, leading to:

$$\begin{aligned} [K_x]^{-1} &= ([K_a] + [\Delta K])^{-1} \\ &= [[K_a](I) + [K_a]^{-1}[\Delta K]]^{-1} \\ &= [K_a]^{-1} - [K_a]^{-1}[\Delta K][K_a]^{-1} + [K_a]^{-1}[\Delta K][K_a]^{-1}[\Delta K][K_a]^{-1} - \dots \\ &= [K_a]^{-1} - \left(\sum_{r=1}^{\infty} (-1)^r ([K_a]^{-1}[\Delta K])^r \right) [K_a]^{-1} \end{aligned} \quad (2-16)$$

When that matrix $[\Delta K]$ is small compared with $[K_a]$, the matrix product $([K_a]^{-1}[\Delta K])^r$ tends to zero as the exponent "r" becomes large. Under these conditions, the flexibility matrix $[K_x]^{-1}$ in equation (2-16) can be approximated by:

$$[K_x]^{-1} \cong [K_a]^{-1} - [K_a]^{-1}[\Delta K][K_a]^{-1} \quad (2-17)$$

so that $[\Delta K] \cong [K_a] ([K_a]^{-1} - [K_x]^{-1}) [K_a]$ (2-18)

Equation (2-18) can be used to estimate the stiffness error matrix $[\Delta K]$ by constructing each of the two flexibility matrices from the corresponding modal data. A flexibility matrix can be expressed in terms of modal data as follows:

$$[K_a]^{-1} = [\phi_a]_{N \times N} [\omega_a^2]_{N \times N}^{-1} [\phi_a]_{N \times N}^T \quad (2-19)$$

$$[K_x]^{-1} = [\phi_x]_{N \times N} [\omega_x^2]_{N \times N}^{-1} [\phi_x]_{N \times N}^T \quad (2-20)$$

It is realised that, in practice, modal data from measurements are incomplete in two aspects; one, the number of modes which can be studied ($m < N$) and two, the number of coordinates which are measured to describe the mode shapes ($n < N$). Due to these two sources of incompleteness, the flexibility matrices in equations (2-19) and (2-20) are necessarily approximated using:

$$[K_a]_{n \times n}^{-1} \cong [\phi_a]_{n \times m} [\omega_a^2]_{m \times m}^{-1} [\phi_a]_{m \times n}^T \quad (2-21)$$

$$[K_x]_{n \times n}^{-1} \cong [\phi_x]_{n \times m} [\omega_x^2]_{m \times m}^{-1} [\phi_x]_{m \times n}^T \quad (2-22)$$

Therefore, a stiffness error matrix can be estimated using the incomplete experimental modal data and the corresponding analytical modal data from the following expression:

$$[\Delta K] \cong [K_a] ([\phi_a]_{n \times m} [\omega_a^2]_{m \times m}^{-1} [\phi_a]_{m \times n}^T - [\phi_x]_{n \times m} [\omega_x^2]_{m \times m}^{-1} [\phi_x]_{m \times n}^T) [K_a] \quad (2-23)$$

The error matrix thus deduced can be used to identify and to locate the difference(s) between the experimental stiffness matrix (which is supposed to be correct) and the

analytical one (which is believed to contain errors).

A similar procedure can be applied in the case of the mass matrix. The mass error matrix $[AM]$ is defined as the difference between the experimental mass matrix and the analytical one:

$$[\Delta M] = [M_x] - [M_a] \quad (2-24)$$

Following similar algebra to that used for the stiffness case, the mass error matrix can be estimated as:

$$[\Delta M] \cong [M_a] ([M_a]^{-1} - [M_x]^{-1}) [M_a] \quad (2-25)$$

or
$$[\Delta M]_{n \times n} \cong [M_a]_{n \times n} \left([\phi_a]_{n \times m} [\phi_a]_{m \times n}^T - [\phi_x]_{n \times m} [\phi_x]_{m \times n}^T \right) [M_a] \quad (2-26)$$

Again, the incomplete experimental modal data and the corresponding analytical modal data are used in to evaluate the mass error matrix $[AM]$.

The essence of the EMM should be noticed. First of all, it does not presume or require an accurate analytical mass matrix ($[M_a] \cong [M_x]$) for analytical stiffness matrix improvement. Physically, this means that the stiffness matrix is not determined with a mass matrix being its direct reference basis. Instead, a group of measured modes is used as the reference basis. This point is reasonably acceptable in many practical cases such as the determination of stiffness matrix of a car body where a significant amount of mass comes from attached objects. (It should be borne in mind here that although the mass matrix $[M_a]$ is not the direct reference basis, it is an implicit one due to the derivation of $[\phi_a]$ and $[\lambda_a]$, from $[M_a]$ and $[K_a]$). Similarly, the EMM does not presume an accurate analytical stiffness matrix ($[K_a] \cong [K_x]$) for the analytical mass matrix improvement, with the same advantage. Lastly, the EMM focuses the analytical stiffness matrix improvement on the flexibility matrix, where lower frequency modes dominate. This agrees with the fact that,

in practical measurements, only the lower frequency modes are readily available. Nevertheless, according to the nature of its approximation, the EMM could be applied repeatedly, in an iterative process, - a feature which is discussed below.

2-3-2 Validation of the Assumption Made by the EMM

Since the Error Matrix Method (EMM) first appeared as a useful tool for analytical model improvement^[16], a number of applications have been reported in recent literature^{[17],[18],[19]}. However, the assumptions made by the method have not yet been fully assessed and this task will be addressed below. The fundamental assumption suggested by the EMM is the supposition that the matrix product $([K_a]^{-1}[\Delta K])^r$ in equation (2-17) goes to zero as "r" becomes large so that the higher terms in equation (2-17) can be ignored.

Assumption: matrix product $([K_a]^{-1}[\Delta K])^r$ goes to zero as "r" becomes larger so that terms for $r \geq 2$ can be ignored.

This assumption eventually raises a number of subsequent questions if the course of the derivation of the EMM is carefully inspected, and this, in turn, raises a query about the physical meaning behind the mathematical manipulation upon which the EMM is derived.

- (1) Is $[K_x]^{-1} \cong [K] - \left(\sum_{r=1}^{\infty} (-1)^r ([K_a]^{-1}[\Delta K])^r [K_a] \right)$ a good approximation of $[K_x]^{-1}$?
- (2) Is $[K_x] \cong ([K_a] - \sum_{r=1}^{\infty} (-1)^r ([K_a]^{-1}[\Delta K])^r [K_a])^{-1}$ a good approximation of $[K_x]$?
- (3) Will $[K_x]$ thus approximated preserve the connectivity of the original $[K_a]$?
- (4) Will $[K_x]$ thus approximated preserve the correct location of stiffness errors?

In order to answer these questions and so to assess the fundamental assumption, it is appropriate to perform some numerical studies for which the exact stiffness error matrix is

known so that it can be used in the assessment.

A case study has been carried out. The system used was an 8 degree-of-freedom discrete system shown in Figure 2-1. The lumped masses are connected by light stiffness components. In order to define a similar, but slightly different system, it is supposed that the stiffness component between coordinates 2 and 3 is not correctly represented by the analytical model: the analytical estimate for this component was $1.5\text{E}+6$ N/m in comparison with the correct stiffness $1.95\text{E}+6$ N/m, which is 30% larger than the analytical stiffness quantity. Apart from this difference, the analytical model coincides with the experimental model both in stiffness and in mass conditions. Table 2-1 contains the simulated experimental (or correct) stiffness matrix and the analytical (or approximate) stiffness matrix while the correct $[\mathbf{AK}]$ for this case is shown in Figure 2-2. It is to be demonstrated by this numerical study that the questions put forward above can be answered positively and, in turn, the assumption employed by the EMM is validated.

It can be seen by re-examining equation (2-16) that the matrix product $([\mathbf{K}_a]^{-1}[\Delta\mathbf{K}])^r$ ($r=1,2,\dots$) is virtually a weighting factor for matrix $[\mathbf{ka}]$ in each term on the right hand side of the equation. Therefore, the product $([\mathbf{K}_a]^{-1}[\Delta\mathbf{K}])^r$ can be assessed by comparing it with a unity matrix $[\mathbf{I}]$. It is found in this case study that this matrix product truly becomes smaller and smaller as the exponent r increases and an indication of how this matrix product decays is presented in Table 2-2. These results are the matrix products $([\mathbf{K}_a]^{-1}[\Delta\mathbf{K}])^r$ as r increases. They are equally scaled by a unity matrix and, therefore, are comparable quantitatively. The results in Table 2-2 have shown, as the first stage, that the assumption stated above is justified as far as the estimation of $[\mathbf{K}_x]^{-1}$ is concerned. In other words, it is found that matrix product $([\mathbf{K}_a]^{-1}[\Delta\mathbf{K}])^r$ becomes smaller and smaller when r increases and hence equation (2-17) represents a good approximation of the flexibility matrix $[\mathbf{K}_x]^{-1}$.

Thus, attention is now turned to examine whether this flexibility matrix will represent a good approximation of the stiffness matrix when it is developed, because small errors in a flexibility matrix may not still mean the same degree of small errors after a matrix inversion takes place. To examine this, stiffness matrices which are obtained by inverting the approximate flexibility matrices (taking into account the first two and then more terms on the right hand side) in equation (2-16) are compared with the correct stiffness matrix $[K_x]$ in Table 2-3. It is clearly seen that the approximate stiffness matrices thus deduced are very close to the correct one. Perhaps more interestingly, it is noted that these approximate stiffness matrices preserve the correct connectivity of the system. This suggests that the assumption is mathematically reasonable because of the good approximation for both flexibility and stiffness matrix estimation, and physically sensible because of the preservation of the correct connectivity of the system.

Further examination of Table 2-3, by comparing the correct stiffness matrix with the approximate ones deduced from inverting flexibility matrices in equation (2-17), reveals that each approximate stiffness matrix indicates the correct location of the stiffness errors (elements **2,2;2,3;3,2;3,3** in the stiffness matrix). This suggests that the mathematics and the physics are satisfactorily consistent in the EMM before modal data are introduced into it (in equation 2-22). Nevertheless, the stiffness matrix thus estimated is merely an approximation. It is again interesting to find that repeated use of equation (2-17) results in estimated stiffness matrices which improve progressively towards the correct stiffness matrix. Table 2-4 shows the $[AK]$ obtained when equation (2-17) is used iteratively and indicates that the EMM could be used in this way with the convergence to the correct answer.

It has been demonstrated by the detailed case study that the stiffness error matrix derived by the EMM in equation (2-18) is an acceptably good estimate which also preserves the correct connectivity and the error location of a system and questions (1)-(4) raised above

have been answered positively. However, in a real case, the number of measured vibration modes will generally be insufficient and [AK] has to be estimated by equation (2-23) using less than all the vibration modes. Table 2-5 shows the stiffness error matrix for this case study of 8DOF system using the first four modes only. It can be seen by comparing Table 2-5 with Table 2-1 that the connectivity is no longer preserved but, nevertheless, the stiffness errors can still be located (elements **2,2;2,3;3,2;3,3**). This suggests that an incomplete set of modes will not maintain the connectivity characteristics and will make the error location less clear, although this may still be identifiable if the number of modes used is sufficiently large. It is worth mentioning that an insufficient number of modes losing the connectivity is an inevitable consequence of all approaches in model improvement.

2-4 MODEL IMPROVEMENT USING ITERATION

Since it is inevitable that experimental data will be incomplete, model improvement performed by any approach has to be an approximation or optimization with certain aspects. The Constraint Minimization Method (CMM)^[9] tends to modify the analytical model in a single optimization effort so that the modified model can represent perfectly all the measured modes involved while the correctness of the remaining modes of the thus optimized model (which are not experimentally identified) is actually rather problematic. As a matter of fact, those remaining modes of the modified model normally do not represent the corresponding modes presumably observed experimentally since the optimized model could have enormously changed the connectivity of the system the original model describes and, hence, the optimized model is determined to be unable to predict the vibration characteristics of the system in the frequency range (normally high frequency range) where no experimental data exist.

Therefore, on the whole, the modified model could not satisfactorily represent the dynamic characteristics of a structure since the principle does not ensure the correctness of the unmeasured modes. Similarly, the EMM aims at comparing the available measured

modes with the corresponding analytical modes to locate errors existing in the analytical model. Again, the incompleteness of the modes involved and the approximate nature of the method makes the results approximate and violation of the connectivity condition is also inevitable. To overcome this problem, it is thought that an iteration procedure could be employed in the model improvement analysis, using the available measured modes repeatedly so that the effects of the approximate nature of the EMM could be minimized and the violation of connectivity condition could hopefully be diminished and as a result, the improvement may be more efficient and effective.

2-4-1 Strategy of the Iteration Process

If the stiffness case is considered, and the stiffness error matrix $[AK]$ is small, then - in theory - it might be hoped to obtain a reasonably good approximation of the true error matrix $[AK]$ by a single application of the EMM using all the available modes observed in measurement. If the analytical model is modified by adding this estimated stiffness error matrix to the original stiffness matrix, then the modified model may be supposed to be closer to the correct model than the original analytical one and can be regarded as the new analytical model. At this stage, revised analytical modes can be found from an eigensolution for this new analytical model and a second stiffness error matrix can be estimated using the EMM a second time. On each repetition of this process, a smaller and smaller $[AK]$ should be obtained and if the obtained $[AK]$ is added each time to the analytical stiffness matrix, then the consequently modified stiffness matrix should converge to the correct one. The whole procedure is illustrated in Figure 2-3.

It is worth noting, before describing specific applications of the iteration technique, that because the Constraint Minimization Method (CMM) is an optimization approach, the stiffness or mass matrix thus modified is a uniquely optimized result and any iteration process can only lead to the very same result. Thus, there is no point in using iteration for the CMM. However, the Error Matrix Method (**EMM**) is fundamentally an approximation approach and is thus suitable for iterative application.

242 Criteria for the Assessment of the Iteration Results

In order to assess the results of the iteration process suggested in the last Section, certain criteria have to be defined. Since the model improvement process takes the measured modes as its basis, it is thought that the analytical modes of each modified model should be compared with the measured modes in such a way as to quantify the closeness of the two sets of vibration modes. However, merely assessing the closeness of the two sets of vibration modes is not enough since the number of measured modes is incomplete and a modified analytical model producing the analytical modes which are very close, or even identical to, the available measured modes could easily be obtained, such as the result of applying the CMM. However, such a model still does not describe correct vibration characteristics of the objective system or structure. In other words, identity of the two sets of modes does not necessarily mean a perfect model. Therefore, since model improvement results in varying the analytical model by correlating the two groups of vibration modes, it is intended that the each modified stiffness matrix (or mass matrix) could be compared with the correct stiffness matrix. Consequently, a suitable criterion would be based on both the modal parameters (natural frequencies and mode shapes) and the spatial parameters (elements in the stiffness matrix or mass matrix) in order to assess the correctness of the modified stiffness matrix on both a modal and the global model scale.

The parameters which were chosen in this study are:

$$\text{Percentage of frequency error} = |((\omega_x)_p - (\omega^{(r)})_p) / (\omega_x)_p \times 100\%$$

$$\text{Percentage of } p^{\text{th}} \text{ mode shape error} = 100\% \times \left\{ \sum_{q=1}^N (|\varphi_{pq}|_x - |\varphi_{pq}|^{(r)})^2 \right\}^{1/2} / \sum_{q=1}^N |\varphi_{pq}|_x$$

$$\begin{aligned} \text{Percentage of total mode shape error} \\ = 100\% \times \left\{ \sum_{p=1}^N \sum_{q=1}^N (|\varphi_{pq}|_x - |\varphi_{pq}|^{(r)})^2 \right\}^{1/2} / \sum_{p=1}^N \sum_{q=1}^N |\varphi_{pq}|_x \end{aligned}$$

$$\text{Percentage ratio of elements of stiffness matrices} = 100\% \times (k^{(r)})_{pq} / (k_x)_{pq}$$

where $(\omega^{(r)})_p$, $\varphi_{pq}^{(r)}$ and $(\mathbf{k}^{(r)})_{pq}$ are the natural frequency of p^{th} mode, element "pq" of the mode shape matrix and element "pq" of the stiffness matrix, of the improved model after the r^{th} iteration respectively, and \mathbf{k}_{pq} is the element "pq" of experimental stiffness matrix. It should be noted that this procedure implies a re-computation of the "analytical" solution after each iteration using the modified model and the new analytical modes each time are compared with the corresponding measured modes and so is the modified stiffness matrix each time with the correct stiffness matrix.

It is known that, in practice, a measurement exercise cannot provide data of all the modes of a structure and, also, the correct stiffness matrix is generally unknown. Hence, the current intention is to evaluate the feasibility of the iteration approach using a simulated vibrating system whose 'experimental' and 'analytical' models are given. Thus, while all the simulated experimental modes are in fact known in this case, only some of them actually participate in the iteration process to modify the analytical stiffness matrix. The complete stiffness matrix (from the 'experimental' model of the system) is also assumed to be known in order to calculate the ratio of elements of stiffness matrices.

2-5 NUMERICAL STUDY

In this section, a numerical study is presented for two tasks. The first is to assess the stability of using the EMM or the CMM to locate errors existing in an analytical stiffness matrix when the number of experimental modes for which data exist varies and, the second one is to establish the feasibility of using the iteration technique for the EMM.

The first and perhaps the primary goal for model improvement is to use available experimental modal data to **localize** the errors existing in an analytical model. The EMM was designed to facilitate this location task and the CMM **also** seeks to achieve the same

goal by optimizing the analytical stiffness matrix. However, despite the inaccuracy of experimental data, the number of measured modes may be very limited and this feature could be vital to obtaining the correct location.

Also, as suggested above, the stiffness error matrix $[AK]$ is usually small compared with the analytical stiffness matrix $[K_a]$ and it may be expected that if the EMM is applied iteratively, and each time the analytical stiffness matrix is updated by the estimated error matrix $[AK]$, then the resultant error matrix $[AK]$ should become smaller and smaller and the updated matrix $[K_a]$ should approach the correct stiffness matrix.

The typical system on which the numerical study was based is the 8DOF system in Figure 2-1 which was used in the previous **investigation**^[16] to validate the basic assumption made by the EMM. There are two Case Studies simulating different ‘analytical’ stiffness matrices while the simulated ‘experimental’ stiffness matrix is the same as in Table 2-1. Throughout, the mass matrix is supposed to be unchanged during the study. These two Case Studies will be referred to again in the next chapter.

Case One The ‘analytical’ and ‘experimental’ stiffness matrices (of course, both are analytical in fact) are shown in Table 2-1. Here, all 8 ‘analytical’ and ‘experimental’ modes can be found by eigensolving, as in Table 2-6. In order to locate the stiffness errors introduced between coordinates 2 and 3 in the system (or on elements of **2,2;2,3;3,2;3,3** in the analytical stiffness matrix) by evaluating the stiffness error matrix $[AK]$, both the CMM and the EMM are used with different numbers of modes being involved.

Figure 2-4 shows the results of the estimated error matrix $[AK]$ using the CMM (on the left hand side) and the EMM (on the right hand side) with the simulated experimental modes involved being the first 2, 4, 6 and 8 modes respectively. It was found from Figure 2-4 that when the number of modes is small (say 2 out of the total of **8**), the errors in the analytical stiffness matrix are not confidently **localized**. As the number of modes

used is increased, the stiffness error location becomes clearer. The results suggests that error location using either the EMM or the CMM relies significantly on the number of measured modes for which data are available.

Once the error matrix $[AK]$ is estimated by either the EMM or the CMM, the analytical model can be updated by adding the obtained $[AK]$ into the original stiffness matrix $[K_a]$. This is effectively the current technique for improving the analytical model. In addition to the fact that the thus-modified stiffness matrix often does not make sense physically, the vibration modes represented by the improved model cannot be correct - for the CMM case, the improved model can represent the experimental modes which have been used to estimate $[AK]$ and other modes may well be incorrect; for the EMM case, all the vibration modes of the improved model may be either inaccurate or incorrect although they may be closer to those vibration modes if observed experimentally. Table 2-7 shows the natural frequency and mode shape errors of those modes deduced from the analytical model improved by the CMM using the first four experimental modes. It can be seen that the first four analytical modes show perfect agreement with the experimental modes which were used to improve the analytical model - both the mode shape errors and the frequency errors being zeros - while the remaining modes are quite inconsistent, showing errors in both mode shapes and natural frequencies. The similar results for the EMM case are presented in Table 2-8. These results indicate that one single application of the current methods cannot effectively improve an analytical model when the number of experimental modes is incomplete.

Case Two This second case study seeks to assess the effectiveness of the iteration process applied with the EMM. To simulate the experimental stiffness condition, the system shown in Figure 2-1 is used again and the spring component connecting coordinates 2 and 3 is increased by 30 per cent and the neighbouring spring component between coordinates 3 and 4 is decreased by 15 per cent, resulting in changes to 7 elements in the analytical stiffness matrix $(2,2; 2,3; 3,2; 3,3; 3,4; 4,3$ and $4,4)$, while the mass matrix

again remains unchanged. The ‘analytical’ and ‘experimental’ stiffness matrices are shown in Table 2-9. Thus, all the 8 analytical and experimental modes are eigen-solved by using the simulated ‘analytical’ model and ‘experimental’ model respectively and they are shown in Table 2-10.

The EMM was applied iteratively using just the first four simulated experimental modes and the results from the iteration are assessed by the parameters defined in the early part of this chapter. The total mode shape error after each iteration is shown in Figure 2-5, and the ratios of elements 2,2; 2,3; 3,2; 3,3; 3,4; 4,3 and 4,4 of the experimental stiffness matrix to these in the improved stiffness matrix each time are shown in Table 2-11. It can be seen from Figure 2-5 and Table 2-11 that the iteration results do not improve after a certain number of iterations. The corrected model does not represent experimental vibration modes and, further, the spatial parameters (ratios of elements of stiffness matrices) vary irregularly.

The same case was studied further by using the first six of the 8 experimental modes (rather than the first 4). Again, the total mode shape error after each iteration was calculated (in Figure 2-6) and the ratios of elements from the two stiffness matrices are shown in Table 2-12. Comparing Figure 2-6 with Figure 2-5 and Table 2-12 with Table 2-11 one finds that, as the number of modes involved increases, the effect of the model improvement process tends to be a little better than the earlier case, but is still not really adequate. Meanwhile, the need to use such a large number of modes would generally be impractical because the number of measured modes in real cases could be very limited.

One possibility for the failure of the direct iteration technique to bring about significant improvements is that it might be over-demanding to try to “correct” **all** of the n^2 elements in the stiffness matrix $[K_a]$ using only a restricted number of measured modes $[\phi_x]$, constituting only $n \times m$ elements ($m \leq n$). On closer consideration of the model improvement study, it is generally found that not all the elements in matrix $[K]$ need to be

adjusted or corrected. Indeed, the error is more than likely to be concentrated in one or a few comparatively **localized** regions within the matrix $[K_a]$. Hence, the improvement process might be more effective if it were to concentrate on that part of the system where the errors are believed to exist. This idea is developed in the next chapter.

2-6 CONCLUSIONS

The identification of structural dynamic characteristics is nowadays dealt with by both analytical methods and modal testing and analysis methods. Both have their particular advantages and the model improvement study has evolved in order to provide a better understanding of structural dynamic characteristics by correlating the analytical model of a structure with the experimentally-observed vibration modes. Among the developed techniques, the Constraint Minimization Method (CMM) and the Error Matrix Method (EMM) are two typical methods. The former tends to optimize the analytical model by using the limited number of measured modes and the latter one focuses on locating the errors existing in the analytical model. The key difference between these two methods is the premise of a correct mass matrix required by the CMM.

The assumption made by the EMM - of the matrix product $([K_a]^{-1}[\Delta K])^r$ in equation (2-17) approaching zero as the exponential "r" becomes larger - has been investigated and it has been found that the assumption is mathematically acceptable and physically sensible.

It is also shown that, if the number of measured modes is insufficient, then the EMM does not succeed in achieving the correct error location, but neither does the CMM. It is also discovered that direct application of an iteration process to the EMM does not lead to an ideal analytical model. In fact, divergence often occurs even when the number of modes involved is reasonably large.

This results suggests that there is a demand to locate more precisely where the errors are in the analytical model alternatively and to refine the iteration process so that it could improve the analytical model properly.

2.5E+06	-1.5E+06	0.0E+00	0.0E+00	0.0E+00	0.0E+00	0.0E+0	0.0E+00
-1.5E+06	3.0E+06	-1.5E+06	0.0E+00	0.0E+00	0.0E+00	0.0E+00	0.0E+00
0.0E+00	-1.5E+06	4.5E+06	-3.0E+06	0.0E+00	0.0E+00	0.0E+00	0.0E+00
0.0E+00	0.0E+00	-3.0E+06	4.9E+06	0.0E+00	0.0E+00	0.0E+00	0.0E+00
0.0E+00	0.0E+00	0.0E+00	0.0E+00	2.8E+06	-1.0E+06	0.0E+00	0.0E+00
0.0E+00	0.0E+00	0.0E+00	0.0E+00	-1.0E+06	4.0E+06	-3.0E+06	0.0E+00
0.0E+00	0.0E+00	0.0E+00	0.0E+00	0.0E+00	-3.0E+06	4.5E+06	-1.5E+06
0.0E+00	0.0E+00	0.0E+00	0.0E+00	0.0E+00	0.0E+00	-1.5E+06	4.0E+06

Analytical stiffness matrix

2.5E+06	-1.5E+06	0.0E+00	0.0E+00	0.0E+00	0.0E+00	0.0E+0	0.0E+00
-1.5E+06	3.45E+06	-1.95E+06	0.0E+00	0.0E+00	0.0E+00	0.0E+00	0.0E+00
0.0E+00	-1.95E+06	4.95E+06	-3.0E+06	0.0E+00	0.0E+00	0.0E+00	0.0E+00
0.0E+00	0.0E+00	-3.0E+06	4.9E+06	0.0E+00	0.0E+00	0.0E+00	0.0E+00
0.0E+00	0.0E+00	0.0E+00	0.0E+00	2.8E+06	-1.0E+06	0.0E+00	0.0E+00
0.0E+00	0.0E+00	0.0E+00	0.0E+00	-1.0E+06	4.0E+06	-3.0E+06	0.0E+00
0.0E+00	0.0E+00	0.0E+00	0.0E+00	0.0E+00	-3.0E+06	4.5E+06	-1.5E+06
0.0E+00	0.0E+00	0.0E+00	0.0E+00	0.0E+00	0.0E+00	-1.5E+06	4.0E+06

Experimental stiffness matrix

Table 2- 1

Simulated analytical and experimental stiffness matrices

0.00000	0.09396	0.09396	0.00000	0.00000	0.00000	0.00000	0.00000
0.00000	0.15659	-0.15659	0.00000	0.00000	0.00000	0.00000	0.00000
0.00000	-0.08077	0.08077	0.00000	0.00000	0.00000	0.00000	0.00000
0.00000	-0.04945	0.04945	0.00000	0.00000	0.00000	0.00000	0.00000
0.00000	0.00000	0.00000	0.00000	0.00000	0.00000	0.00000	0.00000
0.00000	0.00000	0.00000	0.00000	0.00000	0.00000	0.00000	0.00000
0.00000	0.00000	0.00000	0.00000	0.00000	0.00000	0.00000	0.00000
0.00000	0.000	0.00000	0.00000	0.00000	0.00000	0.00000	0.00000

0.00000	0.02230	0.02230	0.00000	0.00000	0.00000	0.00000	0.00000
0.00000	0.03717	-0.03717	0.00000	0.00000	0.00000	0.00000	0.00000
0.00000	-0.01917	0.01917	0.00000	0.00000	0.00000	0.00000	0.00000
0.00000	-0.01174	0.01174	0.00000	0.00000	0.00000	0.00000	0.00000
0.00000	0.00000	0.00000	0.00000	0.00000	0.00000	0.00000	0.00000
0.00000	0.00000	0.00000	0.00000	0.00000	0.00000	0.00000	0.00000
0.00000	0.00000	0.00000	0.00000	0.00000	0.00000	0.00000	0.00000
0.00000	0.00000	0.00000	0.00000	0.00000	0.00000	0.00000	0.00000

0.00000	0.00529	0.00529	0.00000	0.00000	0.00000	0.00000	0.00000
0.00000	0.00882	-0.00882	0.00000	0.00000	0.00000	0.00000	0.00000
0.00000	-0.00445	0.00445	0.00000	0.00000	0.00000	0.00000	0.00000
0.00000	-0.00279	0.00279	0.00000	0.00000	0.00000	0.00000	0.00000
0.00000	0.00000	0.00000	0.00000	0.00000	0.00000	0.00000	0.00000
0.00000	0.00000	0.00000	0.00000	0.00000	0.00000	0.00000	0.00000
0.00000	0.00000	0.00000	0.00000	0.00000	0.00000	0.00000	0.00000
0.00000	0.00000	0.00000	0.00000	0.00000	0.00000	0.00000	0.00000

Table 2-2
 $([K_a]^{-1}[\Delta K])^r$ for Case 1 when $r=1,2,3$

2.5E+06	-1.5E+06	0.0E+00	0.0E+00	0.0E+00	0.0E+00	0.0E+00	0.0E+00
-1.5E+06	3.59E+06	-2.09E+06	0.0E+00	0.0E+00	0.0E+00	0.0E+00	0.0E+00
0.0E+00	-2.09E+06	5.09E+06	-3.0E+06	0.0E+00	0.0E+00	0.0E+00	0.0E+00
0.0E+00	0.0E+00	-3.0E+06	4.9E+06	0.0E+00	0.0E+00	0.0E+00	0.0E+00
0.0E+00	0.0E+00	0.0E+00	0.0E+00	2.8E+06	-1.0E+06	0.0E+00	0.0E+00
0.0E+00	0.0E+00	0.0E+00	0.0E+00	-1.0E+06	4.0E+06	-3.0E+06	0.0E+00
0.0E+00	0.0E+00	0.0E+00	0.0E+00	0.0E+00	-3.0E+06	4.5E+06	-1.5E+06
0.0E+00	0.0E+00	0.0E+00	0.0E+00	0.0E+00	0.0E+00	-1.5E+06	4.0E+06

2.5E+06	-1.5E+06	0.0E+00	0.0E+00	0.0E+00	0.0E+00	0.0E+00	0.0E+00
-1.5E+06	3.42E+06	-1.92E+06	0.0E+00	0.0E+00	0.0E+00	0.0E+00	0.0E+00
0.0E+00	-1.92E+06	4.92E+06	-3.0E+06	0.0E+00	0.0E+00	0.0E+00	0.0E+00
0.0E+00	0.0E+00	-3.0E+06	4.9E+06	0.0E+00	0.0E+00	0.0E+00	0.0E+00
0.0E+00	0.0E+00	0.0E+00	0.0E+00	2.8E+06	-1.0E+06	0.0E+00	0.0E+00
0.0E+00	0.0E+00	0.0E+00	0.0E+00	-1.0E+06	4.0E+06	-3.0E+06	0.0E+00
0.0E+00	0.0E+00	0.0E+00	0.0E+00	0.0E+00	-3.0E+06	4.5E+06	-1.5E+06
0.0E+00	0.0E+00	0.0E+00	0.0E+00	0.0E+00	0.0E+00	-1.5E+06	4.0E+06

2.5E+06	-1.5E+06	0.0E+00	0.0E+00	0.0E+00	0.0E+00	0.0E+00	0.0E+00
-1.5E+06	3.46E+06	-1.96E+06	0.0E+00	0.0E+00	0.0E+00	0.0E+00	0.0E+00
0.0E+00	-1.96E+06	4.96E+06	-3.0E+06	0.0E+00	0.0E+00	0.0E+00	0.0E+00
0.0E+00	0.0E+00	-3.0E+06	4.9E+06	0.0E+00	0.0E+00	0.0E+00	0.0E+00
0.0E+00	0.0E+00	0.0E+00	0.0E+00	2.8E+06	-1.0E+06	0.0E+00	0.0E+00
0.0E+00	0.0E+00	0.0E+00	0.0E+00	-1.0E+06	4.0E+06	-3.0E+06	0.0E+00
0.0E+00	0.0E+00	0.0E+00	0.0E+00	0.0E+00	-3.0E+06	4.5E+06	-1.5E+06
0.0E+00	0.0E+00	0.0E+00	0.0E+00	0.0E+00	0.0E+00	-1.5E+06	4.0E+06

Table 2-3

Stiffness matrix obtained by inverting the approximate flexibility matrices in equation (2-16) taking into account from the **first two, three** and four terms on the right hand side.

0.00000	0.00000	0.00000	0.00000	0.00000	0.00000	0.00000	0.00000
0.00000	363677.	-363677.	0.00000	0.00000	0.00000	0.00000	0.00000
0.00000	-363677.	363677.	0.00000	0.00000	0.00000	0.00000	0.00000
0.00000	0.00000	0.00000	0.00000	0.00000	0.00000	0.00000	0.00000
0.00000	0.00000	0.00000	0.00000	0.00000	0.00000	0.00000	0.00000
0.00000	0.00000	0.00000	0.00000	0.00000	0.00000	0.00000	0.00000
0.00000	0.00000	0.00000	0.00000	0.00000	0.00000	0.00000	0.00000
0.00000	0.00000	0.00000	0.00000	0.00000	0.00000	0.00000	0.00000

0.00000	0.00000	0.00000	0.00000	0.00000	0.00000	0.00000	0.00000
0.00000	83147.	-83147.	0.00000	0.00000	0.00000	0.00000	0.00000
0.00000	-83147.	83147.	0.00000	0.00000	0.00000	0.00000	0.00000
0.00000	0.00000	0.00000	0.00000	0.00000	0.00000	0.00000	0.00000
0.00000	0.00000	0.00000	0.00000	0.00000	0.00000	0.00000	0.00000
0.00000	0.00000	0.00000	0.00000	0.00000	0.00000	0.00000	0.00000
0.00000	0.00000	0.00000	0.00000	0.00000	0.00000	0.00000	0.00000
0.00000	0.00000	0.00000	0.00000	0.00000	0.00000	0.00000	0.00000

0.00000	0.00000	0.00000	0.00000	0.00000	0.00000	0.00000	0.00000
0.00000	3172.	-3172.	0.00000	0.00000	0.00000	0.00000	0.00000
0.00000	-3172.	3172.	0.00000	0.00000	0.00000	0.00000	0.00000
0.00000	0.00000	0.00000	0.00000	0.00000	0.00000	0.00000	0.00000
0.00000	0.00000	0.00000	0.00000	0.00000	0.00000	0.00000	0.00000
0.00000	0.00000	0.00000	0.00000	0.00000	0.00000	0.00000	0.00000
0.00000	0.00000	0.00000	0.00000	0.00000	0.00000	0.00000	0.00000
0.00000	0.00000	0.00000	0.00000	0.00000	0.00000	0.00000	0.00000

Table 2-4
[AK] for Case 1, obtained by repeatedly using equation (2-18)

-5075.	12072.	7563.	-4973.	4548.	-157.	1123.	21190.
12072.	311520.	-354154.	5010.	-8096.	-76033.	68394.	-50770.
7563.	-354154.	370633.	-11732.	-11750.	138287.	127229.	43541.
-4973.	5010.	-11732.	630.	5211.	-41879.	38543.	-17 176.
4548.	-8096.	-11750.	5211.	-4039.	1244.	-2952.	-22504.
-157.	-76033.	138287.	-41879.	1244.	173770.	167646.	76132.
1123.	68394.	127229.	38543.	-2952.	167646.	161751.	-69036.
21190.	-50770.	43541.	-17176.	-22504.	76132.	-69036.	20994.

Table 2-5

Stiffness error matrix for Case 1 by the EMM using the first 4 modes

Mode No.	1	2	3	4	5	6	7	8	
Nat. Freq. Hz	21.373	33.858	78.452	89.864	103.423	212.566	296.473	406.767	
mode shapes	x1	.07057	.08130	.05016	.05977	.12481	.22656	.52016	.80582
	x2	.07373	.01048	-.00267	.26796	.25354	.30933	.36546	-.38938
	x3	.06631	-.05485	.14783	.03574	.28551	.13239	-.26471	.07730
	x4	.04279	-.03918	.20808	.10846	.10775	-.32322	.10084	-.01170
	x5	-.04571	-.05066	.03370	.08651	.13254	.22928	.52365	.80923
	x6	-.06263	.04423	.21387	-.03252	.24891	.33844	.40893	-.40756
	x7	-.06325	.07242	.15945	.11500	.26519	.12384	-.27473	.08122
	x8	-.02595	.03320	-.04266	-.03719	.29410	-.33922	.10193	-.01164

Vibration modes for the analytical model of Case 1

Mode No.	1	2	3	4	5	6	7	8	
Nat. Freq. Hz	21.384	34.443	79.597	93.286	103.494	213.326	303.898	410.018	
mode shapes	x1	.06989	.08018	.05977	.05086	.12412	.21841	.56229	.77958
	x2	.07284	.00282	.04372	.26106	.24496	.29917	.36014	-.40978
	x3	.06700	-.05084	.14785	.02759	.28540	.13883	-.25943	.08887
	x4	.04324	-.03673	.22139	.07998	.10615	-.32638	.09066	-.01314
	x5	-.04563	-.05329	.05016	.07670	.13098	.22107	.56596	.78284
	x6	-.06277	.04561	.21024	-.07046	.25604	.32209	.39508	-.42654
	x7	-.06349	.07418	.17019	.10602	.26163	.13174	-.26746	.09244
	x8	-.02606	.03396	-.05188	-.01579	.29418	-.34245	.09140	-.01305

Vibration modes for the experiemntal model of Case 1

Table 2-6

All analytical and experimental vibration modes for Case 1

Mode No.	1	2	3	4	5	6	7	8
before	0.054	1.699	1.439	3.668	0.069	0.356	2.443	0.793
after	0.000	0.000	0.000	0.000	0.095	0.365	2.468	0.797

Percentage frequency errors

Mode No.	1	2	3	4	5	6	7	8	total
before	0.728	5.764	10.86	19.18	1.368	3.181	5.279	4.514	50.87
after	0.000	0.000	0.000	0.000	0.642	3.369	5.332	4.486	13.83

Percentage mode shape errors

Table 2-7

Percentage errors before and after the model is improved by the CMM using the first 4 experimental modes

Mode No.	1	2	3	4	5	6	7	8
before	0.054	1.699	1.439	3.668	0.069	0.356	2.443	0.793
after	0.009	0.281	0.225	0.114	0.187	0.413	2.773	0.886

Percentage frequency errors

Mode No.	1	2	3	4	5	6	7	8	total
before	0.728	5.764	10.86	19.18	1.368	3.181	5.279	4.514	50.87
after	0.108	0.917	3.403	34.51	6.251	3.828	5.956	5.003	59.97

Percentage mode shape errors

Table 2-8

Percentage errors before and after the model is improved by the EMM using the first 4 experimental modes

2.5E+06	-1.5E+06	0.0E+00	0.0E+00	0.0E+00	0.0E+00	0.0E+0	0.0E+00
-1.5E+06	3.00E+06	-1.50E+06	0.0E+00	0.0E+00	0.0E+00	0.0E+00	0.0E+00
0.0E+00	-1.50E+06	4.50E+06	-3.0E+06	0.0E+00	0.0E+00	0.0E+00	0.0E+00
0.0E+00	0.0E+00	-3.0E+06	4.9E+06	0.0E+00	0.0E+00	0.0E+00	0.0E+00
0.0E+00	0.0E+00	0.0E+00	0.0E+00	2.8E+06	-1.0E+06	0.0E+00	0.0E+00
0.0E+00	0.0E+00	0.0E+00	0.0E+00	-1.0E+06	4.0E+06	-3.0E+06	0.0E+00
0.0E+00	0.0E+00	0.0E+00	0.0E+00	0.0E+00	-3.0E+06	4.5E+06	-1.5E+06
0.0E+00	0.0E+00	0.0E+00	0.0E+00	0.0E+00	0.0E+00	-1.5E+06	4.0E+06

Analytical stiffness matrix

2.5E+06	-1.5E+06	0.0E+00	0.0E+00	0.0E+00	0.0E+00	0.0E+0	0.0E+00
-1.5E+06	3.45E+06	-1.95E+06	0.0E+00	0.0E+00	0.0E+00	0.0E+00	0.0E+00
0.0E+00	-1.95E+06	4.75E+06	-2.8E+06	0.0E+00	0.0E+00	0.0E+00	0.0E+00
0.0E+00	0.0E+00	-2.8E+06	4.7E+06	0.0E+00	0.0E+00	0.0E+00	0.0E+00
0.0E+00	0.0E+00	0.0E+00	0.0E+00	2.8E+06	-1.0E+06	0.0E+00	0.0E+00
0.0E+00	0.0E+00	0.0E+00	0.0E+00	-1.0E+06	4.0E+06	-3.0E+06	0.0E+00
0.0E+00	0.0E+00	0.0E+00	0.0E+00	0.0E+00	-3.0E+06	4.5E+06	-1.5E+06
0.0E+00	0.0E+00	0.0E+00	0.0E+00	0.0E+00	0.0E+00	-1.5E+06	4.0E+06

Experimental stiffness matrix

Table 2-9

Simulated analytical and experimental stiffness matrices for Case 2

Mode No.	1	2	3	4	5	6	7	8	
Nat. Freq. Hz	21.373	33.858	78.452	89.864	103.423	212.566	296.473	406.767	
mode shapes	x1	.07057	.08130	.05016	.05977	.12481	.22656	.52016	.80582
	x2	.07373	.01048	-.00267	.26796	.25354	.30933	.36546	-.38938
	x3	.06631	-.05485	.14783	.03574	.28551	.13239	-.26471	.07730
	x4	.04279	-.03918	.20808	.10846	.10775	-.32322	.10084	-.01170
	x5	-.04571	-.05066	.03370	.0865 1	.13254	.22928	.52365	.80923
	x6	-.06263	.04423	.21387	-.03252	.2489 1	.33844	.40893	-.40756
	x7	-.06325	.07242	.15945	.11500	26519	.12384	-.27473	.08122
	x8	-.02595	.03320	-.04266	-.03719	.29410	-.33922	.10193	-.01164

Vibration modes for the analytical model of Case 2

Mode No.	1	2	3	4	5	6	7	8	
Nat. Freq. Hz	21.314	34.428	79.411	93.203	102.684	210.721	302.901	409.954	
mode shapes	x1	.06991	.08023	.05787	.04678	.12727	.20900	.56453	.78043
	x2	.07328	.00272	.04137	.25358	.25431	.28997	.36685	-.40960
	x3	.06782	-.05110	.14243	.01794	.29096	.14051	-.25630	.08786
	x4	.04267	-.03621	.22214	.07650	.10725	-.32802	.08502	-.01230
	x5	-.04527	-.05354	.04833	.07248	.13473	.21160	.56824	.78369
	x6	-.06239	.045 16	.20443	-.07982	.25980	.3 1193	.40230	-.42634
	x7	-.06313	.0737 1	.16551	.09659	.27005	.13451	-.26476	.09147
	x8	-.02589	.03372	-.05512	-.02046	.28827	-.3479 1	.08665	-.01235

Vibration modes for the experimental model of Case 2

Table 2- 10

All analytical and experimental vibration modes for Case 2

iteration No.	k_{ij}	22	23 (32)	33	34 (43)	44
0		87.0	76.9	94.7	107.1	104.3
1						
4		96.3 89.1	94.1 61.4	99.8 85.1	102.9 92.0	101.8 99.4
8		96.1	77.7	93.3	96.6	100.1
12		95.6	79.4	96.6	100.4	101.5
16		95.1	77.6	97.0	100.7	101.6
20		95.9	78.3	98.1	101.6	101.9

Table 2- 11
 Percentage ratios of elements of stiffness matrices $(k_{ij}^{(r)}/k_{ij}) \%$
 (Direct iteration using the first four modes in Case 2)

iteration No.	k_{ij}	22	23 (32)	33	34 (43)	44
0		87.0	76.9	94.7	107.1	104.3
1		96.9	93.6	99.0	95.9	97.8
4		97.8	96.0	99.0	100.6	100.5
8		97.8	96.0	99.1	100.8	100.6
12		97.8	96.0	99.2	101.0	101.6
16		97.8	96.0	99.3	100.7	101.7
20		97.8	96.1	99.3	101.1	101.7

Table 2-12
 Percentage ratios of elements of stiffness matrices $(k_{ij}^{(r)}/k_{ij}) \%$
 (Direct iteration using the first six modes in Case 2)

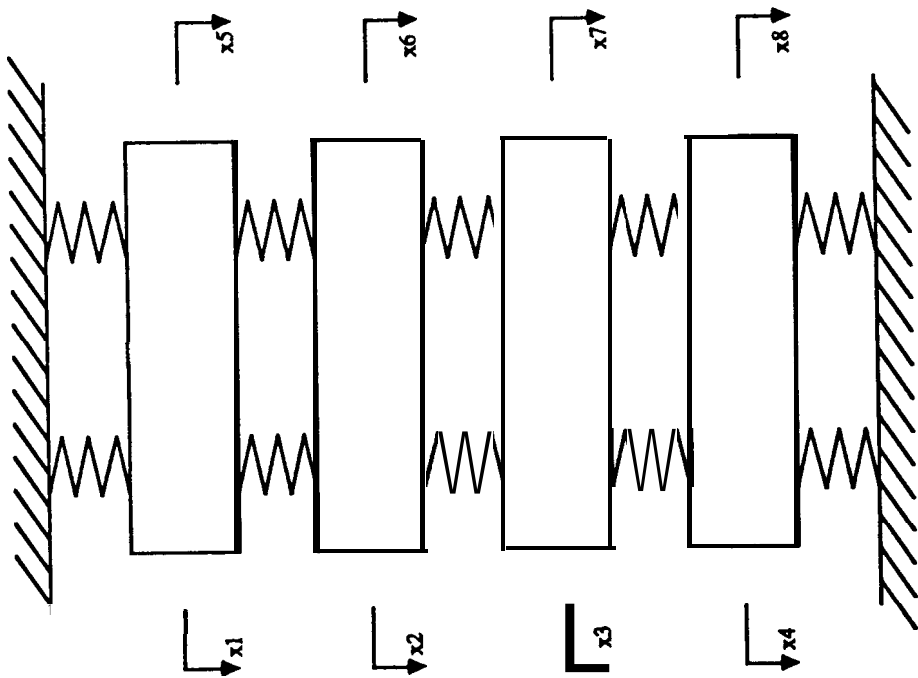


Figure 2-1 An 8DOF vibrating system

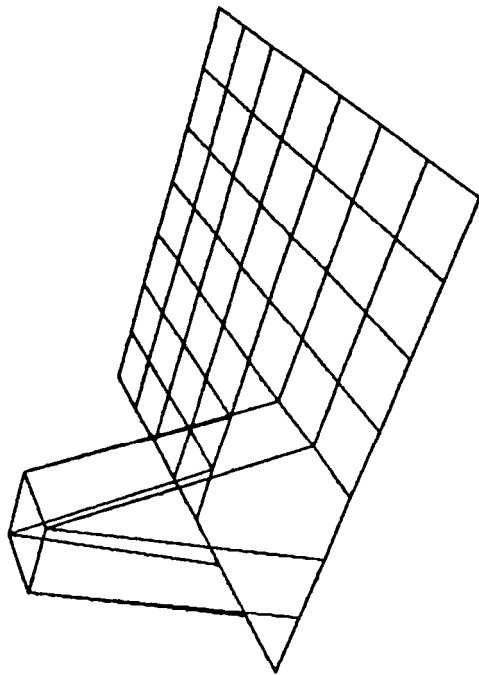


Figure 2-2 Correct stiffness error matrix for Case One

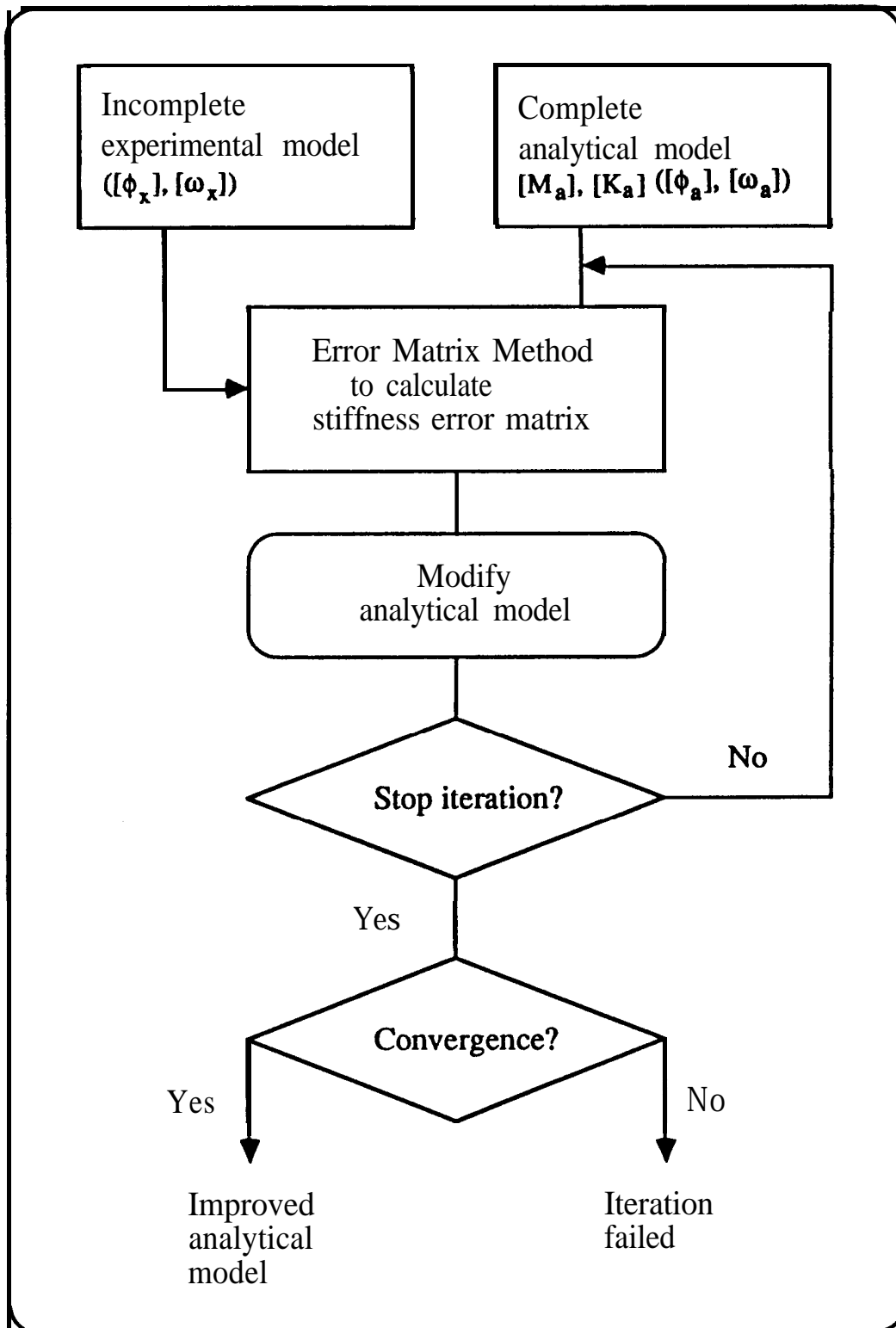


Figure 2-3 Iteration process to improve an analytical model

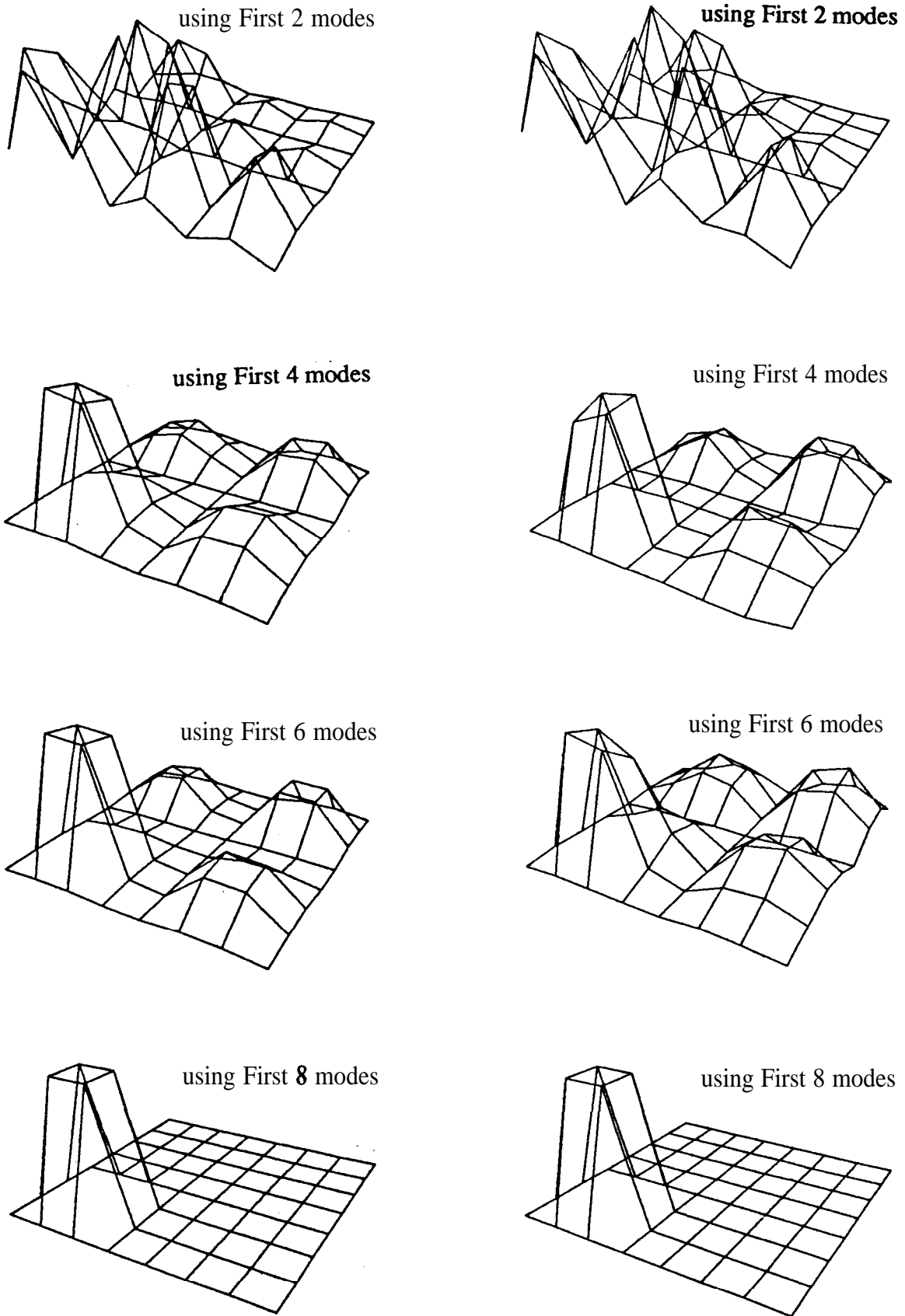


Figure 2-4 Stiffness error matrix [AK] for Case One, estimated by the CMM (left-hand side) and the EMM (right-hand side) using first 2, 4, 6 and 8 modes respectively.

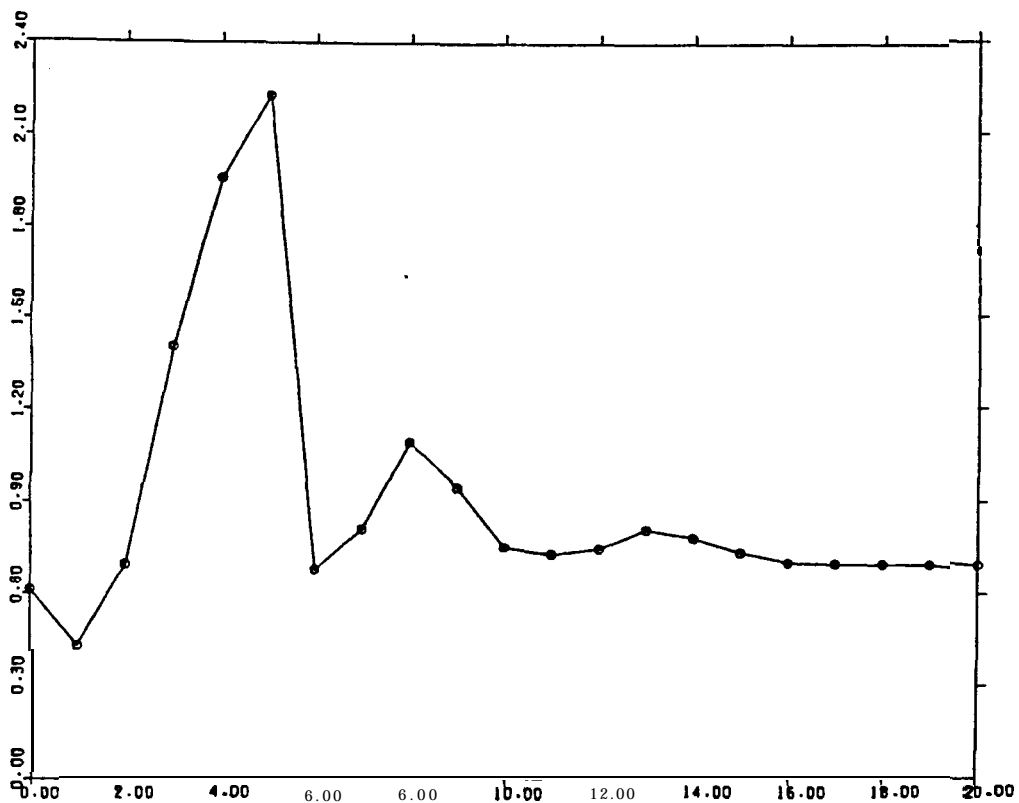


Figure 2-5 Percentage of total mode shape errors for Case Two after each iteration using the EMM with the first 4 modes.

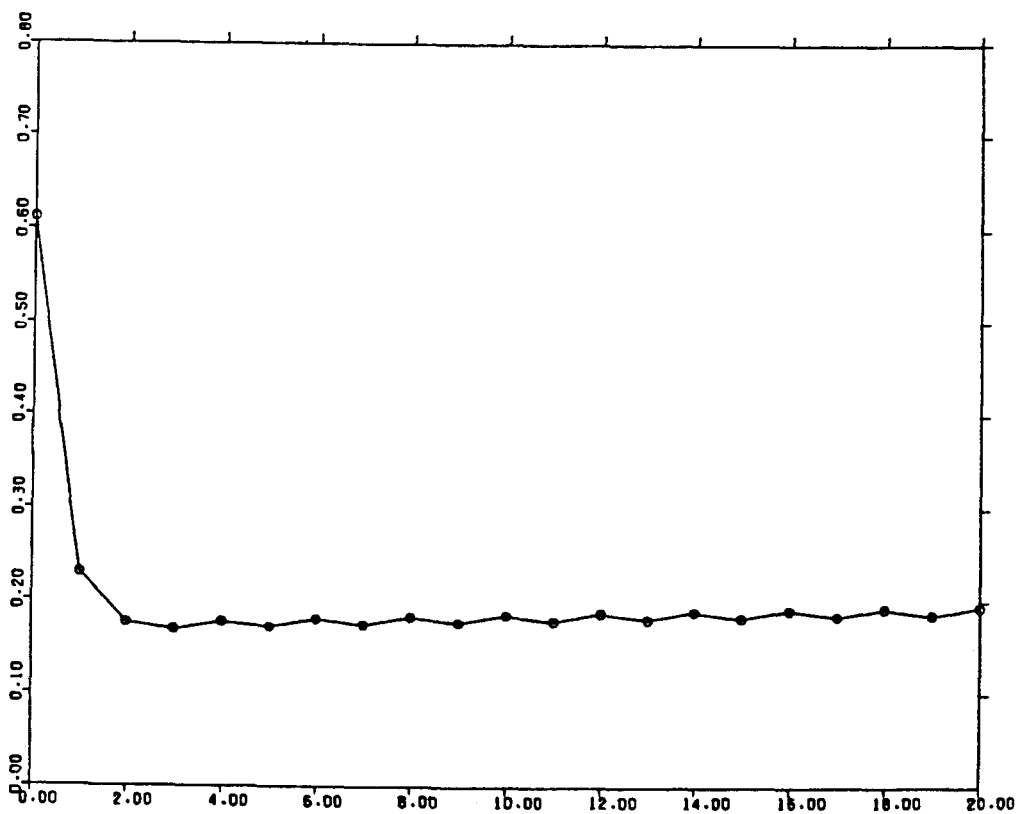


Figure 2-6 Percentage of total mode shape errors for Case Two after each iteration using the EMM with the first 6 modes.

CHAPTER 3

CHAPTER 3

LOCATION OF MISMODELLED REGIONS

- NEW DEVELOPMENTS

3-1 PRELIMINARIES

It was noted in the last Chapter that when the number of modes for which data are available is insufficient - a situation which is very likely in practice - techniques such as the CMM and the EMM might not successfully serve the purpose of locating errors in the analytical model. It was also found that using an iteration process directly in an attempt to improve the analytical model may end up with an unsatisfactory result. In fact, the iteration often diverged from the expected answer. This is mainly because the information contained in the measured modes is rather limited and it is over-demanding to try to correct the whole analytical stiffness or mass matrix.

Although one has to accept the fact that the modes available for the attempt can be very limited, it is also generally accepted that errors in the analytical model are normally localised or isolated rather than spread throughout the whole model, since the FE technique has been highly developed and computer facilities nowadays are sophisticated.

It is therefore believed that the major errors in the model should be located before an attempt is made to improve the analytical model. If this location were successful, then the model could be improved locally and this would be much more efficient. The attempt by the CMM or the EMM to improve the whole analytical mass or stiffness matrix using only a limited number of modes is not physically realistic.

3-2 STRUCTURAL CONNECTIVITY IN AN ANALYTICAL MODEL

The first and intuitive attempt to locate errors is to use the structural connectivity defined by the analytical model itself. As described above, the structural connectivity inherent in the analytical model should **generally** be respected during the model improvement and hence this provides an obvious form of **localization**. As far as the stiffness properties are concerned, this suggests that errors - if there are any - can only occur in the non-zero elements of the analytical stiffness matrix $[K_a]$. It is known that theoretically the experimental stiffness matrix which is normally a banded matrix can be derived from the modal data and the correct mass matrix, provided they are available:

$$[K_x] = [M_x]_{N \times N} [\phi_x]_{N \times N} [\omega_x^2]_{N \times N} [\phi_x]^T_{N \times N} [M_x]_{N \times N} \quad (3-1)$$

To simulate the practical case where only the first m modes are available, the experimental stiffness matrix can be taken to consist of two parts, including the first m modes and the remaining (N-m) modes respectively:

$$[K_x] = [M_x]_{N \times N} [\phi_x]_{N \times m} [\omega_x^2]_{m \times m} [\phi_x]^T_{m \times N} [M_x]_{N \times N} \\ + [M_x]_{N \times N} [\phi_x]_{N \times (N-m)} [\omega_x^2]_{(N-m) \times (N-m)} [\phi_x]^T_{(N-m) \times (N-m)} [M_x]_{N \times N} \quad (3-2)$$

$$= [K_x]_1 + [K_x]_2 \quad (3-3)$$

These two matrices can be shown schematically in Figure 3-1. Although neither is a banded matrix, when be put together they will form the banded matrix $[K_x]$. Normally, only matrix $[K_x]_1$ can be determined from experimental modal data due to the incompleteness of the measured modes. However, it can be said that all the elements in matrix $[K_x]_1$ which do not fall in the area band defined by the structural connectivity in $[K_a]$ are supposed to be the errors because of the insufficient modes used and they will be

changed into zeros if more and more modes are involved. Therefore, those elements violating connectivity should be suppressed artificially, as in Figure 3-2, since they are known to be zero. The iteration process can therefore be applied with the connectivity requirement imposed as the means of error location, albeit only approximate. Physically, this implies that only those stiffness property changes physically allowed by the system or structure will be accepted.

As previously explained, the CMM is an optimization approach and, therefore, is not directly applicable as an iteration approach. However, if the connectivity could be imposed on the optimized stiffness or mass matrix by the CMM, as described above, then it will become possible to apply the CMM iteratively. Each time, the connectivity suggested by the original analytical model is enforced onto the resultant mass or stiffness matrices obtained by the CMM.

A number of numerical studies were carried out using the EMM and the CMM iteratively with the connectivity condition being imposed each time on the improved analytical stiffness matrix as described above. However, it is found that this refined iteration procedure does not generally produce much improved results. In fact, in the case where the number of modes used is limited, so that directly applying the EMM or the CMM to update the analytical model tends to diverge, this new iteration considering the connectivity was unsuccessful.

It can be said that by considering the connectivity we confine the errors to occur inside the connectivity area. The philosophy of the approach is simply requiring the errors to be such that they cannot violate the connectivity while it does not pinpoint exactly where they are in the analytical model. If the errors existing in the analytical model could be located exactly, and the iteration process implemented merely to correct these errors, the improved model would be desirable. The results in Chapter 2 have shown that, due to the limited number of modes, the EMM or the CMM could not exactly locate the errors and direct iteration could not succeed either, so that a new technique needs to be developed to

enable the exact error location using limited number of modes and to facilitate the iteration with this exact error location.

3-3 LOCATION OF MISMODELLED REGIONS IN THE ANALYTICAL MODEL

3-3-1 The Analytical Stiffness Case

It is generally believed that in most practical cases the mass properties of a vibration structure are somewhat easier to model than are the stiffness properties. As a result, the analytical mass matrix is generally acceptably accurate due to the highly sophisticated theoretical modelling techniques used and so, when the stiffness matrix case is investigated here, it is hence presumed that the analytical mass matrix is the same as the experimental one ($[M_a]=[M_x]$). Any areas in the analytical stiffness matrix where errors exist are generally small and local compared with the whole matrix and these areas are called “mismodelled region(s)” here. The aim becomes to pinpoint these regions using the limited number of measured modes when existing techniques do not effectively serve that purpose.

According to definition, the stiffness error matrix is:

$$[\Delta K] = [K_x] - [K_a] \quad (3-4)$$

Equation (3-4) can be post-multiplied on both sides by the incomplete measured mode shape matrix $[\phi_x]$, leading to:

$$[\Delta K][\phi_x] = [K_x][\phi_x] - [K_a][\phi_x] \quad (3-5) ,$$

Although the experimental stiffness matrix $[K_x]$ is unknown, so that the right hand side of equation (3-5) cannot be specified, the measured modal data should satisfy the following relationship,

$$[\mathbf{K}_x][\phi_x] = [\mathbf{M}_x][\phi_x][\omega_x^2] \quad (3-6)$$

where the mass matrix $[\mathbf{M}_x]$ here could be replaced by the accurate analytical mass matrix so that the right hand side of equation (3-6) consist of all known matrices. Thus, substituting equation (3-6) into equation (3-5) yields:

$$[\Delta\mathbf{K}][\phi_x] = [\mathbf{M}_a][\phi_x][\omega_x^2] - [\mathbf{K}_a][\phi_x] \quad (3-7)$$

Post-multiplying both sides of equation (3-7) by the transpose of the incomplete measured mode shape matrix, $[\phi_x]^T$, leads to:

$$[\mathbf{AK}]([\phi_x][\phi_x]^T) = [\mathbf{M}_a][\phi_x][\omega_x^2][\phi_x]^T - [\mathbf{K}_a]([\phi_x][\phi_x]^T) \quad (3-8)$$

It is clear that matrix $([\phi_x][\phi_x]^T)$ cannot be inverted to obtain the stiffness error matrix $[\mathbf{AK}]$, because the mode shape matrix $[\phi_x]$ does not contain all the modes and is rank deficient. However, it is of considerable interest to note that matrix product in the left hand side of equation (3-8) happens to provide an indication of the mismodelled regions, and this matrix product can be derived from the right hand side of the equation which consists of all known matrices. This is explained further in the following.

Equation (3-8) can be transposed to become:

$$([\phi_x][\phi_x]^T)[\Delta\mathbf{K}] = [\phi_x][\omega_x^2][\phi_x]^T[\mathbf{M}_a] - ([\phi_x][\phi_x]^T)[\mathbf{K}_a] \quad (3-9)$$

and both equations (3-8) and (3-9) are illustrated in Figure 3-3. Since it is supposed that the mismodelled region(s) in $[\mathbf{K}_a]$ is usually a local and isolated area, this region can be represented in Figure 3-3 as a small shaded area on the left hand side. It is clear that equation (3-8) indicates the rows in $[\mathbf{K}]$ which contain errors. Since the stiffness matrices $[\mathbf{K}_a]$ and $[\mathbf{K}_x]$ are usually symmetrical, as is matrix $[\mathbf{AK}]$, equation (3-8) has actually located the mismodelled region. In common with equation (3-8), equation (3-9)

shows the columns in matrix $[K_a]$ which contain errors and consequently locates the **mismodelled** region. Therefore, the **mismodelled** region can be located by either using equation (3-8) to locate the rows in $[K_a]$ containing errors or equation (3-9) to locate the columns in $[K_a]$ containing errors. It will be visually more obvious to add these two equations to form the results shown in Figure 3-4, where the overlapped area indicates exactly where is the mismodelled region of the stiffness matrix.

Further examination reveals that equation (3-5) and its derivatives can be written using as few as just one measured mode $\{\phi_x\}_i$ ($i=1, 2, \dots, N$) at a time, rather than all the available measured modes $[\phi_x]$, giving:

$$[\Delta K]\{\phi_x\}_i = [K_x]\{\phi_x\}_i - [K_a]\{\phi_x\}_i \quad (3-10)$$

Following the same procedure of matrix manipulation from equations (3-5) to (3-8) leads to:

$$[\Delta K](\{\phi_x\}\{\phi_x\}^T) = \omega_x^2[M_a]\{\phi_x\}\{\phi_x\}^T - [K_a](\{\phi_x\}\{\phi_x\}^T) \quad (3-11)$$

Equation (3-11) shows that only one measured mode is needed as far as the location of the mismodelled region is concerned, provided that this mode is vibrationally sensitive to $[\Delta K]$. Thus, the location of the mismodelled regions in $[K_a]$ can be performed by using any one of the measured modes or combination of **the** measured modes and this provides the error location with an alternative indication which could make the location process more reliable.

It should be noted that throughout the development of the theory above, there is no assumption that matrix $[\Delta K]$ is small necessary to qualify the feasibility of the theory. This is unlike the cases of the EMM or other methods. Although the theory here

obviously cannot be used to update the matrix $[K_a]$ by any kind of iteration process - rather, it can only be employed to locate the errors from $[K]$ using the measured mode(s) - it is clear that the location of the mismodelled regions is the primary concern for the model improvement study in most times and it has been shown above that the model improvement could hardly be effective or sensible if this location is not provided

3-3-2 The Analytical Mass Case

The same methodology as described in the last section can also be applied to the mass matrix case where a mass error matrix $[AM]$ exists. In practice, it can be said that cases where the analytical mass matrix is less reliable than the stiffness matrix are relatively rare. As far as the joints between the components of a structure are concerned, stiffness modelling errors are expected to be much more serious than those for the mass. However, there are still some practical structures for which the mass modelling could be technically very demanding and the credibility of the resultant analytical mass matrix may be questioned.

In a similar way to the last section, this analysis first presumes that the analytical stiffness matrix is acceptably accurate so that it can be taken as the same as the experimental one ($[K_a]=[K_x]$) when the mass matrix case is investigated. Also, the area(s) in the analytical mass matrix where errors exist is generally small and local compared with the whole matrix and such areas are similarly called “mismodelled region”. The aim becomes the pinpointing of these regions using the limited number of measured modes available.

The mass error matrix is defined as:

$$[\Delta M] = [M_x] - [M_a] \quad (3-12)$$

Equation (3-12) can be post-multiplied on both sides by the incomplete measured mode

shape matrix $[\phi_x]$ and the natural frequency matrix $[\omega_x^2]$, leading to:

$$[\Delta M][\phi_x][\omega_x^2] = [M_x][\phi_x][\omega_x^2] - [M_a][\phi_x][\omega_x^2] \quad (3-13)$$

Substituting equation (3-6) into equation (3-13) will lead to:

$$[\Delta M][\phi_x][\omega_x^2] = [K_a][\phi_x] - [M_a][\phi_x][\omega_x^2] \quad (3-14)$$

post-multiplying equation (3-14) on both sides by the transpose of the **mode shape matrix** $[\phi_x]$ will finally yield:

$$[\Delta M]([\phi_x][\omega_x^2][\phi_x]^T) = [K_a][\phi_x][\phi_x]^T - [M_a]([\phi_x][\omega_x^2][\phi_x]^T) \quad (3-15)$$

The right hand side of equation (3-15) consists of known matrices. Compared with equation (3-8), it is found that this equation provides a significant indication of the mismodelled region(s) in the analytical mass matrix, although the matrix product $([\phi_x][\omega_x^2][\phi_x]^T)$ cannot be inverted to obtain $[\Delta M]$ directly. If equation (3-15) is transposed, giving:

$$([\phi_x][\omega_x^2][\phi_x]^T)[\Delta M] = [\phi_x][\phi_x]^T[K_x] - ([\phi_x][\omega_x^2][\phi_x]^T)[M_a] \quad (3-16)$$

then, combining equations (3-15) with (3-16) will indicate the **mismodelled** regions in $[M_a]$ clearly and can be presented pictorially in Figure 3-4, as for the stiffness case.

Of course, equation (3-15) can also be written using any one of the **measured modes**, yielding:

$$[\Delta M](\omega_x^2\{\phi_x\}\{\phi_x\}^T) = [K_x]\{\phi_x\}\{\phi_x\}^T - [M_a](\omega_x^2\{\phi_x\}\{\phi_x\}^T) \quad (3-17)$$

Again, the location of the mismodelled regions in $[M_a]$ can be performed by using any

one of the measured modes or different combinations of measured modes and this provides the error location with multiple references which could make the location more reliable.

3-3-3 General Case

The stiffness matrix and mass matrix cases have been investigated separately in the last two sections. In reality, however, a combined situation may well occur and the mismodelled regions in both $[K_a]$ and $[M_a]$ need to be located simultaneously using the mode shapes from measurement. In this case, the premise of $[M_a]=[M_x]$ for equation (3-7) is no longer applicable and equation (3-12) should be substituted into equation (3-7) to deal with this problem. This leads to:

$$[\Delta K][\phi_x] = ([M_a] + [\Delta M])[\phi_x][\omega_x^2] - [K_a][\phi_x] \quad (3-18)$$

Post-multiplying both sides of this equation by the transpose of the measured incomplete mode shape matrix $[\phi_x]$ yields:

$$\begin{aligned} & [\Delta K]([\phi_x][\phi_x]^T) - [\Delta M]([\phi_x][\omega_x^2][\phi_x]^T) \\ & = [M_a]([\phi_x][\omega_x^2][\phi_x]^T) - [K_a]([\phi_x][\phi_x]^T) \end{aligned} \quad (3-19)$$

Equation (3-19) may also be obtained by substituting equation (3-4) into equation (3-14).

Akin to equations (3-8) and (3-15) to locate the mismodelled regions in $[K_a]$ and $[M_a]$ separately, equation (3-19) facilitates the error location in the same way. However, the complication involved here is the coexistence of $[AK]$ and $[\Delta M]$ and equation (3-19) only provides the location of the mismodelled regions in the analytical model. Therefore, it is to be identified from the results of equation (3-19) which error region is caused by

[AK] and which by [AM].

3-4 DIRECT NUMERICAL CALCULATION OF [AK]

In addition to revealing mismodelled regions in the analytical mass and stiffness matrices, the advantage of the location technique proposed in the previous section is that it offers the possibility of estimating [AK] (or $[\Delta M]$) by immediate numerical calculation, provided the number of measured modes is sufficient. It is believed that the errors in the analytical model are often local and isolated while, without the effective error location, the model could normally be updated artificially everywhere in such a way that the resultant model would severely violate the structural connectivity and dramatically alter the physical properties in a way which is not practically sensible or acceptable. However, instead of simply applying methods such as the EMM and the CMM to end up with this undesirable new model, the measured modes may well be adequate to quantify these local and isolated errors, once they have been localized, and the analytical model *can* be updated in a way which not only preserves the connectivity but also presents the correct dynamic characteristics of the system or structure without sacrificing the physical properties.

This section investigates the implementation of this numerical calculation. Only the [AK] case is dealt with here and it is presumed that the analytical mass matrix $[M_a]$ is correct and hence $[M_x]$ is used in following formulations when $[M_a]$ occurs in the analysis. The principle is equally valid for estimation of $[\Delta M]$.

Using one measured mode $\{\varphi_x\}_i$ (instead of the set, $\{\phi_x\}$), equation (3-7) becomes:

$$[\Delta K]\{\varphi_x\}_i = (\omega_x^2)_i[M_x]\{\varphi_x\}_i - [K_a]\{\varphi_x\}_i \quad (3-20)$$

The right hand side of this equation consists of known quantities. If it is supposed, for

the sake of simplicity, that there is only one mismodelled region and that this lies in the upper left hand corner of [AK], having dimension $\beta \times \beta$, so that equation (3-20) can be illustrated schematically as shown in Figure 3-5.

Matrices $[M_x], [K_a]$ and $[AK]$ can each be partitioned into a set of column vectors:

$$\begin{aligned}
 [AK] &= [\{\Delta_1\}, \{\Delta_2\}, \dots, \{\Delta_\beta\}, \{\Delta_{\beta+1}\}, \dots, \{\Delta_N\}] \\
 [M_x] &= [\{M_x\}_1, \{M_x\}_2, \dots, \{M_x\}_\beta, \{M_x\}_{\beta+1}, \dots, \{M_x\}_N] \\
 [K_a] &= [\{K_a\}_1, \{K_a\}_2, \dots, \{K_a\}_\beta, \{K_a\}_{\beta+1}, \dots, \{K_a\}_N]
 \end{aligned}$$

where $\{\Delta\}_\beta, \{M_x\}_\beta$ and $\{K_a\}_\beta$ ($\beta=1,2,\dots,N$) are the β^{th} columns in matrices $[AK]$, $[M_x]$ and $[K_a]$ respectively.

Equation (3-20) can then be rewritten as a set of linear simultaneous equations:

$$\left. \begin{aligned}
 \{\Delta_1\}^T \{\varphi_x\}_r &= (\omega_x^2)_r \{M_x\}_1^T \{\varphi_x\}_r - \{K_a\}_1^T \{\varphi_x\}_r \\
 \{\Delta_2\}^T \{\varphi_x\}_r &= (\omega_x^2)_r \{M_x\}_2^T \{\varphi_x\}_r - \{K_a\}_2^T \{\varphi_x\}_r \\
 &\dots\dots\dots \\
 \{\Delta_\beta\}^T \{\varphi_x\}_r &= (\omega_x^2)_r \{M_x\}_\beta^T \{\varphi_x\}_r - \{K_a\}_\beta^T \{\varphi_x\}_r \\
 \{\Delta_{\beta+1}\}^T \{\varphi_x\}_r &= (\omega_x^2)_r \{M_x\}_{\beta+1}^T \{\varphi_x\}_r - \{K_a\}_{\beta+1}^T \{\varphi_x\}_r \\
 &\dots\dots\dots \\
 \{\Delta_N\}^T \{\varphi_x\}_r &= (\omega_x^2)_r \{M_x\}_N^T \{\varphi_x\}_r - \{K_a\}_N^T \{\varphi_x\}_r \quad r=1, 2, \dots, m
 \end{aligned} \right\} \quad (3-21)$$

It can be seen that equation (3-21) contains as many as $N \times m$ linear simultaneous equations. Since the $(\beta \times \beta)$ region of errors in $[AK]$ is symmetrical, the number of linear

simultaneous equations required for numerical determination of $[AK]$ is only $\beta(\beta+1)/2$ out of the total number of $N \times m$ in equation (3-21), provided these equations are independent one another. As each mode can produce up to β linear simultaneous equations, this means the number of measured modes required is reduced to $(\beta+1)/2$ - which is relatively small. However, further algebra reveals that the linear simultaneous equations in (3-21) are not independent. Further, it is concluded that only β modes are needed in order to obtain the $[AK]$ by solving the first β linear simultaneous equations numerically.

It will naturally be the case in practice that more than one localized mismodelled region in $[K_a]$ has to be dealt with. For instance, suppose that there are two such regions, as shown in Figure 3-6, having dimensions $(\beta \times \beta)$ and $(\alpha \times \alpha)$ respectively. Since the two non-zero regions can be dealt with separately in terms of the numerical calculation described above, the number of modes needed to obtain matrix $[AK]$ will still be β , provided here $\alpha < \beta$.

3-5 NUMERICAL ASSESSMENT OF LOCATION TECHNIQUE AND REFINED ITERATION PROCESS

The location of the mismodelled regions in an analytical model by a limited number of measured vibration modes is, in most cases, the primary goal since it pinpoints the failure of the theoretical analysis and provides the analyst with useful information of which part of the structure or system needs to be carefully reanalysed. On the other hand, once the mismodelled regions in the analytical model have been successfully located, the analytical model can also be improved by the available measured modes using existing techniques such as the iterative EMM. Unlike the direct iteration procedure introduced earlier this time only the localized regions in the analytical model will be modified while the remaining major parts in the model can be kept unchanged. Figure 3-7 shows the strategy of this refined iteration process to improve an analytical model. It can be said that this

refined iteration is physically more sensible than the direct iteration applied in the last chapter which tends to modify the whole analytical model.

The dynamic system used to assess the location technique introduced here is the same as that used in the last chapter. The two case studies investigated there are studied further here: the system description and corresponding simulated analytical model and the experimental modes being as in the last Chapter.

The mismodelled region in the analytical stiffness matrix $[K_a]$ will then be located using the new technique developed in this chapter. Once the region has been accurately located, a refined iteration process similar to that direct iteration used in the last Chapter and the slightly improved iteration introduced in the beginning of this Chapter can be used. The refinement for this new iteration process will be in conjunction with the proposed location results and will include restriction of any changes in matrix $[K_a]$ to the mismodelled region which has been located. Any other changes (beyond the **localized** region) indicated by the results of EMM or the CMM will be regarded as errors caused by the incompleteness of the experimental modes and will not be admitted.

Case Study 1 The simulated analytical and experimental stiffness matrices used in this study are for the system shown in Figure 2-1 and are the same as those shown in Table 2-1, and the simulated experimental modes are in Table 2-6. The actual stiffness error matrix is shown in Figure 2-2 and indicates a mismodelled region in the analytical stiffness matrix. Equation (3-1 1) can be used to locate this mismodelled region and Figure 3-8 shows the results of using equation (3-1 1) with a single mode at a time - from mode 1 to mode 8 - and it can be seen that each mode locates errors on **rows 2 and 3 of matrix** $[K_a]$, indicating errors on elements **2,2; 2,3; 3,2; 3,3** of the matrix - which are, in fact, exactly in the mismodelled region. Comparing Figure 3-8 with Figure 2-4 indicates that the location technique suggested in this chapter is much more accurate and efficient and requires considerably fewer experimental modes than other existing methods.

Case Study 2 The simulated analytical and experimental stiffness matrices in this study are the same as those shown in Table 2-7 while the corresponding simulated experimental modes are in Table 2-8. In order to locate exactly the mismodelled region in matrix $[K_a]$, equation (3-1 1) is used in turn with each mode individually, as in Case Study 1. Figure 3-9 shows the results of using equation (3-1 1) with single mode each time (from modes 1 to 4) and it can be seen that the result for each mode locates the same mismodelled region - on elements 2,2; 2,3; 3,2; 3,3; 3,4; 4,3; 4,4 of matrix $[KJ]$ - it can also be seen from Table 2-7 that this located region is correct.

Since the mismodelled region in matrix $[K_a]$ has been successfully located, the iteration process can then be carried out to improve the analytical model by updating matrix $[K_a]$. This time, only the **localized** region in the original matrix $[K_a]$ will be modified by the results of the EMM or the CMM using the first four modes (the same as the case studied in Chapter 2). The total mode shape error is then recorded in Figure 3-10 and the ratios of elements of stiffness matrices are presented in Table 3-1. It can be seen by comparing Figure 3- 10 with Figure 2-7 and Table 3-1 with Table 2-9 that using this refined iteration process on the same case as before shows significant advantages over using direct iteration. Furthermore, a much faster rate of convergence to the correct solution has been achieved than that when only the connectivity was considered.

3-6 CONCLUSIONS

Since the number of vibration modes which can be measured on practical structures is likely to be limited, the corresponding analytical model cannot usually be corrected by a simple application of either the EMM or the CMM, because the results violate the connectivity of the analytical model and could be unacceptably approximate. Under these circumstances, the iteration process is introduced, seeking to improve the analytical model

iteratively and to produce an eventually satisfactory result. This direct iteration process was found in the last chapter to be relatively unsuccessful for model improvement since the iteration can hardly converge to the correct answer.

A first attempt to improve the iteration process was made by applying the connectivity requirements of the analytical model. It is noted that the improved or corrected analytical model must preserve the connectivity of the original model, based on a physical view of a vibration system the model describes. The results of the EMM and the CMM (which violate connectivity each time in the iteration process) are errors due to the insufficiency of the number of measured modes (and other approximations incurred) and should not be taken into account in the model improvement. This slightly improved iteration process has been assessed numerically but has not given convincing results. A possible reason for the relative lack of success of this refined iteration process is that even when connectivity is preserved, the model improvement still implies that all the non-zero stiffness (and/or mass) properties theoretically predicted are erroneous and it tends to “improve” the whole of the analytical model (albeit preserving the connectivity conditions).

It is concluded that difficulties in constructing an analytical model for the vibration properties of a structure are generally encountered only in some local parts of it due to sophisticated analytical modelling techniques now available. Therefore, errors in an analytical model are generally localised and can be referred to as **“mismodelled regions”** in the analytical model. A sensible model improvement procedure should thus seek to modify these mismodelled regions only, rather than to improve the whole analytical prediction. Hence, an exact location of these mismodelled regions from the analytical model is crucial.

Considering the practical situation where the number of measured modes is very limited, and the current methods such as the EMM or the CMM cannot always locate the mismodelled regions in a clear-cut way, a new method has been proposed in this chapter which enables the location to be made with a very limited number of measured modes

(even with only one measured mode). The method is successfully evaluated using the same test cases as before in contrast to less successful location using conventional techniques. It is also proposed in this chapter that if the number of modes is greater than the dimension of the mismodelled region (or the dimension of the biggest mismodelled regions if there are more than one), the exact model correction can be carried out by numerical calculation.

The iteration process to improve the analytical model can now be refined, once the mismodelled regions have been exactly located in the analytical model. Only these mismodelled regions are modified each time in the iteration process by repeatedly using the measured vibration modes. The results have shown marked advantages over those for direct iteration, or for iteration considering connectivity constraints only. It is therefore suggested that the analytical model improvement should be carried out in this way.

	k_{ij}	22	23 (32)	33	34 (43)	44
Iteration No.						
0		87.957	76.923	94.737	107.143	104.255
1		96.300	94.408	99.786	102.920	101.758
4		100.073	99.65 1	100.026	100.195	100.171
8		100.066	99.767	99.839	99.969	99.964
12		100.060	99.795	99.839	99.855	99.952
16		100.054	99.8 14	99.852	99.873	99.955
20		100.049	99.831	99.90 1	99.878	99.959

Table 3- 1

Percentage ratios of elements of stiffness matrices $(k_{ij}^{(r)}/k_{ij}) \%$
 (Location and iteration using the first four modes in Case 2)

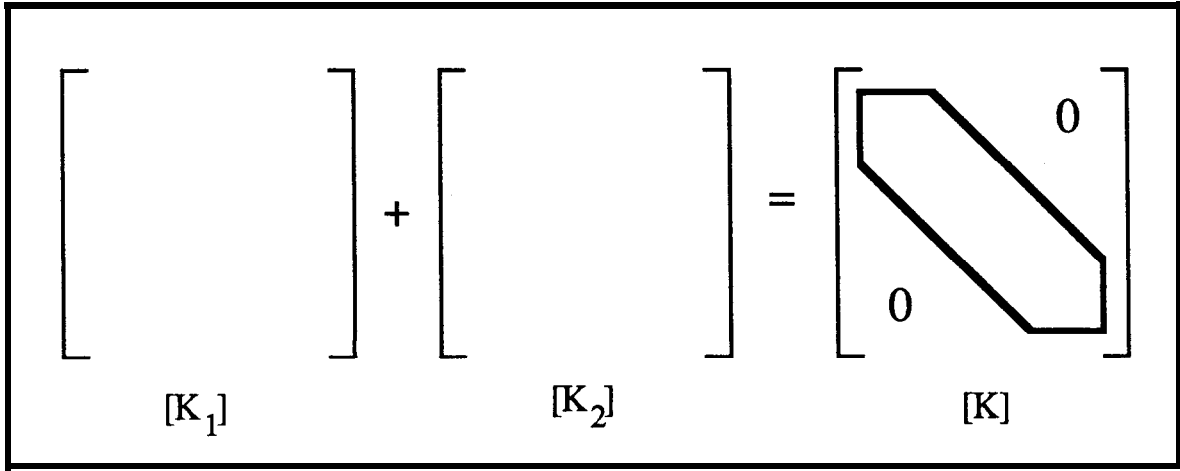


Figure 3- 1 Illustrations of equation (3-3)

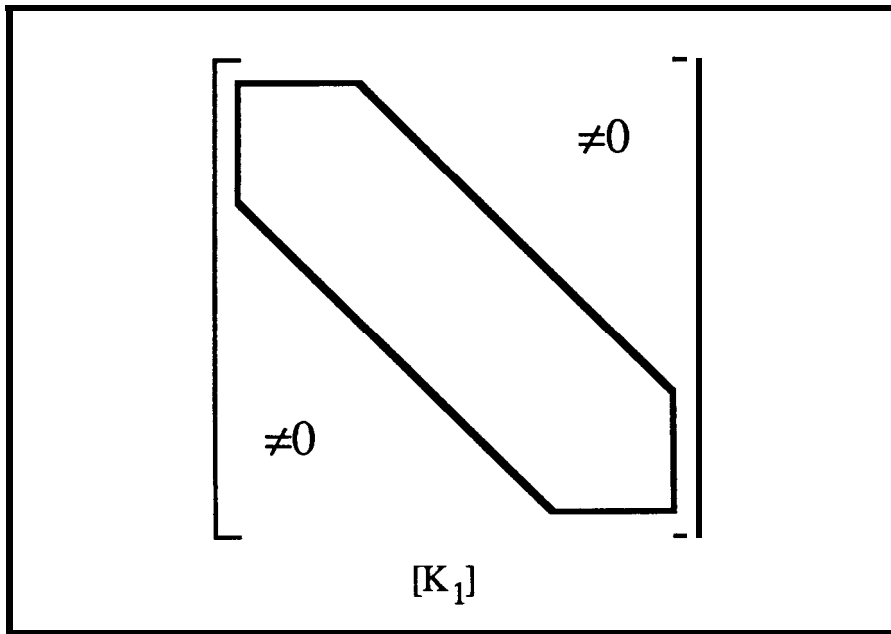


Figure 3-2 Forcing $[K_1]$ to be a banded matrix by correct connectivity

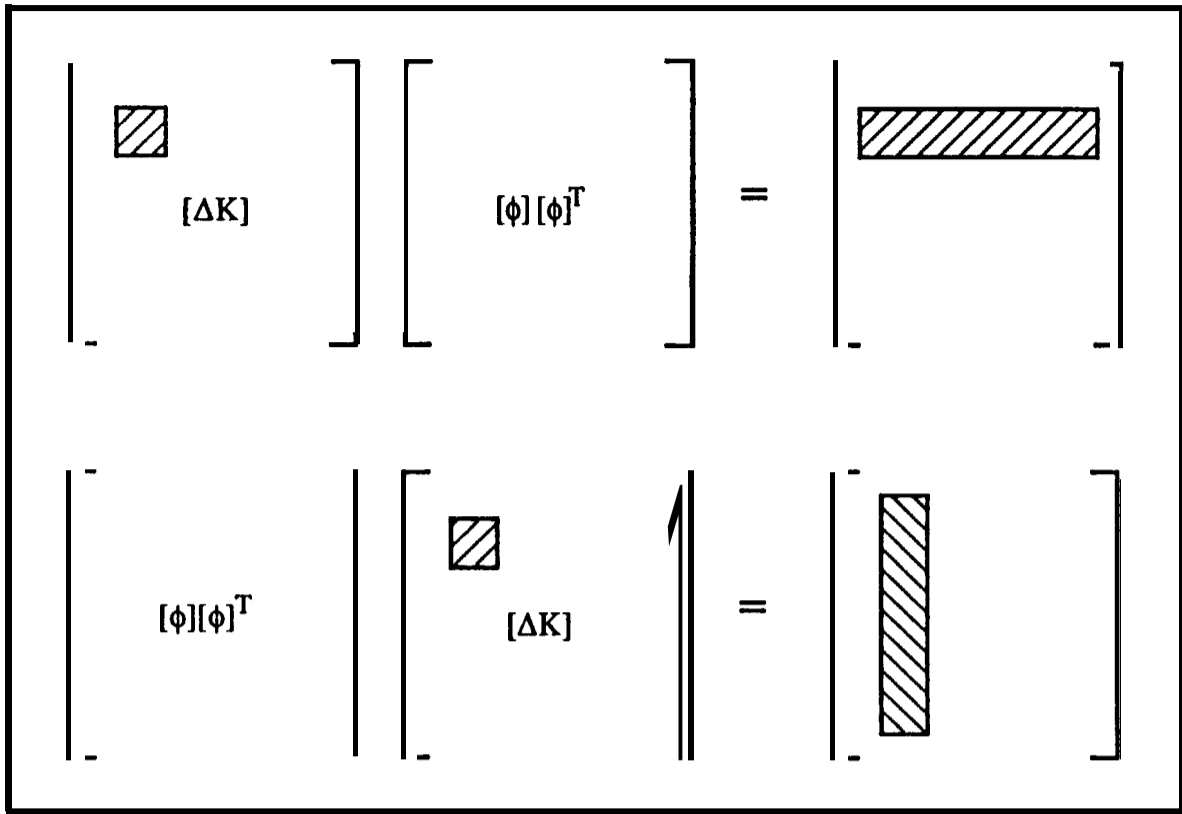


Figure 3-3 Illustrations of equations (3-8) and (3-9)

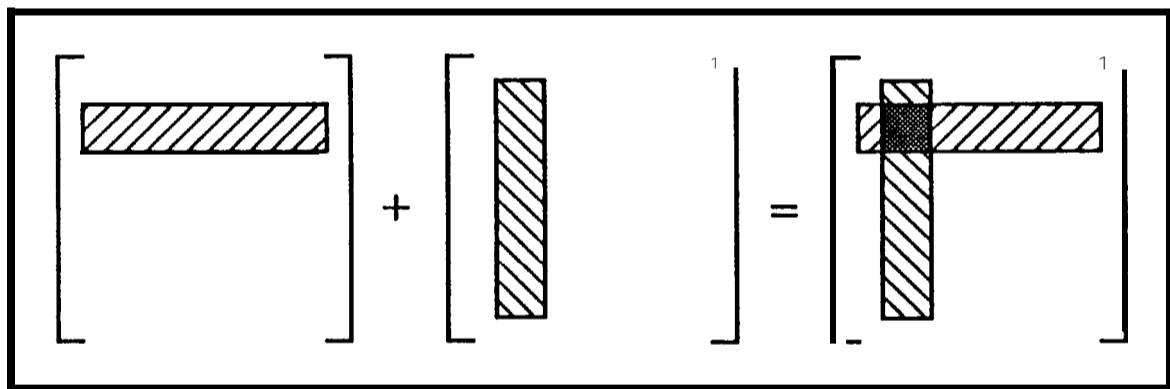


Figure 3-4 Location of the mismodelled region in $[AK]$

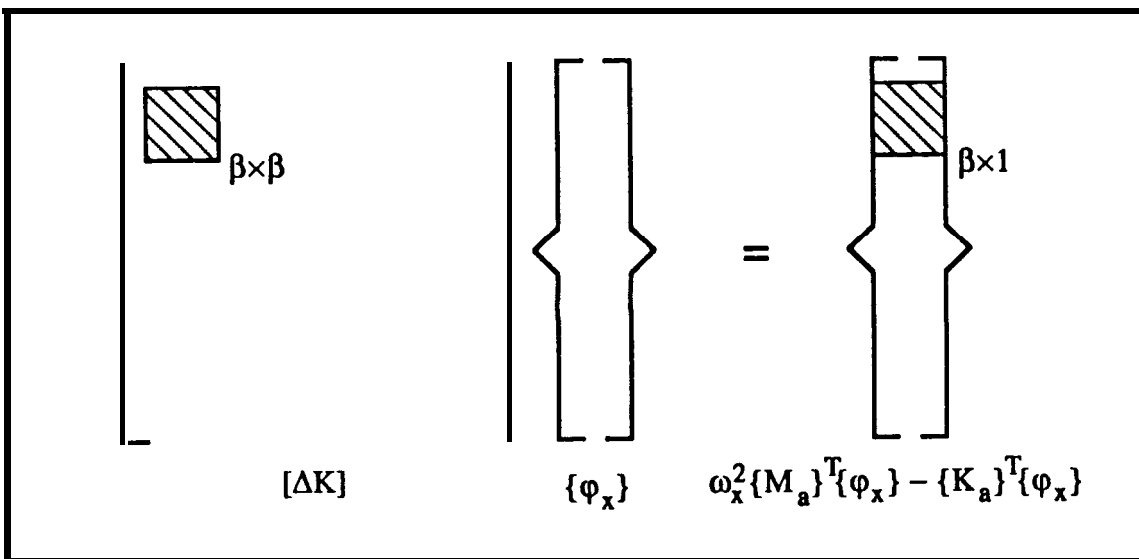


Figure 3-5 Schematical presentation of equation 3-21 when only one mistmodelled region exists

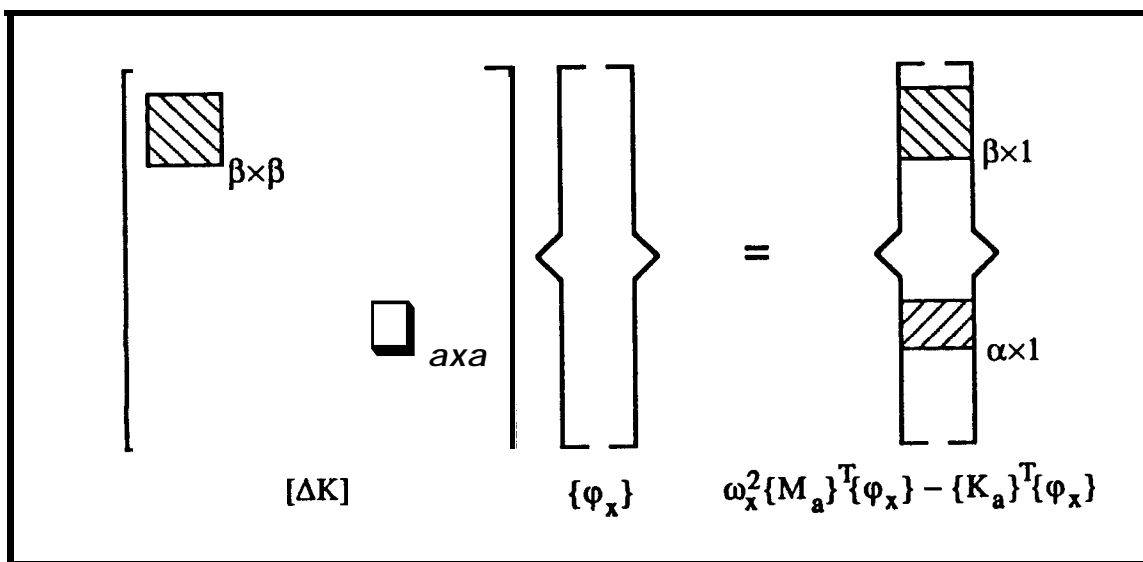


Figure 3-6 Schematical presentation of equation 3-21 when more than one mistmodelled region exist

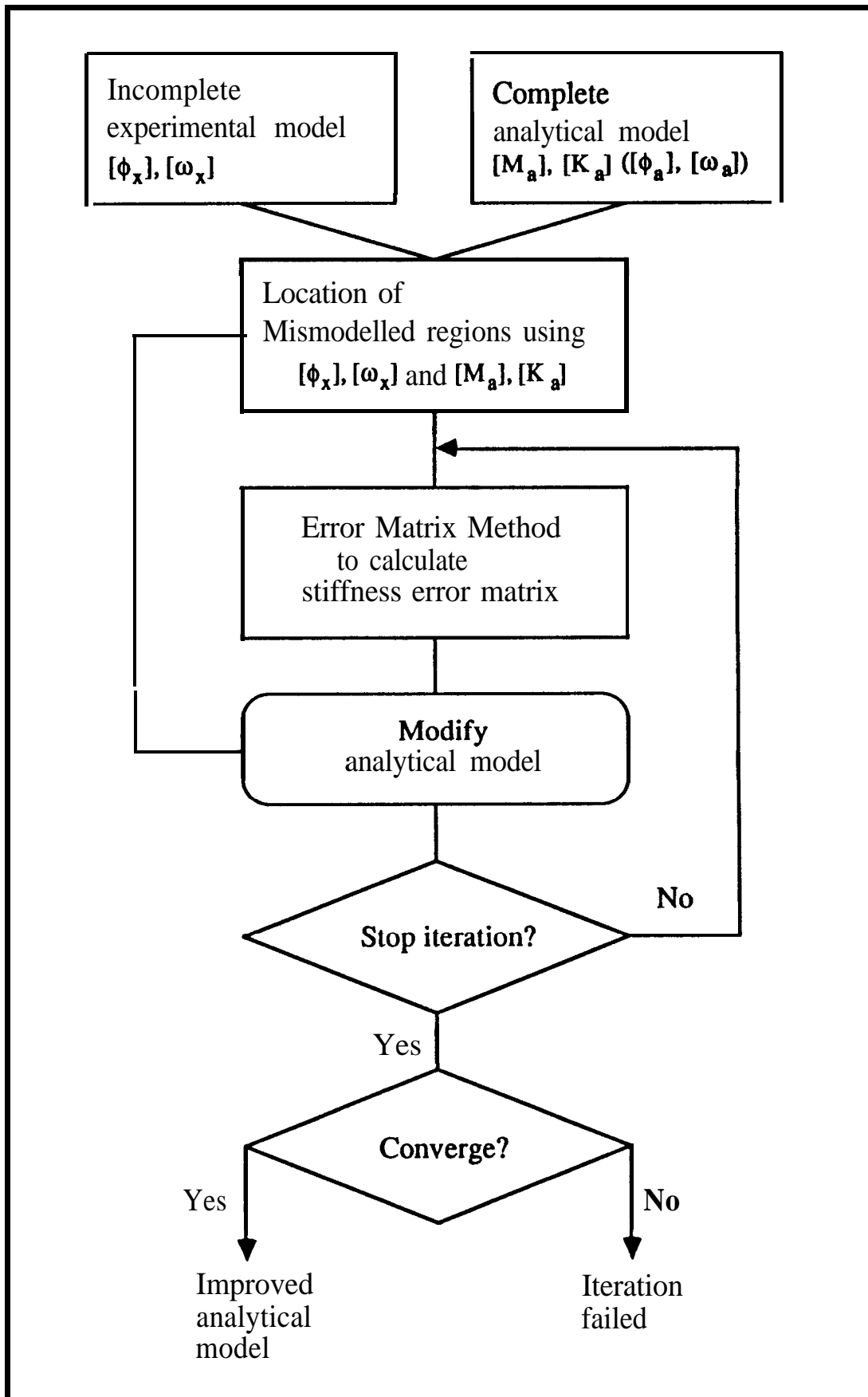


Figure 3-7 Refined iteration process to improve an analytical model

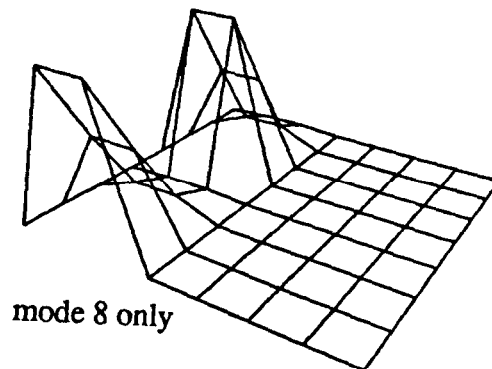
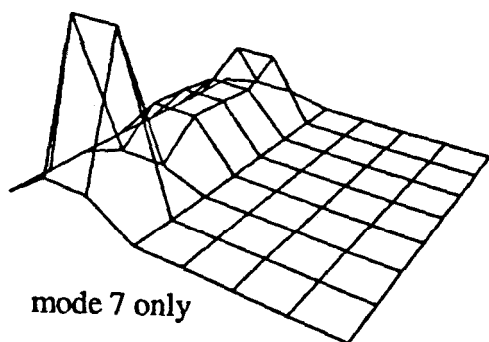
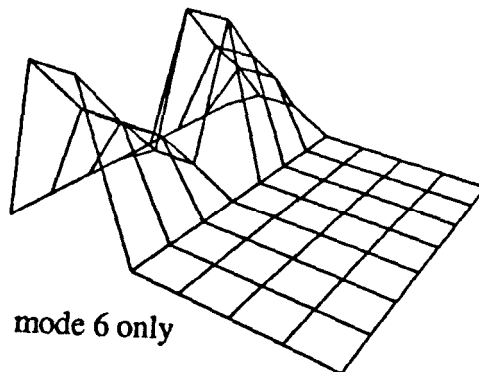
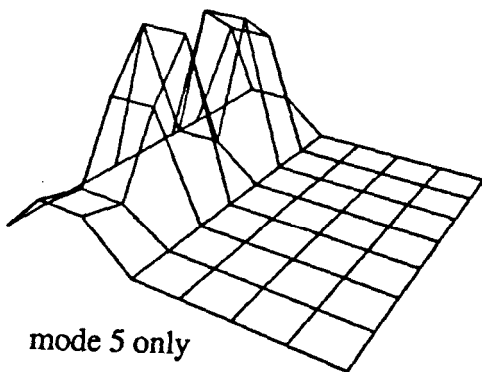
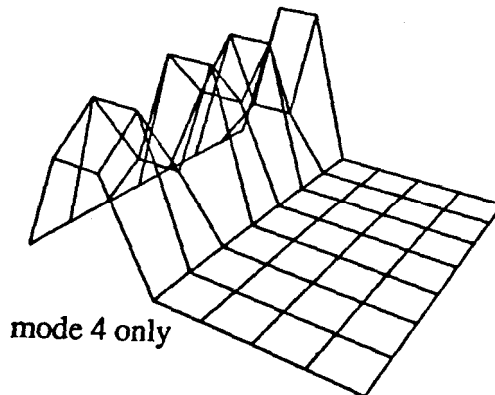
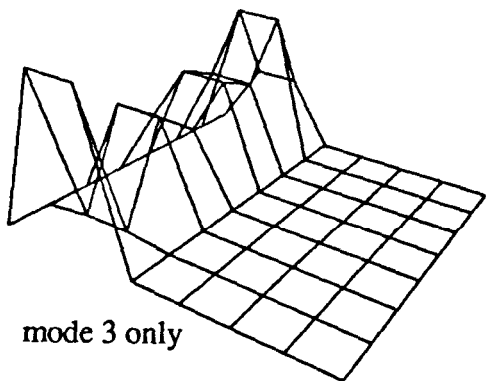
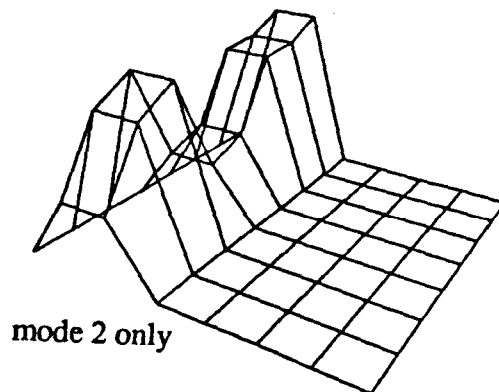
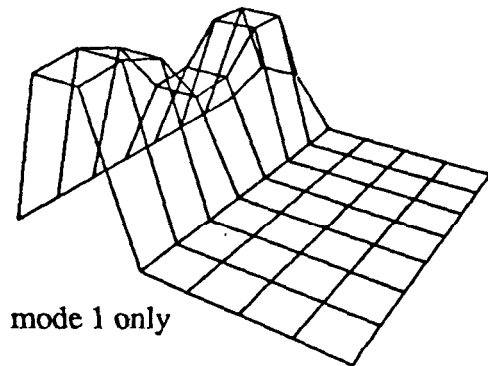


Figure 3-8 Location of stiffness error for Case One using experimental modes from 1 to 8 individually.

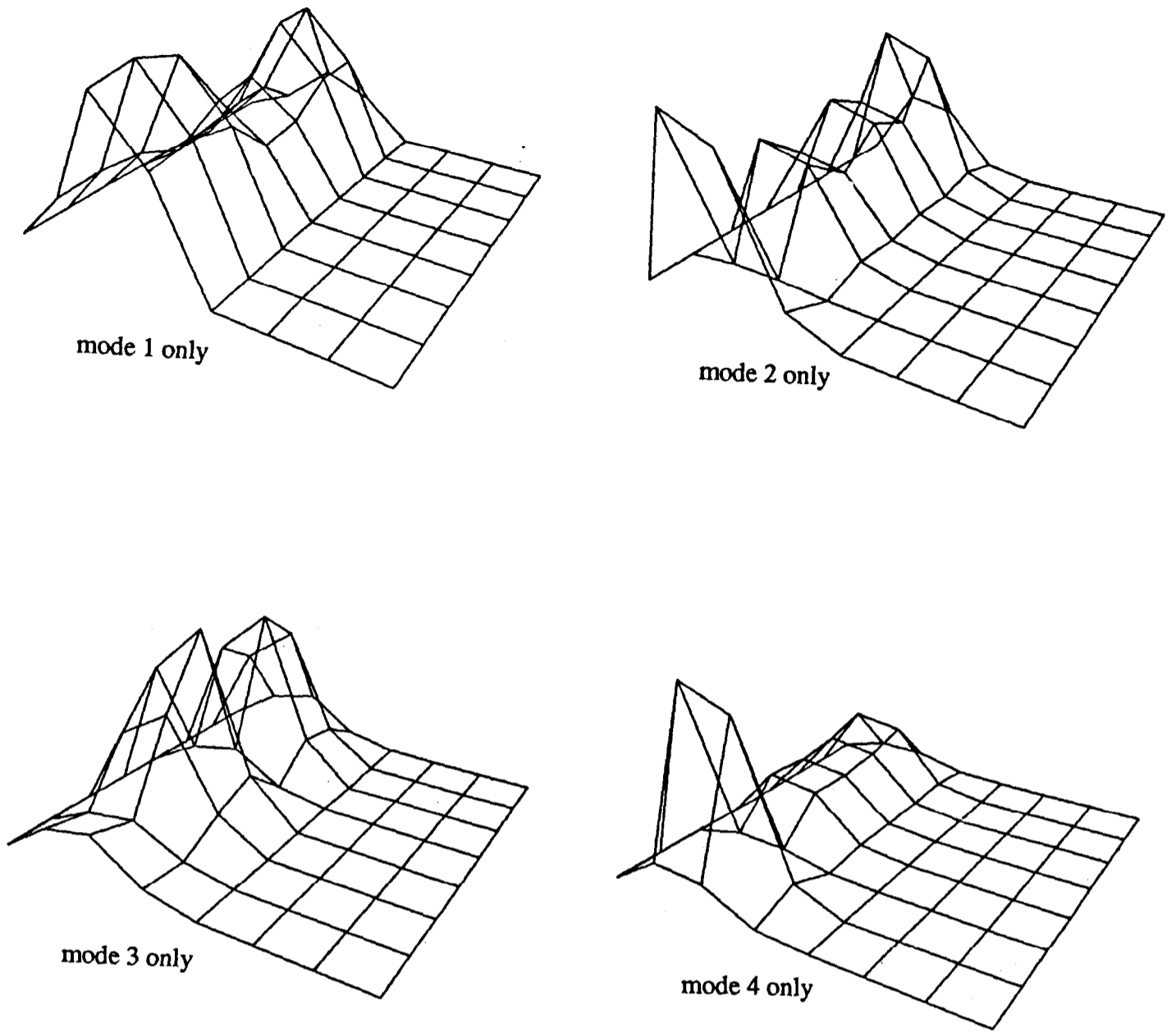


Figure 3-9 Location of stiffness error for Case One using experimental modes **from** 1 to 4 individually.

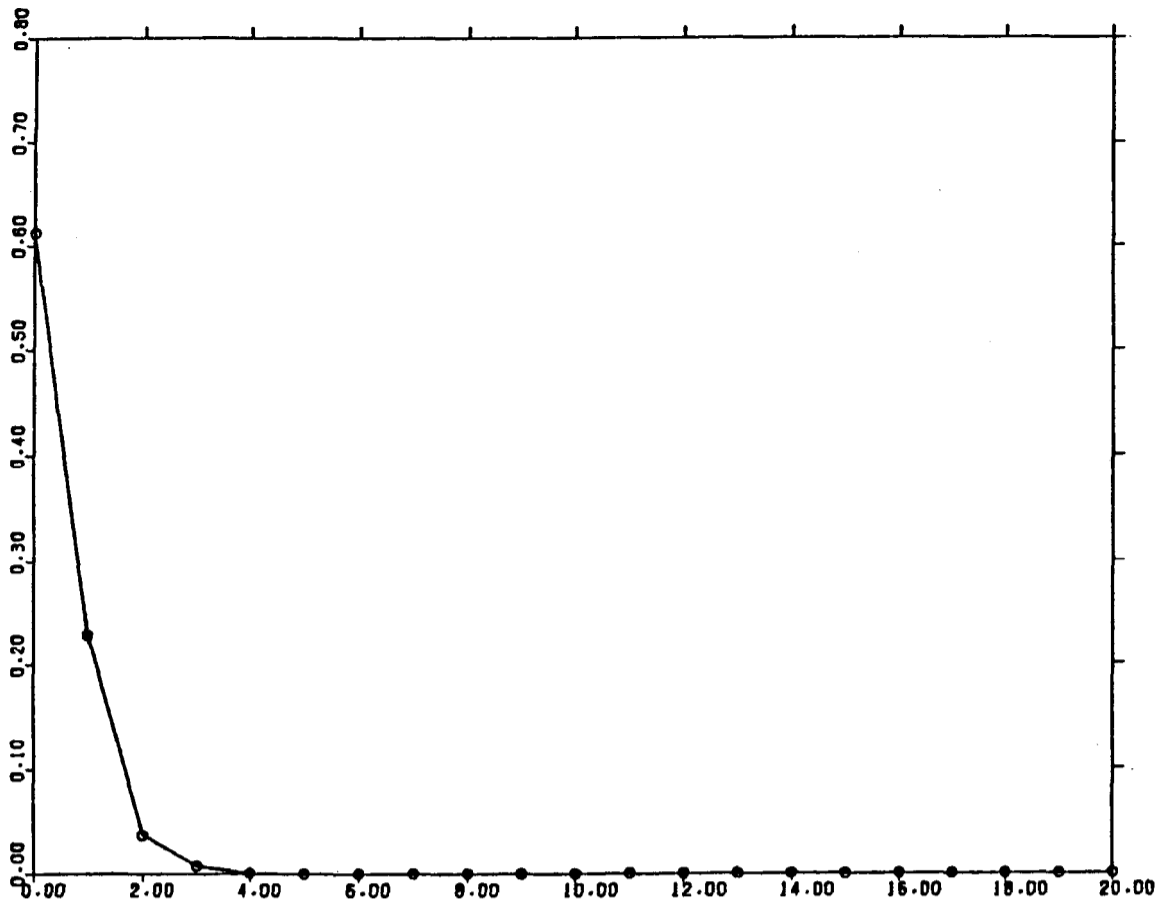


Figure 3- 10 Percentage of total mode shape errors for Case Two after each iteration using the EMM and the stiffness error location results.

CHAPTER 4

CHAPTER 4

IDENTIFICATION OF DAMPING PROPERTIES OF VIBRATING STRUCTURES

4-1 PRELIMINARIES

In the previous Chapters, the location of **mismodelled** regions in an analytical model and the subsequent model improvement using measured vibration modes have been dealt with. When a structure is lightly damped, the vibration modes identified from measurement are often regarded technically as real modes, and it has been suggested that the mismodelled regions can be located effectively by using just a few measured modes. Moreover, once those regions have been successfully located, the analytical model improvement can be focussed in the located regions with the iterative process often producing convincing results which are physically sensible (in contrast to the less convincing results of conventional techniques in many cases).

However, some practical structures are more heavily damped and the measured modal data in such cases are sometimes no longer real. This provokes difficulty in applying the theory discussed in the last two Chapters for investigating the analytical model. Besides, theoretical modelling cannot generally predict the damping properties in detail and so the most likely form for a damping matrix is one which is 'proportional' to the mass and/or stiffness properties, in which case the analytical vibration modes are still real. Although this proportional damping model can readily be applied theoretically, it rarely represents the correct damping properties of real structures.

There have been a number of approaches reported in the literature^{[28]-[32]} which seek to deduce the undamped vibration modes from the measured damped complex modes so that the deduced real modes could be used to modify the erroneous analytical stiffness or mass matrix. In that case, the new development in the previous chapters could be applicable for error location from an analytical model and for the subsequent model improvement. However, the undamped modes thus deduced are often merely a rough approximation since the experimentally identified complex modes are essentially incomplete and the deduction itself relies to some extent on the analytical model which is erroneous. Furthermore, these approaches are not applicable to the location of the damping elements in a structure since they stand on extracting the undamped modes and, in the process, throw away that information concerning the damping properties. It is therefore thought that the experimentally identified complex modes could be used in order to locate the damping elements.

The identification of dynamic characteristics of a damped structure becomes more complicated due to the fact that the erroneous analytical model is to be modified at the same time as the damping properties remain to be investigated. It is believed that it would be possible to investigate the damping properties when the analytical stiffness matrix is relatively accurate. However, this Chapter will consider the general case, i.e. when the structure is damped and its analytical stiffness matrix is in error, and suggests that it is possible to locate the mismodelled regions in the stiffness matrix and meanwhile to locate the damping elements. It will also be shown that the iteration process followed by a successful location could convincingly quantify the damping matrix and the errors existing in the analytical stiffness matrix separately.

4-2 CURRENT APPROACHES FOR **STUDYING** DAMPING PROPERTIES

The damping properties of a practical structure are perhaps the most difficult aspect to investigate, compared with the mass and stiffness characteristics. The difficulty results mainly from the the fact that the damping in a vibrating structure cannot be specified by

analytical methods in the same precise way as can the mass and stiffness characteristics. For some lightly damped structures, the theoretical modelling often assumes them to be undamped and for other cases, where the damping existence cannot be ignored, a linear and proportional damping model is often used. This theory suggests that distribution of damping in a structure takes the same form as that of the mass or stiffness (or both) properties, hence the hysteretic damping matrix $[H]$ or viscous damping matrix $[C]$ could be described by:

$$[H] = \alpha[K] + \beta[M] \quad (4-1)$$

or

$$[C] = \gamma[K] + \delta[M] \quad (4-2)$$

The notable advantage of using this proportional damping model is that the mode shapes of a structure with such damping are identical to the corresponding undamped model and the natural frequencies will be just slightly different. (It is of interest to note that proportional damping models defined by equations 4-1 and 4-2 are not the only cases to produce the identical modes with the undamped ones and the more general condition is discussed in literature^[28]). However, due to the increasing complexity of the dynamic structures to be studied and more stringent demands on the analytical models to include an accurate damping matrix, this assumption of proportional damping becomes less and less appropriate to cope with practical applications.

It is believed that the nature and extent of the damping present in most practical structures can only be determined by experiment. Indeed, measured modal data which come from a successful measurement contain “true” information about the damping properties of a structure. To investigate the information on the damping properties from measurement, it is supposed that the dynamic characteristics of the vibrating structure can be described by a discrete multi-degree-of-freedom system whose equations of motion are as below^[33]:

$$(-\omega^2[M_x] + [K_x] + i[H])\{q\}e^{i\omega t} = \{F\}e^{i\omega t} \quad (4-3)$$

where it is presumed that the damping is of the hysteretic type and $\{q\}$ is a vector of complex harmonic amplitudes. Or, in case of the other widely used damping type -

viscous damping - the equations of motion will be:

$$(-\omega^2[\mathbf{M}_x] + \omega i[\mathbf{C}] + [\mathbf{K}_x])\{\mathbf{q}\}e^{i\omega t} = \{\mathbf{F}\}e^{i\omega t} \quad (4-4)$$

Under the circumstance of single point excitation, the receptance of the system between points "j" and "k" with hysteretic or viscous damping can be **defined** respectively by:

$$\alpha_{jk} = \sum_{r=1}^N \frac{{}_r A_{jk} + i {}_r B_{jk}}{1 - (\omega/\omega_r)^2 + i \eta_r} \quad (4-5)$$

$$\alpha_{jk} = \sum_{r=1}^N \frac{{}_r A_{jk} + i(\omega/\omega_r) {}_r B_{jk}}{1 - (\omega/\omega_r)^2 + 2i(\omega/\omega_r)\xi_r} \quad (4-6)$$

where A, B are the real and imaginary parts of the modal "constant".

Information about the damping properties is contained in the complex modal constant, the natural frequency ω_r (which slightly differs from the undamped natural frequency) as well as the damping loss factor η_r (or ξ_r). The major drawbacks of this information are: (1) it is normally insufficient because of the incompleteness of the measured modal data and, (2) it does not explicitly yield the damping distribution in the structure.

If, in any case, only a few damped vibration modes rather than a representative damping model are of interest in a given practical application, then these damped modes can generally be identified experimentally to fulfil the requirement. However, as far as the stringent demands on the analytical models are concerned to include the damping matrix, the incomplete damping information revealed by the measured modes are certainly not straightforward to enable it. In the literature, effort has been paid to the derivation of a damping matrix directly from a limited number of measured **modes**[34]-[38] as well as to derive the mass and stiffness matrices. Such derivation may be appropriate in the cases where the vibration characteristics of a structure will be defined only by the experimentally-specified number of coordinates and the same number of modes.

4-3 IDENTIFICATION OF DAMPING TYPE FROM MEASURED DATA

The first phase to use the damping information revealed by the measured modes will be to identify the damping type. Although attempts have been made to introduce new damping models in vibration analysis^[39], the hysteretic and viscous damping models are still the most often encountered models used for vibrating structures.

4-3-1 Methodology for Identification of Damping Types

One conventional basic modal analysis approach curve-fits the receptance Nyquist circle based on the SDOF assumption^[33]. This approach gives a damping loss factor but is unable to specify clearly the damping type.

One alternative approach to the Nyquist plot curve-fitting is to use the reciprocal of receptance data^{[40], [41]}. In this case, the SDOF model for the r^{th} mode of a structure with hysteretic or viscous damping, presuming the residual effects of other modes are negligible, will yield the reciprocal of receptance data respectively as:

$$\begin{aligned} \frac{1}{\alpha_H} &= \frac{\omega_r^2 - \omega^2 + i\eta\omega_r^2}{C_r} \\ &= \text{Re}(1/\alpha_H) + \text{Im}(1/\alpha_H)i \end{aligned} \quad (4-7)$$

$$\begin{aligned} \frac{1}{\alpha_V} &= \frac{\omega_r^2 - \omega^2 + 2i\omega\omega_r\xi}{C_r} \\ &= \text{Re}(1/\alpha_V) + \text{Im}(1/\alpha_V)i \end{aligned} \quad (4-8)$$

When the modal constant C_r is a real quantity, the imaginary parts of the reciprocal receptance data become:

$$\text{Im}(1/\alpha_H) = \eta\omega_r^2/C_r \quad (4-9)$$

$$\text{or } \text{Im}(1/\alpha_v) = 2\omega_r \omega \xi / C_r \quad (4-10)$$

In a plot of the imaginary part of $1/\alpha$ against frequency ω (Figures 4-1a and 4-1b), these two damping types are indicated by **either** a horizontal line for hysteretic damping **or** a straight line with non-zero slope for viscous damping. Equations (4-9) and (4-10) are the basis of the identification of damping types.

The simplicity of thus identifying the type of damping is, however, sometimes undermined by the practical situation in which we can hardly rely on the modal constant from the measured data to be real, especially when the damping magnitude is significant. The complexity of the modal constant, as often exists, will tend to mix the real and imaginary parts of the receptance data and hence the reciprocal of the receptance data will not be so directly able to identify the damping type. In order to identify the damping when the mode is complex, it is now proposed that the complexity of the modal constant can be removed once its phase angle is accurately identified by Nyquist circle curve-fitting.

4-3-2 Removal of Complexity from Measured Data

A complex modal constant can be written as the expression in equations (4-7) or (4-8) multiplied by a complex number ($\cos\theta + i\sin\theta$) with unity modulus. The effect of the complexity of the modal constant in the Nyquist circle will thus be to rotate the whole circle from the original position by an angle θ , as illustrated in Figure 4-2. Hence, the reciprocal of the receptance data with a complex modal constant is given as:

$$\begin{aligned} 1/\alpha &= \text{Re}(1/\alpha) + \text{Im}(1/\alpha)i \\ &= [\text{Re}(1/\underline{\alpha}) + \text{Im}(1/\underline{\alpha})i][(\cos\theta - i\sin\theta)] \end{aligned} \quad (4-11)$$

where $\underline{\alpha}$ is referred to as the receptance when the modal constant is real.

Thus, it can be thought that the measured data are in such a form that a set of receptance data with no complexity are transformed by a complex quantity with unity modulus and so the measured data could be subjected to equation (4-11). The phase angle θ in equation (4-11) may be deduced by the Nyquist circle curve-fitting and, consequently, the purely real and imaginary parts (before being transformed by the complexity) can be deduced from equation (4-11), being respectively:

$$\begin{aligned} \operatorname{Re}(1/\underline{\alpha}) &= \operatorname{Re}(1/\alpha)\cos\theta - \operatorname{Im}(1/\alpha)\sin\theta \\ \operatorname{Im}(1/\underline{\alpha}) &= \operatorname{Im}(1/\alpha)\cos\theta + \operatorname{Re}(1/\alpha)\sin\theta \end{aligned} \quad (4-12)$$

Thus, data $\operatorname{Im}(1/\underline{\alpha})$ can be used to identify the damping type, as described above.

4-4 LOCATION OF DAMPING ELEMENTS FROM A STRUCTURE

4-4-1 Usual Damping Condition of a Vibrating Structure

From the point of view of modal analysis, the damping properties of a vibrating system defined by equations (4-3) or (4-4) can be specified by the system's modal data (i.e. by the damped natural frequencies, complex modal constants and, above all, the damping loss factors) in equations (4-5) or (4-6) respectively. However, these modal data are not directly related to the spatial distribution of damping in the system. For instance: given a damping matrix, the modal data (especially those damping loss factors which most significantly reflect the damping properties) will change if there is a change in the stiffness matrix. As has been discussed in the last two Chapters, the theoretically-predicted stiffness matrix will generally contain errors, and so the damping properties indicated by the modal data should be treated with considerable care.

Fortunately, unlike the mass and stiffness characteristics which are generally contributed to by all parts of a structure, the most significant damping in structures usually comes from the joints between the various components^{[42],[43]}. In other words, it can be said that damping mainly occurs at or between a restricted number of coordinates in terms of

the analytical model, and so the usual assumption of proportional damping will not satisfactorily cope with such practical cases. Figure 4-3 shows schematically a damping matrix which could be regarded as representing a ‘true’ damping matrix case for a practical structure.

Hence, it is supposed that useful information about the damping distribution in a structure could be revealed by **localizing** the damping elements in a vibration model determined from measurements, such as those obtained from a modal test. If the damping elements can be successfully **localized** by the measured data, then the damping matrix of the corresponding analytical model of the structure will be provided in an acceptable form, similar to that in Figure 4-3, rather than conventionally assuming it to be proportional to the mass and stiffness matrices as in equations (4-1) and (4-2), and any further attempt to quantify the damping level could be directed to those **localized** elements.

4-4-2 The Approach for Damping Element Location

When hysteretic damping exists in a vibrating structure, it is generally accepted that the damping matrix $[H]$ can be combined with the stiffness matrix $[K_x]$ (or $[K_a]$ if it comes from the analytical model and is with errors) to form what is called ‘complex stiffness matrix’, (as was introduced in Chapter 3):

$$[K_c] = [K_x] + i[H] \quad (4-13)$$

For the sake of simplicity, it is first assumed that the mass and stiffness properties of the analytical model of the structure are acceptably accurate when the location of damping elements from the structure is investigated and, hence, the stiffness matrix $[K_x]$ in equation (4-13) can be adequately represented by the analytical stiffness matrix. The more general case, with an **erroneous** analytical model, will be considered later. Since the structure is damped, its measured vibration modes will be complex and the mode shape matrix, denoted by $[\phi_x]$, will be incomplete with less than all the modes included.

Equation (4- 13) can be post-multiplied by the complex mode shape matrix $[\phi_x]$, yielding:

$$[K_c][\phi_x] = [K_x][\phi_x] + i[H][\phi_x] \quad (4- 14)$$

Since the following relationship holds for the experimental model,

$$[K_c][\phi_x] = [M_x][\phi_x][\omega_x^2] \quad (4-15)$$

it can be substituted into equation (4-13) to eliminate the unknown complex stiffness matrix $[K_c]$ and, by rearranging and post-multiplying the resultant equation on both sides by the transpose of the measured complex mode shape matrix $[\phi_x]^T$, yields:

$$i[H][\phi_x][\phi_x]^T = [M_x][\phi_x][\omega_x^2][\phi_x]^T - [K_x][\phi_x][\phi_x]^T \quad (4-16)$$

In common with the approach developed in Chapter 3 to locate the mismodelled regions in the mass and stiffness properties of the analytical model, equation (4- 16) can be used in a similar way to locate the damping of the structure by pinpointing the significant elements in the damping matrix. It should be noted that the incomplete measured mode shape matrix $[\phi_x]$ and the measured natural frequency matrix $[\omega_x^2]$ are both complex while the structure's stiffness, mass and damping matrices are all real. With this in mind, equation (4-16) can be split into two equations, representing its real and imaginary parts respectively. It is the imaginary part of equation (4-16) which enables the location of the damping by pinpointing the significant elements in the damping matrix $[H]$. Moreover, equation (4-16) can be written using as few as just one measured complex mode to cope with the practical situation when the number of measured complex modes could be strictly limited.

As mentioned earlier, a complication of damped structures lies in the argument that the analytical model is erroneous when the damping properties remain to be investigated. It is believed that it would be somewhat easier to investigate the damping properties when the

analytical stiffness matrix is effectively accurate. However, to consider the general case, when the analytical stiffness matrix is not correct, equation (4-13) will become:

$$[\mathbf{K}_c] = [\mathbf{K}_a] + [\Delta\mathbf{K}] + i[\mathbf{H}] \quad (4-17)$$

The derivation from equation (4-13) to equation (4-16) will now yield:

$$[\mathbf{AK}] [\phi_x] [\phi_x]^T + i[\mathbf{H}] [\phi_x] [\phi_x]^T = [\mathbf{M}_x] [\phi_x] [\omega_x^2] [\phi_x]^T - [\mathbf{K}_a] [\phi_x] [\phi_x]^T \quad (4-18)$$

Comparison of equation (4-18) with equation (4-16) indicates that equation (4-18) tends to locate the mismodelled regions in the analytical stiffness matrix and the damping elements simultaneously. Theoretically, when equation (4-18) is split into its real and imaginary parts, the effects of $[\mathbf{AK}]$ and $[\mathbf{H}]$ will show up in both and it is thought that closer inspection of the structure might be helpful in order to identify the non-zero parts in $[\mathbf{AK}]$ and $[\mathbf{H}]$ from the results of equation (4-18). However, it can generally be expected that the effect of $[\mathbf{AK}]$ will dominate the real part of equation (4-18) and that of $[\mathbf{H}]$ the imaginary one. Again, equation (4-18) can be written using as few as only one measured complex mode. The application of equation (4-18) will be presented later in this chapter.

4-5 ESTIMATION OF DAMPING MATRIX

4-S-1 Extension of the EMM to Estimate Damping Matrix

Once the significant elements in the damping matrix $[\mathbf{H}]$ have been **localized**, the attention of the damping property investigation is consequently turned to the possible evaluation of the damping matrix itself using the limited number of measured complex modes available. Although the standard EMM (Chapter 2) is available to estimate the stiffness or mass error matrices $[\mathbf{AK}]$ or $[\mathbf{AM}]$, there is no corresponding technique to estimate the damping matrix and the following paragraphs develop the EMM in order to facilitate the damping matrix estimation.

For generality, the analytical stiffness matrix $[K_a]$ (assumed to be derived from an FE analysis, or similar) is taken to be erroneous, albeit only slightly. The error is denoted in Chapter 2 as $[AK]$, is called ‘the stiffness error matrix’ and is usually small compared with $[K_a]$. It is convenient to define here a complex stiffness error matrix $[\Delta K_c]$ which is the difference between the correct complex stiffness matrix in equation (4-13) (which is, in practice, unavailable) and the (real) analytical stiffness matrix, i.e.:

$$[\Delta K_c] = [K_c] - [K_a] \tag{4-19}$$

$$\begin{aligned} &= ([K_x] + i[H]) - ([K_x] - [\Delta K]) \\ &= [\Delta K] + i[H] \end{aligned} \tag{4-20}$$

The real part of this complex stiffness error matrix $[AK_c]$ is effectively the stiffness error matrix defined by the EMM in Chapter 2 while the imaginary part of $[AK_c]$ represents the damping matrix.

From equation (4-19), the correct complex stiffness matrix $[K_c]$ can be written as:

$$[K_c] = [K_a] + [\Delta K_c]$$

Inverting both sides leads to:

$$\begin{aligned} [K_c]^{-1} &= ([K_a] + [\Delta K_c])^{-1} \\ &= ([I] + [K_a]^{-1}[\Delta K_c])^{-1}[K_a]^{-1} \\ &= \{ [I] - ([K_a]^{-1}[\Delta K_c]) + ([K_a]^{-1}[\Delta K_c])^2 - \dots \} [K_a]^{-1} \\ &= [K_a]^{-1} - ([K_a]^{-1}[\Delta K_c])[K_a]^{-1} + ([K_a]^{-1}[\Delta K_c])^2[K_a]^{-1} - \dots \end{aligned} \tag{4-21}$$

Since matrices $[AK]$ and $[H]$ can be assumed to be small compared with $[K_a]$, similar validation to that used in Chapter 2 shows that matrix product $([K_a]^{-1}[\Delta K_c])^n$ approaches

a zero matrix as n increases, i.e.:

$$([K_a]^{-1}[\Delta K_c])^n \rightarrow [0] \text{ as } n \rightarrow \infty.$$

Then, equation (4-21) becomes:

$$[K_c]^{-1} \approx [K_a]^{-1} - [K_a]^{-1}[\Delta K_c][K_a]^{-1}$$

so $[K_a]^{-1}[\Delta K_c][K_a]^{-1} \approx [K_a]^{-1} - [K_c]^{-1}$

and $[AK_c] \approx [K_a] ([K_a]^{-1} - [K_c]^{-1}) [K_a]$ (4-22)

Since the real **part** of the complex stiffness error matrix $[\Delta K_c]$ is defined as $[AK]$, and the imaginary part as $[H]$, equation (4-22) can be split into its real and imaginary parts to yield both the stiffness error matrix and the damping matrix:

$$\begin{aligned} [AK] &= \text{Real} ([AK_c]) \\ &\approx \text{Real} \{ [K_a] ([K_a]^{-1} - [K_c]^{-1}) [K_a] \} \\ &\approx [K_a] ([K_a]^{-1} - \text{Real}([K_c]^{-1})) [K_a] \end{aligned} \quad (4-23)$$

$$\begin{aligned} [H] &= \text{Imag} ([\Delta K_c]) \\ &\approx \text{Imag} \{ [K_a] ([K_a]^{-1} - [K_c]^{-1}) [K_a] \} \\ &\approx [K_a] \{ \text{Imag} ([K_c]^{-1}) \} [K_a] \end{aligned} \quad (4-24)$$

Equations (4-23) and (4-24) indicate that the stiffness error matrix $[AK]$ and damping matrix $[H]$ can be estimated separately when they coexist. Estimation of the damping matrix can thus be implemented by estimating the imaginary part of $[AK_c]$ only,

In order to use an incomplete set of vibration modes to estimate the stiffness error matrix $[AK]$ and the damping matrix $[H]$, the analytical flexibility matrix $[K_a]^{-1}$ and the experimental complex flexibility matrix $[K_c]^{-1}$ must be approximated by the corresponding real and complex modal data:

$$[K_a]^{-1} = [\phi_a]_{n \times m} [\omega_a^2]^{-1}_{m \times m} [\phi_a]^T_{m \times n} \quad (4-25)$$

$$[K_c]^{-1} = [\phi_x]_{n \times m} [\omega_x^2]^{-1}_{m \times m} [\phi_x]^T_{m \times m} \quad (4-26)$$

Therefore, the stiffness error matrix in equation (4-23) and the damping matrix in equation (4-24) can be obtained using the modal data as:

$$\begin{aligned} [AK] &= \text{Real} ([\Delta K_a]) \\ &\approx [K_a] ([\phi_a][\omega_a^2]^{-1}[\phi_a]^T - \text{Real} \{ [\phi_x][\omega_x^2]^{-1}[\phi_x]^T \}) [K_a] \end{aligned} \quad (4-27)$$

$$\begin{aligned} [H] &= \text{Imag} ([\Delta K_c]) \\ &\approx [K_a] (\text{Imag} \{ [\phi_x][\omega_x^2]^{-1}[\phi_x]^T \}) [K_a] \end{aligned} \quad (4-28)$$

It should be borne in mind that the damping matrix estimated by equation (4-28) will be a full matrix, 'predicting' damping properties throughout the structure. This is due to the limited number of modes available from measurement and is contradictory to the usual damping condition of a vibrating structure as indicated above (i.e. damping concentrated at relatively few points). It also needs to be noted that as the number of measured modes increases, the significant elements in damping matrix $[H]$ will show up more and more clearly in the damping matrix estimated by equation (4-28) and such a trend could be an additional means of **confirming** the damping element location suggested in §4-4.

One interesting feature in estimating the damping matrix is that close modes will play a

significantly important part in the process. Since the damping matrix $[H]$ is small compared with $[K_x]$, it can be regarded as a complex perturbation of $[K_x]$. The complex stiffness matrix $[K_c]$ (i.e. $[K_x] + i[H]$) is then the result of this perturbation. According to perturbation theory, the consequence of a perturbation $i[H]$ on the stiffness matrix $[K_x]$ is that each complex mode shape $\{\phi_c\}_r$ ($r=1,2 \dots n$) after perturbation can be expressed as a combination of the corresponding real mode shape $\{\phi_x\}_r$ before perturbation plus a contribution of all the other (real) mode shapes. Mathematically:

$$\{\phi_c\}_r = \{\phi_x\}_r + \sum_{s=1}^n (\omega_r^2 - \omega_s^2)^{-1} \{ \{\phi_x\}_s^T i[H] \{\phi_x\}_r \} \{\phi_x\}_s$$

If two modes, r and s , are very close to each other, then, since $(\omega_r^2 - \omega_s^2)$ is small, they will both contribute significantly to the change of each mode shape. This means that close modes are likely to have a considerable effect in the perturbation $i[H]$ on $[K_x]$ and may be expected to contain significant information of the perturbation on mode shapes so that they will be especially effective in estimating the damping matrix. Therefore, the damping matrix estimated using equation (4-28) will be more accurate if two measured vibration modes are very close and are employed in the estimation.

4-5-2 Iterative Approach to Improve the Estimation of $[H]$

Since the significant elements in the damping matrix $[H]$ can be localized before the damping matrix itself is estimated by equation (4-28), the elements in $[H]$ estimated by equation (4-28) which are not localized by means of the measured complex vibration modes will be regarded as errors introduced by the insufficiency of the number of measured modes and will be artificially suppressed, as used in the stiffness error matrix case studied in Chapter 3. The same argument will be applied to the stiffness error matrix $[AK]$ estimated by equation (4-27). In addition, matrices $[H]$ and $[AK]$ thus estimated will be expected to be rough estimates since the number of measured complex modes used will

significantly important part in the process. Since the damping matrix $[H]$ is small compared with $[K_x]$, it can be regarded as a complex perturbation of $[K_x]$. The complex stiffness matrix $[K_c]$ (i.e. $[K_x] + i[H]$) is then the result of this perturbation. According to perturbation theory, the consequence of a perturbation $i[H]$ on the stiffness matrix $[K_x]$ is that each complex mode shape $\{\phi_c\}_r$ ($r=1,2 \dots n$) after perturbation can be expressed as a combination of the corresponding real mode shape $\{\phi_x\}_r$ before perturbation **plus** a contribution of all the other (real) mode shapes. Mathematically:

$$\{\phi_c\}_r = \{\phi_x\}_r + \sum_{s=1}^n (\omega_r^2 - \omega_s^2)^{-1} \{ \{\phi_x\}_s^T i[H] \{\phi_x\}_r \} \{\phi_x\}_s$$

If two modes, r and s , are very close to each other, then, since $(\omega_r^2 - \omega_s^2)$ is small, they will both contribute significantly to the change of each mode shape. This means that close modes are likely to have a considerable effect in the perturbation $i[H]$ on $[K_x]$ and may be expected to contain significant information of the perturbation on mode shapes so that they will be especially effective in estimating the damping matrix. Therefore, the damping matrix estimated using equation (4-28) will be more accurate if two measured vibration modes are very close and are employed in the estimation.

4-5-2 Iterative **Approach to Improve the Estimation of $[H]$**

Since the significant elements in the damping matrix $[H]$ can be localized before the damping matrix itself is estimated by equation (4-28), the elements in $[H]$ estimated by equation (4-28) which are not localized by means of the measured complex vibration modes will be regarded as errors introduced by the insufficiency of the number of measured modes and will be artificially suppressed, as used in the stiffness error matrix case studied in Chapter 3. The same argument will be applied to the stiffness error matrix $[AK]$ estimated by equation (4-27). In addition, matrices $[H]$ and $[AK]$ thus estimated will be expected to be rough estimates since the number of measured complex modes used will

often be very limited. However, with the knowledge of the location results, this estimation can be carried out iteratively with the limited number of measured complex modes in order to achieve a reasonably accurate damping matrix. The process can be illustrated as in Figure 4-4 and is subjected to a numerical case study below.

4-6 NUMERICAL ASSESSMENT OF DAMPING PROPERTY INVESTIGATION

A series of numerical studies were carried out in order to validate the technique proposed above for locating the damping in a vibrating structure. Also, by examining the damping matrix obtained using an incomplete set of measured vibration modes, an attempt is made to produce an acceptable damping matrix for the structure based on the accurate damping element location.

The system used for the numerical study was the same as that shown in Figure 2-1 and used in the previous two Chapters, with the exception that it is now supposed to include

one hysteretic damper, with a value of 4.5×10^5 N/m, attached between coordinates 6 and 7, thus forming the system shown in Figure 4-5. The correct damping matrix for the system is shown in Figure 4-6. Three damping cases are investigated:

- (i) when the analytical stiffness matrix is reliable;
- (ii) when the analytical stiffness matrix is erroneous and;
- (iii) when close modes exist for the system.

These three cases are denoted as "Case **D1**, Case **D2** and Case **D3**" respectively. For all the various cases investigated, the mass matrix remains unchanged (and correct).

Case D1 The stiffness matrix of the system is the same as the analytical stiffness matrix in Table 2-1 and is supposed to be correct. Thus, all 8 simulated 'analytical' modes and 'experimental' modes can be obtained by eigensolution. It should be noted that the 'analytical' modes are real and the 'experimental' modes are complex since the system is now damped and the 'analytical' model does not include the damping properties. Table

4-1 presents all eight undamped and damped natural frequencies and damping loss factors.

Equation (4-16) is applied to locate the non-zero elements in the damping matrix $[H]$. To simulate the practical situation of having only a limited number of measured vibration modes, and to assess the feasibility of the approach proposed in this Chapter, only one simulated measured complex mode is used at a time in applying equation (4-16). Figure 4-7 provides graphical presentations of the location results obtained by equation (4-16) using one mode at a time - from mode 1 to mode 4. This figure suggests that the damping element can be located by using as few as one measured complex mode, provided this measured mode is sensitive to the damper.

Case D2 To consider the more general practical situation, it is thought that the analytical stiffness matrix will often be erroneous for a damped structure and hence, the case of coexistence of $[AK]$ and $[H]$ has to be investigated numerically in order to lend fully support to the approach developed in this Chapter. To simulate this case, it is supposed that the analytical and the experimental stiffness matrices are the same as Case 1 investigated in the previous two Chapters (Chapters 2 and 3) while the damping condition is the same as for Case D1 above. The stiffness error matrix $[AK]$ is then the same as that in Figure 2-2. The objectives of this case study are first, to locate both the **mismodelled** region in the analytical stiffness matrix between coordinates 2 and 3 and the damping element between coordinates 6 and 7 and, second, to assess the possibility of determining both $[AK]$ and $[H]$ accurately using the iterative process illustrated in Figure 4-4.

Table 4-2 presents the natural frequencies and damping loss factors for both undamped analytical and damped "experimental" cases. It is interesting to note - by comparing Table 4-1 with Table 4-2 - that the damping loss factors in these two cases are quite different from each other, even though the damping distribution in the system is the same in both cases. This supports the suggestion made in the early part of this Chapter that a given damping matrix may not present a unique set of damping loss factors in the modal data,

because the damping loss factors depend on mass and stiffness properties as well as the damping distribution. However, it can be seen from the results detailed below that correct damping element location will still be achieved.

To locate the mismodelled region in $[K_a]$ and the significant elements in $[H]$, equation (4-18) is used with any one of the measured complex modes. Figure 4-8 shows the results of using equation (4-18) with just one mode at a time. The left-hand column in the figure is the real part of equation (4-18) and the right-hand column the imaginary part. It is clear from this Figure that results from each application consistently pinpoint the correct location of the stiffness errors in the analytical matrix $[K_a]$ (between coordinates 2 and 3) and the damping element between coordinates 6 and 7.

Once the correct location for $[K_a]$ and $[H]$ has been achieved, equations (4-27) and (4-28) can be used to calculate respectively the stiffness error matrix $[AK]$ and the damping matrix $[H]$. It is **also** attempted in this case study to assess the iterative process suggested in Figure 4-4. Accordingly, the first four complex modes were used together in applying equations (4-27) and (4-28) iteratively and for each iteration the results were modified in accordance with the correct location already available. Figures 4-9 to 4-14 show the natural frequency errors, the damping loss factor errors of all 8 modes, the total mode shape errors of the real and imaginary parts of the mode shapes and the errors of each mode shape. All the results indicate the notable success of the iteration process. The final improved analytical stiffness matrix and the constructed damping matrix are considered to be accurate enough, when compared with the correct stiffness and damping matrices.

Case D3 It can be seen from Tables 4-1 and 4-2 that neither Case **D1** nor Case D2 has any close modes (close in the sense of natural frequencies). To investigate the effect of close modes on damping element location, the stiffness matrix of Case **D1** is adjusted so that the undamped and damped natural frequencies and damping loss factors are as shown in Table 4-3. It can be seen that modes 4 and 5 are very close to each other in this new

configuration and hence only these two modes are used in equation (4-28) to calculate a damping matrix. The result shown in Figure 4-15 indicates clearly the dominance of these two modes in estimating the damping element between coordinates 6 and 7 and confirms that close modes can be decisive in investigating the damping properties of a vibration system.

4-7 CONCLUSIONS

The difficulty of investigating the damping properties of a vibrating structure lies mainly in two aspects (in addition to the inevitable practical situation of incompleteness in the measured vibration modes): (1) the damping properties cannot be specified by analytical methods in the same way as can the mass and stiffness characteristics, and (2) the damping properties of a structure have to be investigated in many cases where the analytical model of it is erroneous in the stiffness and/or mass properties as well.

It is expected that the damping properties of most vibrating structures are not distributed in a similar way to the mass and stiffness, and so the conventional proportional damping model is not appropriate to represent the true damping distribution. Rather, damping often comes from the joints between the various components of a structure, or from the structural failures such as internal cracks. Therefore, it is believed to be more appropriate to investigate the damping properties by first locating the major damping elements using the measured complex vibration modes and then, if the number of measured vibration modes is adequate, estimating the damping matrix based on the suggestion of a successful damping element location.

It is believed that modal data from a successful measurement contain the necessary information about the structure's damping properties. However, the information provided by the **experimental** modal data does not reveal explicitly the spatial or global damping distribution of the structure. Moreover, the information can be misinterpreted when the erroneous analytical model of the structure is applied to investigate the damping

properties.

An analytical approach has been developed to locate the damping elements in a vibrating system using a very limited number of measured complex vibration modes. Case studies using the approach have demonstrated that the mismodelled regions in an analytical stiffness matrix can be located by the **real** part of equation (4-18) while the damping distribution is revealed by its imaginary part. Once a successful location has been achieved for both $[\mathbf{K}_a]$ and $[\mathbf{H}]$, improving matrix $[\mathbf{K}]$ and estimating $[\mathbf{H}]$ can then be implemented by using the extended EMM in a iterative process. Encouraging results based on simulated data have been obtained that validate the analytical approach. Furthermore, it has been found that close modes contain much more valuable information about the complexity of the system than do isolated modes, suggesting that they are especially important in methods for constructing the damping distribution. It is suggested that the approach proposed in this Chapter is feasible in investigating the damping properties of vibrating structures.

UNDAMPED NATURAL FREQUENCIES	NATURAL FREQUENCIES	DAMPED DAMPING LOSS FACTORS
21.3729 Hz	21.3729 Hz	.00000
33.8582 Hz	33.8756 Hz	.00776
78.4522 Hz	78.4983 Hz	.00523
89.8641 Hz	89.8756 Hz	.03052
103.4225 Hz	103.4224 Hz	.00028
212.5663 Hz	212.7217 Hz	.01140
292.4734 Hz	296.6479 Hz	.06077
406.7665 Hz	406.5155 Hz	.01643

Table 4-1
Natural frequencies and damping loss factors for Case D1

UNDAMPED NATURAL FREQUENCIES	NATURAL FREQUENCIES	DAMPED DAMPING LOSS FACTORS
21.3729 Hz	21.3834 Hz	.00001
33.8582 Hz	34.4070 Hz	.00771
78.4522 Hz	79.5351 Hz	.00293
89.8641 Hz	93.0651 Hz	.03648
103.4225 Hz	103.4838 Hz	.00005
212.5663 Hz	213.3700 Hz	.00918
292.4734 Hz	303.3162 Hz	.05499
406.7665 Hz	409.3685 Hz	.01804

Table 4-2
Natural frequencies and damping loss factors for Case D2

UNDAMPED NATURAL FREQUENCIES	NATURAL FREQUENCIES	DAMPED DAMPING LOSS FACTORS
5.0029 Hz	5.0045 Hz	.00375
8.8321 Hz	8.8483 Hz	.02667
20.3547 Hz	20.3561 Hz	.00049
24.0661 Hz	24.2047 Hz	.04409
25.5812 Hz	25.4991 Hz	.02115
51.6245 Hz	51.6300 Hz	.00279
79.9811 Hz	78.0000 Hz	.04938
114.8575 Hz	114.8295 Hz	.00966

Table 4-3
Natural frequencies and damping loss factors for Case D3

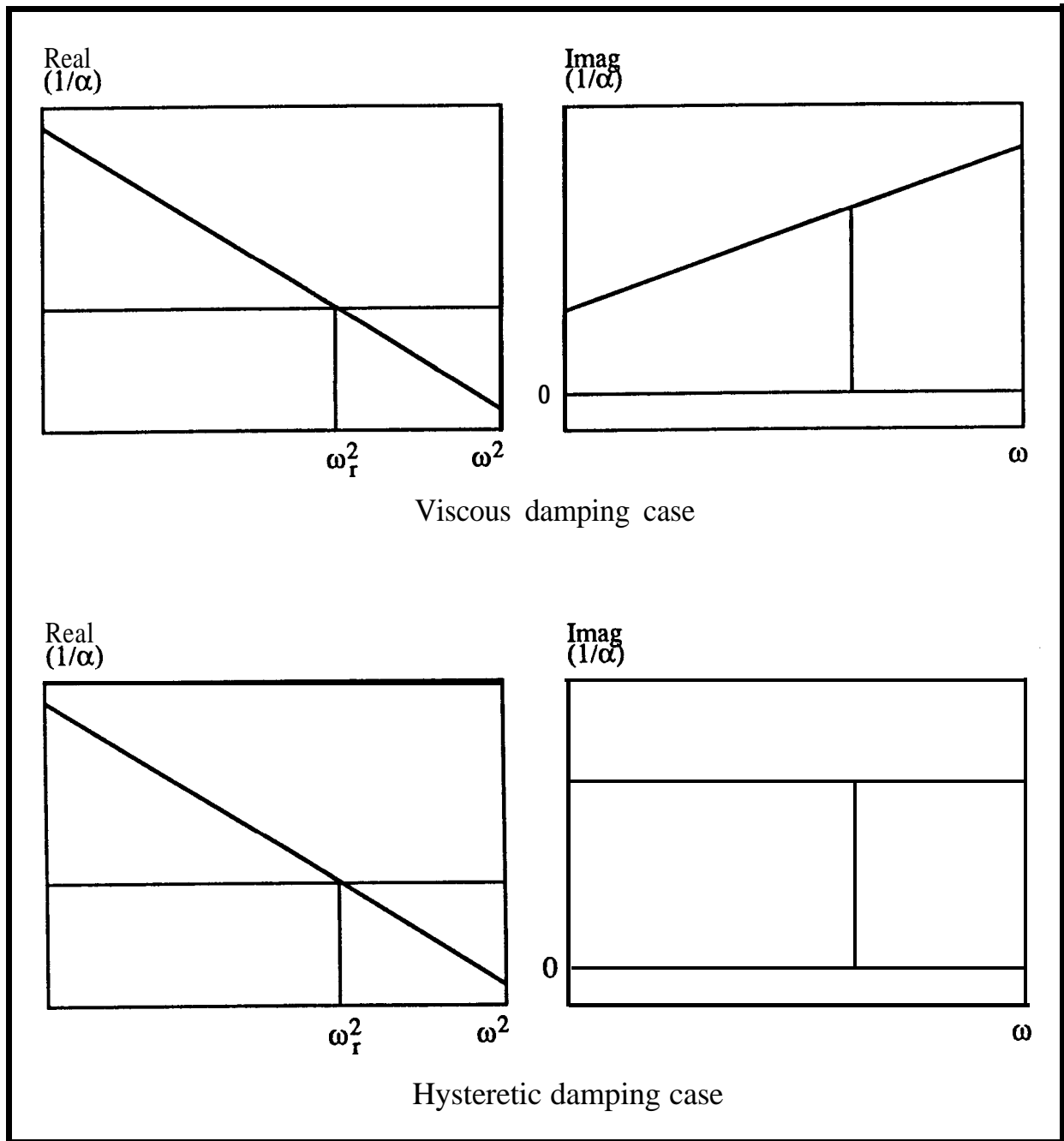


Figure 4- 1 Reciprocal of receptance data of one vibration mode with viscous or hysteretic damping

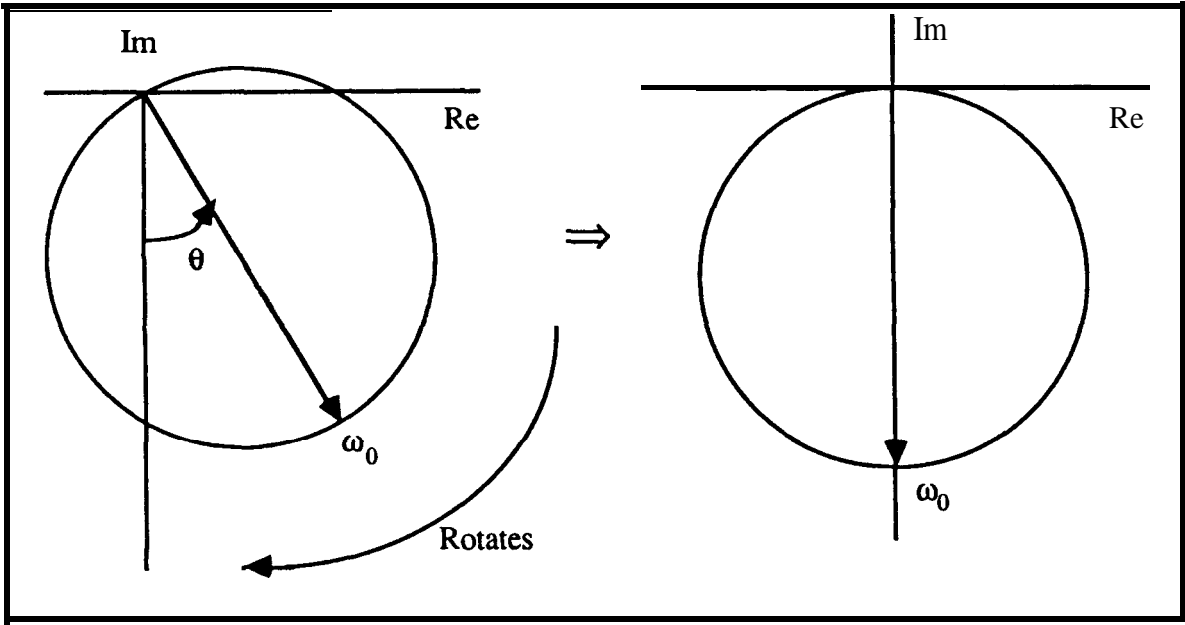


Figure 4-2 Rotate the Nyquist circle to remove the effect of complexity

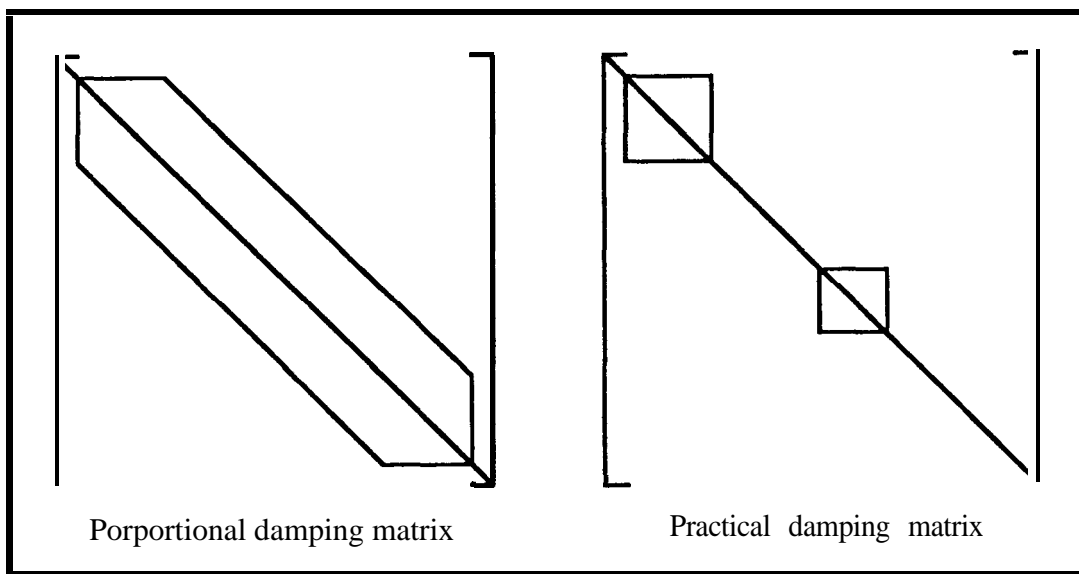


Figure 4-3 A typical practical damping matrix compared with a proportional damping matrix

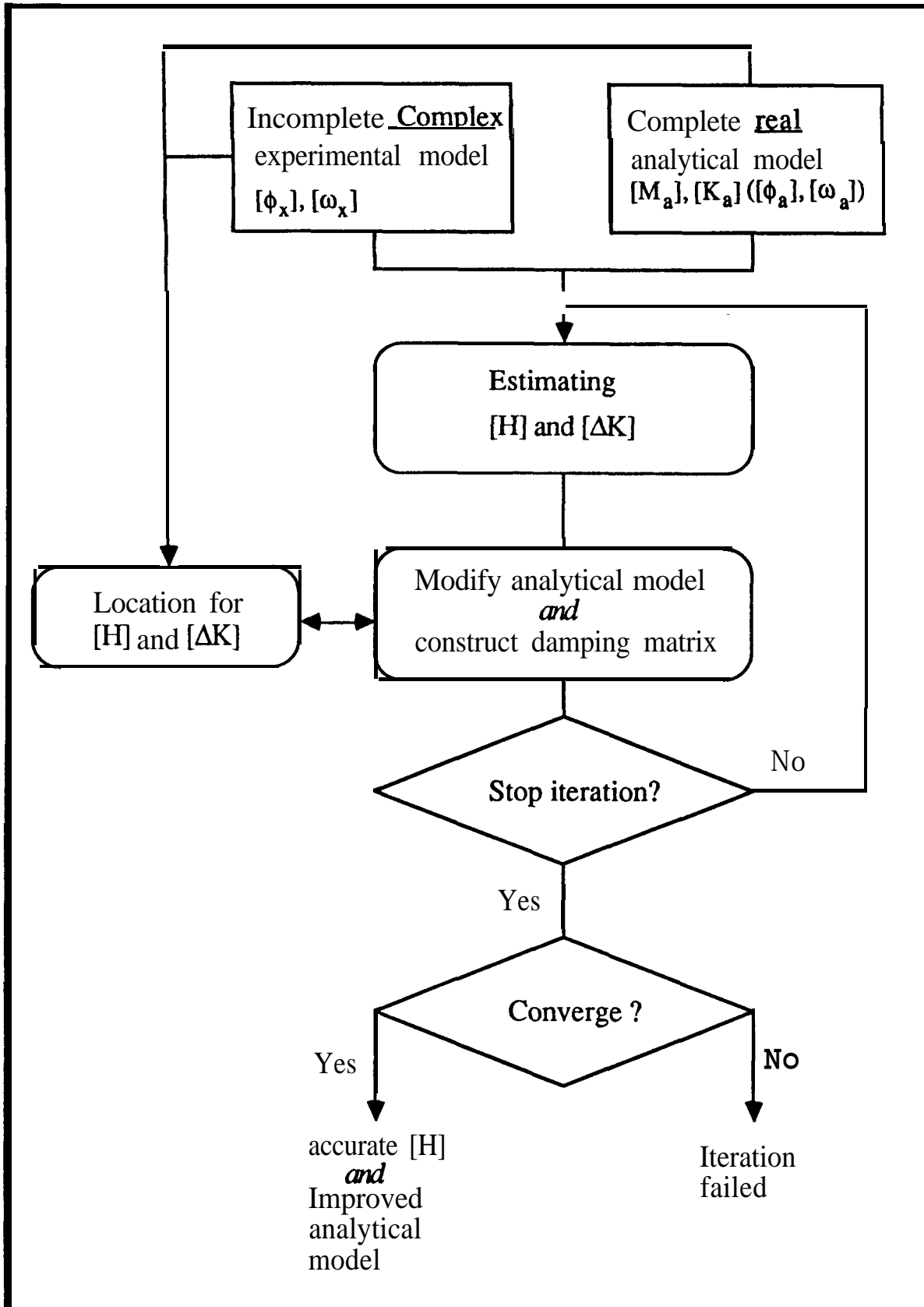


Figure 4-4 Iteration process to estimate [H] and to improve [K_a]

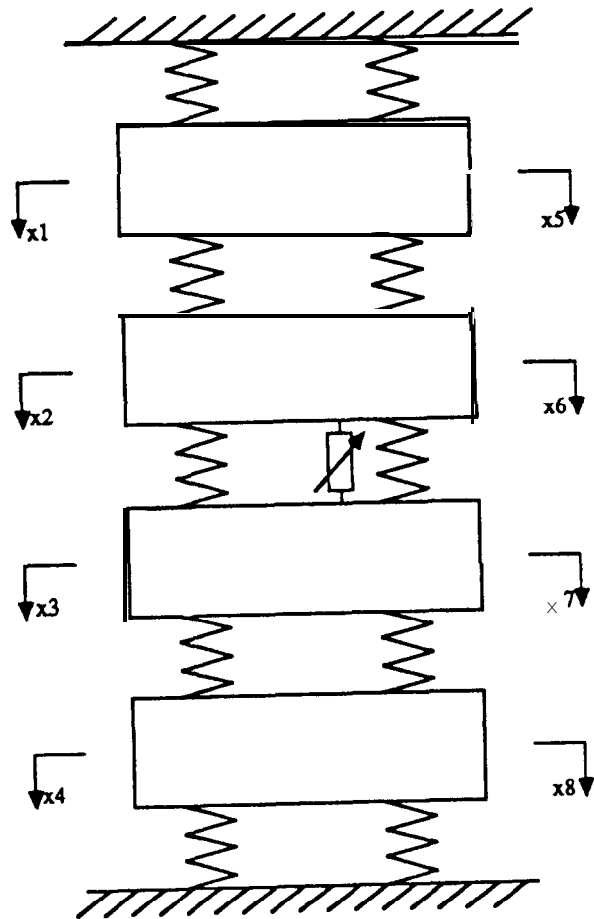


Figure 4-5 An 8DOF system with an incorrect stiffness component and a theoretically unpredicted damper.

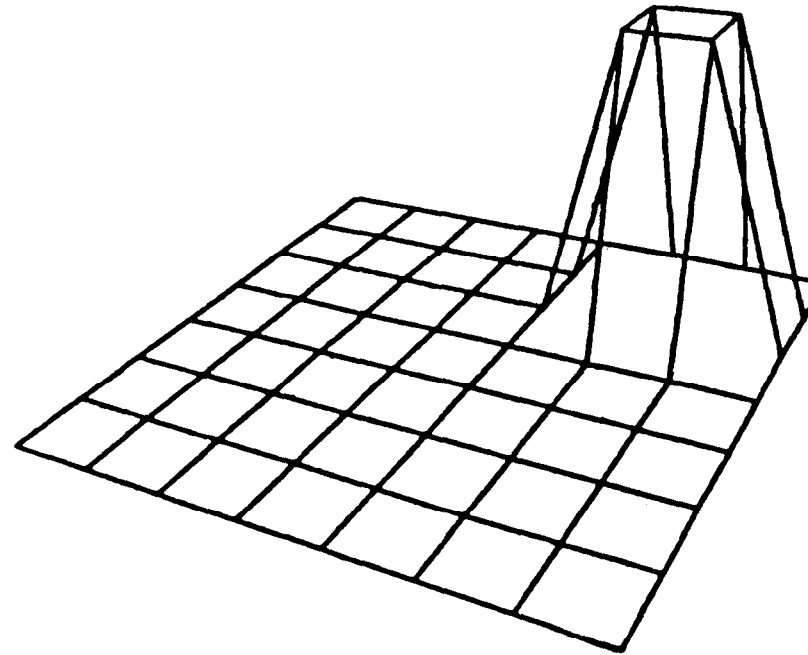
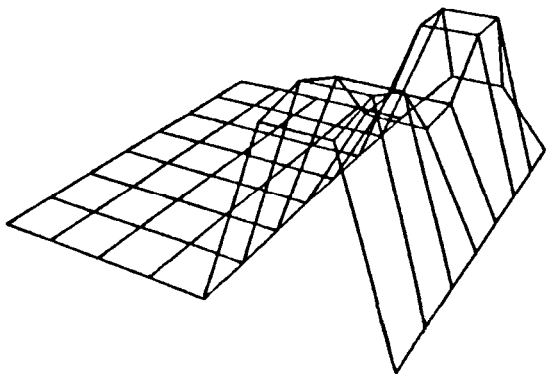
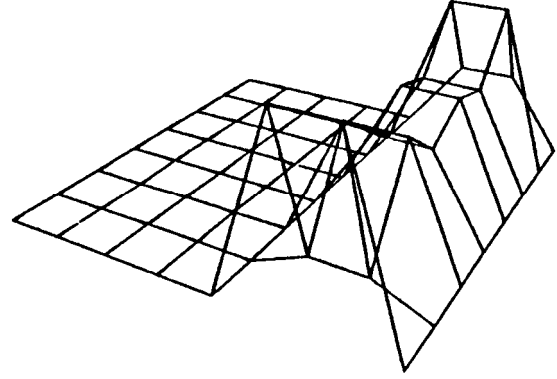


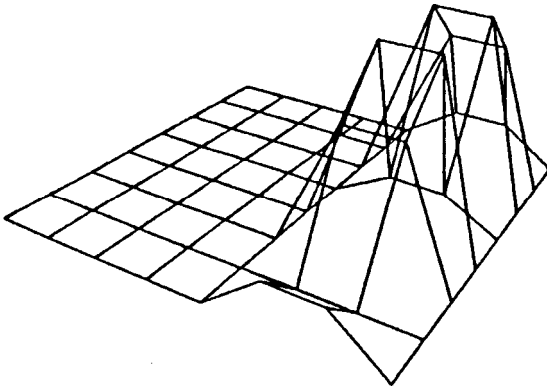
Figure 4-6 Correct damping matrix for the system shown in Figure 4-5.



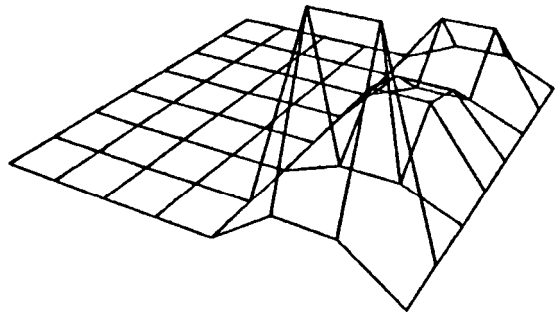
mode 1 only



mode 2 only



mode 3 only



mode 4 only

Figure 4-7 Graphical presentations of the location results for Case **D1** using equation (4-16) with modes from 1 to 4 individually.

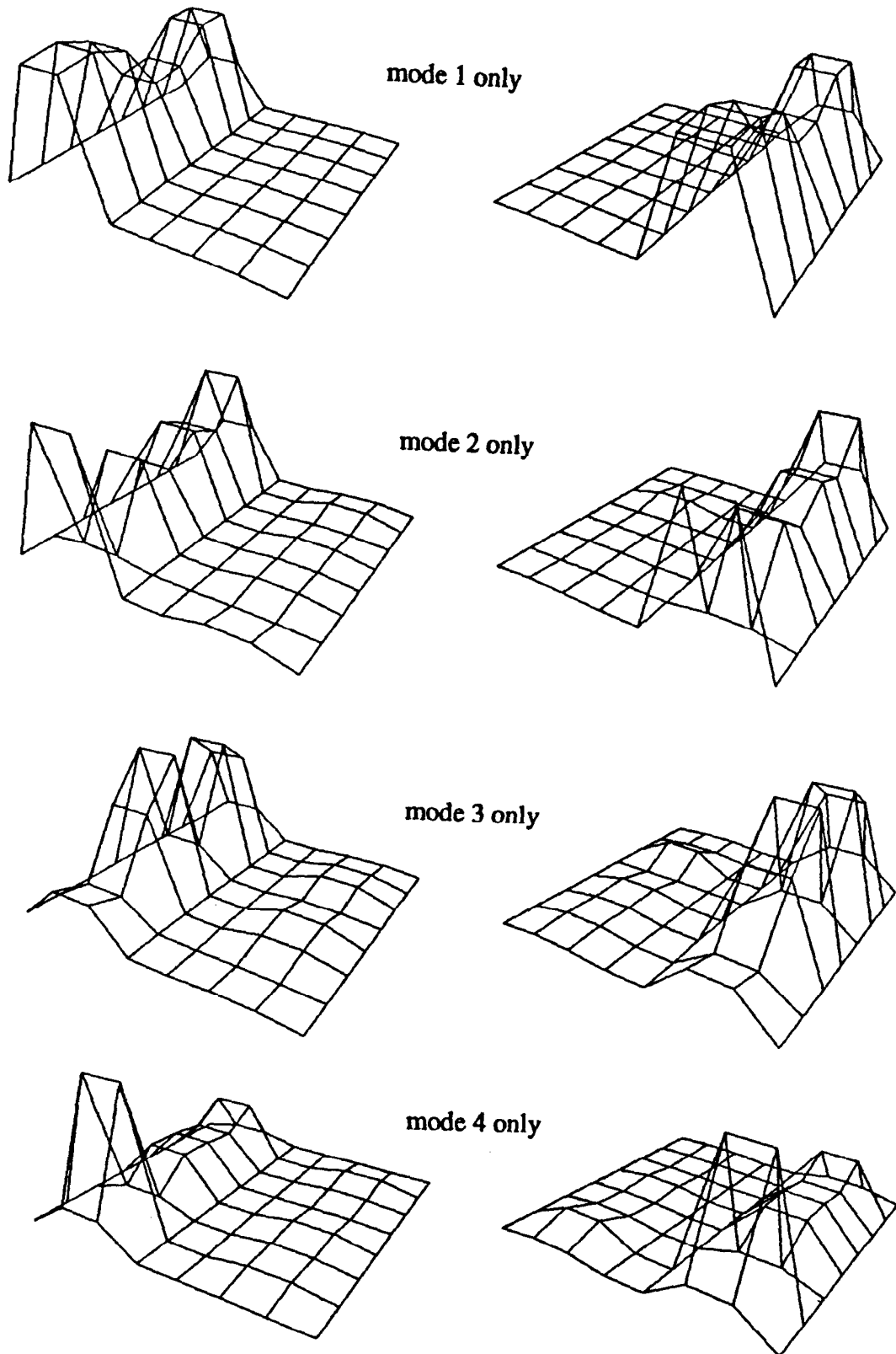


Figure 4-8 Graphical presentations of the location results for Case D2 using equation (4-16) with modes **from** 1 to 4 individually.
Left-hand side column: location of stiffness errors.
Right-hand side column: location of damping elements.

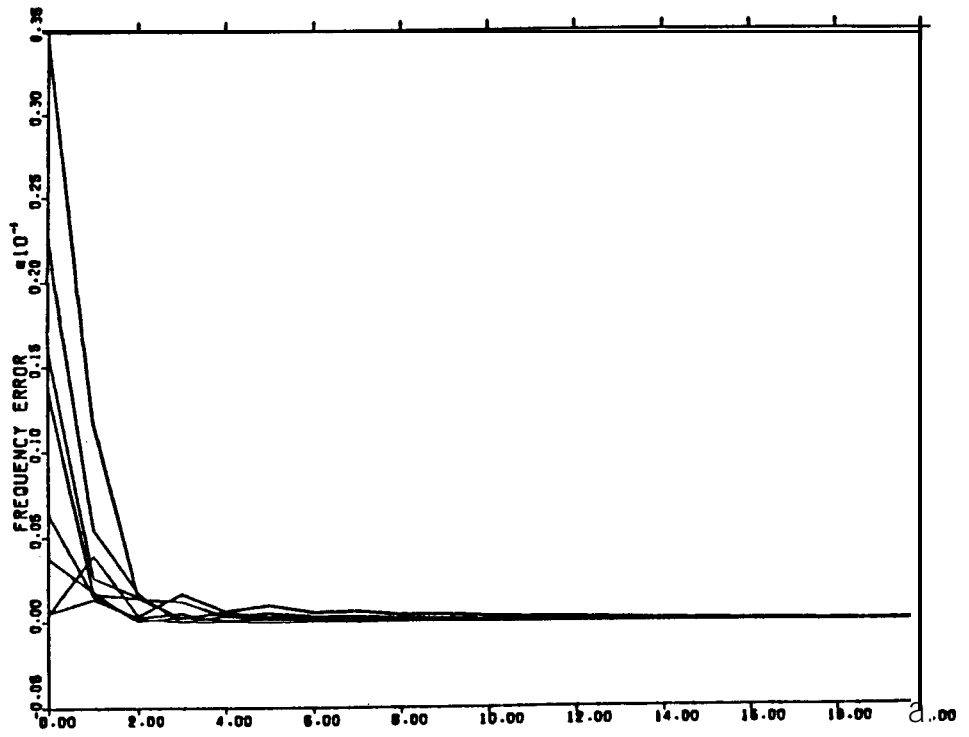


Figure 4-9 Percentage errors of all 8 natural frequencies for Case D2 after each iteration using the EMM and the error location results.

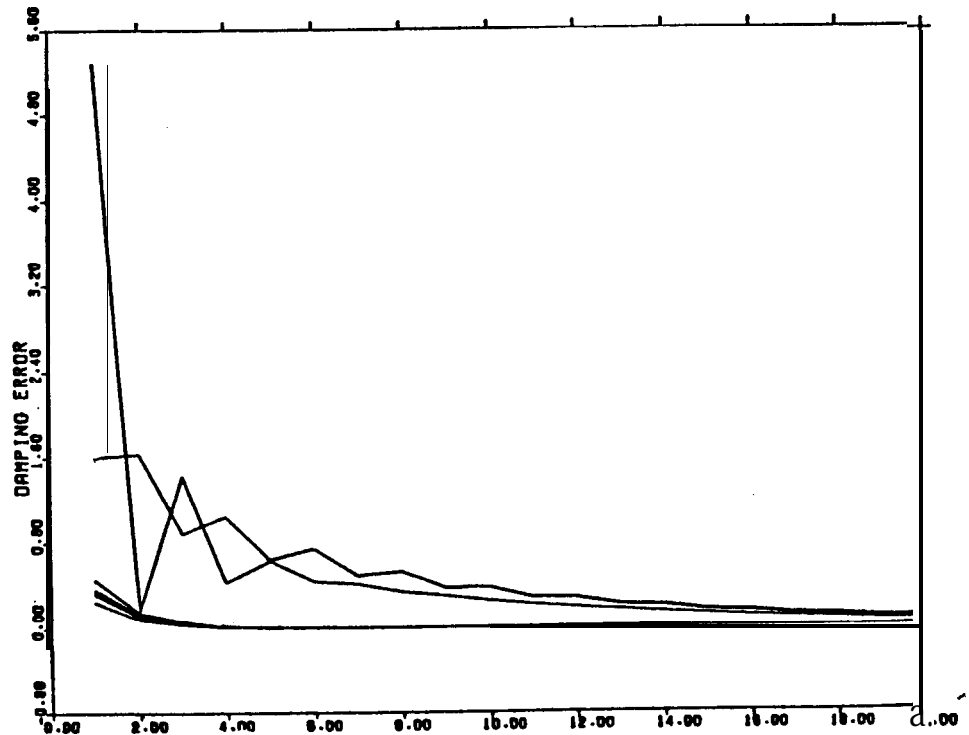


Figure 4-10 Percentage errors of all 8 damping loss factors for Case D2 after each iteration using the EMM and the error location results.

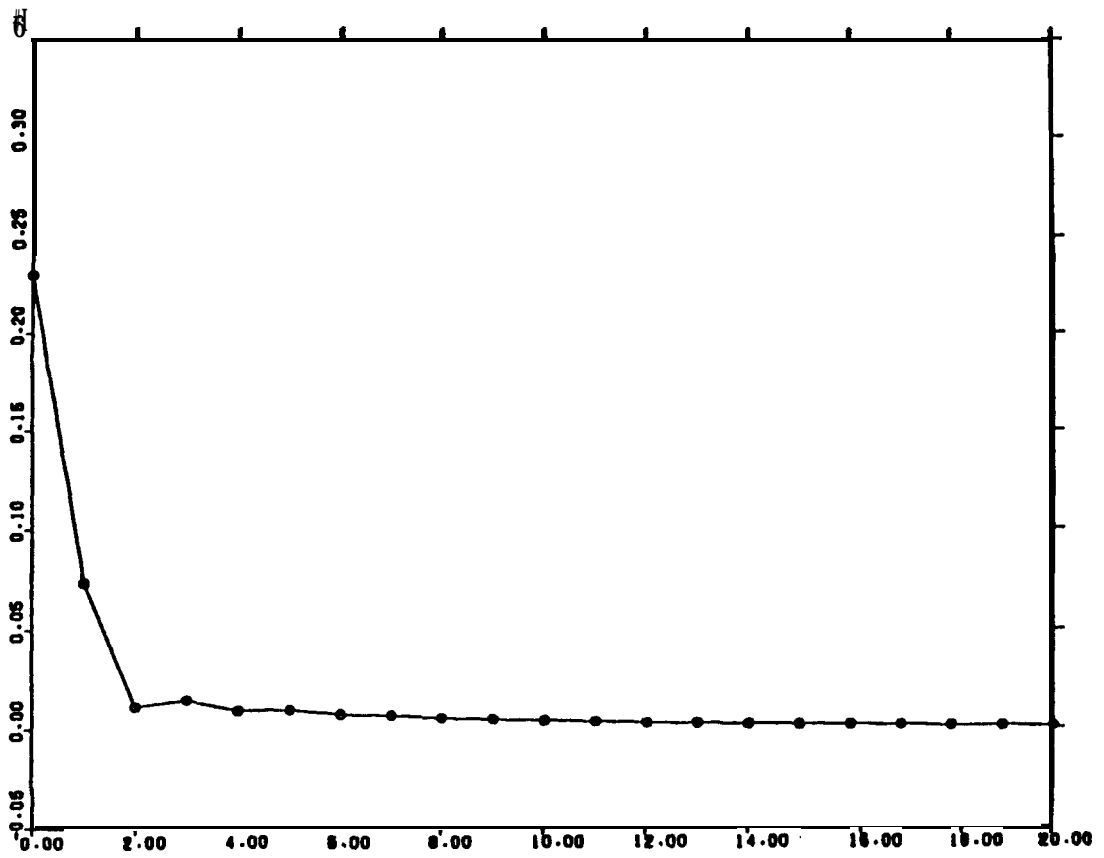


Figure 4-11 Percentage of total mode shape errors (real parts) for Case D2 after each iteration using the EMM and the error location results.

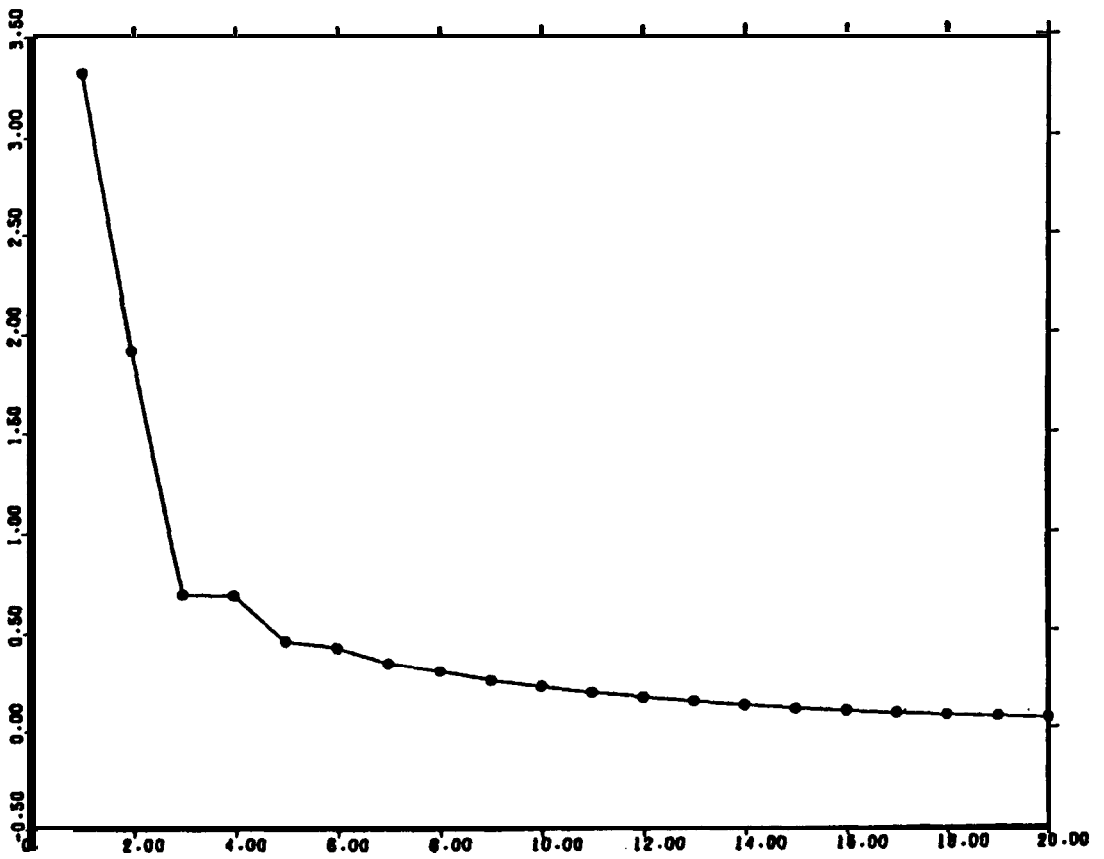


Figure 4-12 Percentage of total mode shape errors (imaginary parts) for Case D2 after each iteration using the EMM and the error location results.

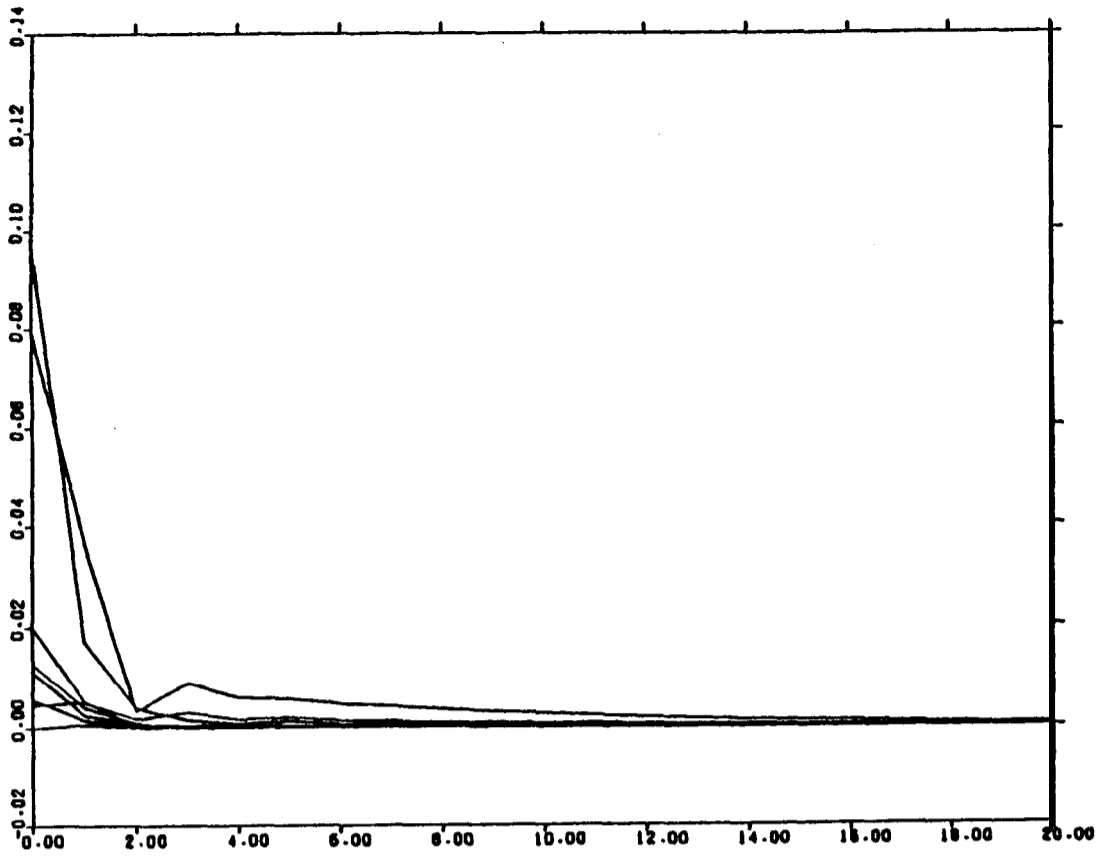


Figure 4-13 Percentage errors of all 8 mode shapes (real parts) for Case Two after each iteration using the EMM and the error location results.

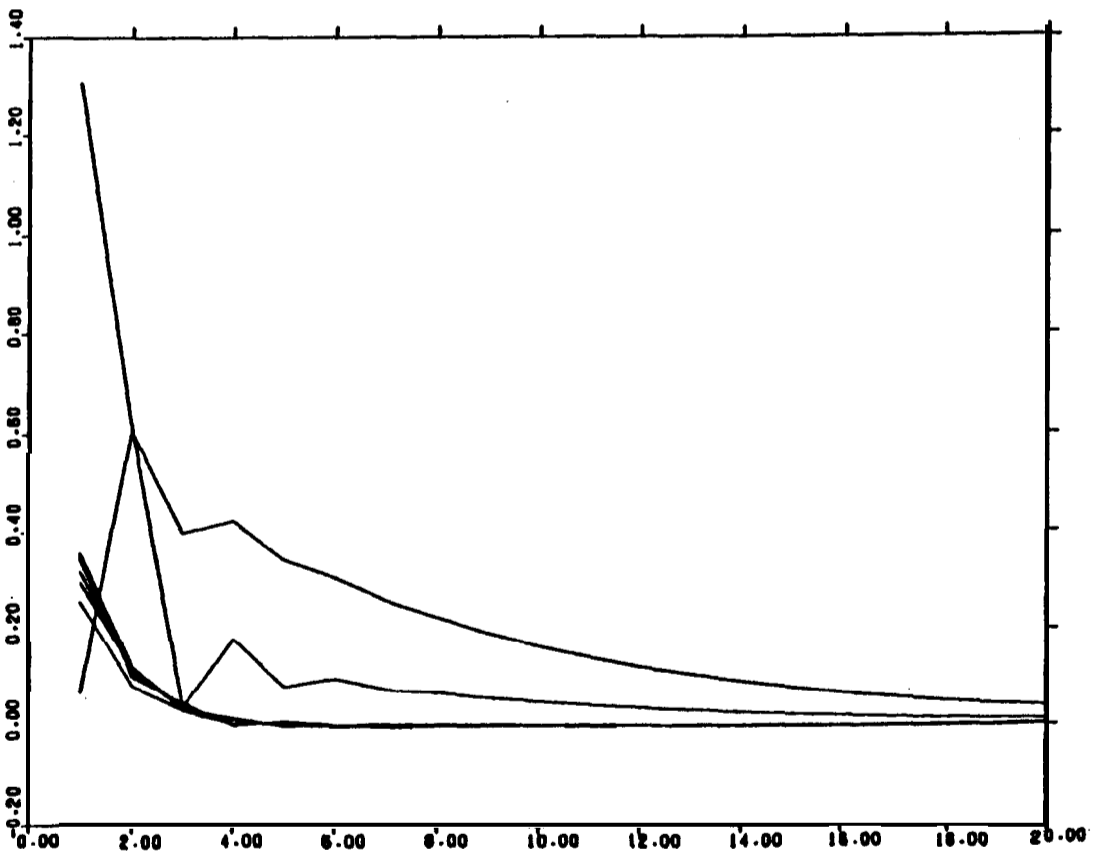


Figure 4- 14 Percentage errors of all 8 mode shapes (imaginary parts) for Case Two after each iteration using the EMM and the en-or location results.

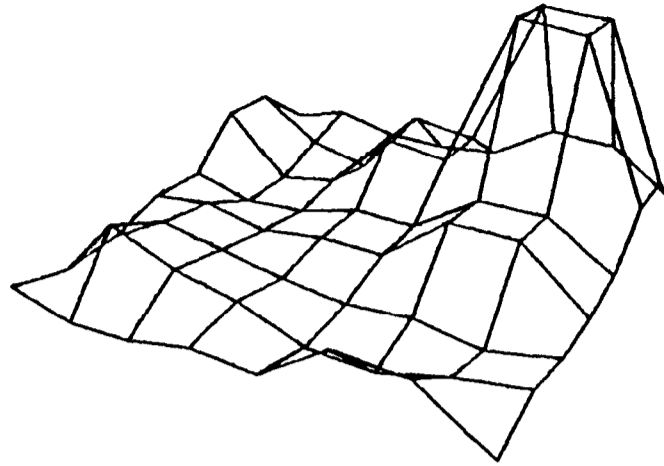


Figure 4-15 Effect of two close complex modes in Case D3 in estimating damping matrix using equation (4-28).

CHAPTER 5

CHAPTER 5

COMPATIBILITY OF MEASURED MODES AND ANALYTICAL MODEL

5-1 PRELIMINARIES

As described earlier, the incompleteness of the set of the measured modes has two aspects. First, the number of modes available from measurement (m) is usually very limited ($m < N$) and second, the number of coordinates identifiable by measurement (n) is less than the number of coordinates specified in the analytical model ($n < N$).

It has been shown in the earlier part of the thesis that, theoretically, the mismodelled regions in an analytical model could be located from just a few measured modes using the new approaches proposed in Chapters 3 and 4 when neither the basic EMM nor the CMM are successful in doing so. However, the location of mismodelled regions can be implemented only when the measured modes are compatible with the analytical mass and stiffness matrices in terms of specified coordinates and, in the majority of cases, this compatibility is not present.

Usually, an analytical model will employ a far greater number of coordinates to describe the vibration characteristics of a structure than is practical for the measured data. The reason for the measured modes to have a limited number of coordinates lies mainly on two counts: (1) vibration measurement is too expensive to permit testing many coordinates and (2) some coordinates may be either technically difficult to test (such as rotation coordinates) or physically inaccessible (such as those coordinates specified by the analytical model which are 'inside' the structure). Experience has shown that modal tests

of typical structures may be limited to some 50 points while the analytical model of a structure could be theoretically as fine as possible and, due to the sophisticated computer facilities nowadays, and examples involving up to thousands of coordinates are not unusual in practice.

The attempt to locate the mismodelled regions in an analytical model and probably proceeding to update it cannot be implemented directly if an incompatibility between the measured vibration modes and the analytical model exists. To overcome this incompatibility, much effort has been devoted. In principle, two strategies are possible: (i) to condense the analytical model so that it is compatible with the measured modes or (ii) to expand the measured modes somehow to the full set of coordinates of the analytical model, possibly by using the analytical model itself.

5-2 MODEL CONDENSATION BY GUYAN REDUCTION

The problem of this incompatibility of the measured modes and the analytical model was first dealt with effectively by Guyan^[21]. In his paper, he suggested that the mass matrix of a real structure can be reduced, as well as the stiffness matrix, by eliminating the coordinates at which no forces are applied. This matrix reduction method was then employed in vibration studies to 'condense' an analytical model to be compatible with measured data. More specifically, the analytical mass and stiffness matrices can each be partitioned into four submatrices respectively, as follows:

$$[M] = \begin{bmatrix} [M_{11}] & [M_{12}] \\ [M_{21}] & [M_{22}] \end{bmatrix} \quad [K] = \begin{bmatrix} [K_{11}] & [K_{12}] \\ [K_{21}] & [K_{22}] \end{bmatrix} \quad (5-1)$$

where, $[M_{11}]$ and $[K_{11}]$ are $n \times n$ submatrices corresponding to those coordinates experimentally tested. To be compatible with the measured modes, the analytical model is also condensed so that the condensed model contains the following two matrices:

$$[K_a]_R = [K_{11}] - [K_{12}][K_{22}]^{-1}[K_{21}] \quad (5-2)$$

and $[M_a]_R = [M_{11}] - [M_{12}][K_{22}]^{-1}[K_{21}] -$

$$([K_{22}]^{-1}[K_{12}])^T([M_{21}] - [M_{22}][K_{22}]^{-1}[K_{21}]) \quad (5-3)$$

The mathematical consequence of this **Guyan** reduction - as it is now widely referred to - is that the eigen-problem is closely but not exactly preserved. An implicit assumption inherent in the derivation of **Guyan** reduction from the viewpoint of structural dynamics was later revealed by **Kidder**^[22] and is introduced as **below** in §5-3.

5-3 EXPANSION OF MEASURED MODES BY THE ANALYTICAL MODEL

The vibration characteristics of an undamped system can be described by its eigen-equations:

$$(-\omega_r^2[M] + [K])\{\phi\}_r = \{0\} \quad (5-4)$$

where ω_r and $\{\phi\}_r$ can be any one of the total N natural frequencies and the corresponding mode shapes.

If the vibration mode $\{\phi\}_r$ is partitioned into those elements relating to coordinates of specific interest and those which are not, then equation (5-4) can be rearranged so that those coordinates specifically of interest will be on the upper part of the mode shape vector $\{\phi\}_r$ and those which are not will be on the lower part. The mass and stiffness matrices will also be rearranged accordingly. Equation (5-4) will then become:

$$\left(-\omega_r^2 \begin{bmatrix} [M_{11}] & [M_{12}] \\ [M_{21}] & [M_{22}] \end{bmatrix} + \begin{bmatrix} [K_{11}] & [K_{12}] \\ [K_{21}] & [K_{22}] \end{bmatrix} \right) \begin{Bmatrix} \{\phi_1\}_r \\ \{\phi_2\}_r \end{Bmatrix} = \{0\} \quad (5-5a,b)$$

and during the elimination of the sub-mode $\{\phi_2\}_r$, it can be pointed out that the approximation nature of **Guyan** reduction implies the pre-requisite that:

$$\omega_r^2([K_{22}][M_{22}])^\infty \rightarrow [0]$$

It can be shown that such a condition will be reasonable only for the low frequency case and hence there may be an acceptable agreement between the low frequency vibration modes of a vibration model and those of the condensed model but this agreement is expected to deteriorate for high frequency modes. Moreover, it is found from equation (5-5) that the sub-mode $\{\varphi_2\}_r$ of a vibration mode $\{\varphi\}_r$ can be expanded by means of the mass and stiffness matrices and the sub-mode $\{\varphi_1\}_r$:

$$\{\varphi_2\}_r = -(-\omega_r^2[M_{22}] + [K_{22}])^{-1}(-\omega_r^2[M_{21}] + [K_{21}])\{\varphi_1\}_r \quad (5-6)$$

Once the sub-mode $\{\varphi_2\}_r$ is obtained by equation (5-6) and is added into sub-mode $\{\varphi_1\}_r$, rearrangement of the coordinates should be performed to recover the original order in mode shapes corresponding to the mass and stiffness matrices.

If a measured vibration mode of a structure is defined at some of the coordinates of its analytical model, then the mode can be expanded to the same coordinate scale compatible with the analytical model using equation (5-6), based upon the analytical mass and stiffness matrices. A measured mode thus expanded is effectively interpolated by the analytical model. If the analytical model contains errors, it can be imagined that those interpolated coordinates in the expanded measured mode will not contain any information of the errors existing in the analytical model. Use of this mode expansion approach has been reported in the literature^[15] and practical cases^[14].

5-4 COMMENTS OF DIFFERENT APPROACHES

5-4-1 Guyan Reduction

The **Guyan** reduction was originally developed not for the location of mismodelled regions from the analytical model of a dynamic structure, but for condensing the analytical model of a structure to an economical size so that the dynamic characteristics of the structure could be described in fewer coordinates by a condensed model which possesses reasonably similar natural frequencies and mode shapes of the structure. In order to use the **Guyan** reduction for the process of locating the mismodelled regions in the analytical model, it will be necessary to condense the analytical model down to those coordinates which were tested experimentally. No doubt, the condensed analytical model will be much smaller in size than the original one. Hence, the computational effort in calculating the analytical vibration modes will be reduced greatly for any approach requiring those analytical modes, such as the EMM, if it is to be used for the error location and the model improvement. However, the approach of locating the mismodelled regions by the application of this model condensation technique could sometimes be severely undermined both in theory and in practice for the following reasons. **Guyan** reduction does not preserve the eigensolution of the model exactly and hence the analytical modes deduced **from** the condensed model will not, in some cases, represent the true analytical properties of the modelled structure. This in itself may not be a serious problem compared with the possible consequence that the mismodelled regions existing in the analytical model could very likely be scattered during the model condensation process so that location of the mismodelled regions in the analytical model may become more difficult.

For instance, if an analytical stiffness matrix $[K_a]$ contains modelling errors, then the mismodelled regions could be scattered into all its four partitioned submatrices in equation (5-1) by the reduction process, depending on the choice of the coordinates experimentally identified.

Figure 5-1 shows an $N \times N$ analytical stiffness matrix $[K_a]$ before **Guyan** reduction with four erroneous elements A,B,B,C on rows r and $r+1$ of the matrix. In order to condense the stiffness matrix using the **Guyan** reduction approach, the matrix should firstly be partitioned by equation (5-1). If the measured and unmeasured coordinates are alternate from the first one to the number N coordinate, and row r in matrix $[K_a]$ corresponds to a measured coordinate while row $r+1$ does not, then matrix $[K_a]$ will be partitioned in such a way that the four submatrices are as shown in Figure 5-2. It can be seen that the erroneous elements A,B,B,C are now scattered into these four submatrices and the condensed stiffness matrix by **Guyan** reduction in equation (5-2) is as shown in Figure 5-3 and does not exhibit the original error location. If it happens that both rows r and $r+1$ correspond to the measured coordinates, then all the four erroneous elements in matrix $[K_a]$ will contribute to submatrix $[K_{11}]$ and the correct location of mismodelled regions is preserved in the condensed stiffness matrix under these conditions. However, it must be recognised that this is not always possible in **real** life.

It is also worth noting from equation (5-3) that the the mismodelled regions in the analytical stiffness matrix will pollute the analytical mass matrix since the mass matrix condensation process makes use of the analytical stiffness matrix. It can be seen from the last example that it would be unrealistic to expect the condensed analytical stiffness matrix $[K_a]_R$ in equation (5-2) still to hold the same location of the **mismodelled** regions as the original $[K_a]$ does. Nevertheless, it is accepted that the **Guyan** reduction is the most effective technique at present, as far as the model condensation is concerned, and it can be very useful in reducing an analytical model, provided the model is relatively accurate.

In consequence, it is suggested that great care should be taken when **Guyan** reduction is to be used to condense an analytical model since the correct location of **mismodelled**

regions depends markedly on the coordinates experimentally identified and could possibly be violated in practical cases when the number of these coordinates is necessarily restricted.

S-4-2 Expansion of Measured Modes

Another strategy for coping with the incompatibility of the measured modes and the analytical model is to expand the measured modes to the same coordinate set as the analytical model, possibly using the analytical model itself. The possibility of scattering the errors in the model is then avoided due to the fact that this process does not change the connectivity in the original analytical model. It needs to be emphasised here that such a mode expansion approach does not change the measured vibration modes at all: what the approach does is to use the analytical model to interpolate those coordinates in the experimental model which are not measured. Then, since the measured modes are expanded by the analytical mass and stiffness matrices, it can be expected that modes thus obtained are not exactly the same as those modes actually measured at all the coordinates. In common with employing the **Guyan** reduction technique to condense the analytical model to the coordinates tested, in the attempt to locate the the mismodelled regions in the model which are to be pinpointed using those coordinates, location using the expanded measured modes could only define the the mismodelled regions by those coordinates tested and other coordinates in the expanded measured modes which were not tested cannot be expected to be able to possess any error location information. This is further explained below.

Suppose that coordinates i and $i+1$ of a structure in Figure 5-4 are two among all of the measured coordinates, while in the analytical model, ten coordinates are specified between (and including) i and $i+1$ and, further, among these ten coordinates, modelling errors exist between coordinates j and $j+1$ and there is no other modelling errors situated in other part of the structure.

If the model condensation procedure described above is used in order to apply methods such as the EMM and the CMM, then the dynamic characteristics of the structure defined by all the ten coordinates will be concentrated into coordinates i and $i+1$ and, further, coordinates i and $i+1$ will also contain the dynamic characteristics information from all other coordinates of the structure due to the condensation process specified by equations (5-1), (5-2) and (5-3). It is hoped that an error location result will pinpoint the **mismodelled** regions between coordinates i and $i+1$, provided the modelling errors situated between these two coordinates (or more precisely, between coordinates j and $j+1$) are not scattered into other part of the analytical model. Clearly, there is no point whatsoever to expect any approach to locate the mismodelled regions between coordinates j and $j+1$, because these two coordinates are not actually measured and the measured mode shapes do not include them

If the measured modes are expanded using the analytical model, then the location technique proposed in the early part of this thesis could be used to locate the mismodelled regions and again, the mismodelled regions could only be defined between coordinates i and $i+1$. However, in this case, there is no risk of the errors being scattered in the analytical model and misleading the error location process.

5-5 EXPANSION OF MEASURED COMPLEX MODES

In the previous studies, only the undamped case has been considered. The vibration modes from measurement have been supposed to be effectively real so that they can be expanded using the analytical model. As already mentioned, such applications have been found in the literature, although not for the purpose of error location. However, some vibrating structures are significantly damped and the vibration modes experimentally identified will be complex. In order to use such measured modes to locate the mismodelled regions in the analytical model and to locate the damping components from the vibrating structure, the measured complex modes have to be expanded in some way to the full coordinate set. Although there is no appropriate analytical damping matrix in

existence, it is suggested that the measured complex modes could still be expanded in a similar way as for the case of measured real modes, if some technical difficulties could be solved.

A complex mode from measurement includes the natural frequency ω_x , the damping loss factor η_x and the complex mode shape $\{\varphi_x\}$. If the expanded complex mode shape is denoted as $\{\varphi_x\}$ and which is:

$$\{\varphi_x\} = \{ \{\varphi_{x1}\}^T | \{\varphi_{x2}\}^T \}^T \quad (5-7)$$

where the first sub-mode $\{\varphi_{x1}\}$ is the complex mode shape as identified experimentally and the second sub-mode $\{\varphi_{x2}\}$ is the yet to be determined part of the complex mode shape corresponding to the coordinates defined in the analytical model. Then, the usual eigen-equations in equation (5-5) can be similarly partitioned into two parts, representing respectively the coordinates in the complex mode shape $\{\varphi_{x1}\}$ experimentally identified and those remaining to be specified from the analytical model, ($\{\varphi_{x2}\}$):

$$\left(-(\omega_x^2(1+\eta i)) \begin{bmatrix} [M_{11}] & [M_{12}] \\ [M_{21}] & [M_{22}] \end{bmatrix} + \begin{bmatrix} [K_{11}] & [K_{12}] \\ [K_{21}] & [K_{22}] \end{bmatrix} \right) \begin{Bmatrix} \{\varphi_{x1}\} \\ \{\varphi_{x2}\} \end{Bmatrix} = \{0\} \quad (5-8a,b)$$

The sub-mode $\{\varphi_{x2}\}$ of $\{\varphi_x\}$ can then be expanded by means of the analytical mass and stiffness matrices:

$$\{\varphi_{x2}\} = - \{ -\omega_x^2(1+\eta i)[M_{22}] + [K_{22}] \}^{-1} \{ -\omega_x^2(1+\eta i)[M_{21}] + [K_{21}]\{\varphi_{x1}\} \} \quad (5-9)$$

This mode expansion approach involves mathematically inverting a complex matrix and this technical problem is discussed in Appendix 2. Thus, the measured complex modes can then be expanded to the full coordinate set to be compatible with the analytical model, based upon the analytical mass and stiffness matrices. Again, sorting the coordinates in the expanded complex mode in equation (5-7) to the same order as the original analytical

model will have to be done.

5-6 ASSESSMENT OF **APPROACHES** FOR COMPATIBILITY

The different approaches discussed and developed above to solve the problem of incompatibility between the measured modes and the analytical vibration model of a structure need to be fully assessed. It is thought that it would be appropriate to carry out some specific numerical studies to assess these approaches. The system used in the assessment is the 21 degree-of-freedom system in Figure 5-5. The analytical stiffness and mass matrices can be constructed as the stiffness components and the masses are given and hence all the simulated real analytical vibration modes are known.

It is supposed that the analytical model of the system has two ‘defects’, one being that the stiffness component between coordinates 5 and 6 is underestimated by 20% and the other being that there is a hysteretic damper in between coordinates 13 and 14. By considering these two defects, the “experimental” model of the system can be constructed and thus, the complex experimental vibration properties can be computed and are used to facilitate this study. Table 5- 1 shows natural frequencies and damping loss factors of all 21 modes for both models. The correct stiffness error matrix and the damping matrix of the system is shown in Figure 5-6 and Figure 5-7 respectively.

If a modal test is conducted on the system using all the 21 coordinates, so that the experimental vibration modes are defined in terms of the full coordinate set, then the measured modes are completely compatible with the analytical model and there is no requirement either to condense the model or to expand the modes. The measured complex modes can then be used to locate the stiffness mismodelled region in matrix $[K_a]$ and the damping elements in matrix $[H]$. Figure 5-8 shows the location results of the approach proposed in Chapter 4 using each of modes 1, 2 or 3 respectively and it can be seen from this figure that both the stiffness errors between coordinates 5 and 6 and the damper

between coordinates 13 and 14 are well **localized**.

In order to simulate the practical case where the experimental vibration modes are defined at less coordinates than in the analytical model, the coordinates with odd numbers in the complex experimental mode shape matrix are selected, representing the mode shapes which are experimentally identified. Then, these modes are expanded by equation (S-9) using the analytical stiffness and mass matrices. The thus-expanded modes are then used to locate the stiffness mismodelled region in matrix $[K_a]$ and the damping elements in matrix $[H]$.

Figure 5-9 shows the location results using the expanded modes 1, 2, 3, 5, 7 and 9 individually. Since the even-numbered coordinates in the expanded modes are expanded by the analytical model, the stiffness errors and the damping will not be expected to show up on these coordinates. Therefore, the mismodelled region in matrix $[K_a]$ will now be defined between coordinates 5 and 7, both being experimentally-identified coordinates. Indeed, the results using every expanded mode in Figure 5-9 indicate consistently the stiffness errors between coordinates 5 and 7, with coordinate 6 showing no stiffness modelling errors. The same argument for location of the damper between coordinates 13 and 14 is validated by Figure 5-9. The results using all the expanded modes in it consistently locate the damping distribution between coordinates 13 and 15.

5-7 CONCLUSIONS

In practice, a degree of incompatibility always exists between the analytical model of a vibrating structure and the vibration modes which are identified experimentally. If this incompatibility problem is not resolved, then no further use can be made of the measured vibration modes to improve the analytical model.

Basically, there are two approaches to bridge this incompatibility: one seeks to condense

the analytical model to those coordinates which are or can be identified experimentally and the other attempts to expand the measured vibration modes using the existing analytical model to the full set of coordinates.

No doubt, model condensation is a very economical means of studying the vibration characteristics of a practical structure, considering the possible large numbers of coordinates involved. As far as the location of the modelling errors and damping components is concerned, however, it is believed that model condensation approach can be quite vulnerable since the modelling errors in the analytical model will probably be scattered during the condensation process and which will mislead the location effort.

In order to preserve the correct location of modelling errors in the analytical model, and the correct damping distribution, it is suggested in this Chapter that the measured vibration modes be expanded on the basis of the analytical model so that the expanded modes can be used to locate the modelling errors and the damping distribution. A complex mode expansion technique is also proposed.

Numerical assessment is carried out to validate the feasibility of the mode expansion technique and results of using the expanded modes to locate the stiffness modelling errors and the damping distribution simultaneously. It is suggested by the notable results that such a mode expansion technique can be used in practical modal studies.

21 DOF System		Analytical model	Experimental model	
Mode No.	Undamped frequency (Hz)	frequency (Hz)	Damped frequency (Hz)	damping loss factor
1	10.247	10.433		.040673
2	26.615	26.974		.079168
3	48.950	48.995		.000944
4	65.561	66.574		.095412
5	77.270	78.512		.038553
6	94.436	94.401		.005943
7	129.425	129.805		.001260
8	154.283	156.197		.006836
9	165.128	166.831		.003896
10	184.810	184.808		.001321
11	205.195	205.197		.000040
12	221.929	221.932		.000685
13	249.918	249.873		.016287
14	269.443	279.794		.000172
15	283.824	288.980		.000297
16	290.790	290.928		.000263
17	292.867	307.798		.000001
18	330.097	330.097		.000000
19	371.159	388.123		.000000
20	47 1.907	47 1.907		.000047
21	491.147	491.147		.000153

Table 5- 1

Natural frequencies and damping loss factors of the 21 DOF system

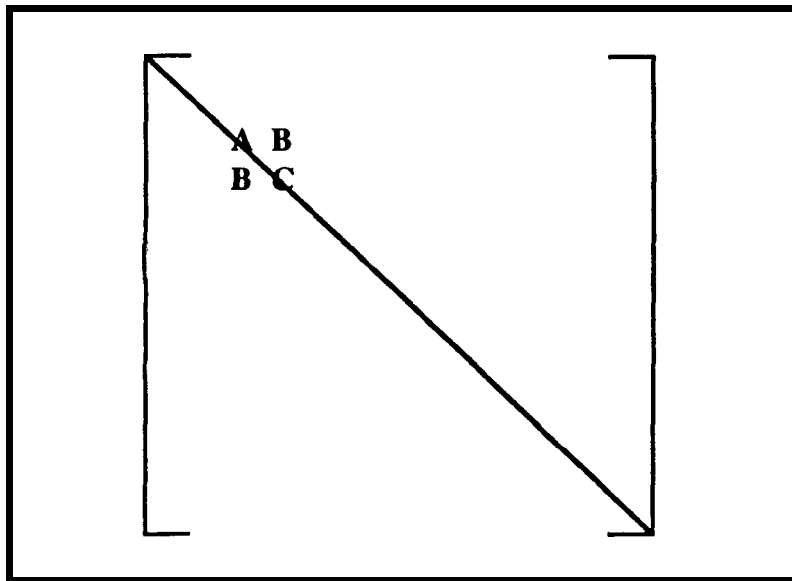


Figure 5-1 An analytical **stiffness** matrix with four erroneous elements

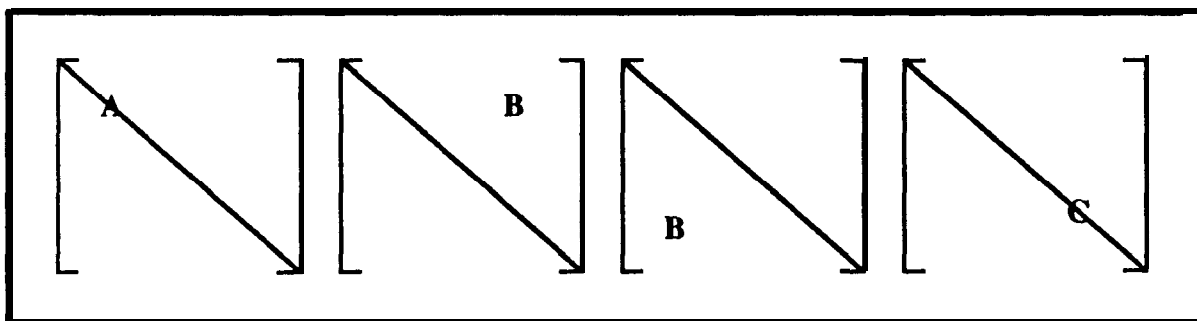


Figure 5-2 Erroneous elements scattered into four submatrices

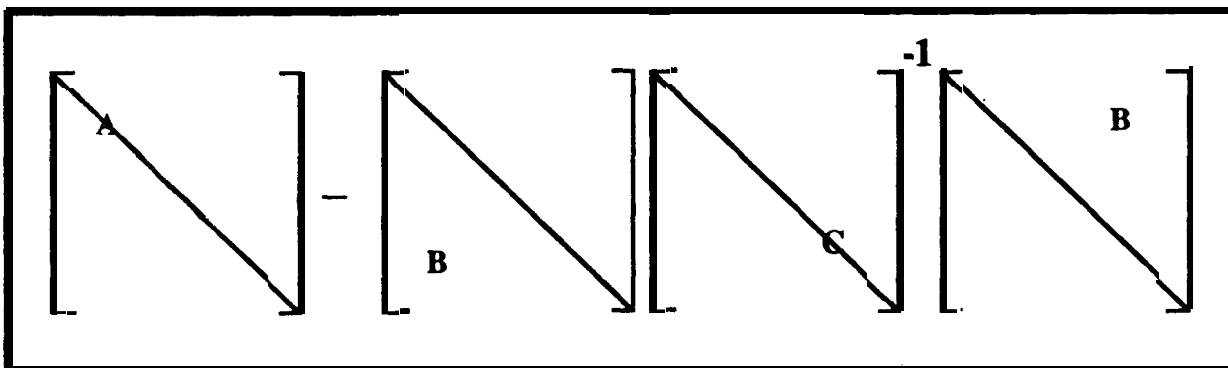


Figure 5-3 **Guyan** reduction process

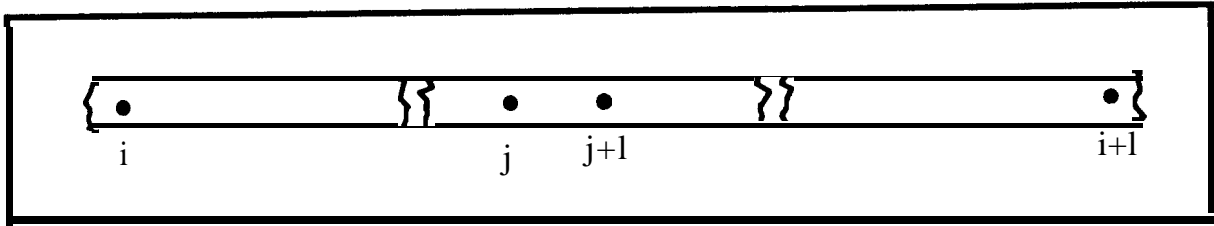


Figure 5-4 A structure with coordinates "i" and "i+1" being tested

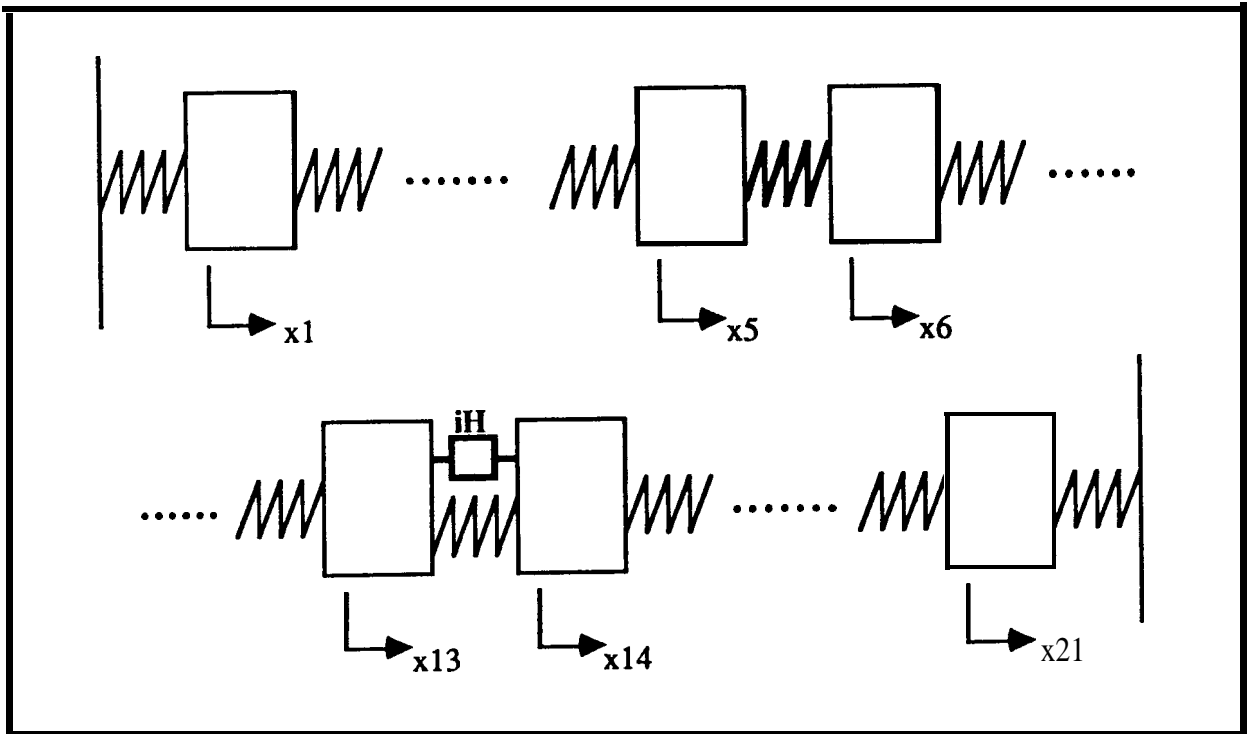


Figure 5-5 A 21 DOF system with an incorrectly predicted **stiffness component** and an unpredicted hysteretic damper

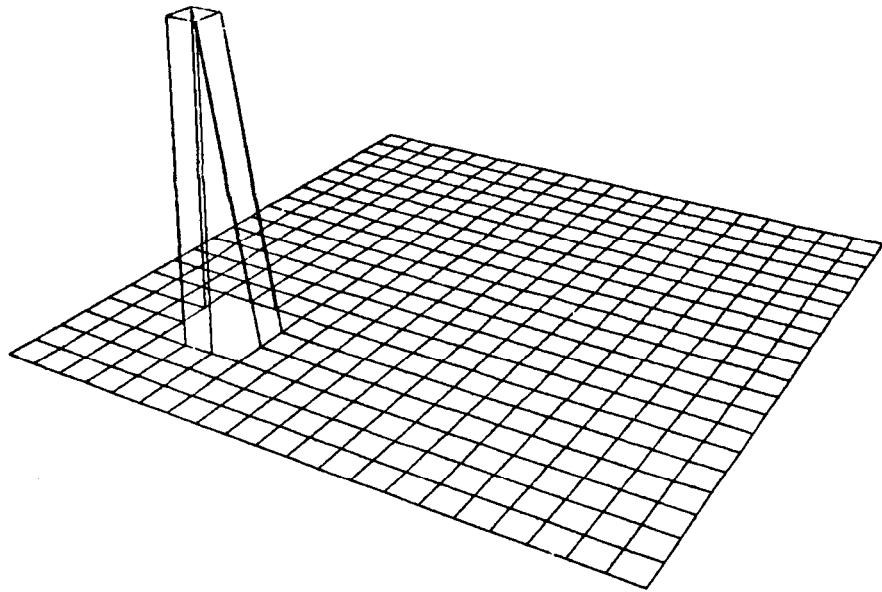


Figure 5-6 Correct stiffness error matrix $[AK]$ for the system shown in Figure 5-5.

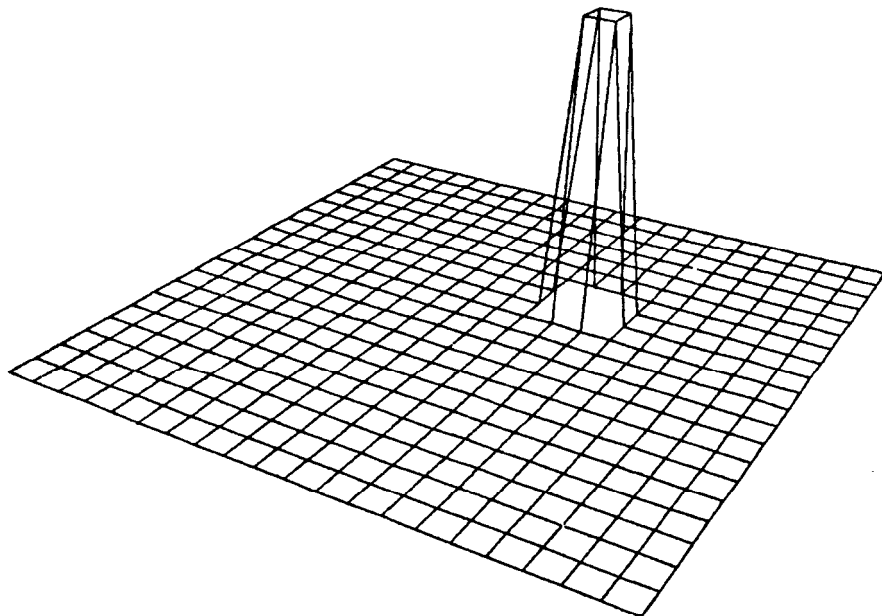


Figure 5-7 Correct damping matrix $[H]$ for the system shown in Figure 5-5.

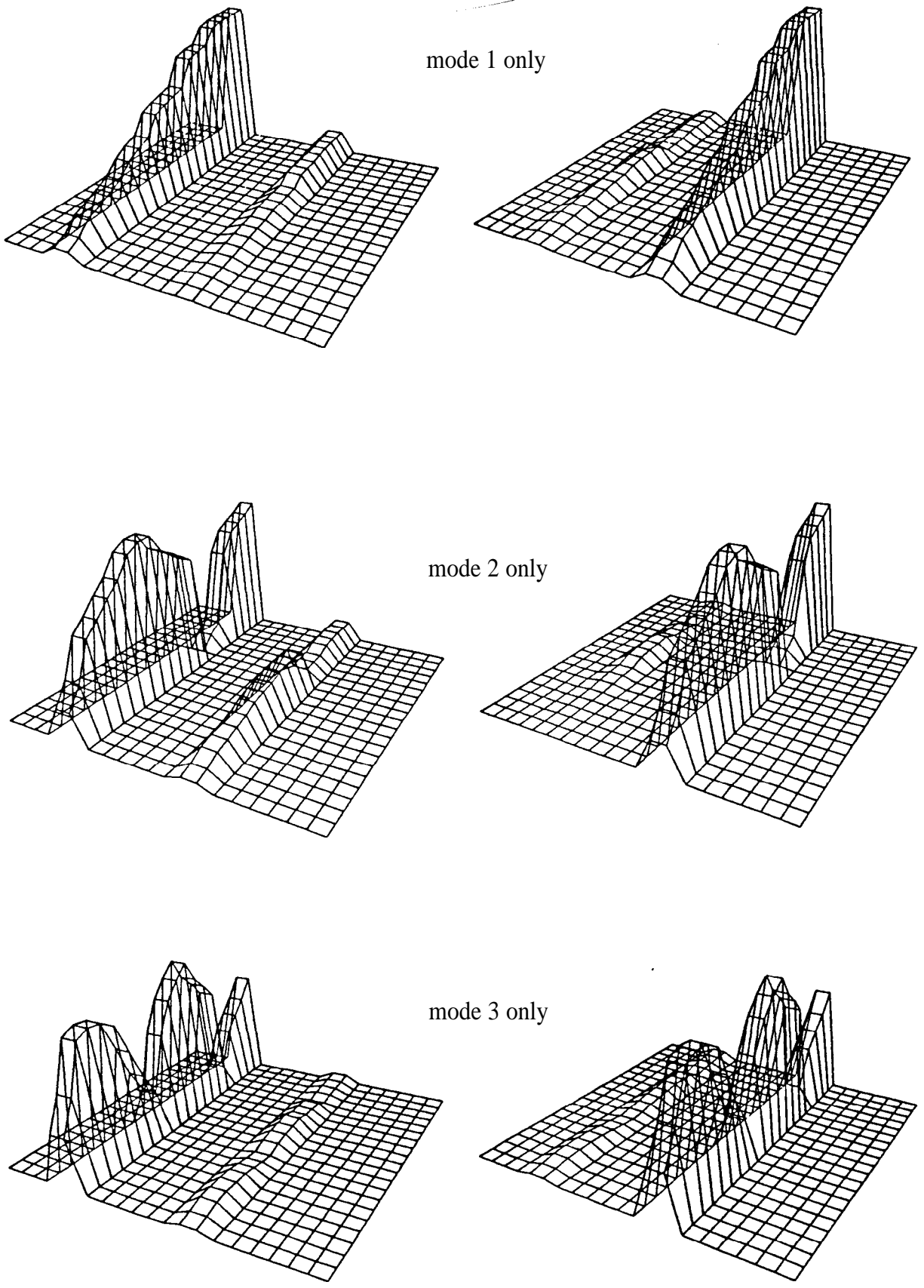


Figure 5-8 **Location** of stiffness errors and damping elements in the system shown in Figure 5-5 using experimental modes 1, 2 and 3 respectively.

Left-hand side column: location of stiffness errors.

Right-hand side column: location of damping elements.

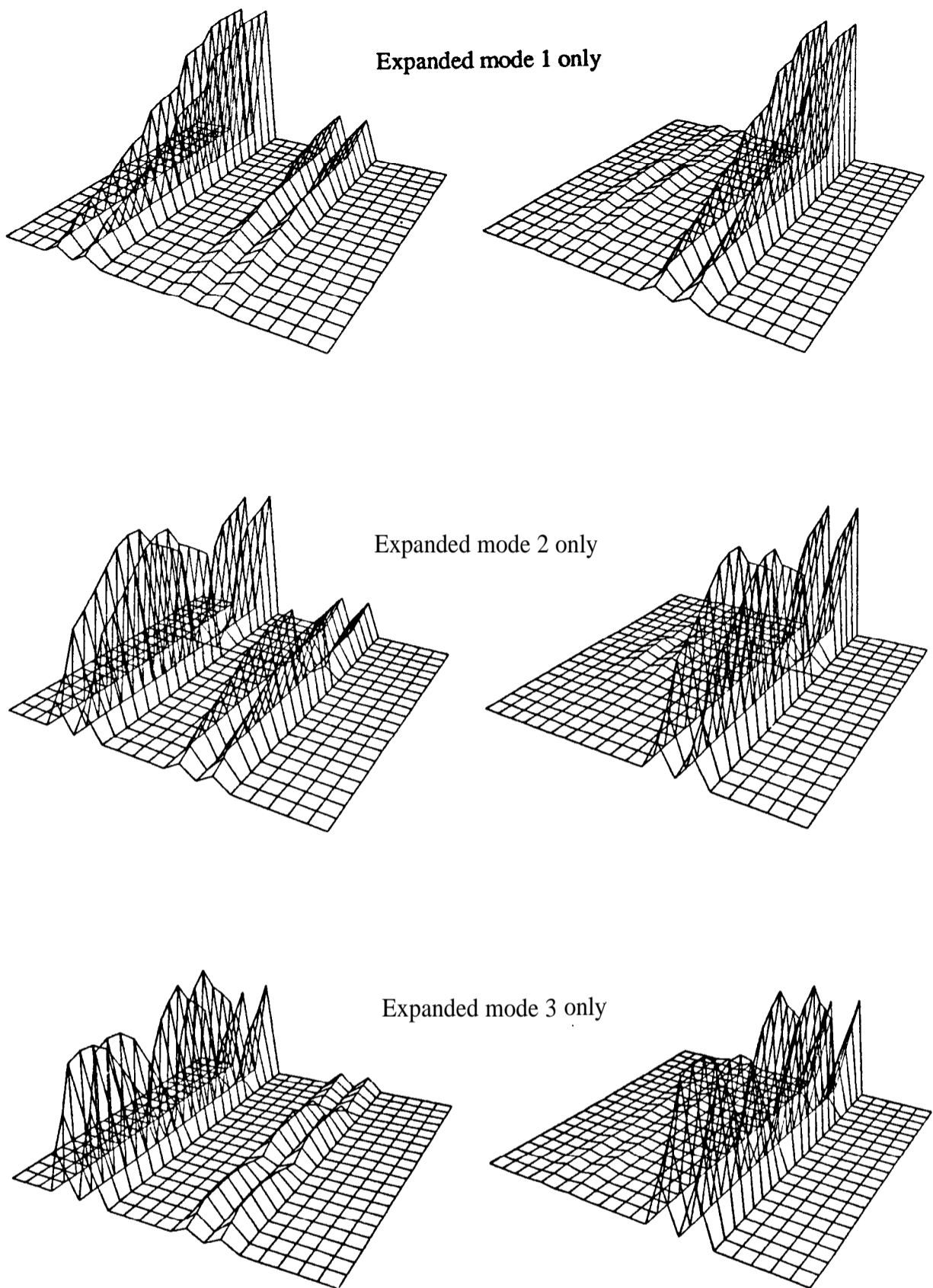


Figure 5-9 Location of stiffness errors and damping elements in the system shown in Figure 5-5 using experimental modes 1, 2 and 3 individually after the experimental modes are expanded.

Left-hand side column: location of stiffness errors.

Right-hand side column: location of damping elements.

CHAPTER 6

CHAPTER 6

APPLICATION OF MODELLING ERROR LOCATION TO A PRACTICAL STRUCTURE

6-1 INTRODUCTION

In the early parts of this thesis, it has been noted that the dynamic characteristics of a structure are widely investigated by two approaches, these being theoretical modelling and experimental testing. It has also been stressed that the dynamic characteristics can be fully and correctly understood only if these two approaches are made in parallel, in order to offset the weaknesses of both. The strong demand in vibration research and engineering practice to use the measured vibration modes in order to improve the analytical model of a vibration structure has also been identified.

Several methods which currently facilitate the model improvement process have been reviewed and studied in Chapter 2. It is found that the main drawback of these methods is that the resultant improved analytical stiffness or mass matrix does not adequately represent the structure modelled analytically since these methods attempt to modify the whole analytical model and end up with an 'improved' model which violates the actual connectivity of the structure. The vibration characteristics deduced by a thus-improved model will therefore not be correct and even the iteration process suggested in Chapter 2 cannot overcome this drawback and achieve the correct model. In addition, we lack an appropriate method to investigate the damping properties of vibrating structures and the proportional damping assumption is believed to be impractical in real life applications.

Since it is realized that, for most vibrating structures, the **modelling** errors inherent in their analytical models are usually local - due to the sophisticated modelling techniques - and

these local errors in the models are referred to as the '**mismodelled**' regions, it then becomes extremely important for the model improvement methods to be able to localize these regions using a limited number of measured vibration modes. Without this location, the models cannot be modified in the right areas and the model improvement can be neither structurally meaningful and nor computationally efficient. A new approach has been developed in Chapter 3 to enable the localisation of mismodelled regions using as few as just one measured vibration mode. It has also been established that once the mismodelled regions are localized, an iterative improvement of the analytical model can become remarkably **efficient**. A similar philosophy has been applied to an investigation of the damping properties and again, it is proposed that the major damping components of a vibration structure can be located using a limited number of complex modes obtained by modal testing and it then becomes promising to construct a meaningful damping matrix for the analytical model by using the measured complex modes and the existing analytical model, even if this contains some errors.

Although these approaches to localize the mismodelled regions from an analytical model and the damping components of a vibration system have been successfully validated using numerical case studies, it is necessary to investigate a real structure using the same approach in order to demonstrate satisfactorily the feasibility of the applying the approach in practice. This Chapter investigates the vibration characteristics of a beam structure using both theoretical modelling and modal testing and analysis, in an attempt to demonstrate that the local errors in the analytical model of the structure can be successfully localized by applying the approach developed in this thesis.

6-2 ANALYTICAL MODELLING OF THE **STRUCTURE**

The structure used in this study is the beam shown in Figure 6-1, with a uniform cross section but with a joint, which is ignored in the predicted model. The structure actually consists of two beam subsystems connected by a nut and bolt so that the tightness of the joint can be adjusted to produce different local stiffness conditions. The beam is made of

steel and is about 2m long with cross section of **25mm x 18.5mm**.

A finite element analysis is carried out for this beam structure, ignoring the joint, so that the structure is regarded as a uniform beam shown in Figure 6-2. This is divided into 9 equal length beam elements and, taking into account both the translational and the rotational displacements in directions x and θ_z as shown in Figure 6-3, mass and stiffness matrices can be derived for the beam element (Appendix 3). Global analytical mass and stiffness matrices which form the analytical model of the structure can then be constructed. The analytical mass and stiffness matrices thus obtained have a dimension of 20×20 . It is believed that the analytical mass matrix of this structure is reasonably accurate since the structure does not have any sudden changes of section while the analytical stiffness matrix obviously does not represent the true stiffness distribution because it does not take account of the local stiffness change near the joint

The analytical vibration modes of the structure are obtained by the eigen-solution of the analytical model. Table 6-1 shows all the 20 natural frequencies of the analytical modes, including two zero natural frequencies for the rigid body modes. The left hand column in Table 6-2 shows the mode shape vectors of 4, 5, and 6 analytical vibration modes derived by the analytical model. It can be seen that the analytical vibration modes are defined in both the rotational and translational coordinates and these are alternately positioned in the mode shape vectors. Specifically, those odd-numbered coordinates are translational coordinates and the even-numbered rotational ones.

6-3 MODAL TESTING AND ANALYSIS OF THE BEAM STRUCTURE AND THE COMPARISON OF ITS MODAL MODEL AND FE MODEL

The modal testing was carried out with the structure supported by two soft strings at its ends, simulating a free-free boundary condition, as shown in Figure 6-4. The testing was

carried out at ten translational coordinates in the x direction, as indicated in the Figure 6-4. As suggested by the modal testing theory, one column of the FRF matrix of a system is theoretically sufficient to extract the modal model of the system, provided the excitation point is selected such that all the interesting vibration modes can be excited. After careful examination, it was decided that structure was to be excited at point 3 (coordinate 5) where all the interested modes show up. Equipment set-up is also displayed in Figure 6-4. The frequency response analyser used in this test was Solartron 1250 analyser which facilitates standard discrete sinusoidal signal. The Modal Testing software 'POLAR' is used for the data acquisition and software 'MODENT' used for the analysis. Both programs are developed in the Modal Testing Unit in this department and, in this study, they were run on an HP computer.

A fast sinusoidal excitation sweep was used first in the frequency range of interest in order to identify the vibration modes. Then, a roomed sinusoidal excitation was used in the test and the acceleration response at each coordinate was recorded while the excitation force is applied on point 3, so that the frequency response function (FRF) could be obtained from the frequency response analyser. Figure 6-5 shows a typical frequency response function obtained in measurement. Its counterpart in the Argand plane is shown in Figure 6-6. The data exhibit quite clearly-defined modal properties for the structure within the measured frequency range.

In this study, only three vibration modes were measured and analysed for the purpose of stiffness error location. The measured natural frequencies of these three modes are shown in the right hand column of Table 6-1. Table 6-2 compares these three measured vibration modes with those predicted by the analytical model. The difference between the measured natural frequencies and those predicted analytically, and that between the mode shapes, is apparent and is expected to be caused by the fact that the analytical model does not correctly model the true stiffness distribution of the beam structure because of the joint. Figure 6-7 shows the FRF data measured from point 6 within a certain frequency range and the corresponding FRF data predicted by the FE model. It can be clearly seen that the

vibration modes predicted theoretically exhibit different dynamic characteristics of the structure from the vibration modes obtained experimentally. Again, this is due to the different stiffness conditions which apply to the analytical and experimental configuration.

6-4 LOCATION OF THE MISMODELLED REGION IN ANALYTICAL STIFFNESS MATRIX USING MEASURED VIBRATION MODE

641 Expansion of Measured Vibration Modes

In order **to localize** the modelling errors in the analytical stiffness matrix, the incompatibility between the analytical model and the measured vibration modes in terms of the coordinates specified has to be overcome first. As proposed in Chapter 5, the three measured vibration modes are expanded to include those rotational coordinates which are not measured, using the analytical mass and stiffness matrices. The three thus-expanded measured mode shapes (rearranged to the original coordinate order as the analytical mode shapes adopt) are listed in Table 6-2, together with the corresponding analytical mode shapes for the sake of easy comparison. It can be seen **from** Table 6-2 that the measured translational coordinates in the expanded mode shapes are unchanged while the rotational coordinates in the expanded mode shapes are effectively interpolated into the mode shapes by the analytical model. In addition, the measured natural frequencies are not changed during this mode shape expansion procedure.

6-4-2 Location of Mismatched Region in the Analytical Stiffness Matrix

The three expanded measured vibration modes are then used to locate the errors in the analytical stiffness matrix. Figure 6-8 shows the results of locating the errors using each expanded measured vibration modes individually and then using three measured modes together, and this figure indicates that each result consistently points to the same region in the analytical stiffness matrix where stiffness modelling errors exist. Namely, the errors are confined in those elements between rows 13 and 17, corresponding to the testing

points between 7 and 9.

To interpret the results shown in Figure 6-8, it has to be noted that the unpredicted joint in the beam structure (ignored in the analysis) is situated between the test points 7 and 8 and, according to the explanation of Chapter 5, the stiffness modelling errors should be located between test points 7 and 8 (which correspond to the global coordinates between 13 and 16). However, the results in Figure 6-8 for using each expanded measured vibration consistently indicate the stiffness modelling errors between testing points 7 and 9, which relate to global coordinates 13 to 18. This is eventually answered by inspection of the structure. Since the joint which is sited between test points 7 and 8 is close to point 9 side, the significant tightness of the joint eventually affects the stiffness condition between points 8 and 9, so that the modelling errors are indicated not only between points 7 and 9, but also between 8 and 9.

To be fully convinced of the location obtained above using the measured vibration modes, one extreme condition is now considered. It is understood that the measured modal data values could possibly vary due to the testing conditions, numerical calculation errors etc. In order to simulate the possibility of different test results, and the consequence of that on the location of the stiffness modelling errors in this study, all the measured natural frequencies and mode shapes of the three modes are perturbed by five percent random errors and these revised measured modes are then used, as before for the unperturbed modes, to locate the errors in the analytical stiffness matrix. Figure 6-9 shows the results using the revised modes 4, 5 and 6 individually and it can be seen that just the same modelling error location is obtained, as before. This shows that the correct modelling error location can be achieved even the measured data have some realistic errors.

6-5 CONCLUSIONS

A practical application of the approach proposed in the early part of this thesis to locate the **mismodelled** region in the analytical model of a structure has been carried out. The

primary purpose of this part of the study is to assess the practical feasibility of the approaches proposed so far in this thesis in locating the modelling errors which exist in the analytical model of a structure using just a few number of the measured vibration modes.

The structure upon which the investigation was performed is a beam structure with an analytically ignored joint which causes the modelling errors in the analytical stiffness matrix of the structure. The analytical model is obtained assuming the structure to be a uniform beam and the analytical mass and stiffness matrices can be derived by Finite Element modelling. The stiffness matrix thus derived contains errors relating to the local area where the joint exists while the mass matrix is believed to be acceptably accurate since there is no sudden mass change on the structure.

Modal testing was carried out using the ten translational coordinates of the structure only, as the remaining rotational coordinates defined by the analytical model are technically difficult to test. Only three vibration modes were identified experimentally.

Since an incompatibility exists between the measured vibration modes and the analytical model, the three measured vibration modes were expanded using the analytical mass and stiffness matrices, as suggested in Chapter 5. These three expanded vibration modes were then used to locate the modelling errors assumed to be present in the analytical stiffness matrix.

The results of using the expanded vibration modes individually to locate modelling errors in the analytical stiffness matrix have consistently pinpointed the correct region in the matrix which relates the local area in the structure where the unpredicted joint is situated.

Mode	Natural frequencies(Hz) of complete model	Natural frequencies (Hz) of measured modes
1	0.0000	
2	0.0000	
3	35.0970	
4	98.328 1	78.99
5	196.4980	170.16
6	331.1097	287.83
7	501.6208	
8	701.4584	
9	913.3696	
10	1094.408 1	
11	1598.5626	
12	1811.2545	
13	2076.2880	
14	2398.3894	
15	2824.3952	
16	3430.9070	
17	4355.4700	
18	5758.2817	
19	8079.045 1	
20	8494.8225	

Table 6- 1
predicted and **measured** natural frequencies of the beam structure

Coords	Source analytical model	measured mode	expanded measured
1	0.75065	0.67238	0.67238
2	-3.0957 1		-2.47615
3	0.10554	0.15084	0.15084
4	-2.82288		-2.34668
5	-0.38516	-0.28598	-0.28598
6	-1.51959		-1.54197
7	-0.50100	-0.46880	-0.46880
8	0.49832		0.04462
9	-0.21322	-0.3 1209	-0.31209
10	1.95468		1.41524
11	0.23680	0.07480	0.07480
12	1.90327		1.91141
13	0.50582	0.44332	0.44332
14	0.37366		1.37209
15	0.36850	0.51650	0.51650
16	-1.60837		-1.31651
17	-0.13817	-0.0725 1	-0.0725 1
18	2.86949		-3.25774
19	-0.79146	-0.71877	-0.71877
20	-3.12549		-2.89180

Table 6-2(a) Mode 4 - mode shapes **from** different sources

	Source analytical model	measured mode	expanded measured
Coords			
1	0.757 10	0.75609	0.75609
2	-4.36470		-4.22389
3	-0.12437	-0.08800	-0.08800
4	-3.46185		-3.267 15
5	-0.52608	-0.49158	-0.49158
6	0.07181		0.30012
7	-0.12887	-0.21981	-0.21981
8	2.99139		2.55901
9	0.46508	0.37643	0.37643
10	1.72114		2.10325
11	0.44841	0.49969	0.49969
12	-1.86534		-1.00436
13	-0.15752	0.01540	0.01540
14	-2.93444		-3.09858
15	-0.52382	-0.49303	-0.49303
16	0.07077		-0.40925
17	-0.09219	-0.11456	-0.11456
18	3.578 10		2.93072
19	0.81509	0.52150	0.52150
20	4.48759		2.95846

Table 6-2(b) Mode 5 - mode shapes **from** different sources

	Source analytical model	measured mode	expanded measured
Coords			
1	0.76419	0.67992	0.67992
2	-5.59298		-5.28993
3	-0.31916	-0.32269	-0.32269
4	-3.51529		-3.16451
5	-0.40384	-0.38506	-0.38506
6	2.68520		2.59939
7	0.40342	0.39950	0.39950
8	2.87411		2.77730
9	0.39647	0.40743	0.40743
10	-2.9259 1		-2.67267
11	-0.41110	-0.36426	-0.36426
12	-2.82433		-2.93672
13	-0.3873 1	-0.42412	-0.42412
14	2.983 17		2.61191
15	0.40729	0.333 12	0.333 12
16	2.63293		2.43214
17	0.29849	0.25655	0.25655
18	-3.6487 1		-2.64746
19	-0.84007	-0.51613	-0.51613
20	-5.95857		-4.01821

Table 6-2(c) Mode 6 - mode shapes from different sources

Table 6-2
Mode shapes for vibration modes **4, 5, 6** of the beam structure

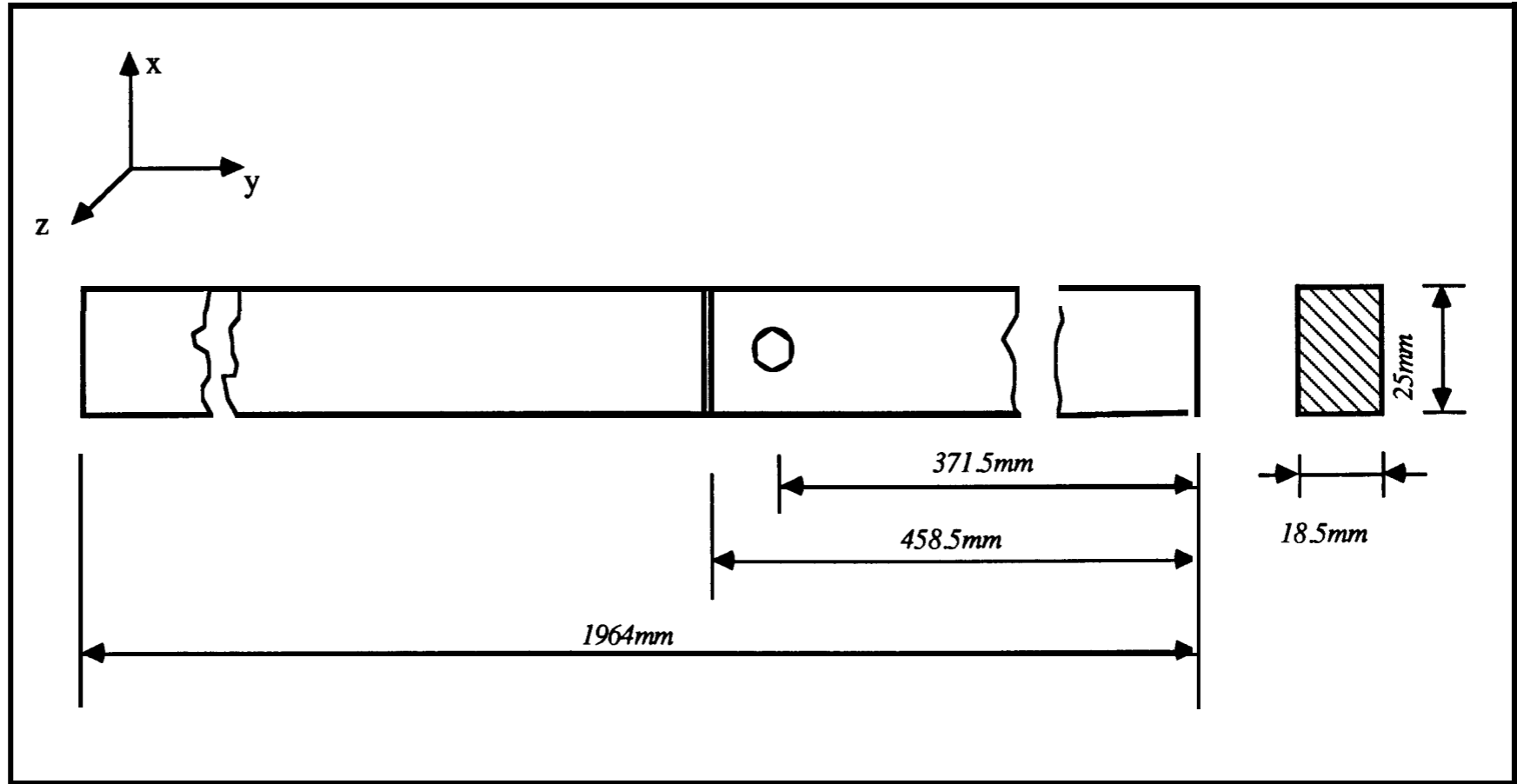


Figure 6-1 a uniform with an unpredicted joint

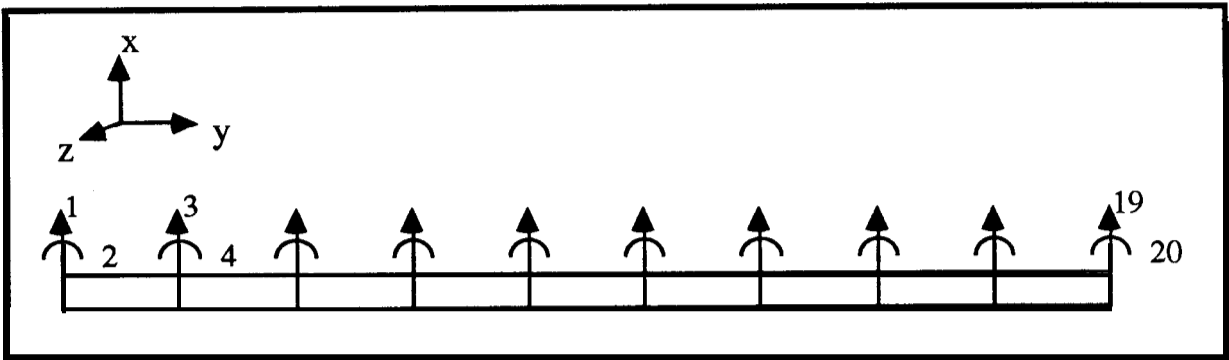


Figure 6-2 FE modelling of a uniform beam

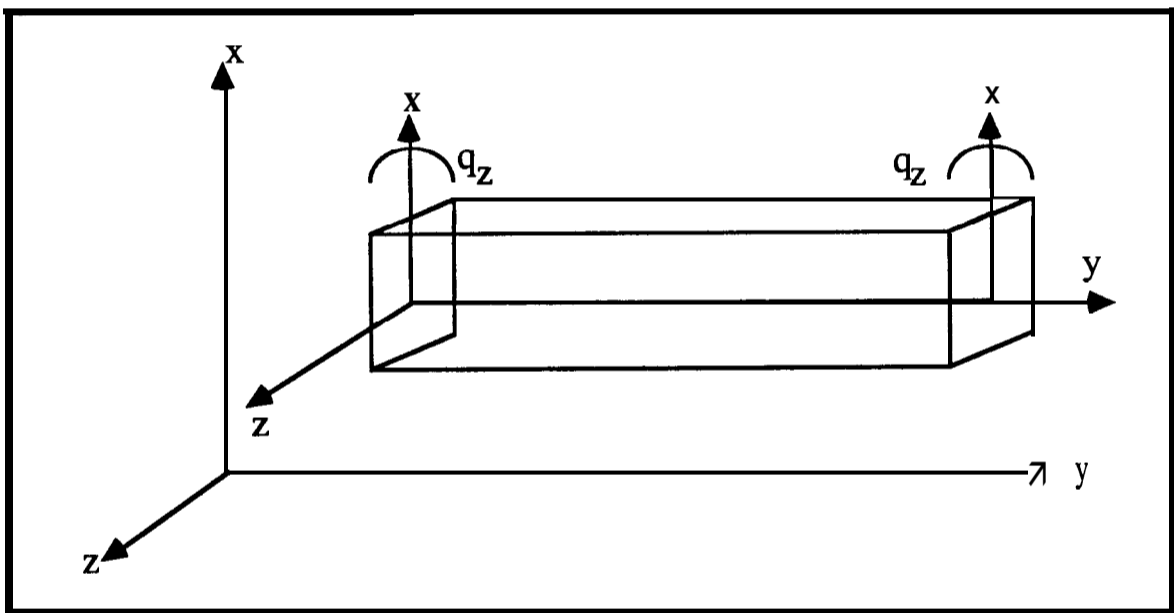


Figure 6-3 A typical beam element for FE analysis

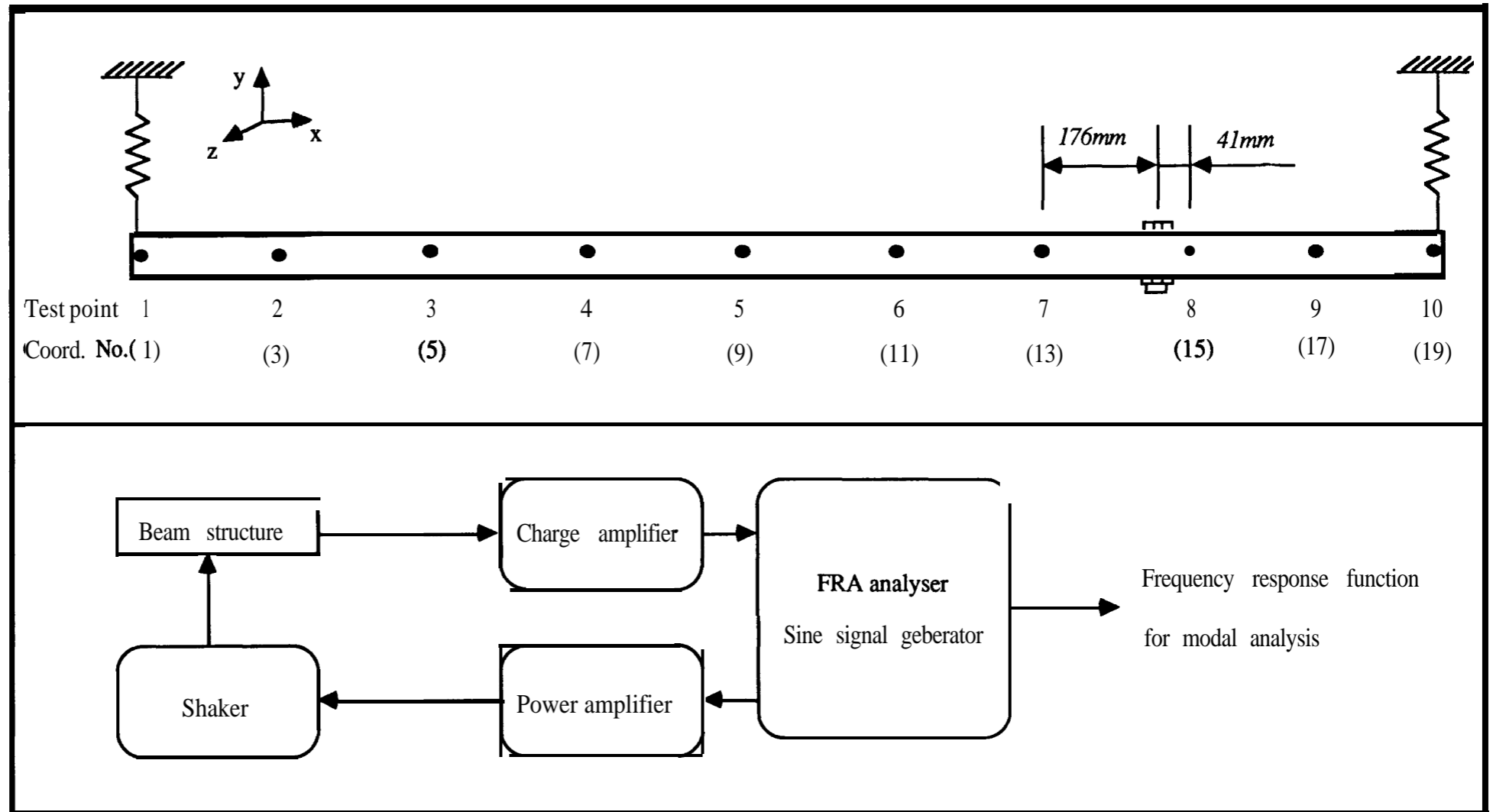


Figure 6-4 Modal testing of the beam structure

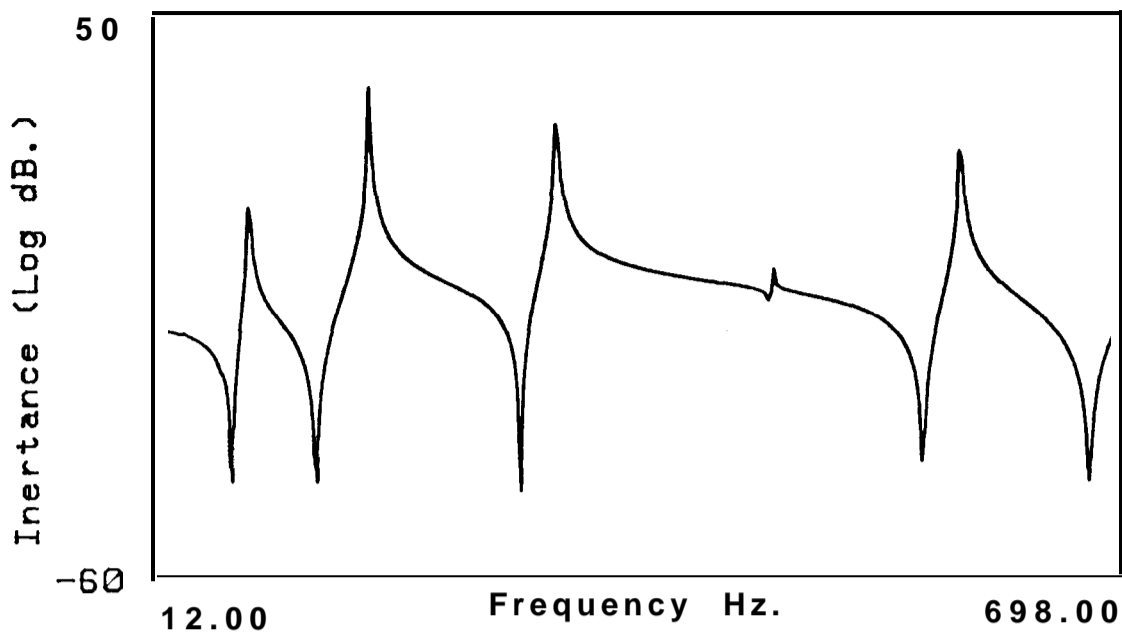


Figure 6-5 A typical frequency response function obtained from modal test of the beam structure shown in Figure 6-4.

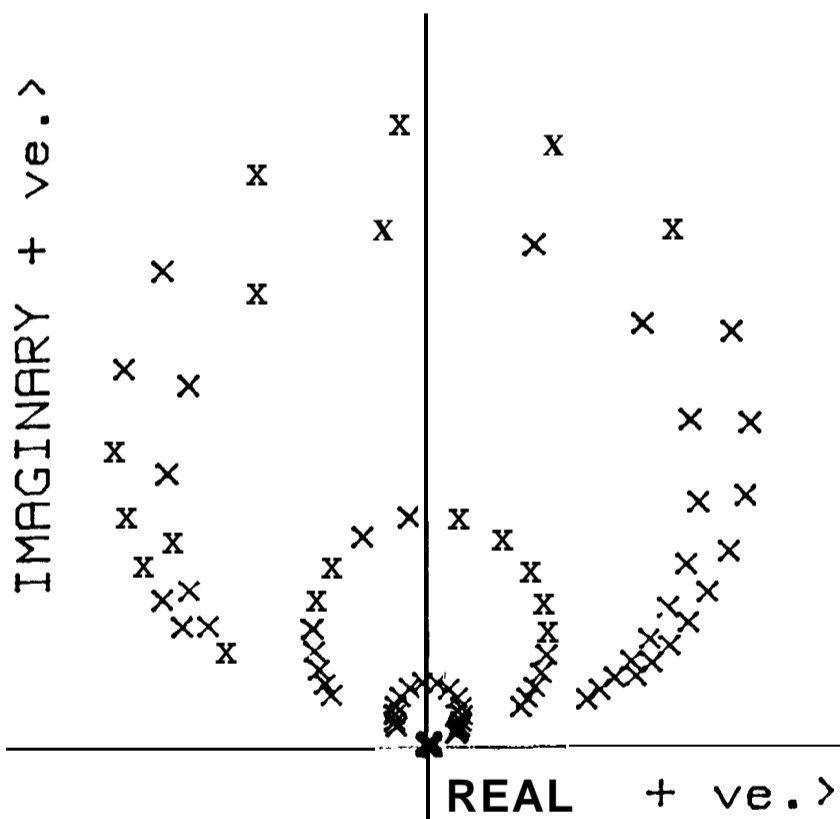


Figure 6-6 The FRF in Figure 6-5 is presented in the Argand plane.

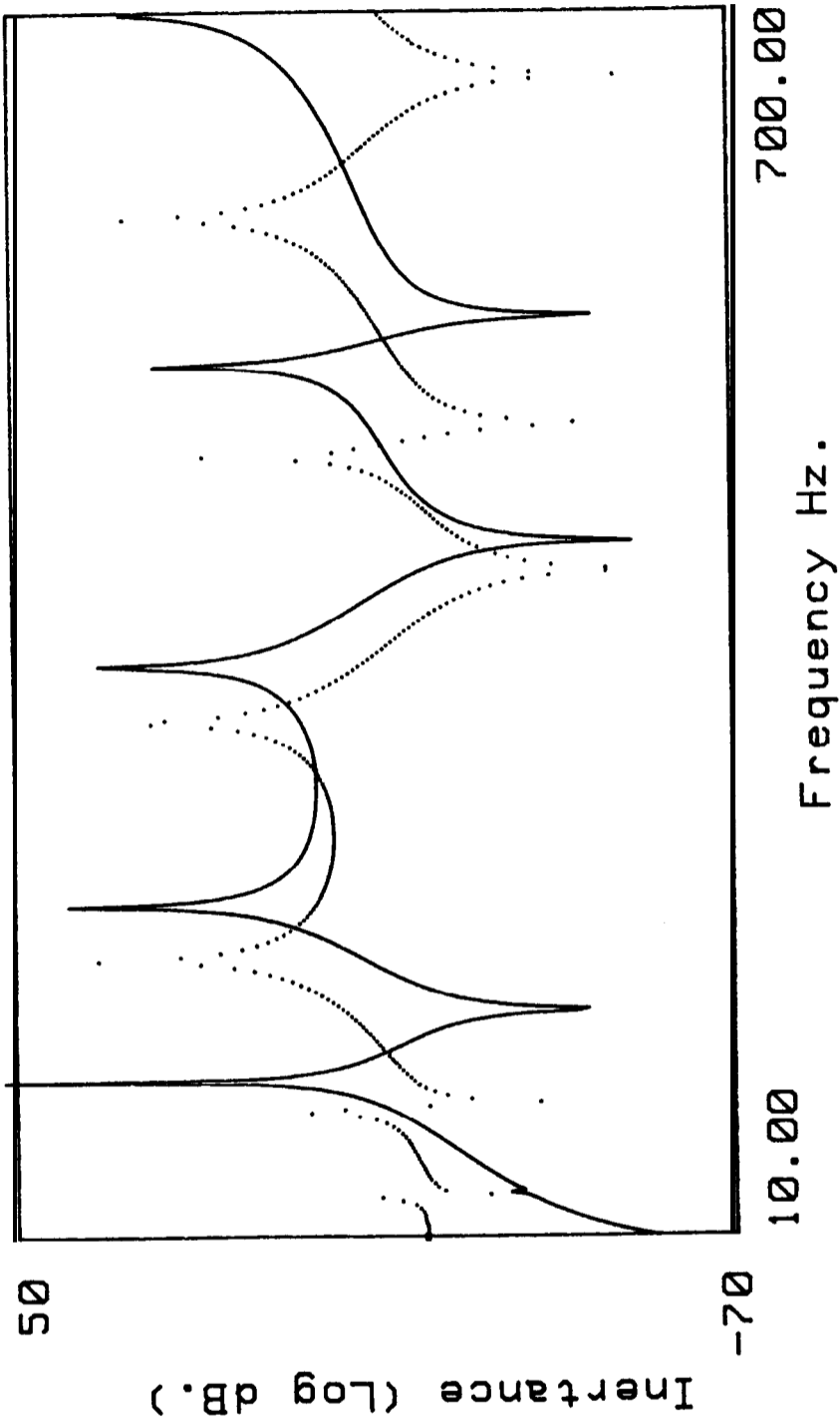


Figure 6-7 The FRF data measured from point 6 of the beam structure and the corresponding FRF data predicted by the FE model.

Dotted line - measured data

Solid line - theoretical data

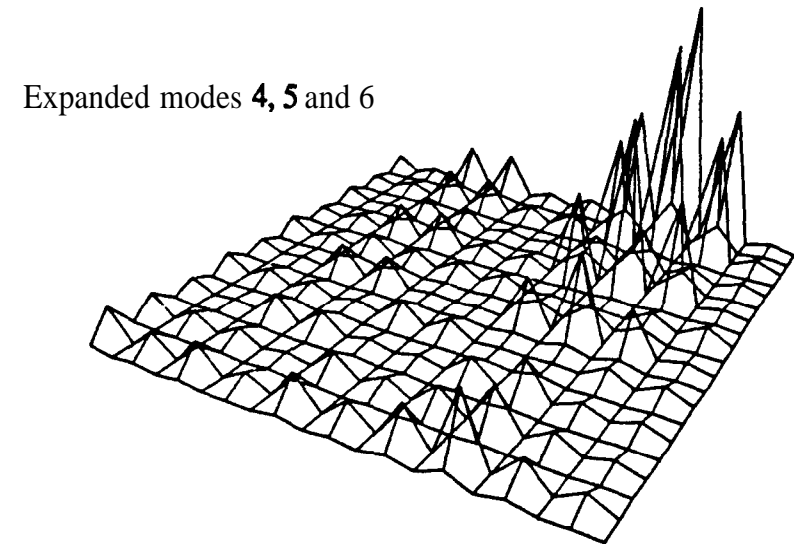
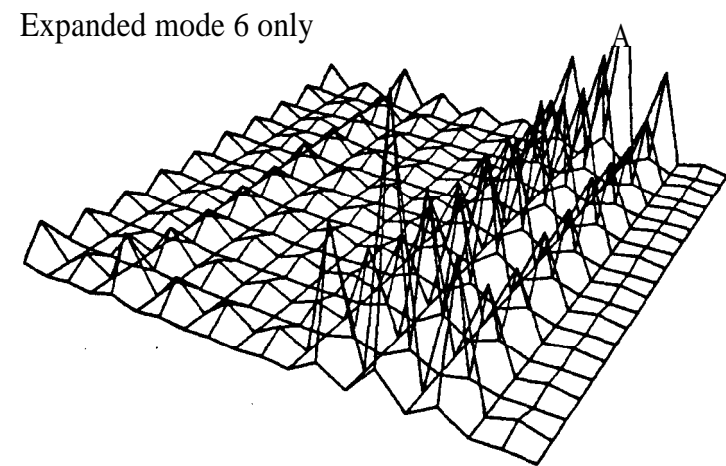
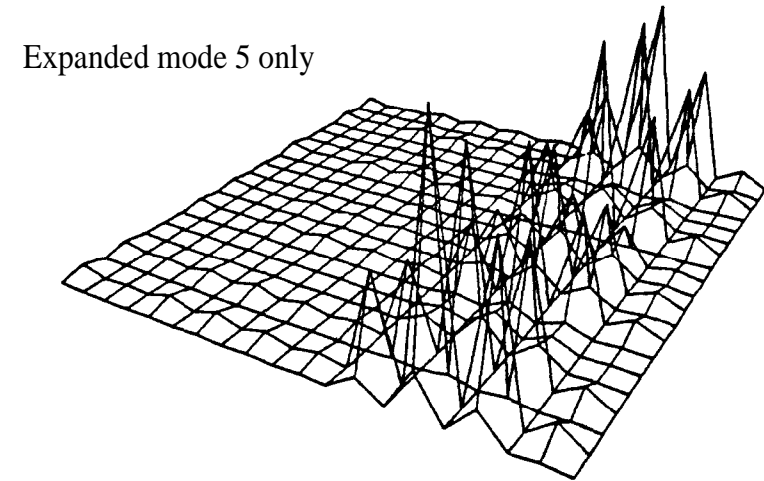
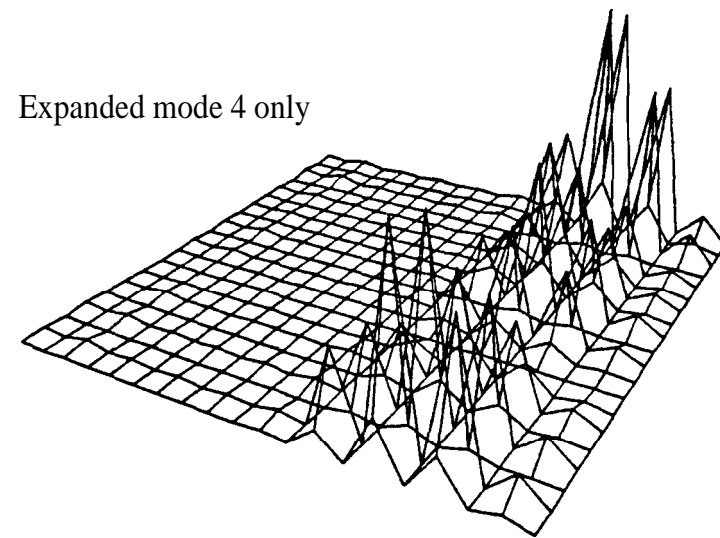


Figure 6-8 Location of **stiffness errors** for the beam structure shown in Figure 6-4 using experimental modes **4, 5** and 6 individually and then together after the experimental modes **are expanded**.

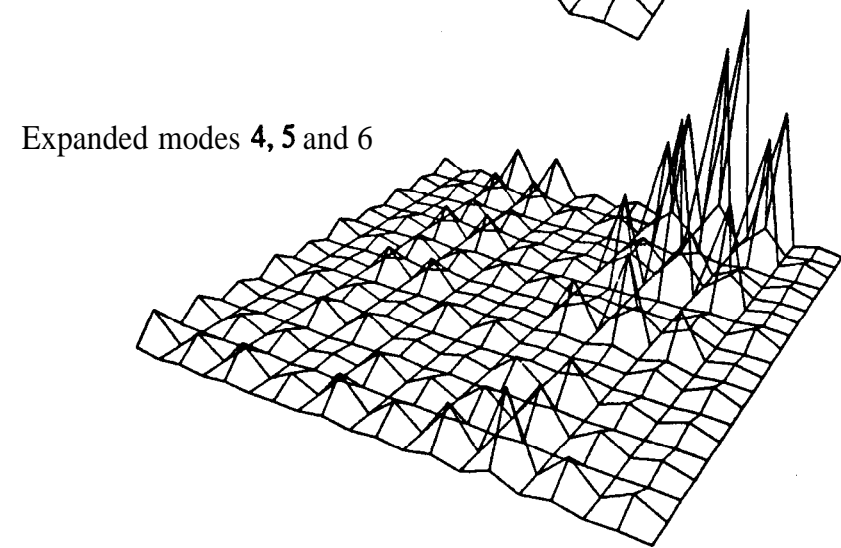
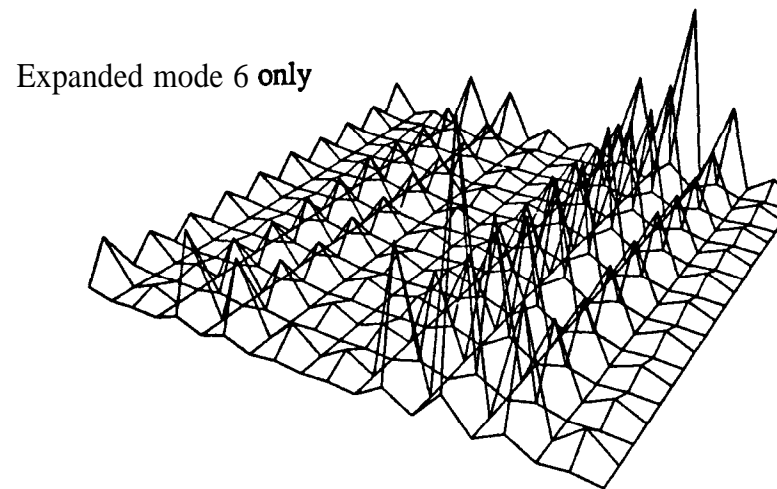
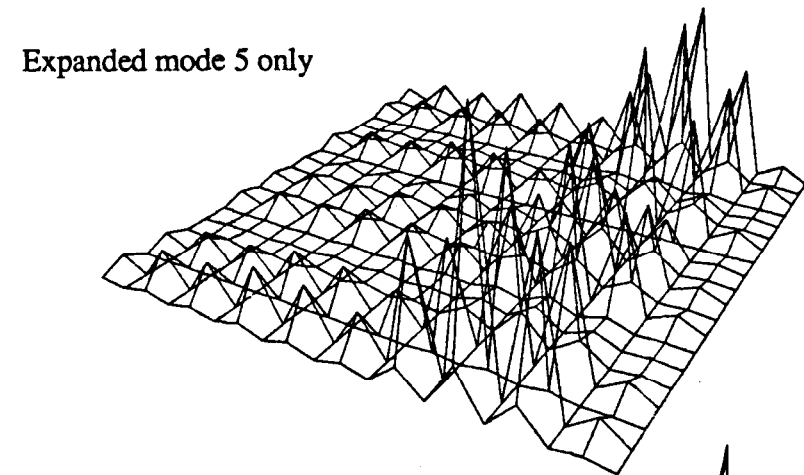
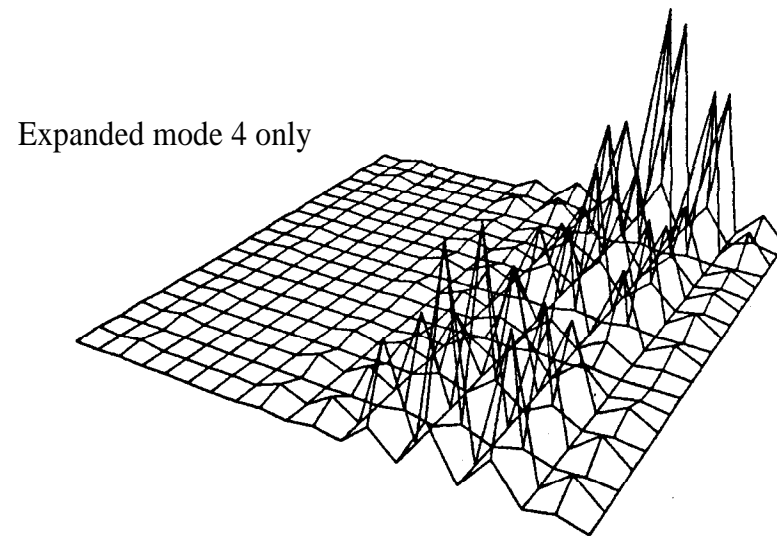


Figure 6-9 Location of stiffness **errors** for the beam structure shown in Figure 6-4 using experimental modes **4, 5** and 6 individually and then together after the experimental modes are expanded and 5% artificial random errors are added into the natural **frequencies** and mode shapes.

CHAPTER 7

CHAPTER 7

MEASUREMENT OF NONLINEARITY

7-1 INTRODUCTION

In the previous Chapters, we have covered one of the most important and demanding topics in the recent vibration research: that of correlating the analytical model of a dynamic structure and its measured vibration modes so that an improved model can be obtained. This is expected to combine the advantages of the two widely used approaches (analytical modelling and experimental testing) in order to understand better the dynamic characteristics of the structure under investigation. The damping properties of a structure have also been studied.

In those previous studies, it is assumed that linearity exists for the structures modelled analytically and tested but it is realised that all real vibrating structures are nonlinear to some degree. However, many of them may be nonlinear to a tolerable extent so that they can still be investigated using the theory for linear structures. For those structures known or suspected to be noticeably nonlinear in their vibration behaviour, the linear assumption fails to be applicable and special analysis is needed to investigate the nonlinearity. Generally, it can be said that nonlinearity is similar to the modelling errors and damping properties discussed earlier in the sense that it also cannot be predicted analytically and can only be identified by experimental measurement.

The study of nonlinearity is very complicated. This results from the fact that the superposition principles whereby the response of a system to different excitations can be added linearly is not valid in the case of nonlinear systems. As a consequence, the dynamic characteristics of nonlinear structures become excitation-dependent and much

less predictable. Since the nonlinearity encountered in vibrating structures is often difficult to identify, and even more difficult to quantify, they are in many practical cases significant to the vibration behaviour of the structure, and the requirement for special investigation methods is clear.

It is noted that theoretical methods have been developed extensively for those nonlinear systems whose equations of motion can be expressed analytically. The fundamental point of the analysis can be classified briefly as linearising either the parameters of a nonlinear system *or* its vibration response. There are currently quite a number of methods which are available to examine the vibration behaviour of a nonlinear system analytically. For example, the Small Oscillation Method is an approach which replaces the nonlinear term in the differential equations of a nonlinear system by its Taylor series with respect to displacement and velocity and considers only the **first** two terms, thereby extracting a linear system which will exhibit a response like the nonlinear system; The **Quasi-harmonic Method**^[54] aims at deriving a periodic solution for a nonlinear system in the form of a power series in ϵ (a parameter which indicates the perturbations of the system and is considered to be very small). Thus, a time-dependent solution which does not differ appreciably from the solution of the corresponding linear equation can be sought. The Method of Krylov and Bogolyubov supposes that the solution to the equation of a nonlinear vibrating system is still in the same form as that of its linear counterpart, except that the amplitude and phase are slightly varying with time and, as a consequence, the approximate solution of the nonlinear system is a periodic function of both the amplitude and phase angle, as **well** as time. An equivalent natural frequency and damping **coefficient** of the nonlinear system subjected to an external excitation can then be obtained as functions of the response **amplitude**^[55]. **Iwan's New Linearisation Method**^[56] is a generalisation of the method of equivalent linearisation. It introduces a weighting function into the averaging integrals used in the equivalent linearisation method and suggests that a nonlinear second order system can be replaced by a linear system in such a way that an average of the difference between the two systems is minimized. It also shows that the replacement is unique and can be accomplished in a straightforward manner.

Apart from the methods **summarized** above for general nonlinear cases, analysis could be further developed to cope with systems having known types of nonlinearity. For instance, such studies can be traced back to dates long before the computer was **available**^[57] or, they can be found from time to time in recent **literature**^{[58],[59]}.

Although many types of nonlinearity have been studied extensively, based on mathematics and analysis used in control engineering, the theory is often not directly applicable to experimental modal analysis of real structures because of the absence of explicit equations of motion for practical vibration situations. The major difficulty in these situations is the detection and identification of the nonlinearity when what is available is the response of a nonlinear structure to excitation by external forces rather than an explicit analytical description. Nevertheless, the theoretical study provides many specific and frequently encountered types of nonlinearity with characteristic response patterns which, in turn, provide a helpful reference in practical modal analysis.

7-2 EXCITATION TECHNIQUES

It is customary to assume that for linear structures, the dynamic characteristics will not vary according to the choice of the excitation technique used to measure them. However, the effects of most kinds of nonlinearity encountered in structural dynamics are generally found to vary with the external excitation and hence the **first** problem of a nonlinearity investigation will necessarily be to decide a proper means of excitation so that the nonlinearity can be easily exposed and then identified. There are currently mainly three types of excitation method widely used in vibration study practice and each of them is discussed below.

7-2-1 Sinusoidal Excitation

Sinusoidal excitation is the traditional excitation technique in vibration testing and also in

recent modal testing practice. Although many other techniques such as random, transient, periodic and pseudo-random excitations etc have been developed, sinusoidal excitation is still commonly applied in practice because of its uniqueness and precision. The main advantages of this excitation can be summarised as:

- (a) sinusoidal excitation can accurately control the input signal level and hence it enables a high input force to be fed into the structure. This is especially significant when large structures are tested,
- (b) for discrete sinusoidal excitation, the signal-to-noise ratio is generally good as the energy is concentrated in one frequency band each time and even swept sinusoidal excitation can normally achieve similar concentrated energy conditions compared with other excitation methods;
- (c) sinusoidal excitation is widely regarded as the best excitation technique for the identification of nonlinearity in most applications of modal testing and analysis;
- (d) when the harmonic distortion effects of nonlinearity are investigated, sinusoidal excitation is also uniquely required.

It is the item (c) that contributes most to the continued wide application of this traditional excitation technique. In this study, sinusoidal excitation is employed for each nonlinearity simulated on an analogue computer in order to facilitate the nonlinearity identification process.

The main drawback of the sinusoidal excitation technique is that it is relatively slow compared with many of the other techniques used in practice. The obvious reason is that the excitation is performed frequency by frequency and, at each step, time is needed for the system to settle to its steady-state response. However, it is believed that for many practices of the identification of structural dynamic characteristics, correct measurement results often become the primary criterion **over** time-saving in the test. For instance, when the modal analysis results are to be used to improve an FE model of the tested structure - an application which appears to be in great demand in recent years and has been exhaustively discussed above - a major concern lies on the precision and comprehension

of the modal analysis results. Consequently, sinusoidal **excitation** is preferred in modal testing in order to provide the post analysis stages with the optimum data.

7-22 **Random Excitation**

Random excitation attracts analysts and researchers primarily because of its potential time saving in obtaining frequency response functions of the tested objects. Using this technique, the system is excited simultaneously at every frequency within the range of interest. This wide frequency band excitation enables the technique to be much faster than sinusoidal excitation. Further, the effects of noise can be successfully eliminated by averaging if the measurement time is long enough.

The derivation of the input and output relationship under random excitation relies on Fourier transform theory and is based upon Duhamel's Integral. As the Duhamel's Integral presumes a linear system behaviour, it has been suggested in the literature that the linearity characteristic of the response from the random excitation is automatically assumed. It will be shown below that this is not true. The actual reason for the inability of random excitation to expose the nonlinearity from the response is the randomness of the amplitude and phase of the input force.

In the measurement, spectral estimates for each recorded data block have random amplitude and random phase. Thus, at each frequency the system can be considered to be excited by different amplitudes and phases, sample after sample. By considering the effect of nonlinearity as noise in the response, it can be understood that after the averaging process the frequency response function obtained from the FFI' analyser will always comply with the behaviour of a linear system. It can then be roughly concluded that as far as the identification of nonlinearity is concerned, conventional random excitation and signal analysis is not a feasible technique in practice.

It should be noted here that the problem of impedance mismatch between the tested

structure and the shaker always exists and this can result in problem of noise. Usually, the spectrum of the excitation signal is uniform along the frequency range of measurement. However, when a mismatch occurs, the spectrum of the excitation force applied to the structure may be distorted, yielding noise problems. The mismatch problem is most serious at the resonances of the structure when the response spectrum at the vicinity of resonance tends to drop because of the low impedance input to the structure, resulting in a low signal-noise ratio.

Sometimes, when the dynamic modelling of a nonlinear system is of concern rather than the identification of nonlinearity, the primary interest will be on extracting a linear model of the system which behaves vibrationally in the frequency range of interest in as similar a manner as possible to the nonlinear system, regardless what type of nonlinearity the system possesses, then random excitation could be an effective technique.

7-23 Transient Excitation

Since the Fourier Transform was **first** developed in the early nineteenth century, the theoretical foundation had been provided for transient testing. However, not until digital computers with **FFT** capabilities were developed did transient excitation and analysis become practically feasible and has now received great interest because of the unique characteristics differing from other excitation techniques.

In transient excitation measurement, the data involved are the time histories of the excitation force $f(t)$ and of the response $x(t)$. The frequency response function is defined by the division of the Fourier Transforms of these two time series signals. The denominator is the Fourier Transform of $f(t)$ whereas the numerator is the Fourier Transform of $x(t)$:

$$H(\omega) = X(\omega)/F(\omega) \quad (7-1)$$

The actual computer analysis approach to obtain the frequency response function depends on the estimates of the auto-spectrum of the force signal and the cross-spectrum of the force and response. The computation is performed as:

$$\begin{aligned} H(\omega) &= X(\omega) / F(\omega) \\ &= X(\omega)F^*(\omega) / F(\omega)F^*(\omega) \\ &= S_{xf}(\omega) / S_{ff}(\omega) \end{aligned} \tag{7-2}$$

where $F^*(\omega)$ is the complex conjugate of the Fourier Transform $F(\omega)$ and $S_{xf}(\omega)$ is the cross-spectrum of the force and the response of the system. Therefore, obtaining the frequency response function in transient testing becomes a matter of spectral analysis.

The form of the forcing function in transient excitation is important. The input forcing function theoretically suggested for transient excitation is of a pulse type. This is, unfortunately, mechanically difficult to achieve in practice. Usually, a mechanical impact is used to generate the required forcing signal. If the impact is well controlled, the forcing signal would have a comparatively short time duration and contain desirable energy spectral properties. However, a very short duration of an impact, covering a broad range of energy distribution in the frequency domain, can be extremely difficult to obtain in practice. This means that in the frequency domain the input force energy at high frequencies is not always large enough to excite the system effectively. Hence, care should be taken when transient excitation is applied to the case where vibration properties at high frequency are of primary interest. Moreover, it is quite obvious that the excitation frequency bandwidth cannot be controlled conveniently.

One possible alternative to the mechanical impact forcing signal is an electrical, instead of mechanical, impulse which can be applied to the **structure** through a conventionally used shaker. Indeed, this type of electrical pulse test has been adapted. Despite the fact that an electrically-produced forcing signal has well controlled amplitude, a desired rectangular

shaped pulse signal is still not easy to achieve due to a number of error sources such as the “digitising error” occurring in the operation of A/D (analogue to digital) conversion. Besides, the frequency characteristics of a shaker could be a problem and this is perhaps more important,

Another forcing function referred to as “rapidly swept sinewave” or “chirp”, which is classified in the transient excitation category, has been employed with success in recent years^[60]. Unlike the discrete **sinewave** used in sinusoidal excitation, the swept **sinewave** here is of constant amplitude and has a sweeping frequency which varies rapidly and continuously with time and has high cut-off rate at the starting and ending frequencies. The time duration of the forcing signal can be as short as a few seconds. However, no evidence has been found to back up the advantage of using such a excitation technique for the purpose of identifying nonlinearity.

7-2-4 Comments on Different Excitation Techniques

Although there are a number of excitation techniques available nowadays for vibration testing, the choice for the modal testing of a dynamic structure is by no means easy, especially when nonlinearity is to be investigated.

Random excitation tends to excite the structure with a random force level and phase at each frequency and thus the response data from a nonlinear system will behave as if the system were linear, as the recorded data blocks are averaged. As the contribution of the nonlinearity to the response differs from noise in that it is a systematic error and cannot be averaged out, the response data from a nonlinear system will appear to be from a linear system which is often referred to as a ‘linearised model’ of the **nonlinear** system, **rather** than the linear part of the nonlinear system. This is illustrated in Figure 7-1. Hence, random excitation is not applicable for the purpose of the identification of nonlinearity. In other cases, when the dynamic modelling of a nonlinear system is of interest, rather than the identification of nonlinearity is sought, the primary concern will be on the extraction

of a linear model of the system which will behave vibrationally in as similar a manner as possible to the nonlinear system in the frequency range of interest, regardless of what type of nonlinearity the system possesses, then random excitation could be an efficient technique.

Transient excitation has noticeable properties of convenience and simplicity and is remarkably fast in performance. It requires less instrumentation (for the case of a mechanical impact test), facilitating mobile experiments. However, transient excitation obviously attracts the same argument as random excitation in not being applicable for the purpose of the detection and identification of nonlinearity. This is mainly because the force level and phase of each data record is similarly not controllable as for the random excitation case and, in addition, the frequency range is also difficult to control. Nevertheless, low coherence often occurs at anti-resonances of the frequency response function data when the impact test is carried out. This is mainly because of the low signal/noise ratio at anti-resonances. This characteristic is different from the random test where low coherence occurs both at resonances and at anti-resonances of the frequency response function data. The reason for this difference is that for the random test, not only can a low signal/noise ratio deteriorate coherence (which is similar to transient excitation case), but also can the bias error do (also known as leakage **problem**)[70].

Sinusoidal excitation can have a well-controlled input force amplitude for each frequency tested, and thus the nonlinearity inherent in the tested structure can then be exposed in the response. In addition, it is most ideal to deduce harmonics when nonlinearity exists. Therefore, this excitation technique is the most desirable one to use in the investigation of nonlinearity. In this study, **only** sinusoidal excitation is applied.

7-3 PRACTICAL CONSIDERATIONS OF NONLINEARITY MEASUREMENTS

As explained above, sinusoidal excitation is strongly favoured in measurement if nonlinearity is expected and is to be studied. However, selecting sinusoidal excitation is

merely the first step towards being able to identify the nonlinearity. There are still a number of possible practical problems which need to be carefully considered, otherwise the measurement will not be successful and, as a consequence, nonlinearity will not be correctly identified.

The main difference between measurement of a linear structure and of a structure with nonlinearity is that the excitation force level becomes significant for the latter case. In fact, the force level becomes vitally important in determining the vibration characteristics of a nonlinear structure. The effect of the excitation force level on the response of a nonlinear structure depends not only upon the degree of the nonlinearity the structure possesses, but also upon what type of nonlinearity it possesses. For many types of either nonlinear stiffness or nonlinear damping, increasing the excitation force level will be similar to enlarging the degree of nonlinearity as far as the response of the nonlinear structure is concerned. Some other types of nonlinearity can be the other way around or even, the excitation force level can be discontinuous (it will not affect the response until it reaches a certain quantity). For instance, cubic stiffness provides a good example of enlarging the degree of nonlinearity being the same as increasing the excitation force level while Coulomb friction tends to affect the response less when the excitation force level increases. Backlash stiffness is a nonlinearity where the excitation force level does not affect the vibration response of a system possessing it until the force level is large enough to make the response level to exceed a given limit.

As the vibration response of a nonlinear system is eventually related to the excitation force level, careful consideration should be taken to select the force level for the measurement. Thus, it would be appropriate to use a relatively large force level for a system with cubic stiffness if the nonlinearity is to be detected and identified. However, great attention should be paid to the characteristics of the shaker which is normally used for vibration measurement, since the shaker tends to distort the force level. In practice, the force level will tend to decrease near resonances and this influences the effect of nonlinearity on the frequency response function data. In order to expose the nonlinearity so that it can be

identified, the following possible steps could be taken in measurement:

- (a) using response control to build up a series of linearised models for the nonlinear system. This method is extremely time-consuming and conventional linear algorithms do not enable the extraction of the linear model of the system, i.e. the damping loss factor and modal constant for the linear model of the system is not obtainable unless very low or very high force conditions obtain, depending on the type of nonlinearity.
- (b) using a controlled force level to measure one frequency response function (FRF) over the frequency range of interest or on the nonlinear mode. In this case, each data point of this FRF comes, in fact, from one FRF of the former case, thus containing the information of that FRF. Therefore, this type of measurement is often applied in practice to study nonlinearity. The problem here is that to obtain a controlled force level in measurement is by no means easy, especially when nonlinearity is significant.

It will be seen later in Chapter 8 that nonlinearity investigation does not necessarily require these conditional measurement above. In fact, it is possible to study nonlinearity and to identify their types simply by using the data from conventional measurement where no control is imposed at all.

74 SIMULATION FOR NON INVESTIGATION

7-4-1 Significance of Simulation of Nonlinearity

For most practical nonlinear structures, the type and extent of the nonlinearity are generally unknown and, further, the extent of the nonlinearity is not controllable for the sake of nonlinearity analysis. The identification of nonlinearity will then be ineffective or even unsuccessful unless the types of nonlinearity the structures often possess are thoroughly studied beforehand so that their characteristics on the vibration behaviour are

well understood and categorised. It is believed that the most effective way to investigate nonlinearity would be to simulate those types of nonlinearity frequently encountered in practice and to thoroughly study their characteristics on the modal data so that those categorised characteristics will then become useful references for the investigation of the practical nonlinear structures.

The advantage of simulation analysis in nonlinearity investigation, besides the practical necessity suggested above, lies mainly in the fact that a nonlinear system can easily be simulated on a device such as an analogue computer by setting up the differential equation which governs the simulated system and the parameters of the system can then be conveniently adjusted to simulate different extents of nonlinearity. Hence, the response of the simulated nonlinear system can be obtained and the vibration characteristics of the nonlinear system can be thoroughly investigated which, in turn, will be referenced for the nonlinearity investigation of practical structures.

7-4-2 Analogue **Simulation of Nonlinearity**

An analogue computer is a device whose component parts can be arranged to satisfy a given set of equations, usually simultaneous ordinary differential equations. As for the vibration study, the equations of motion to which a nonlinear system are subject are usually second order ordinary differential equations, and so the analogue computer is an appropriate device to be used. Figure 7-2 shows some of the basic elements used in this study to construct the nonlinear systems. Because the analogue computer can only integrate a function with respect to time (rather than differentiate it), a differential equation has to be solved for the highest derivative in the equation.

In this study, several nonlinear SDOF systems, having either nonlinear stiffness or nonlinear damping which are believed to be frequently encountered in practice, are simulated on an analogue computer in order to investigate the dynamic behaviour of a system having these types of nonlinearity.

(1) A SDOF System with Hardening Cubic Stiffness

A SDOF system with hardening cubic stiffness and linear viscous damping is governed by the following differential equation of motion:

$$\ddot{x} + 2\xi\omega_0\dot{x} + \omega_0^2(x + \beta x^3) = F(t) \tag{7-3}$$

where ξ - viscous damping ratio of the system;

ω_0 - natural frequency of the system;

β - cubic stiffness coefficient;

$F(t)$ - function of the excitation force.

In order to set up the analogue circuit for this system, equation (7-3) should be rearranged into:

$$\ddot{x} = - (-F(t) + 2\xi\omega_0\dot{x} + \omega_0^2x + \omega_0^2\beta x^3) \tag{7-4}$$

In this study, the viscous damping ratio of the system is chosen as 0.005 and the natural frequency as 10 rad/sec. The analogue circuit which simulates equation (7-4) is shown in Figure 7-3.

(2) A SDOF System with Backlash Stiffness

A system with backlash stiffness and linear viscous damping can be shown in Figure 7-4 and the governing equation of motion is as follows:

$$\ddot{x} + 2\xi\omega_0\dot{x} + \omega_0^2x + \varphi(x) = F(t) \tag{7-5}$$

where:

$$\varphi(x) = \begin{cases} + \delta\omega_0^2x_0 & x > +x_0 \\ 0 & -x_0 < x < +x_0 \\ - \delta\omega_0^2x_0 & x < -x_0 \end{cases}$$

Here, parameter x_0 - which defines the linear response level of the system - is called the

“response limit” and a linear system will have a infinite response limit. The other parameter δ which symbolises the stiffness change is referred to later as “stiffness ratio” and a zero stiffness ratio will mean a linear system.

Again, in order to set up the analogue circuit for the system, equation (7-5) is rearranged into:

$$\ddot{x} = -\{ -F(t) + 2\xi\omega_0\dot{x} + \omega_0^2x + \varphi(x) \} \quad (7-6)$$

With the same viscous damping ratio and the natural frequency as before, the analogue circuit which simulate equation (7-6) is shown in Figure 7-5.

(3) A SDOF System with Piece-wise Stiffness

Piece-wise stiffness is a kind of nonlinear stiffness which is fairly often encountered in practice. It differs from cubic stiffness in that its stiffness change is not continuous and the stiffness effectively consists of a combination of several linear stiffnesses in different response ranges. The backlash stiffness discussed immediately above is a type of piece-wise stiffness. A system with piece-wise stiffness and viscous damping is governed by the following general equation of motion:

$$\ddot{x} + 2\xi\omega_0\dot{x} + \varphi(x) = F(t) \quad (7-7)$$

where $\varphi(x)$ is a piece-wise function, contributing nonlinear stiffness effects and, for instance, this function becomes as below for a bilinear stiffness:

$$\varphi(x) = \begin{cases} \omega_0^2x + \alpha\omega_{01}^2x & x > 0 \\ \omega_0^2x - \beta\omega_{02}^2x & x \leq 0 \end{cases}$$

Again, in order to set up the circuit for a system with piece-wise stiffness, equation (7-7) is rearranged into:

$$\ddot{x} = -(-F(t) + 2\xi\omega_0\dot{x} + \varphi(x)) \quad (7-8)$$

Figure 7-6 shows an analogue circuit which enables us to simulate various types of piece-wise stiffness due to the positions of those switches indicated in this Figure. The piece-wise stiffnesses this circuit enables us to simulate are shown in Table 7-1.

(4) A SDOF System with Nonlinear Quadratic Damping

Nonlinear damping appears to be encountered less often than nonlinear stiffness in practice, although this is actually not the case. This prejudice is partly due to the fact that some dynamic structures are not significantly damped so that nonlinear damping may not contribute as much as nonlinear stiffnesses and hence is not paid as much attention as nonlinear stiffness. For fairly heavily damped structures, nonlinear damping is surely another domain of nonlinearity which cannot be overlooked.

Quadratic damping is one of the many types of nonlinear damping encountered in practical vibration problems. A SDOF system with linear stiffness and quadratic damping can be described by the following equation of motion:

$$\ddot{x} + \alpha |\dot{x}| \dot{x} + \omega_0^2 x = F(t) \quad (7-9)$$

where α is the quadratic damping coefficient.

Equation (7-9) can be rearranged to be suitable for the analogue set-up:

$$\ddot{x} = -(-F(t) + \alpha |\dot{x}| \dot{x} + \omega_0^2 x) \quad (7-10)$$

and the corresponding analogue circuit for this SDOF system having quadratic damping is shown in Figure 7-7.

7-5 THE FREQUENCY RESPONSES OF THE NONLINEAR SYSTEMS

Once a nonlinear system is simulated on an analogue computer, a FRF measurement can be performed as if it were a practical structure. As suggested earlier in this Chapter, sinusoidal excitation is selected to provide the input (force) to the system and the consequent acceleration (or velocity, displacement) of the system is regarded as that of the structure due to the sinusoidal input force. The frequency response function (FRF) of the nonlinear system can then be obtained from a frequency response analyser. The post measurement modal analysis will then be based upon the FRF thus obtained.

However, the most important difference between measuring a simulated nonlinear system and measuring a practical structure should be noted here. When sinusoidal excitation is applied to measure a simulated nonlinear system without using a shaker, the force level for the entire measurement will be constant (mainly controlled by the generator) as the nonlinear property of a shaker which distorts the force level is not present. Therefore, the nonlinearity could be readily exposed and its identification is relatively easy. However, for the measurement of a practical structure, the force level will tend to vary near any resonances which, in turn, influences the effect of the nonlinearity on the frequency response function data.

Figure 7-8 shows the inertance-type frequency response functions obtained from a SDOF analogue system measured using sinusoidal excitation and Figures 7-9 and 7-10 present the corresponding real and imaginary parts plots. The system contains hardening cubic stiffness with different cubic stiffness coefficients. Figure 7-11 shows the frequency response functions of the same system with an unchanged cubic stiffness coefficient while the excitation force level varies and again, the corresponding real and imaginary parts are shown in Figures 7-12 and 7-13. It can easily be seen from Figures 7-10 to 7-13 that increasing the cubic stiffness coefficient has an identical effect on the frequency response function data of the system to increasing the excitation force level. Hence,

although the extent of nonlinearity in practice is virtually impossible to change arbitrarily as the simulated system can be, the effect of different extent of nonlinearity on the the frequency response function of the nonlinear system can still be demonstrated by varying the excitation force level so that the nonlinearity can be fully exposed and identified.

For a SDOF system with backlash stiffness, the frequency response function due to sinusoidal excitation is influenced by the nonlinearity and the excitation force level in a slightly different way to that seen for the cubic stiffness case. There exist three possible conditions for this simulated SDOF system to vary and they are (a) the excitation force level, (b) the response limit and (c) the stiffness ratio - both parameters having been defined in equation (7-5). The frequency response of this system due to the change of each condition is studied.

Figures 7- 14 to 7- 16 show the frequency response functions and their corresponding real and imaginary parts obtained from a SDOF analogue system by using sinusoidal excitation. The system containing hardening backlash stiffness has an unchanged stiffness ratio and response limit as the excitation force level varies. The comparison of Figure 7-14 with Figure 7-11 will reveal the different effects of excitation force level on the frequency response functions in these two cases, although they are all hardening-type stiffness. For the cubic stiffness case, the frequency response function is affected continuously by the excitation force level and this effect becomes greater as the excitation frequency approaches the resonance frequency. However, the effect of increasing the excitation force level for the backlash stiffness case does not show up unless the response of the system exceeds a certain value, and this value is relevant to the excitation force level itself. The difference discovered here could be a useful indication of distinguishing between these two types of hardening stiffness.

Figure 7-17 shows the frequency response functions of the same system containing backlash stiffness with an unchanged *stiffness* ratio and a constant excitation level while the response limit varies. It is evident by comparing Figure 7-17 with Figure 7-14 that

the response limit varies. It is evident by comparing Figure 7-17 with Figure 7-14 that decreasing the response limit of the system will have a similar effect on the frequency response function to increasing the excitation force level. Figure 7-18 shows the frequency response functions with an unchanged response limit and a constant excitation level while the stiffness ratio of the system varies. It is interesting to note that the consequence of different stiffness ratios does not show up until the response reaches a certain level - which is believed to be the response limit of the system - and the frequency response functions diverge more from the one without nonlinearity as the stiffness ratio becomes bigger. For nonlinear damping cases, such a SDOF system also simulated on analogue computer with quadratic damping, measurement can be carried out similarly using sinusoidal excitation. Figure 7-19 shows the FRF data with different extent of quadratic damping. It is evident that the natural frequency of the system changes little, while the response is obviously governed by the damping extent.

As suggested above, the frequency response of a nonlinear system due to random excitation will appear to be that of a linear system. This is because most types of nonlinearity are excitation amplitude-dependent while the random force signal has randomly varying force amplitude and phase angle. Therefore, the response of a nonlinear system due to random excitation becomes an averaged result due to the different force amplitude and as a consequence, the effect of the nonlinearity is linearised. To appreciate this, random excitation is used in the measurement of the simulated nonlinear systems discussed above. The measured frequency response function data eventually show apparently linear behaviour for the nonlinear systems.

To understand fully the linearisation consequence of random excitation tests, questions about the Fourier Transform algorithm have to be answered. As the Fourier Transform is a linear operation, suggestions of this algorithm linearising the nonlinearity could be found in some **literature**^[61]. In this study, a special investigation was carried out: sinusoidal excitation is used for the nonlinear systems while the frequency response analysis is performed by an FFT analyser. It is found that as the excitation frequency

sweeps, the frequency response function obtained by **FFT** exhibits exactly the same results as shown in Figures 7-8 to 7-17 which are obtained from frequency response analyser. This verifies the discussion in the earlier part of this Chapter - the Fourier Transform is not responsible for the linearisation of the effect of nonlinearity in measurement using random excitation. It is the randomness of the force amplitude and phase angle of the input signal which linearise the response of a nonlinear system and makes the system behave as a linear system

7-6 CONCLUSIONS

Nonlinearity is a widely-encountered phenomenon in practical dynamic structures. It is sometimes neglected because of its small extent and little contribution to the vibration response, but for many other cases, lack of proper means to deal with the nonlinearity could be the primary reason for ignoring it.

Theoretically, the main difficulty introduced by the nonlinearity is that the superposition principle whereby the response of a system to different excitations can be added linearly is violated for nonlinear systems. As a consequence, the dynamic characteristics of nonlinear structures become excitation-dependent and much less easily predicted.

It is believed that theory has been highly developed for those nonlinear systems whose equations of motion are expressible analytically. There are currently quite a number of methods which are available to examine the vibration behaviour of a known nonlinear system.

However, since the nonlinearity inherent in vibrating structures is difficult to identify and even much more difficult to quantify, such theory is often not directly applicable to experimental modal analysis because of the absence of explicit equations of motion. The efforts of nonlinearity study in practical vibration analysis are then focussed on the detection and the identification of nonlinearity in structures from measured FRF data

Since the effects of most kinds of nonlinearity frequently encountered in structural dynamics are characteristically variable due to the external excitation, the first problem of the nonlinearity investigation will be to choose a proper excitation force so that the nonlinearity could easily be exposed and then detected and identified. Amongst those excitation methods currently widely used in vibration study, the sinusoidal excitation method is strongly favored for nonlinearity investigation.

Analogue computer simulation is advantageous for nonlinearity investigations. This is mainly because a nonlinear system can easily be simulated on an analogue computer and the parameters of the system can then be conveniently adjusted to represent different extent of nonlinearity. Hence, the response of the simulated nonlinear system can be obtained and the vibration characteristics of the nonlinear system can then be thoroughly investigated which, in turn, will be referenced for the nonlinearity investigation of the practical structures.

SDOF systems with some frequently encountered types of nonlinearity are successfully simulated on an analogue computer. Among those types of nonlinearity are cubic stiffness, backlash stiffness, quadratic damping and various kinds of piece-wise stiffness. Measurement using the sinusoidal excitation method can then be performed to obtain the frequency response functions of these nonlinear systems. The refined modal analysis can be carried out to detect and identify the nonlinearity by analysing these measured frequency response function data and this will be extensively studied in the next Chapter.

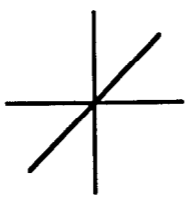
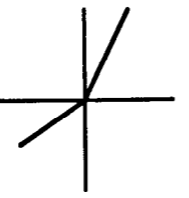
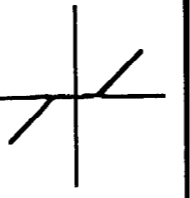
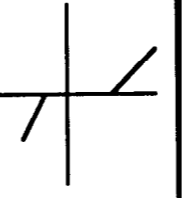
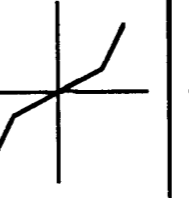
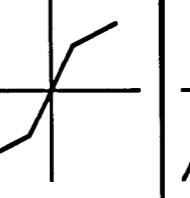
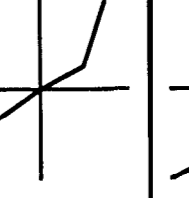
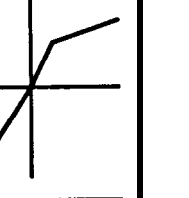
Type	Linear	Bilinear	dead lock	Asymmetric dead lock	Hardening backlash	Softening backlash	Asymmetric hardening backlash	Asymmetric softening backlash
Char								
Condition								
Switch 1	A	A	B	B	A	A	A	A
Stitch 2	Z	X	Y	Y	Y	X	Y	Y
coefficient multiplier k1	0	$0 < k1 < 1$	$\neq 0$	$\neq 0$	$\neq 0$	$\neq 0$	$\neq 0$	$\neq 0$
coefficient multiplier k2	$= 0$	1	1	$\neq 1$	1	1	$\neq 1$	$\neq 1$
Backlash quantity		$E1=0$ $E2=\text{maximum}$	$E1=E2 \neq 0$	$E1 \neq E2 \neq 0$	$E1=E2 \neq 0$	$E1=E2 \neq 0$	$E1 \neq E2 \neq 0$	$E1 \neq E2 \neq 0$

Table 7-1
Various types of piece-wise nonlinear stiffnesses

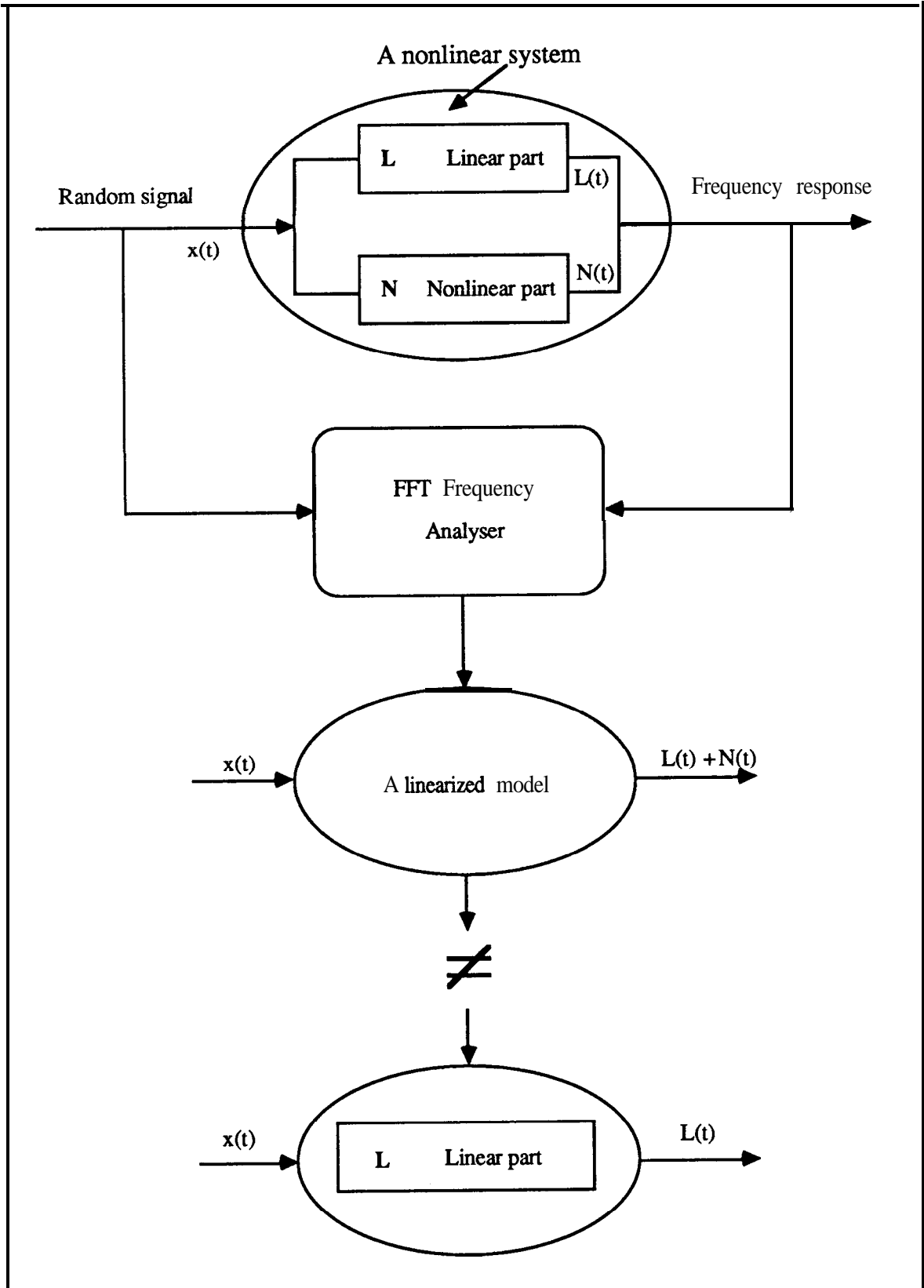


Figure 7-1 Linearisation effect of random excitation test

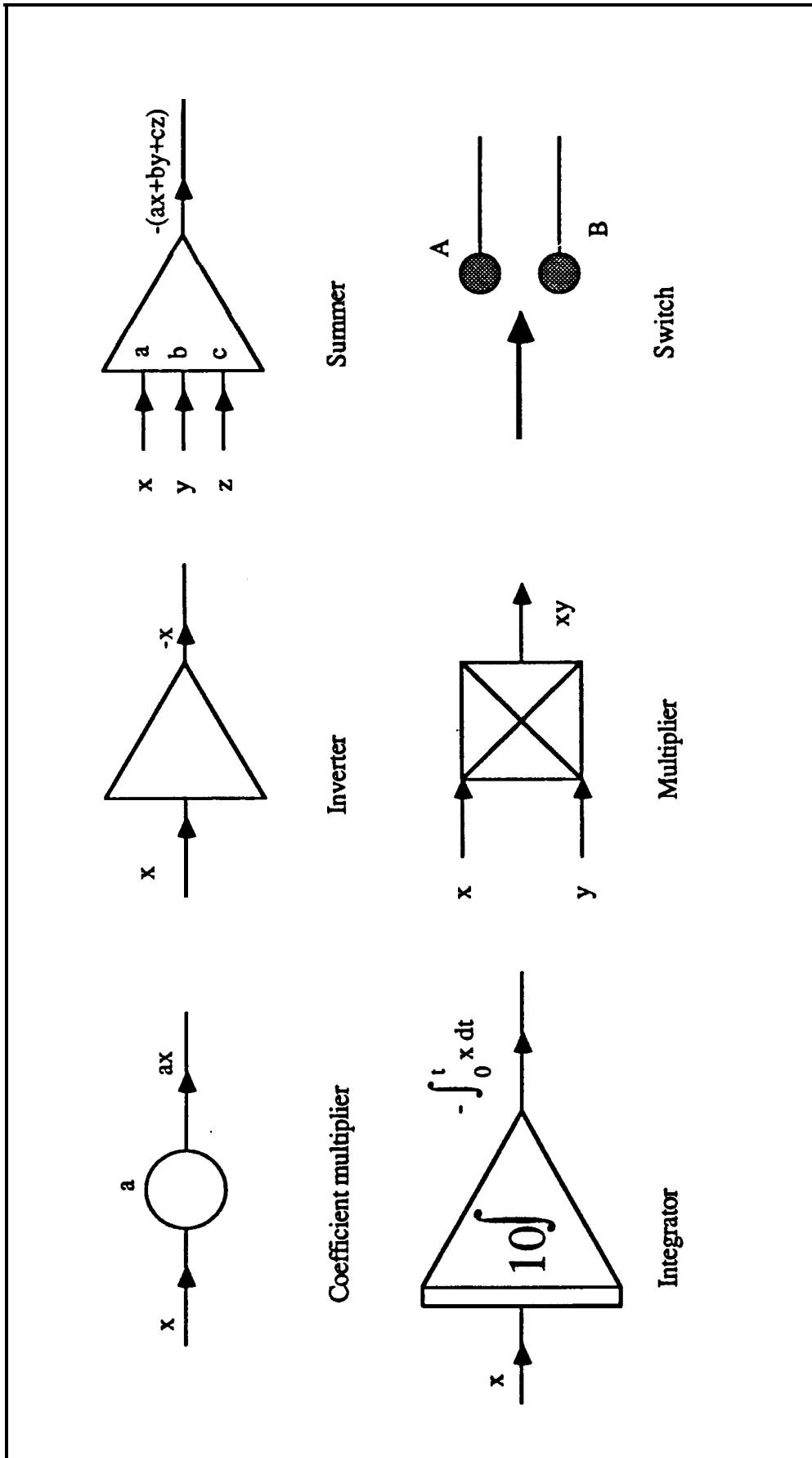


Figure 7-2 Basic elements of an analogue computer

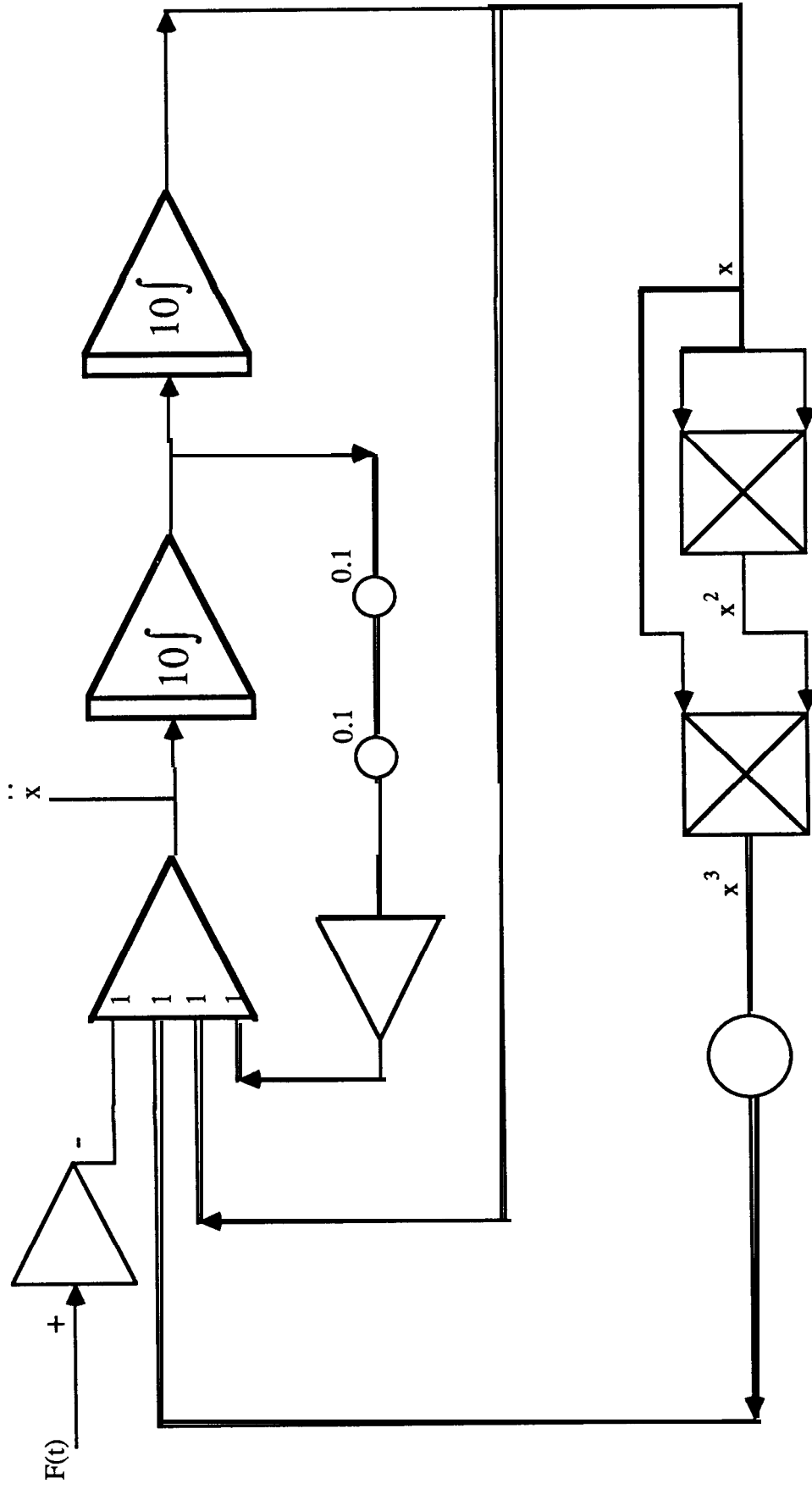


Figure 7-3 A SDOF system with hardening cubic stiffness

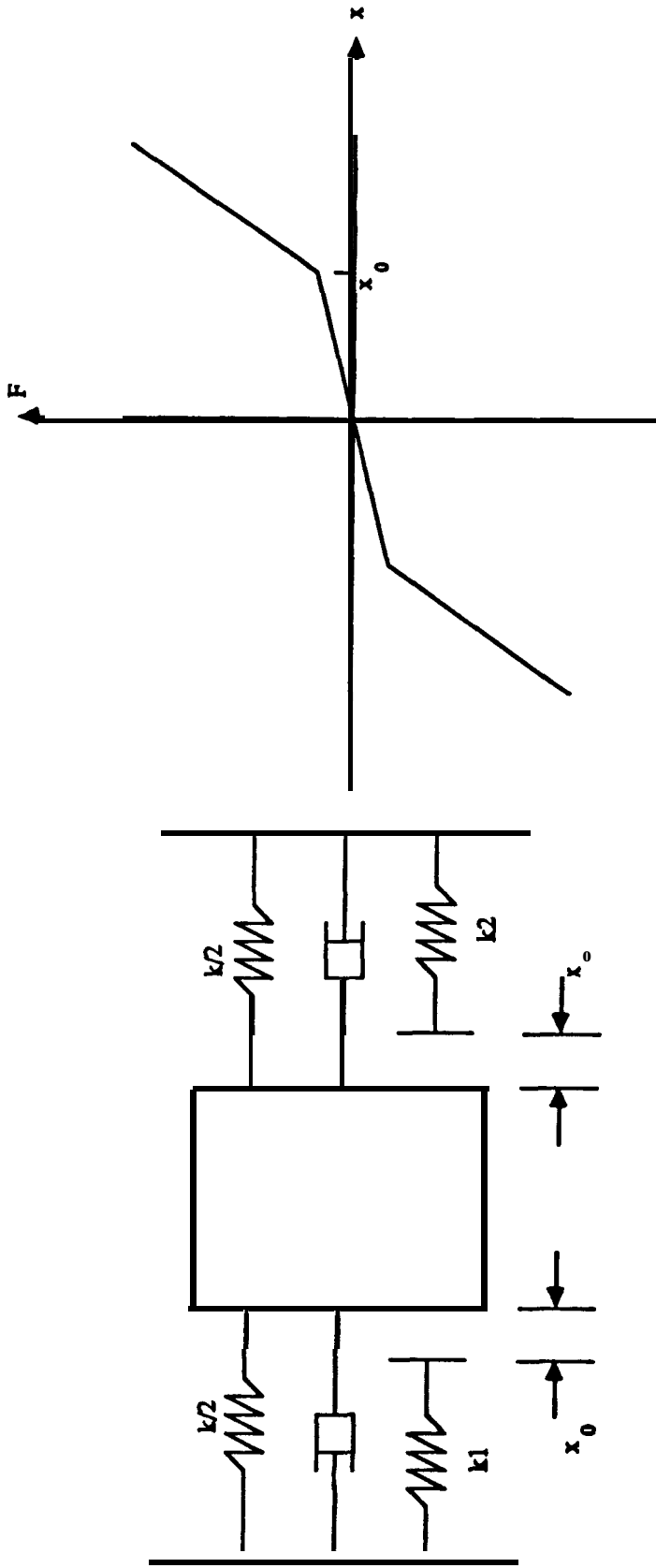


Figure 7-4 A SDOF system with backlash stiffness and its stiffness characteristics

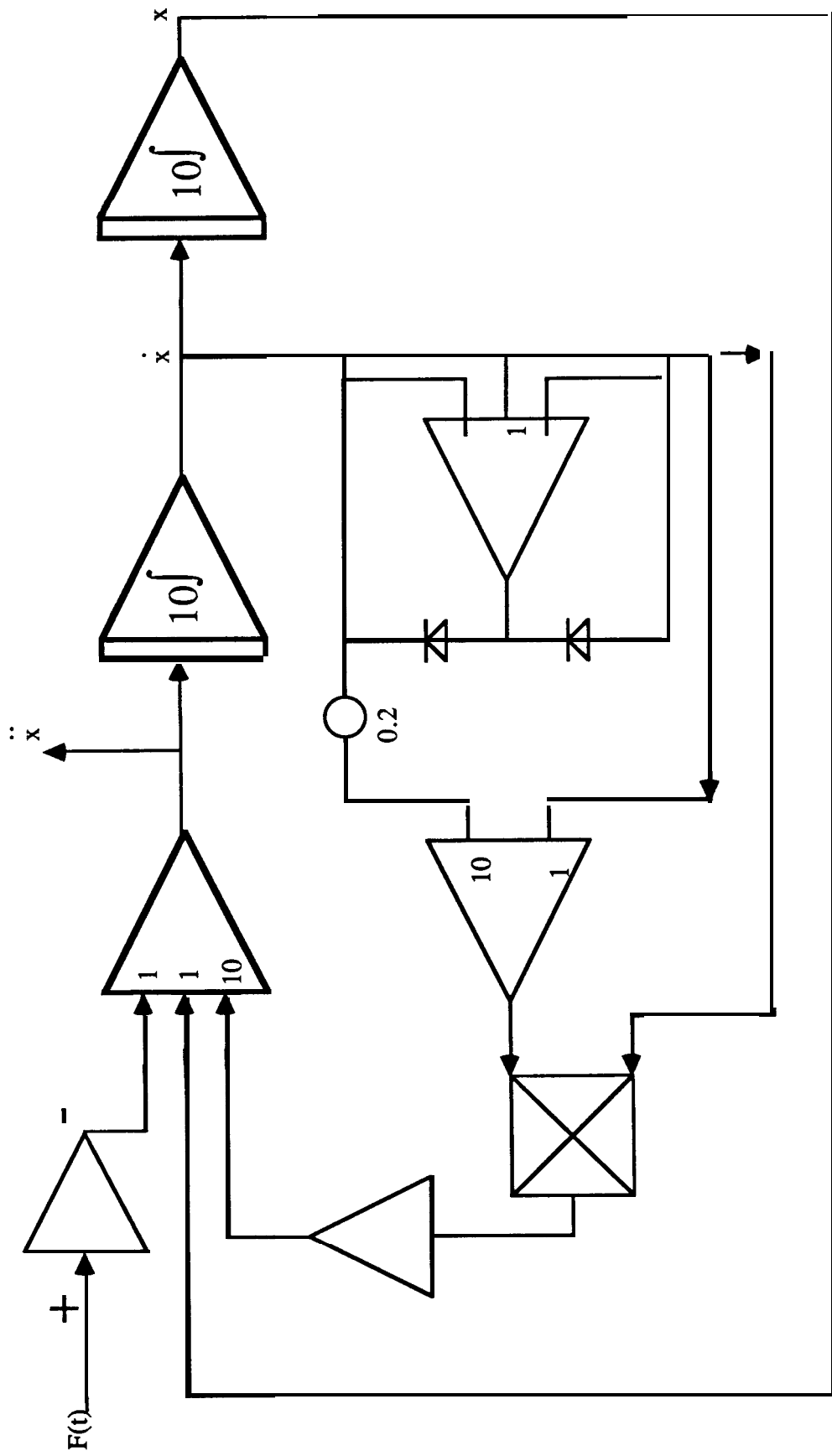


Figure 7-7 A SDOF system with quadratic damping

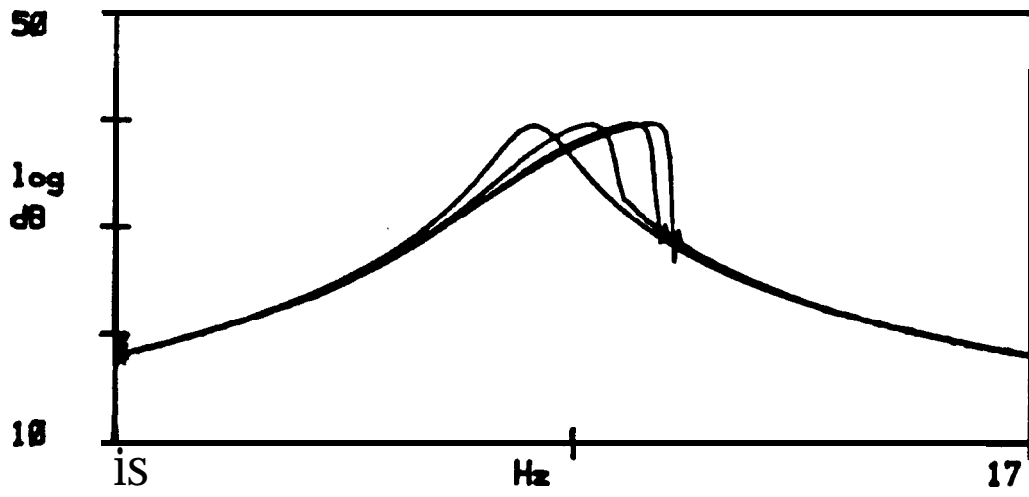


Figure 7-8 Inertance frequency response functions obtained from a SDOF system with different extent of hardening cubic stiffness using sinusoidal excitation.

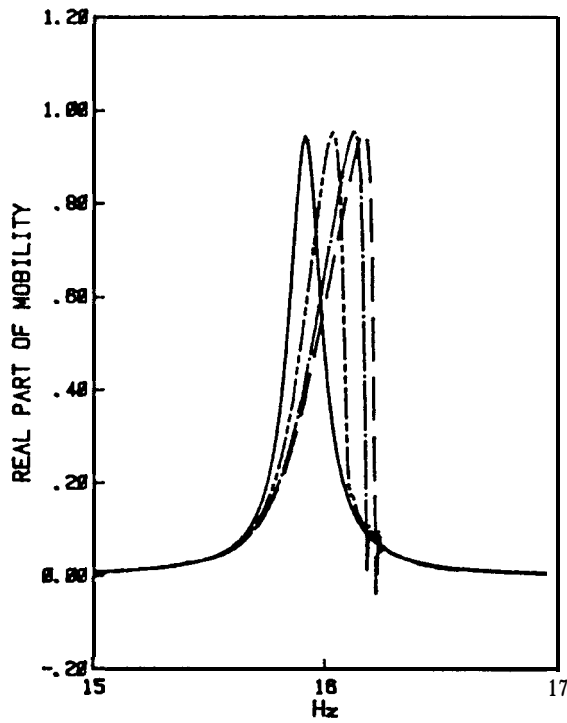


Figure 7-9 Real parts of the frequency response functions shown in Figure 7-8.

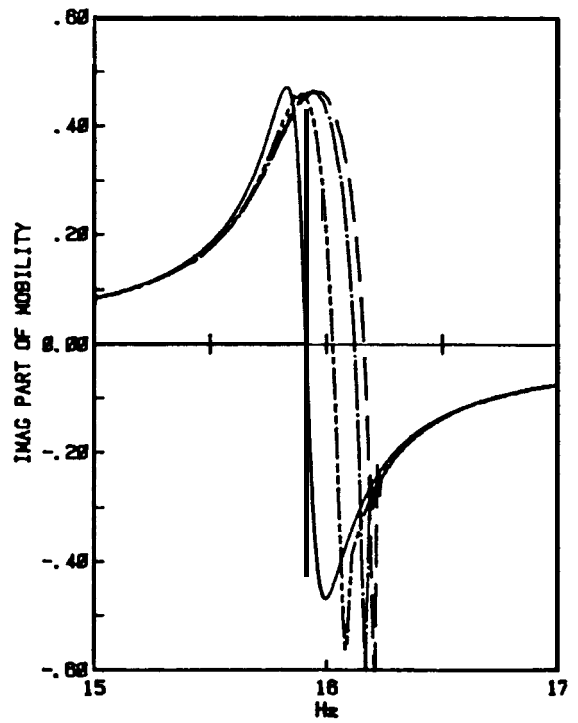


Figure 7-10 Imaginary parts of the frequency response functions shown in Figure 7-8.

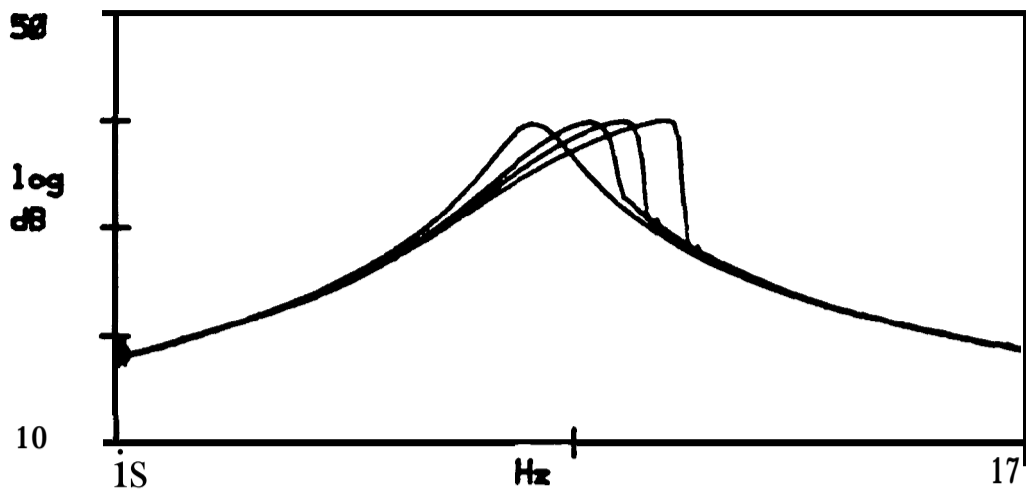


Figure 7- 11 Inertance frequency response functions obtained from a SDOF system with hardening cubic stiffness using different sinusoidal excitation levels.

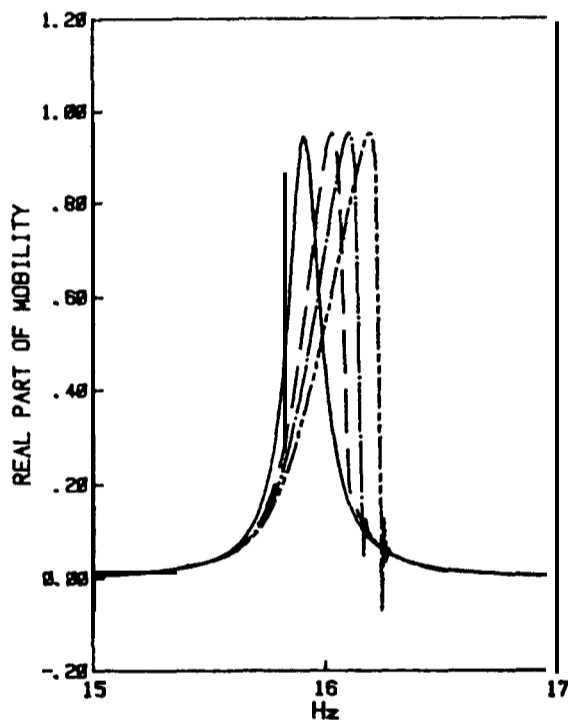


Figure 7-12 Real parts of the frequency response functions shown in Figure 7- 11.

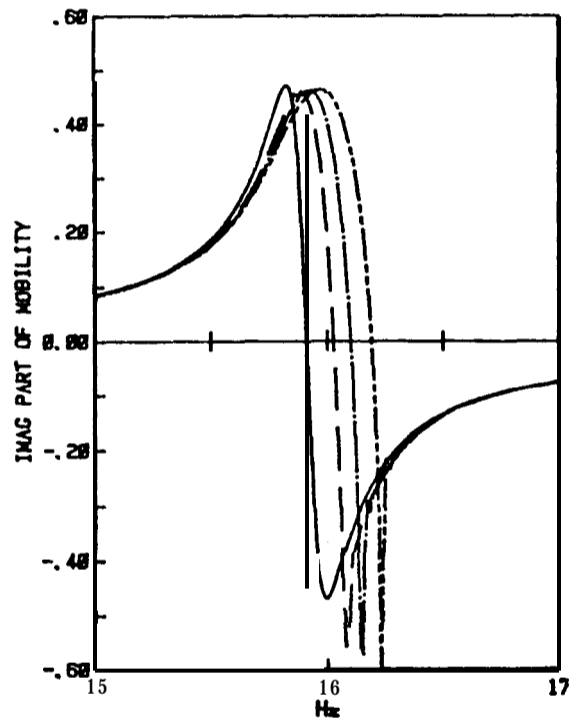


Figure 7-13 Imaginary parts of the frequency response functions shown in Figure 7- 11.

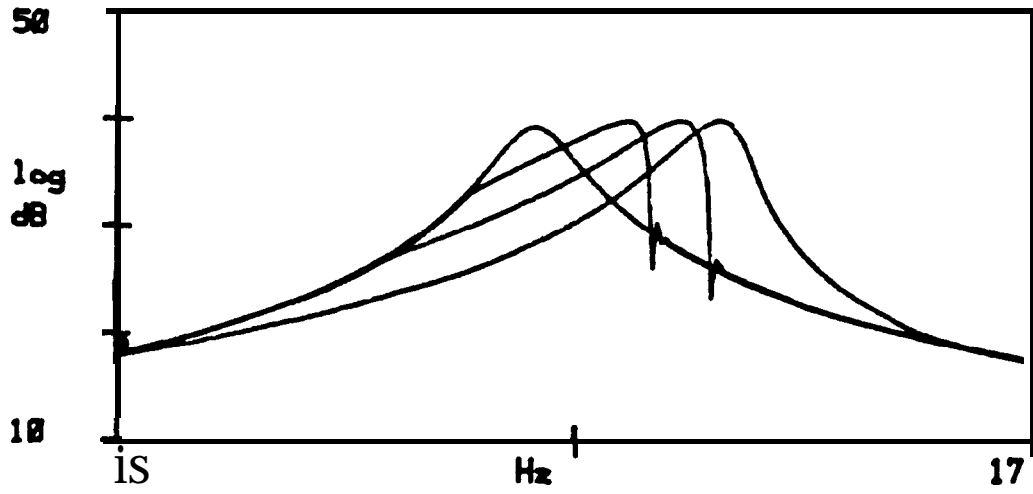


Figure 7-14 Inertance frequency response functions obtained from a SDOF system with hardening backlash stiffness using different sinusoidal excitation levels.

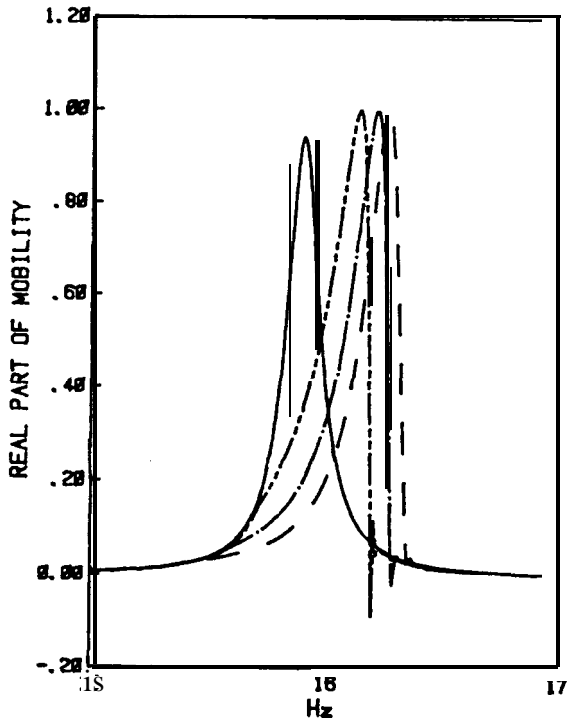


Figure 7-15 Real parts of the frequency response functions shown in Figure 7-14.

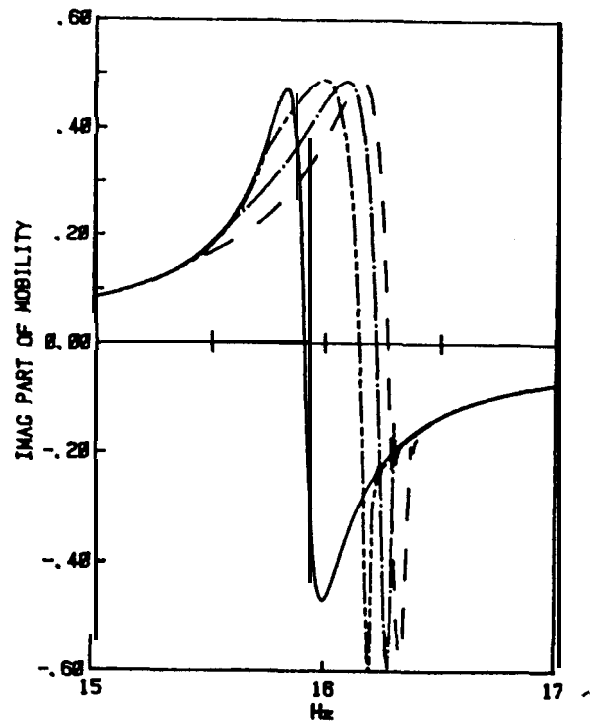


Figure 7-16 Imaginary parts of the frequency response functions shown in Figure 7-14.

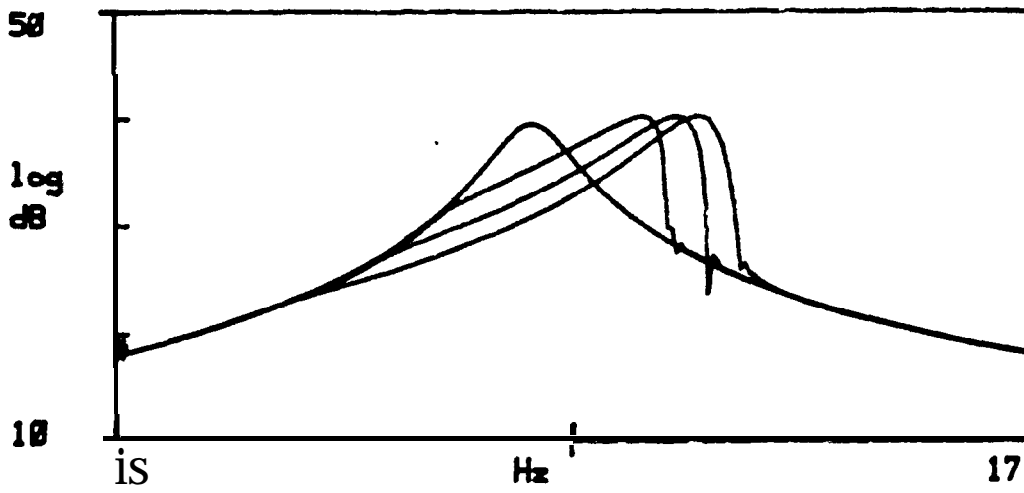


Figure 7-17 Inertance frequency response functions obtained from a SDOF system with different response limits of hardening backlash stiffness using sinusoidal excitation.

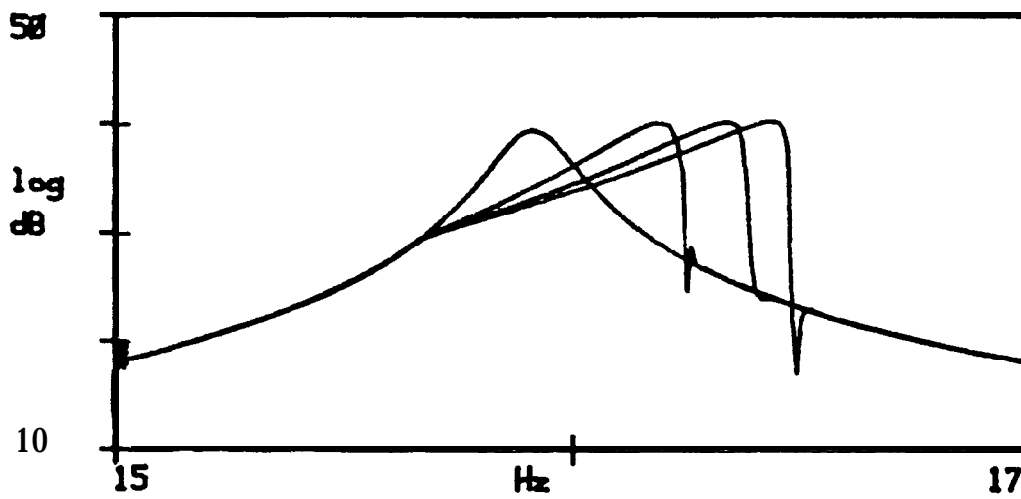


Figure 7-18 Inertance frequency response functions obtained from a SDOF system with different stiffness ratio of hardening backlash stiffness using sinusoidal excitation.

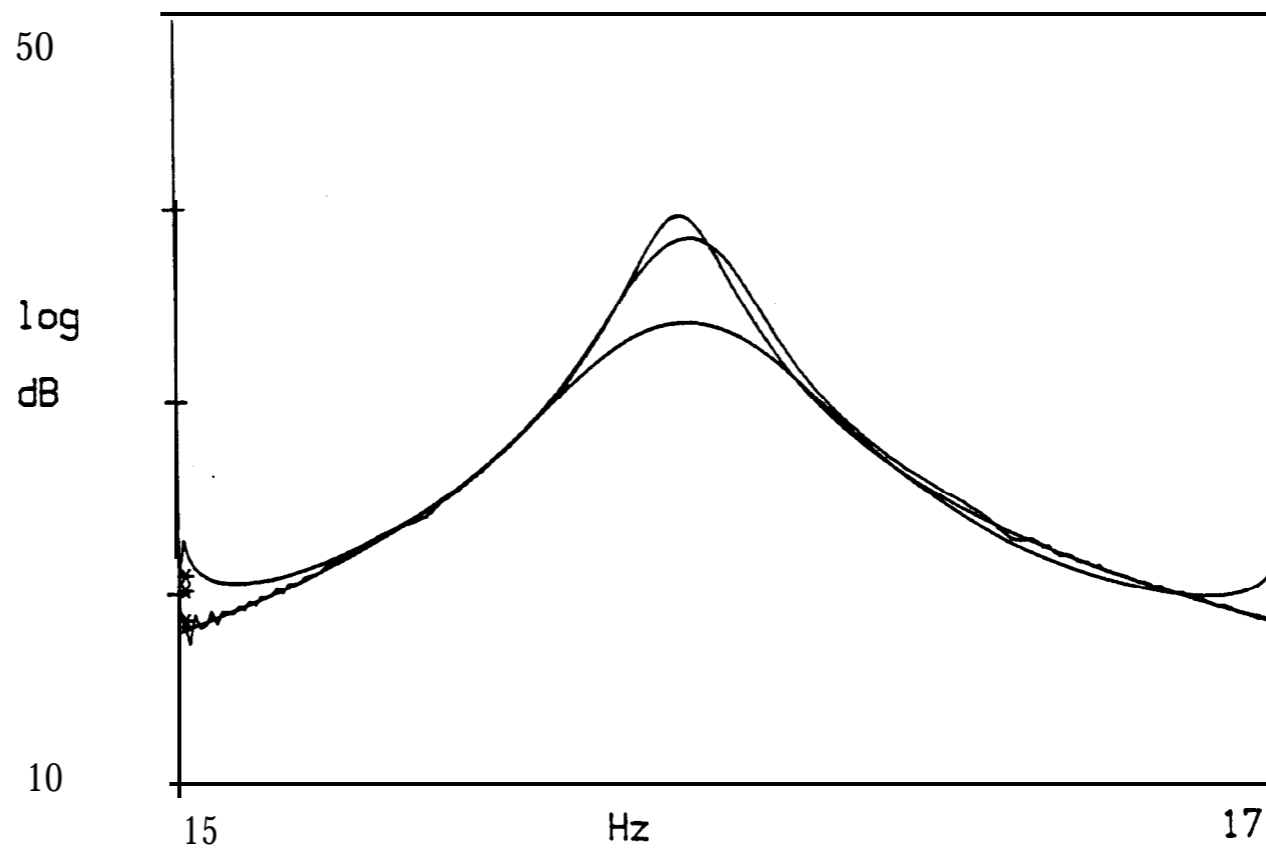


Figure 7-19 Inertance frequency response functions obtained from a SDOF system with different extent of quadratic damping using sinusoidal excitation.

CHAPTER 8

CHAPTER 8

MODAL ANALYSIS OF NONLINEAR SYSTEMS

8-1 CURRENT METHODS AND APPLICATIONS OF MODAL ANALYSIS FOR NONLINEAR SYSTEMS

Once it is suspected that a structure or a system is nonlinear, and measurement is carried out as discussed extensively in the last Chapter, it is necessary to analyse the frequency response function data taking account of the effect of possible nonlinearity. The application of modal analysis methods to such FRF data depends upon the different requirements on the nonlinearity investigation of the system. Generally speaking, there are three possible requirements in practice for the results of modal analysis of a nonlinear system. First, a linearised model may be required whose vibration response will be as close as possible to the actual vibration response of the nonlinear system. Second, the type of nonlinearity might need to be identified in order to enable the possible establishment of a correct mathematical model of the nonlinearity and to seek the possibility of predicting the vibration response of the nonlinear system to a wide range of excitation conditions. Third, the identified type of nonlinearity is to be quantified in some extent.

It is believed that the first requirement - to obtain a **linearized** model for a nonlinear system without seeking the nature of the nonlinearity - is comparatively easy to achieve. In fact, a family of frequency response functions with different random excitation force levels could always be measured, as suggested in the Chapter 7, and a conventional linear modal analysis algorithm be employed to build up a series of models, each of them representing the vibration behaviour of the nonlinear system under conditions of a certain excitation force level. It is worth noting that such an investigation does not tell the nature and extent

of the nonlinearity but, instead, it simplifies the nonlinearity problem by a piecewise **linearization** approach.

However, practice is often confronted with the requirement of understanding the nature, and even the extent, of the nonlinearity of a dynamic structure. Hence, current modal analysis efforts are directed towards the detection of nonlinearity, and the identification of the type and extent of nonlinearity in structures. To summarize, the following three questions are to be answered by the appropriate application of modal analysis methods to structures which might be nonlinear (Figure 8-1).

- (1) Is the system or structure nonlinear?; (detection)
- (2) If yes, what kind of nonlinearity does it exhibit?; and (identification)
- (3) What is the extent of the nonlinearity? (quantification)

A large number of papers dealing with nonlinearity can be found in the literature in recent years. As far as the detection and the identification of nonlinearity from the modal test data is concerned, the methods commonly employed nowadays can be summarised below. It is important to bear in mind that sinusoidal excitation is preferred in modal tests for all these methods in order to let the nonlinearity be properly exposed rather than be averaged out as happens in random excitation conditions. The advantages and disadvantages of those methods currently used and summarised below will be discussed and the direction of further developments will then be pointed out.

8-1-1 Bode Plots

The basis of using Bode plots to detect the possible existence of nonlinearity, and to identify it, is that the nonlinearity should systematically distort the frequency response function data and its real and imaginary parts from the form of the corresponding linear system's FRF data. As the linear system's frequency response function is very well **recognized**, the possible existence of nonlinearity could then be revealed by examining the abnormal behaviour of the real and imaginary parts of the frequency response function

data.

A typical example of nonlinearity being evident in the Bode plot is provided by the frequency response function data shown in Figure 7-11 and its corresponding real and imaginary parts shown on Figures 7-12 and 7-13. The system from which these data are derived has hardening cubic stiffness and it can be seen that this nonlinearity is clearly exposed on the data. Similarly to this cubic stiffness case, the frequency response function and its corresponding real and imaginary parts obtained from another SDOF system, this time with backlash stiffness, are shown in Figures 7-14 to 7-16. Again, the existence of the nonlinearity is apparent from the systematic distortion in the plots.

Although Bode plots of the frequency response function data can reveal the existence of possible nonlinearity in most cases, it is after all merely a straightforward presentation and no analysis of nonlinearity is involved. As a consequence of its simplicity, this method usually cannot distinguish one type of nonlinearity from the other - e.g. the cubic stiffness and backlash stiffness - when their effects on the frequency response function data are fairly similar. Therefore, Bode plots can only be used to provide a rough and basic examination of the existence of nonlinearity.

8-1-2 Reciprocal of Frequency Response Function

The Reciprocal of frequency response function data, which was previously discussed briefly in Chapter 4, is offered as an alternative to modal analysis by the Nyquist circle fit. It is based upon an assumption of SDOF behaviour. Basically, it is supposed that, neglecting the residual effects of all other modes, the r^{th} mode of the frequency response function (receptance) data of a structure will yield:

$$\alpha_{jl} = \frac{rA_{jl}}{\omega_r^2 - \omega^2 + i\eta_r\omega_r^2} \quad (8-1)$$

where: α_{jl} is the receptance between test points j and l ;

- rA_{jl} is modal constant;
- ω_r^2 is the natural frequency;
- η_r is the damping loss factor.

Although the modal constant is in theory a complex quantity, it is often effectively real and is treated thus here for this approach. The corresponding reciprocal of receptance &ta is:

$$\begin{aligned}
 (1/\alpha_{jl}) &= \frac{\omega_r^2 - \omega^2 + i\eta_r\omega_r^2}{rA_{jl}} & (8-2) \\
 &= (\omega_r^2 - \omega^2)/rA_{jl} + i\eta_r\omega_r^2/rA_{jl} \\
 &= \text{Re}(1/\alpha_{jl}) + \text{Im}(1/\alpha_{jl})i
 \end{aligned}$$

Perhaps the most significant advantage of using the reciprocal of receptance data is that the mass and stiffness characteristics (natural frequency and modal constant in modal data) and damping property (damping loss factor in modal data) are separated out into the real and imaginary parts of the data respectively and hence, they can be dealt with separately. In this case, the estimation of natural frequency and modal constant will be considerably less affected by the damping loss factor than happens in the Nyquist circle-fit or MDOF curve-fit, since this estimation is carried out only on the real part of the reciprocal of receptance data, and which is physically quite reasonable. Similarly for the estimation of damping loss factor, for the same reason. In addition, the extraction of modal data from the reciprocal of the receptance data will not require the condition of equal frequency spacing of the data which Nyquist circle-fit does.

The significant advantage of using the reciprocal of the receptance data becomes evident when modal analysis is made of FRF data from systems with nonlinearity. In these cases, the effects of a nonlinear stiffness will show up on the real part of the reciprocal of receptance data while the imaginary part of the data will be dominated by the effect of the damping. Figure 8-2 shows the real and imaginary parts of the reciprocal of FRF data of

a SDOF system with hardening cubic stiffness. It can be seen that the effect of the nonlinear stiffness distorts the real part data noticeably but the imaginary part remains just as for the linear case since the system here does not have any nonlinearity in the damping. In Figure 8-3, similar real and imaginary parts of the reciprocal of FRF data for a SDOF system with hardening backlash stiffness are presented. Again, the effect of the nonlinear stiffness is clearly observed confined to the real part data.

This characteristic - that the effect of stiffness nonlinearity only shows up in the real part - is in contrast with the standard FRF data format where the effect of any type of nonlinearity will influence both its real and imaginary parts equally (e.g. the real and imaginary parts of inertance FRF data). This is due to the fact that the real and imaginary parts of the FRF data are related to each other and it will be seen in later discussion that the **Hilbert** transformation makes use of this relationship between the real and imaginary parts of the FRF data to investigate nonlinearity.

S-1-3 Modal Analysis and the Isometric Damping Plot

The isometric damping plot is one of the simpler methods available for the modal analysis of nonlinear systems. Its application to the detection and identification of nonlinearity relies on the argument that the nonlinearity will distort the spacing of the frequency response function data along the Nyquist circle from their positions when no nonlinearity exists. Its effect is unlike noise on the measurements, which also tends to distort the FRF data, because the distortion provoked by nonlinearity is systematic rather than random. Due to this character of systematic distortion, the damping estimates will vary according to the specific point selection around the Nyquist circle and the nature of the distortion displayed by the different damping estimates indicates the existence of nonlinearity. The following analysis seeks to explain the mechanism in detail.

It is well known that the damping loss factor for a vibration mode can be estimated by curve-fitting the Nyquist circle (as shown in Figure 8-4) and using the following

equation:

$$\eta_r = \frac{\omega_a^2 - \omega_b^2}{\omega_r^2 \{ \tan(\theta_a/2) + \tan(\theta_b/2) \}} \quad (8-3)$$

where ω_a and ω_b are frequencies for two data points, one before and one after the identified natural frequency. Also, it is known that for the FRF data from a linear system without noise pollution, the damping estimate in equation (8-3) will theoretically be the same no matter what pair of points on the Nyquist circle are chosen.

If the system is nonlinear, however, and the nonlinearity distorts the spacing of the FRF data on the Nyquist circle systematically, as noted above, then the damping estimates from equation (8-3) will also vary systematically depending on the different points selected, and variation in damping estimates becomes a good indication of the nonlinearity. Figure 8-5 shows the Nyquist plot of the FRF data for a SDOF system with hardening cubic stiffness and the corresponding isometric damping plot. It can be seen that the nonlinear stiffness produces typical damping variation on the isometric damping plot. In Figure 8-6, a similar Nyquist plot of the FRF data from a SDOF system with hardening backlash stiffness and the isometric damping plot are shown. Again, the damping variation in the isometric damping plot caused by the nonlinearity exhibits a strong characteristic.

8-14 The Hilbert Transform

The Hilbert transform is a method for calculating the imaginary part of a complex frequency response function from its real part (and vice versa), under certain conditions. According to the **Cauchy-Rieman** theorem, a mathematically **harmonic** complex analytical function possesses the property that its real part can be derived from its imaginary part and vice versa. This relationship is known as a Hilbert transform pair. In recent years, **the** Hilbert transform technique has been borrowed from control engineering and applied **to** vibration research for the identification and analysis of nonlinearity in structural

dynamics. In the following, the definition of the Hilbert transform will be briefly reviewed and the basis for its application to modal analysis will be outlined, together with several application examples.

S-141 The Principle of the Hilbert Transform

The Hilbert transform of a mathematical function $f(x)$ is defined as an integral and is denoted as \mathbf{H} :

$$\begin{aligned} F(x) &= \frac{1}{j} \int_{-\infty}^{\infty} f(x') \frac{dx'}{x'-x} \\ &= \mathbf{H}[f(x)] \end{aligned} \tag{8-4}$$

The integral $F(x)$ is a linear functional of $f(x)$ and it can be shown from the theory of random vibration that the integral in equation (8-4) can be obtained by convolving the mathematical function $f(x)$ with $(-\pi x)^{-1}$, namely,

$$F(x) = (-1/\pi x) f(x) \tag{8-5}$$

or $\mathbf{H} [f(x)] = (-1/\pi x) f(x)$

Since the Fourier transform of $(-1/\pi x)$ is $i(\mathbf{s g n co})$, where $\mathbf{s g n}$ is a sign function and i is imaginary unity, it can be said that the Hilbert transform is equivalent to a particular kind of filtering in which the amplitude of the spectral components are left unchanged but their phases are altered by $\pi/2$. Thus, the application of the Hilbert transformations twice in succession will reverse the phase of all components and the results will be the negative of the originals:

$$f(x) = -(-1/\pi x) F(x) \tag{8-6}$$

$$f(x) = -1/\pi \int_{-\infty}^{\infty} F(x') \frac{dx'}{x'-x} \tag{8-7}$$

or

$$f(x) = -\mathbf{H}[F(x)]$$

8-1-4-2 Basis of the Application of the Hilbert Transform to Modal Analysis

The frequency response function of a dynamic system $G(\omega)$, which is a function of frequency ω , is the Fourier transform of $I(t)$, the impulse response function of the system which is a time varying function^[76]:

$$G(\omega) = \int_{-\infty}^{\infty} I(t) e^{-i\omega t} dt \tag{8-8}$$

or $G(\omega) = \mathbf{F}[I(t)]$

where \mathbf{F} denotes the Fourier transformation in this work.

Since the impulse response $I(t)$ from a linear system is real and causal (a system is causal if, for any input, the response at any instant of time does not depend upon the future input: a linear dynamic system should always be causal), it can always be split into even and odd parts:

$$\begin{aligned} I(t) &= I(t)_{\text{even}} + I(t)_{\text{odd}} \\ &= \{I(t) + I(-t)\}/2 + (I(t) - I(-t))/2 \end{aligned} \tag{8-9}$$

and the even and odd parts can be linked together by the following equation:

$$I(t)_{\text{odd}} = I(t)_{\text{even}} \mathbf{sgn}(t) \tag{8-10}$$

Since the Fourier transform of the sign function $\mathbf{sgn}(t)$ is:

$$\mathbf{F}[\mathbf{sgn}(t)] = -i/\pi\omega \tag{8-11}$$

the Fourier transformation of both sides in equation (8-10) yields:

$$\begin{aligned} \mathbf{F}[I(t)_{\text{odd}}] &= \mathbf{F}[I(t)_{\text{even}}] \mathbf{F}[\mathbf{sgn}(t)] \\ &= \mathbf{F}[I(t)_{\text{even}}] (-i/\pi\omega) \end{aligned} \tag{8-12}$$

It can be validated **theoretically**^{[74],[75],[76]} that, for a linear dynamic system, the real part of the frequency response function $G(\omega)$ is the Fourier transform of the even part of the impulse response function $I(t)$, and the imaginary part of $G(\omega)$ is the Fourier transform of the odd part of $I(t)$, namely:

$$\text{Re}(G(\omega)) = \mathbf{F} [I(t)_{\text{even}}] \quad (8-13a)$$

$$\text{Im}(G(\omega)) = \mathbf{F} [I(t)_{\text{odd}}] \quad (8-13b)$$

Thus, it can be shown as below that the imaginary part of the frequency response function $G(\omega)$ can be obtained from the Hilbert transform of its real counterpart (the same argument holds for the other way around):

$$\begin{aligned} \mathbf{H}[\text{Re}G(\omega)] &= (-i/\pi\omega) \text{Re}(G(\omega)) \\ &= \mathbf{F} [\mathbf{F}^{-1}[(-i/\pi\omega) \text{Re}G(\omega)]] \\ &= \mathbf{F} [[\text{sgn}(t) I(t)_{\text{even}}]] \\ &= \mathbf{F} [[I(t)_{\text{odd}}]] \\ &= \text{Im}G(\omega) \end{aligned}$$

Therefore, it is demonstrated by the above analysis that for a linear vibrating system, the entire frequency response function can be constructed by knowledge of either its real or its imaginary parts only or, in other words, either one of them determines completely the vibration characteristics of the system. It should be borne in mind that although it is suggested above that the impulse response is obtained from test, this is merely for the sake of simplicity to depict the theory. In practice, any kind of measurement technique could be used and the inverse of Fourier transformation of the frequency response function should always provide the impulse response of the system, provided this is

linear and no noise pollution is involved.

If a system is nonlinear, then its impulse response from an impulse test is normally still causal, provided the system is time-invariant as most structures in practice are. However, the inverse Fourier transform of the frequency response function obtained from a sinusoidal excitation, which is suggested in Chapter 7 as a favorable measurement technique, would become noncausal due to the **nonlinearity**[74],[75]. Thus, the result of the Hilbert transform of the real part of the FRF data will not be the same as the imaginary part of the FRF as it will be distorted by the nonlinearity, nor will the transform of the imaginary part be the same as the real part, as illustrated in Figure 8-7.

To apply the Hilbert transform to the detection and identification of nonlinearity in vibration studies, the frequency response function of a vibrating system from sinusoidal test is used and the Hilbert transform of its real part can be calculated (as can its imaginary part) and compared with its imaginary part. Any discrepancy between the Hilbert transform of the real part of the FRF and its imaginary part will then indicate the existence of nonlinearity, provided the computation of the Hilbert transform is accurate enough. Once different types of nonlinearity can be simulated, studied and categorized by the Hilbert transformation, the nonlinearity found in test data could be identified with a reference to those categorized nonlinearity.

Figure 8-8 shows the real and imaginary parts of the FRF for a SDOF system with hardening cubic stiffness and also the Hilbert transform of each. It can be seen that the existence of the nonlinear stiffness results in a discrepancy between the original FRF and the Hilbert transform counterparts. In Figure 8-9, a similar FRF of a SDOF system with hardening backlash stiffness and the Hilbert transforms are shown. Again, the discrepancy caused by the nonlinearity is evident. These discrepancies could also be examined in Nyquist plane.

8-2 COMMENTS ON CURRENT METHODS FOR MODAL ANALYSIS OF NONLINEARITY

Amongst those methods currently used for the modal analysis of nonlinear systems and outlined above, the methods based on the Bode plot and on the reciprocal of FRF data can be categorized as types which aim at presenting the FRF data in such a way as to show up the nonlinearity. It might be thought that when the FRF data are presented in some other way, such as the inverse of the Nyquist circle (which is a straight line for linear cases), the effect of an existing nonlinearity could also be expected. Therefore, it is believed that these two methods are convenient for a straightforward inspection for the existence of nonlinearity but this approach is not rigorous enough for a precise modal analysis of the nonlinearity.

On the other hand, two other methods, namely the isometric damping plot and the Hilbert transformation, tend to detect and to identify nonlinearity by investigating its effect on the FRF data. Specifically, the isometric damping plot method demonstrates the spacing distortion caused by the nonlinearity and the Hilbert transform examines the violation of the functional properties of the frequency response function introduced by the nonlinearity.

An overall and thorough examination of the application of these four methods - (i) Bode plot, (ii) reciprocal of frequency response function, (iii) isometric damping plot, and (iv) Hilbert transform - presented above shows that all of them are more or less feasible and convenient for the detection of nonlinearity. In other words, the first question put forward at the beginning of this Chapter can now be answered reasonably convincingly. However, not **all** the methods can be used to identify the nature of the nonlinearity once its existence is confirmed. For instance, the method of reciprocal of FRF data can clearly demonstrate the effect of nonlinear stiffness but cannot identify its actual type clearly. For other more sophisticated methods such as the isometric damping plot, the identification of

the type of nonlinearity becomes possible if those commonly encountered types of nonlinearity are well **categorized** beforehand. However, a conclusive identification is often difficult to achieve, considering the application on the hardening cubic stiffness case and hardening backlash stiffness case. The same argument holds for the Hilbert transformation technique. Moreover, it is clear that unless the type of nonlinearity is identified confidently, its quantification is out of the question.

Apart from the immediate discussion on the identification of nonlinearity types, one important aspect in the modal analysis of nonlinearity which these current methods are not fully able to cope with is the need to obtain the correct modal data when the system is nonlinear. For instance, the modal constant and damping loss factor for a system with nonlinear stiffness should, in theory, be the same constants as if there is no nonlinear stiffness. However, **their** accurate estimation is usually hindered when conventional (linear) modal analysis algorithms are applied to extract modal data from nonlinear **FRF** data.

Based upon the above study and discussion, it can be said that modal analysis of nonlinearity requires further development so that it can more conclusively identify the type of nonlinearity from FRF data and, based on this identification, the extent of the nonlinearity can then be investigated, if required. In addition, the undistorted modal data could be extracted from the nonlinear FRF data. In the following study, a new interpretation of the effect of nonlinearity on FRF data is examined and used as the basis for a new method to facilitate modal analysis of nonlinear structures.

8-3 A NEW INTERPRETATION OF THE EFFECT OF NONLINEARITY ON FRF DATA FROM THE MODAL ANALYSIS VIEWPOINT

8-3-1 Interpretation of FRF Data with Nonlinearity

With reference to vibration theory, it can easily be seen that some types of nonlinearity

have been studied extensively. Using the experimental modal analysis methods discussed above, more types of nonlinearity have been simulated and investigated. However, it is believed that there are some aspects in applying modal analysis to identifying the types of nonlinearity which need to be interpreted theoretically before further development of practical nonlinearity analysis can progress. In the following, some new insights into the modal analysis of nonlinear systems **will** be presented from a very fundamental point of view and, for the sake of simplicity, these are illustrated using a SDOF system with nonlinear stiffness. The discussion commences with the equation of motion of the system with the spatial parameters such as mass and stiffness. It is customary that a SDOF system with cubic stiffness will be described by the Duffing equation, as is often referred to in textbooks:

$$m\ddot{x} + c\dot{x} + kx - \beta x^3 = f \quad (8-14)$$

where m , k , β and c stand for the mass, linear stiffness, cubic stiffness and viscous damping coefficients of the system respectively.

The stiffness characteristics and the frequency response function of the system subjected to a sinusoidal excitation ($f=Fe^{i\omega t}$) are shown in Figures 8-10 and 8-11 respectively. The type of frequency response function (FRF) shown in Figure 8-11 is often observed in modal testing results but its interpretation from the viewpoint of modal analysis has not been fully explored.

Considering a sinusoidal excitation, $f(t)=Fe^{i\omega t}$, equation (8-14) becomes:

$$m\ddot{x} + c\dot{x} + k(1 - \beta x^2/k)x = Fe^{i\omega t} \quad (8-15)$$

or
$$m\ddot{x} + c\dot{x} + k(\hat{x})x = Fe^{i\omega t} \quad (8-16)$$

Here, $k(i)$ is a function of the harmonic amplitude \hat{x} . The receptance of the system **can** then be defined as:

$$a(\omega) = 1/(k(\hat{x}) - \omega^2 m + i\omega c) \quad (8-17)$$

The corresponding receptance for the same system without the nonlinear stiffness can be denoted with a '0' subscript as:

$$\alpha_0(\omega) = 1/(k - \omega^2 m + i\omega c) \quad (8-18)$$

It can be said equivalently that the nonlinear system has different values of stiffness at different response amplitudes. If a sinusoidal excitation with constant force ($F=\text{constant}$) is applied in modal testing, then a receptance FRF of the form in Figure 8-1 1 will be obtained for a SDOF system with softening cubic stiffness.

Since it is realised that the receptance in equation (8-17) has different values at different response amplitudes for a given frequency, a response control technique could be employed experimentally, as described in Chapter 7, in which each measurement is made with the response amplitude being kept at a chosen level in order to linearise the vibration behaviour. Figure 8-12 shows the measurement results of from SDOF system with softening cubic stiffness in the vicinity of the resonance by using different response amplitude controls. It can be seen that, as predicted by theory, each curve conforms to a linear model, although the parameters of the model in each case vary according to the selected response amplitudes. This, in fact, is one procedure for formulating a series of linearized models for the system and thus to determine $k(\hat{x})$ versus \hat{x} .

If we draw a horizontal line on Figure 8-12 to represent a specific value of receptance amplitude (see Figure 8-13), then, for this particular value of the amplitude at the exciting frequency ' ω ' denoted in Figure 8-13, we can take the cross point between the FRF curve and that horizontal line, both representing the conditions of the response amplitude which must be satisfied simultaneously. For each point before resonance thus chosen, there is a corresponding point (ω'') after resonance lying on the same FRF curve. Linking all the

points thus deduced produces a new FRF curve (Figure 8-13) which is found to be of the same form as that in Figure 8-11. In other words, the response of a system with nonlinear stiffness can be constructed from the properties of a family of linear systems, each, in this case, having the same mass and damping properties but different stiffness values. The usually-observed FRF of this nonlinear system with constant excitation level (Figure 8-11) is effectively a combination of the results of all the linear systems, each point relating to one of them.

Based on this observation, it can now be explained in a new way why nonlinearity cannot be identified directly from a single FRF measurement made using random excitation since, in this case, the force level at each excitation frequency varies, causing the response level at this frequency to be an averaged value. The resultant FRF can therefore be shown schematically in Figure 8-14. The curve, in fact, is between the linear FRF (without nonlinearity) and the FRF curve of maximum response level.

8-3-2 Interpretation of the Reciprocal of Receptance Data with Nonlinearity

8-3-2-1 Stiffness Nonlinearity

The reciprocal of receptance data has been previously discussed in Chapter 4 for the identification of damping type and in an earlier part of this Chapter as a tool for the investigation of nonlinearity. It has been found hitherto that this technique is not applicable for the conclusive identification of nonlinearity type by simple and direct implementation. However, an appropriate interpretation of the reciprocal of FRF data from the modal analysis viewpoint, similar to that of the 'standard' FRF data discussed above, will reveal the inherent nonlinearity effect on the reciprocal of receptance data in a way which has not been published so far. In turn, this revelation will suggest a new understanding of the results from modal analysis of systems with nonlinearity, as explained below.

It can be seen from Figure 4-1 that the real part of the reciprocal of receptance for a linear

points thus deduced produces a new FRF curve (Figure 8-13) which is found to be of the same form as that in Figure 8-1. In other words, the response of a system with nonlinear stiffness can be constructed from the properties of a family of linear systems, each, in this case, having the same mass and damping properties but different stiffness values. The usually-observed FRF of this nonlinear system with constant excitation level (Figure 8-1) is effectively a combination of the results of all the linear systems, each point relating to one of them.

Based on this observation, it can now be explained in a new way why nonlinearity cannot be identified directly from a single FRF measurement made using random excitation since, in this case, the force level at each excitation frequency varies, causing the response level at this frequency to be an averaged value. The resultant FRF can therefore be shown schematically in Figure 8-14. The curve, in fact, is between the linear FRF (without nonlinearity) and the FRF curve of maximum response level.

8-3-2 Interpretation of the Reciprocal of Receptance Data with Nonlinearity

8-3-2-1 Stiffness Nonlinearity

The reciprocal of receptance data has been previously discussed in Chapter 4 for the identification of damping type and in an earlier part of this Chapter as a tool for the investigation of nonlinearity. It has been found hitherto that this technique is not applicable for the conclusive identification of nonlinearity type by simple and direct implementation. However, an appropriate interpretation of the reciprocal of FRF data from the modal analysis viewpoint, similar to that of the 'standard' FRF data discussed above, will reveal the inherent nonlinearity effect on the reciprocal of receptance data in a way which has not been published so far. In turn, this revelation will suggest a new understanding of the results from modal analysis of systems with nonlinearity, as explained below.

It can be seen from Figure 4-1 that the real part of the reciprocal of receptance for a linear

system (but with little noise) conforms a straight line when plotted against frequency squared. From equation (8-17), it can also be seen that the reciprocal of the receptance of a SDOF system with a stiffness nonlinearity, and its real and imaginary parts, can be expressed as:

$$1/a(\omega) = k(\hat{x}) - \omega^2 m + i\omega c \quad (8-19)$$

$$\text{Re}(1/\alpha) = k(\hat{x}) - \omega^2 m \quad \text{and} \quad \text{Im}(1/\alpha) = i\omega c$$

As suggested earlier, the most significant advantage of using the reciprocal of receptance is the separation of the stiffness characteristics from the damping property into its real and imaginary parts respectively, and so the interpretation of the reciprocal of the FRF data due to nonlinear stiffness can then be concentrated on the real part of the data:

$$\begin{aligned} \text{Re}(1/\alpha) &= k(\hat{x}) - \omega^2 m \\ &= m (\omega_0^2(\hat{x}) - \omega^2) \end{aligned} \quad (8-20)$$

Equation (8-20) suggests that away from the resonance, where $k(\hat{x})$ is dependent considerably less on the response amplitude, $\text{Re}(1/\alpha)$ will effectively be the same as $\text{Re}(1/\alpha_0)$ - the real part of the reciprocal receptance data of the corresponding linear system deduced from equation (8-18) - while in the vicinity of resonance, each data point of $\text{Re}(1/\alpha)$ effectively represents a different stiffness value $k(\hat{x})$ or natural frequency $\omega_0^2(\hat{x})$, because the amplitude of vibration (\hat{x}) is likely to vary considerably from point to point.

In common with the previous interpretation of the FRF data with nonlinearity, it can be seen here that if the measurement is made with a controlled response amplitude each time, the $\text{Re}(1/\alpha)$ versus ω^2 plot will be of the same form as that for linear case (i.e. a straight line), except that for each of such a condition of constant response amplitude, the

$\text{Re}(1/\alpha)$ data points will be subject to a different linear model with different natural frequency, since the system will take different stiffness quantity for each condition. Schematically, each time the $\text{Re}(1/\alpha)$ points will lie on one straight line which has a different offset due to different **natural** frequency $\omega_0^2(\hat{x})$ (or different stiffness), as shown in Figure 8-15. Since we presume the system has constant mass and damping quantities (i.e. they do not change with the force level) for the nonlinear stiffness case, the modal constant of the system should not, in theory, vary according to force level and hence these straight lines are all parallel one to another. However, one measurement made with a constant force level can include all the **information** contained in those parallel lines. This is because each $\text{Re}(1/\alpha)$ data point in this case comes from one of those parallel lines for response amplitude-controlled measurements and thus contains the necessary information to define that line. Figure 8-16 shows the principle and is actually the counterpart of Figure 8-13 which is for the receptance FRF case.

8-3-2-2 Damping Nonlinearity

Similarly to the nonlinear stiffness case, the interpretation can be extended to the imaginary part of the reciprocal of receptance data to observe the effect of nonlinear damping. In this case, the equation of motion of the system with nonlinear damping can be written as below for a sinusoidal forcing function:

$$m\ddot{x} + c(\hat{x})\dot{x} + kx = Fe^{i\omega t} \quad (8-21)$$

where $c(W)$ represents the nonlinear damping which is a function of the harmonic amplitude \hat{x} , and parameters m and k are mass and stiffness of the system and are supposed to be constant.

Based on the same argument as for the nonlinear stiffness case, it is clear that the effect of nonlinear damping is concentrated in the imaginary part of the reciprocal of receptance data, which takes the simple form:

$$\text{Im}(1/\alpha) = c(\hat{x})\omega \quad (8-22)$$

It is customary that for linear viscous damping case, the imaginary part of the reciprocal of **receptance data** (denoted here as $\text{Im}(1/\alpha_0)$) versus frequency appears to obey a straight line as the harmonic amplitude function $\mathbf{c}(\hat{\mathbf{x}})$ in equation (8-22) is actually a constant. As the damping becomes nonlinear, it can be seen from equation (8-22) that for each constant response amplitude condition, the nonlinear damping will not vary and the system will be subject to a linear damping model. The imaginary part of its reciprocal of receptance data becomes a straight line, just like the linear damping case although this straight line has a different slope **from** the one of $\text{Im}(1/\alpha_0)$ data representing linear damping case, as shown in Figure 8-17. Nevertheless, one set of FRF data obtained with a measurement of constant force level can include all the information of those non-parallel lines. This is because each $\text{Im}(1/\alpha)$ data point in this case conforms to a certain harmonic amplitude and should lie on one of those radial lines, this data point then fully contains the information of that line. Figure 8-18 exhibits the composition of the $\text{Im}(1/\alpha)$ data from a measurement of constant force level.

8-4 A NEW METHOD FOR THE MODAL ANALYSIS OF NONLINEAR SYSTEMS

8-4-1 Modal Analysis of Stiffness Nonlinearity

Having presented the above interpretation of nonlinearity effects on FRF data, it now becomes possible to apply this to the modal analysis of nonlinear systems and to develop a new technique which will be fundamentally different from the conventional methods for the modal analysis of nonlinearity. As the **first** phase of the technique, the modal analysis of stiffness nonlinearity is studied. Nonlinear damping will be discussed later.

Before embarking on a detailed discussion, it is worth re-emphasizing that nonlinear stiffness is a displacement amplitude-dependent property of a dynamic system and that the natural frequency of the system is therefore amplitude-dependent, too. Also for the sake

of simplicity, it is assumed that the system's mass properties are constant in this case (i.e. they do not change with excitation force level) and hence the modal constant of the system with displacement amplitude-dependent stiffness should not, in theory, depend on force level.

Since for a given type of nonlinear stiffness, the reciprocal of receptance data has been thoroughly interpreted from Figure 8-16, it is believed now that by analysing the reciprocal of receptance data in accordance with the knowledge of the above interpretation, the type of nonlinear stiffness can be convincingly identified. In the following, it is supposed at first that the linear modal constant of the nonlinear system 'A' (i.e. the modal constant obtained when assuming the nonlinearity is removed from the system) is known - although this may be very difficult to achieve in practice - although it will be found later that this precondition is not necessary.

S-4-1-1 Description of Methodology

As stiffness nonlinearity is amplitude-dependent, it is supposed that a relationship of response harmonic amplitude versus natural frequency (equivalent to stiffness, since the systems's mass property does not change) is necessary to identify the type of nonlinearity. Further, it would be ideal to quantify the nonlinearity because, unlike other methods such as the isometric damping plot or the **Hilbert** transform to extract certain indications of nonlinearity, this relationship reveals the nonlinear stiffness feature directly and explicitly. If it is supposed that the **Re(1/α)** data of a nonlinear system, such as the curve shown in Figure 8-16, is available from measurements, then a set of parallel lines using the linear modal constant as the slope can be drawn on the plot of **Re(1/α)** versus frequency squared. The line through each FRF data point represents a **linearized** model of the nonlinear system which is valid at a certain response amplitude, as exhibited by Figure 8-13. Since each data point relates to a specific response amplitude, a plot of response harmonic amplitude versus natural frequency is then obtained and this, in turn, shows explicitly the nonlinear stiffness characteristics of the system.

8-4-1-2 Algorithm for Modal Analysis of Nonlinear Stiffness

The algorithm of the above procedure can be initiated from equation (8-20). Using the modal data instead of the spatial parameters such as mass and stiffness, equation (8-20) can be written in terms of modal constant (A) and harmonic amplitude (\hat{x}) as:

$$\text{Re}(1/\alpha) = (\omega_0^2(\hat{x}) - \omega^2)/A \quad (8-23)$$

The plot of data $\text{Re}(1/\alpha)$ against ω^2 is a straight line for data without nonlinearity and the natural frequency ω_0^2 is thus a constant. However, in the case of nonlinear stiffness, the amplitude-dependent natural frequency can be deduced from equation (8-23), yielding;

$$\omega_0^2(\hat{x}) = A(\text{Re}(1/\alpha)) + \omega^2 \quad (8-24)$$

Equation (8-24) consists only of FRF data and modal data and it demonstrates that, if the correct modal constant A is available, the receptance amplitude-dependent natural frequency can be obtained from the reciprocal of receptance data and this is equivalent to obtaining the nonlinear stiffness against the receptance amplitude. It is necessary to mention here that since the linear modal constant is relatively difficult to obtain by conducting a conventional modal analysis procedure on nonlinear data, a new technique will be introduced later in §8-4-3 to derive an accurate modal constant estimate.

The stiffness is a property related to response amplitude (rather than receptance amplitude), and so it is necessary to convert the latter to the former once the natural frequency against receptance amplitude is deduced from equation (8-24). If the force level is constant throughout a measurement (which is ideal but impractical), then the difference between the two amplitudes (response and receptance) would be merely a scale factor, as will be seen later. However, considering the inevitable non-constant force levels in a measurement of a nonlinear system, the response amplitude of each data point is irregularly related to the force level and hence, cannot be obtained **straightforwardly** from

the receptance amplitude of that point. Fortunately, it is found that obtaining response amplitude from receptance amplitude is feasible with knowledge of the force level information because the receptance and the harmonic response under a sinusoidal excitation have a simple relationship:

$$\alpha(\omega) = X e^{i\omega t} / F e^{i\omega t} \quad (8-25)$$

and the harmonic amplitudes of the receptance, response and excitation force are therefore related to one another as:

$$|\alpha(\omega)| = |X(\omega)| / |F(\omega)| \quad (8-26)$$

where $a(\omega)$ and $X(\omega)$ represent the receptance and response amplitude under the excitation frequency ω , and $F(\omega)$ is the excitation force amplitude from the shaker.

Thus, the displacement amplitude can be deduced frequency by frequency from the receptance amplitude and the force level:

$$|X| = |\alpha(\omega)| |F| \quad (8-27)$$

Equation (8-27) reveals the important feature that if the force level is recorded in the measurement, then modal analysis of nonlinear stiffness can be conducted on the FRF data measured without requiring any force or response level control. This means that standard measurements can be made, thus saving a great deal of experimental effort.

Once the response amplitude is deduced by equation (8-27), together with the amplitude-dependent natural frequency obtained from equation (8-24), the stiffness characteristics can be derived explicitly and it becomes possible to identify the type of nonlinear stiffness and, possibly, to quantify it.

8-4-2 Modal Analysis of Damping Nonlinearity

The modal analysis of a damping nonlinearity is based upon the previously developed interpretation and is subjected to the similar methodology as that for stiffness nonlinearity. In common with that case, nonlinear damping is an amplitude-dependent property of a dynamic system. Therefore, unlike the linear system which has a constant damping loss factor, the loss factor of a system with nonlinear damping will be amplitude-dependent. For the sake of simplicity, it can be assumed that the system's mass and stiffness properties are constant when nonlinear damping is studied. The primary aim of modal analysis of systems with a damping nonlinearity would be - like that of stiffness nonlinearity - to identify conclusively the nonlinear damping type and to develop a model (of damping against response amplitude) for the system.

The vibration motion of a system with a damping nonlinearity is described previously by equation (8-21) and the effect of damping nonlinearity on FRF data is concentrated on the imaginary part of the reciprocal of receptance, defined by equation (8-22). As Figure 8-18 shows, each $\text{Im}(1/\alpha)$ data point relates to a different linearized damping model of the system and each data point represents a different damping loss factor due to different response amplitude. Hence, when the FRF data of a system with damping nonlinearity are measured, a series of straight lines can be drawn on the curve of $\text{Im}(1/\alpha)$ against frequency, each of which represents a linear damping model for a certain response amplitude. Further, the damping loss factor corresponding to each data point can be estimated from the straight line which passes through the point in question and represents a linear damping model. Thus, a nonlinear damping model (of damping loss factor against response amplitude) can be deduced.

In order to implement the methodology of modal analysis of damping nonlinearity, equation (8-22) can be rewritten in terms of FRF and modal data, yielding:

$$\text{Im}(1/\alpha) = 2\xi(\hat{x})\omega_0\omega / A \quad (8-28)$$

where $\xi(\hat{x})$ is the response amplitude-dependent damping loss factor which becomes constant if the damping is linear.

Once the linear natural frequency " ω_0 " and modal constant "A" are obtained from either the Nyquist circle-fit or the real part of the reciprocal of receptance data, the damping loss factor for each data point (which corresponds to a different response amplitude, \mathbf{x}) can be evaluated by:

$$\xi(\hat{x}) = \text{Im}(1/\alpha) A / 2\omega_0\omega \quad (8-29)$$

In order to develop the relationship of response amplitude versus damping loss factor, the response amplitude of each data point has to be estimated from the measured data in the **same** way as was introduced for the stiffness nonlinearity case. Specifically, the response amplitude can be derived from equation (8-27) and thus the damping property of the nonlinear system (against the response amplitude) can be then be modelled and the nonlinear damping type be identified.

S-4-3 The Extraction of an Accurate Modal Constant Estimate

It can be seen from the above study for the new method of modal analysis of nonlinearity, that the accuracy of the modal constant estimate is very important. In fact, both equation (8-24) for the analysis of stiffness nonlinearity and equation (8-29) for the analysis of damping nonlinearity require an accurate modal constant estimate. However, an accurate estimation of this parameter can be very difficult to achieve when the measured data are from a nonlinear system. Even for a linear system, the modal constant is often determined after the natural frequency and damping loss factor estimation for the Nyquist circle-fit algorithm and, hence, any inaccuracy in the latter two will directly influence the reliability

of the former.

In order to reduce the influence of an error in the modal constant estimate for subsequent analysis of nonlinearity, an accurate modal constant has to be obtained somehow. In the following, the linear case is first examined to investigate the effect of an erroneous modal constant estimate on the natural frequency estimation using the $\text{Re}(1/\alpha)$ data and to investigate a new method of obtaining an accurate modal constant estimate. Then, it will be shown how the same technique can be introduced into the modal analysis of nonlinear systems to adjust the modal constant estimate so as to achieve a satisfactory nonlinearity analysis.

For a dynamic system with linear stiffness properties, the natural frequency can be evaluated from any $\text{Re}(1/\alpha)$ data point using the following equation, provided the modal constant estimate A is correct:

$$\omega_0^2 = \text{Re}(1/\alpha)A + \omega^2 \quad (8-30)$$

The natural frequency thus estimated should theoretically be the same no matter which data point is employed. Figure 8-19 shows the $\text{Re}(1/a)$ data from a linear system and the receptance amplitude against the natural frequency estimated by equation (8-30) using each data point individually. Clearly, the same natural frequency is obtained from each data point.

If the modal constant estimate is in error by an amount denoted by ΔA , then equation (8-30) will become:

$$\omega_0^2 = \text{Re}(1/\alpha)A + \omega^2 + \text{Re}(1/\alpha)\Delta A \quad (8-31)$$

Equation (8-31) shows that the error in the modal constant estimate will perturb the natural frequency estimation process and produce a systematic discrepancy in the result.

Only at the point when $\text{Re}(1/\alpha)$ is zero is the natural frequency estimated correctly. Equation (8-31) also suggests that since the discrepancy in the natural frequency estimate is systematic due to an error in the modal constant estimate, it should be possible to alter the modal constant estimate with frequency so that when the systematic discrepancy disappears, the correct estimate of modal constant has been achieved, and so has that of the natural frequency. Figure 8-20 shows the results of natural frequency estimation by equation (8-31) with different amounts of AA and it is clear that as AA becomes smaller, the natural frequency estimation from each data point becomes closer to the correct answer.

The technique proposed above to obtain simultaneously correct modal constant and natural frequency estimates is a procedure which is independent of the damping and it can be a useful alternative to the analysis of data *without* nonlinearity so as to improve the modal parameter extraction. For the modal analysis of damping nonlinearity, the correct modal constant and natural frequency estimates are required in equation (8-29) and it is also expected that they can be obtained in this way.

8-5 APPLICATIONS OF THE NEW METHOD FOR THE MODAL ANALYSIS OF NONLINEARITY

The new method for the modal analysis of nonlinearity proposed above has been applied to several systems with various types of nonlinear stiffness or damping in order to assess fully the feasibility of the method. Most of the systems have a SDOF with either one type of nonlinear stiffness or of nonlinear damping. In this study, both analytical and electrical analogue data are used. In a second stage of the assessment, FRF data measured on a practical structure are employed and the nonlinearity is investigated.

8-5-1 Analysis of Stiffness Nonlinearity

A SDOF system with different types of nonlinear stiffness has been simulated on an analogue computer^[63] and studied using the traditional methods including the Hilbert Transform and the isometric damping plot. Among these nonlinear systems, a SDOF system with hardening cubic stiffness is typical and the data measured from it are employed here for this study.

The inertance FRF data and the reciprocal of receptance data of the system have been given previously in Figures 7-8 and 8-2 respectively. The isometric damping plot and the Hilbert Transform of the FRF data with this cubic stiffness have also been presented previously - in Figures 8-5 and 8-7 respectively. It can be seen that the existing nonlinearity is strongly indicated by both the damping plot and the results of the Hilbert Transformation. However, the type of nonlinearity is not conclusively identified since other types of nonlinear stiffness - such as backlash stiffness - may well produce similar indications and it could be extremely difficult to distinguish them from each other in either of these two methods.

By using the new method of analysis, the system's property of response amplitude *versus* the natural frequency (equivalent to the stiffness) evaluated from each $\text{Re}(1/\alpha)$ data point has been obtained as shown in Figure 8-21. Here it can be seen that the system has a continuously changing type of stiffness property and hence the possibility of backlash stiffness is eliminated and cubic stiffness is proposed. For a SDOF system with hardening backlash stiffness, the reciprocal of receptance data has been shown earlier in Figure 8-3. It has been found that the isometric damping plot and the Hilbert Transform results in this case could easily be misinterpreted as if the system has cubic stiffness. However, by using the new method of modal analysis, the backlash type of stiffness characteristics of the system can be shown as in Figure 8-22 which exhibits the true

nonlinear stiffness type and is rather clearly distinguishable from the cubic stiffness characteristic.

8-5-2 Analysis of Damping Nonlinearity

When the new method is applied to the study of damping nonlinearity, the results are as encouraging as those for stiffness nonlinearity. The FRF data from a SDOF with different extents of quadratic damping are shown in Figure 7-19 in the last chapter. The existence of quadratic damping could be suspected from the typical apple-shape Nyquist plot provided its extent is rather large and measurement force constant. However, the isometric damping plot does not clearly indicate this nonlinearity.

On the other hand, the FRF data with quadratic damping can be analysed using the new method proposed in this Chapter, with the results shown in Figure 8-23. The plot on the right hand side is the imaginary part of the reciprocal of receptance and that on left hand side is the analysis result. Figure 8-23 demonstrates that the damping loss factor of the system varies linearly according to the response amplitude and this happens to coincide with the characteristic of a quadratic damping model. Figure 8-24 shows the imaginary part of the reciprocal of receptance of a SDOF system with a dry friction type of nonlinear damping and the analysis result. Again, the extent of the nonlinear damping at different response amplitude is clearly uncovered. Therefore, it can be seen that the new method of modal analysis is quite useful in conclusively identifying the type of nonlinear damping as well as identifying that of nonlinear stiffness.

8-5-3 Practical Applications of the New Method

In practical applications of techniques to study nonlinearity, it is believed that - with **the** exception of the possible uncertainty of the exact type of nonlinearity - the primary problem lies in the difficulty of applying constant force or constant response measurement conditions, both being strictly required by conventional methods of nonlinearity analysis.

If the force is not kept constant, then the nonlinearity cannot generally be fully exposed and conventional methods cannot produce convincing results for analysis of nonlinearity. Likewise, if the response is not well controlled, then a linearized model of a nonlinear system cannot be obtained.

However, by using the new method, neither force control nor response control is required in the measurement whereas the nonlinearity can still be analysed. In the following, a typical example from measurements on the analogue computer is given first to simulate a practical measurement where no force control is used and it will be seen that the nonlinearity is successfully analysed. Second, a practical example from measuring a vibrating structure known to exhibit nonlinear characteristics is then studied and the nonlinearity investigated.

The FRF data shown in Figure 8-25 are obtained from the model of a SDOF system with cubic stiffness added. The measurement is carried out in such a way that the force level simulates the practical case; i.e. near resonance, the force applied to the system decreases significantly due to the characteristics of the shaker. The actual force level recorded in the measurement is presented in Figure 8-26. It is evident that the FRF data in Figure 8-25 do not indicate the existence of nonlinearity as would be expected if the force level were kept constant throughout the resonance frequency range. Moreover, neither the reciprocal of receptance plot shown in Figure 8-27, nor the modal analysis results given by Figure 8-28, provides any significant indication of a cubic stiffness characteristic. All this is attributed to the non-constant **force** level employed in measurement.

The same FRF data were then analysed using the new method proposed in this Chapter. The system is known not to have any damping nonlinearity, and the analysis correctly indicates a linear damping model by the form of the imaginary plot of $(1/\alpha)$. However, the nonlinear stiffness is clearly indicated by the relationship of natural frequency against response amplitude exhibited in Figure 8-29. The continuous natural frequency change with response amplitude coincides with the cubic stiffness model. Hence, it suggests that

the new method does not necessarily require force control or response control to be applied during measurements in order to achieve a successful nonlinearity analysis, both being extremely difficult to achieve in practice.

A practical structure referred to as the “NASTRAN structure” was then investigated. The structure was known to possess certain type(s) of stiffness **nonlinearity**^[61] while the exact nature of the nonlinearity is still unknown. In this study, a discrete sine sweep was used to measure FRF data, covering the first mode of the structure, although neither the force nor the response was controlled in measurement. Hence, the structure was measured in just the same way as would be used if no considerations were taken of the existence of nonlinearity. The inertance FRF data obtained and the force level generated by the shaker are shown in Figures 8-30 and 8-31 respectively. It can be seen from these figures that since the force level was not controlled, the FRF data does not show indications of nonlinearity. The same conclusion is drawn from results of the modal analysis presented in Figure 8-32 by circle-fitting a Nyquist plot of the FRF.

The new method was applied to the measured data and a nonlinear stiffness characteristic was clearly revealed by the results shown in Figure 8-33. The stiffness change with response amplitude suggests that the first vibration mode of the structure is subjected to a softening backlash type of stiffness since the stiffness appears to be constant within a certain response amplitude range, while beyond this range, the stiffness tends to decrease as the response amplitude increases. By close observation of the structure, it can be supposed that this could be due to the joints by which components of the structure are connected. If the response amplitude is very small, then there is effectively no slip within the joints but as the amplitude increases, the slip does occur, thereby reducing the stiffness of the structure.

8-6 CONCLUSIONS

Once nonlinearity is suspected in a structure, different strategies can be applied to deal

with it, depending upon the different requirements. Despite the difficulty in extracting correct modal data in the presence of nonlinearity, the main problems put forward by the nonlinearity for modal analysis are: (1) Whether a dynamic system or structure is nonlinear?; (2) If yes, what type of nonlinearity is it? and, possibly, (3) What is the extent of the nonlinearity?

In coping with the reality of nonlinearity in structural dynamics, it is understood that there are three common requirements for the modal analysis which can be summarized as: (1) detecting the existence of nonlinearity and then linearising it without need for the knowledge of its type; (2) identifying the type of the nonlinearity and (3) quantifying the identified nonlinearity in order to devise a correct model for the nonlinear system for subsequent analysis purposes, such as response prediction.

Four commonly-used methods for the modal analysis of nonlinearity have been reviewed in detail in this Chapter. It is noted that both the Bode plot and the reciprocal of receptance methods are merely different presentations of the FRF data intended to show up any systematical distortion caused by existence of nonlinearity. They are very convenient in the nonlinearity detection stage but not so applicable for the identification of nonlinearity type or its quantification.

The isometric damping plot and the **Hilbert** Transform both seek more specific indications of the different types of nonlinearity. Apart from the evident results these methods provide in validating the existence of nonlinearity, conclusive identification of its type relies on a lot of prior studies and **categorization** of different types of nonlinearity commonly encountered in reality but, even then, some types of nonlinearity have similar indications in the results of both methods and could mislead the identification.

On considering the measurement of a practical structure, it is realized that to achieve a satisfactory control on either the force or the response levels is often extremely difficult. Nevertheless, the detection of nonlinearity and identification of its type performed by the

above methods strictly requires the FRF data from measurement with a fairly constant force level. Moreover, the modelling of the identified stiffness nonlinearity relies on a number of measurements with different amount of response control. These requirements impose significant demands on the measurement **process(es)** associated with nonlinearity studies.

Based upon the SDOF assumption, a new interpretation of the effect of nonlinearity in the FRF data, and subsequently in the reciprocal of receptance data, is made. It is made essentially from the viewpoint of modal analysis rather than the theory deduced from known differential equations. It is shown that since a dynamic system having a stiffness nonlinearity will take a different stiffness value with each different response amplitude, every FRF data point from a measurement with constant force actually relates to a specific FRF data curve measured with a constant response and so, in effect, contains all the information of the latter curve. Therefore, it is possible to use one FRF curve measured with constant force to identify the type of nonlinearity and to model it. The same interpretation is made for damping nonlinearity case.

Based on this interpretation, a new method is proposed to analyse the nonlinearity from measured FRF data. In addition to deriving an indication of the nonlinearity, this method aims at discovering the relationship between the vibration response amplitude and the extent of the nonlinearity (such as stiffness or damping quantity) from the FRF data measured using sinusoidal excitation. Since this method reveals directly the nonlinearity characteristics as a function of response amplitude, it provides more conclusive identification results and immediately suggests the reference for quantifying or modelling the nonlinearity. It is also seen that the condition of constant force is not necessary when measuring the FRF data for the subsequent modal analysis. In fact, satisfactory analysis can be carried out as long as the response amplitude varies sufficiently to expose the nonlinearity. As a consequence, the new method also suggests a technique to extract correct modal data in case of nonlinearity.

In addition to requiring neither force nor response control in measurement, another major advantage of the method developed here is its simplicity, both of application and interpretation. By separating the stiffness and damping effects (into the real and imaginary parts of the reciprocal of FRF), there is the immediate benefit of establishing the type of element in which any nonlinearity exists. Then, it is possible to extract the nonlinear characteristic by a simple modal analysis process without further complex analysis.

Although the method is predicated on the assumption of a SDOF model, and the extension to truly MDOF systems is difficult, this difficulty is a feature shared by most (if not all) studies of non-linearity in practical modal analysis applications. In view of the impracticability of dealing with actual structural nonlinearity in any but an approximate way, this new approach has distinct advantages in such applications.

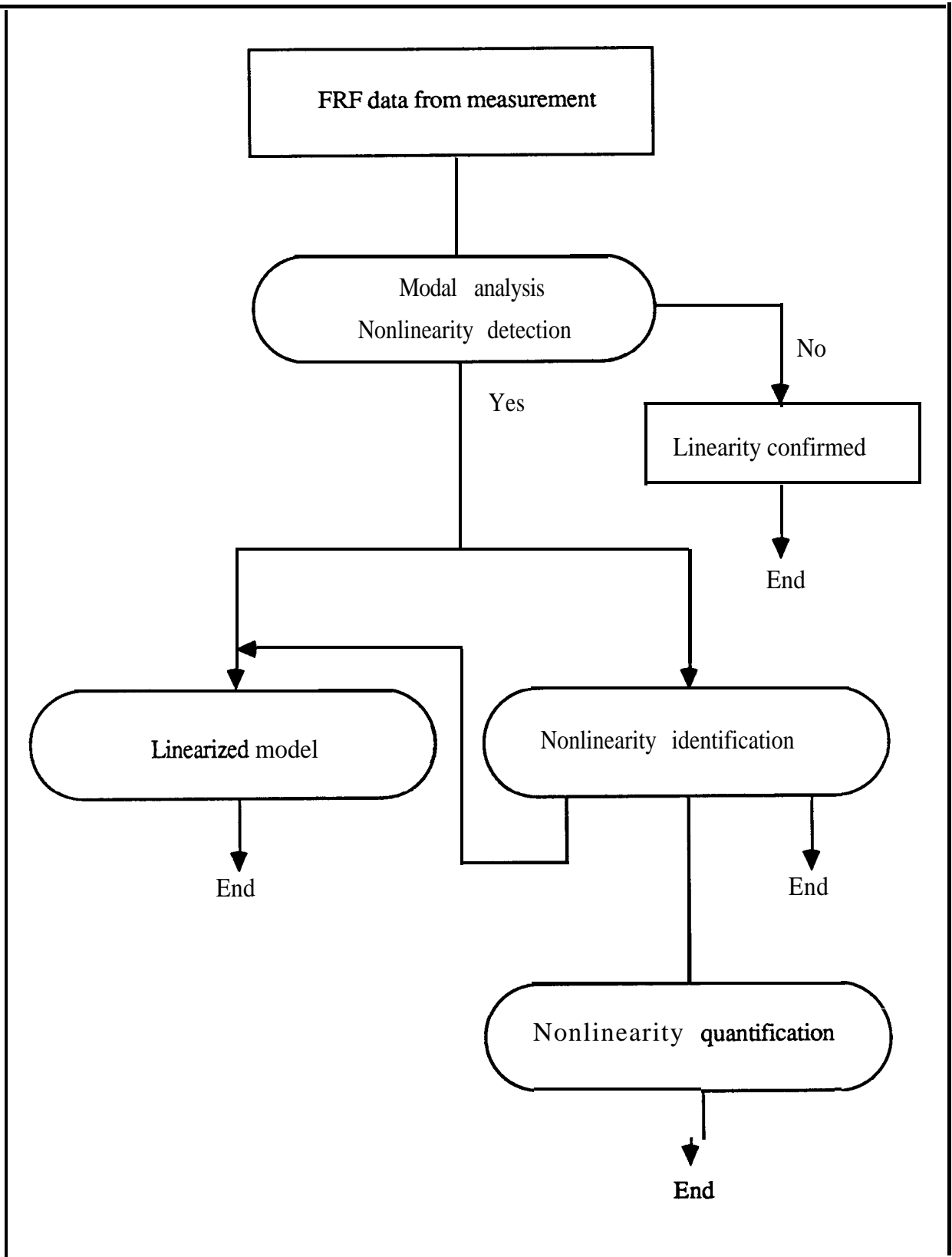


Figure 8-1 The strategy of modal analysis of nonlinearity

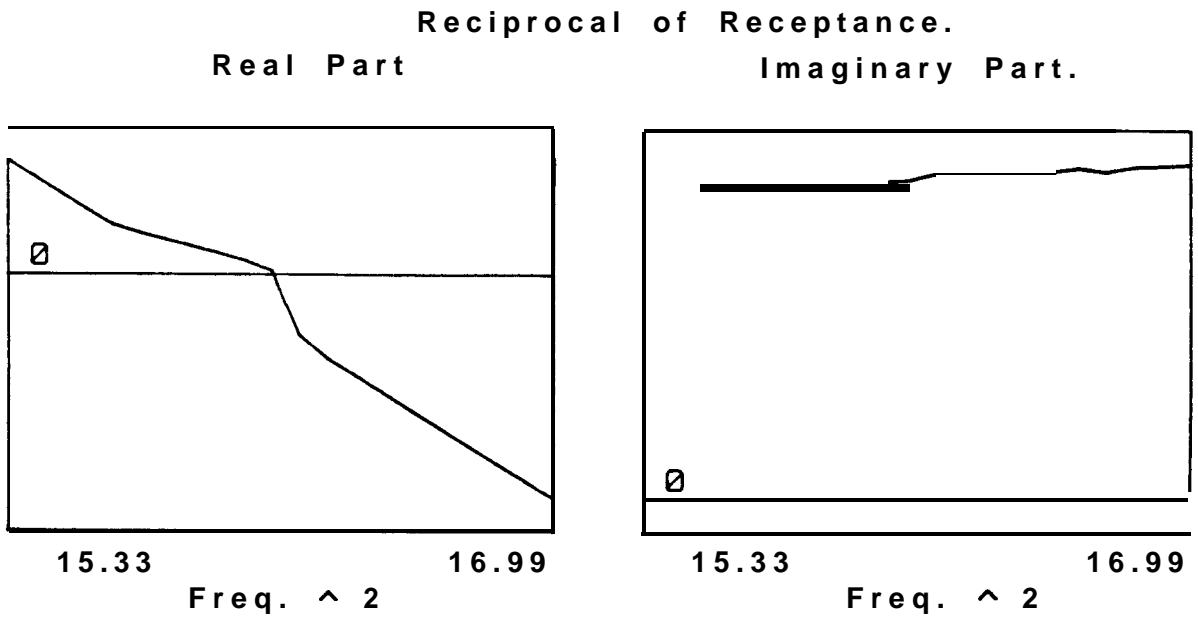


Figure 8-2 Real and imaginary parts of the reciprocal of FRF data from the SDOF system with hardening cubic stiffness

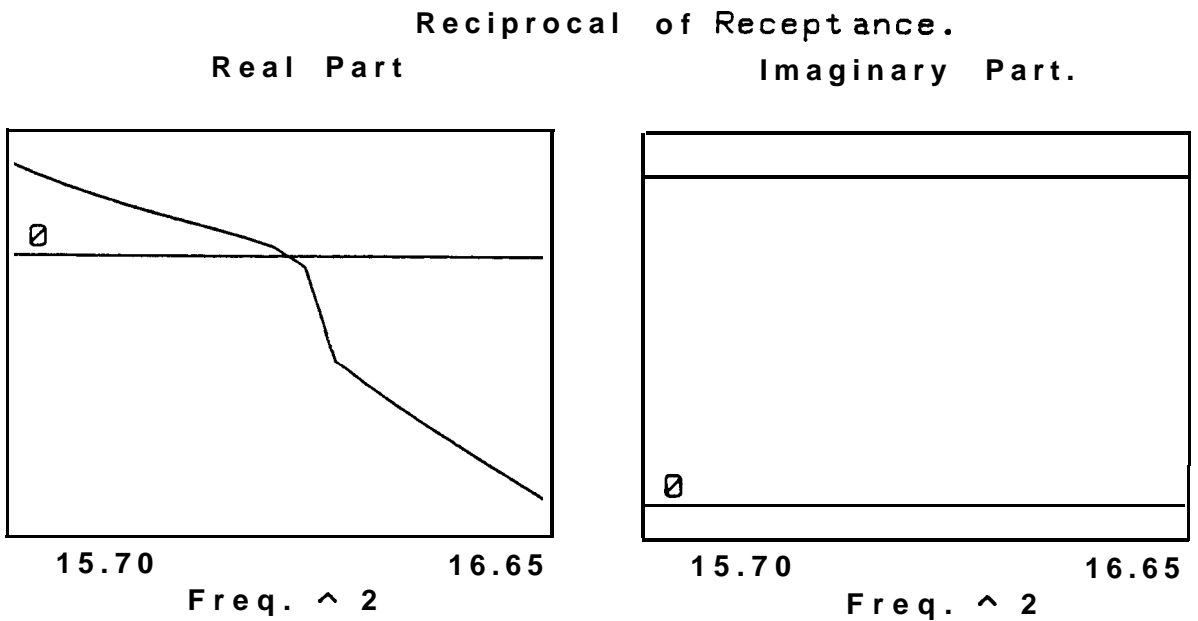


Figure 8-3 Real and imaginary parts of the reciprocal of FRF data from the SDOF system with hardening backlash stiffness

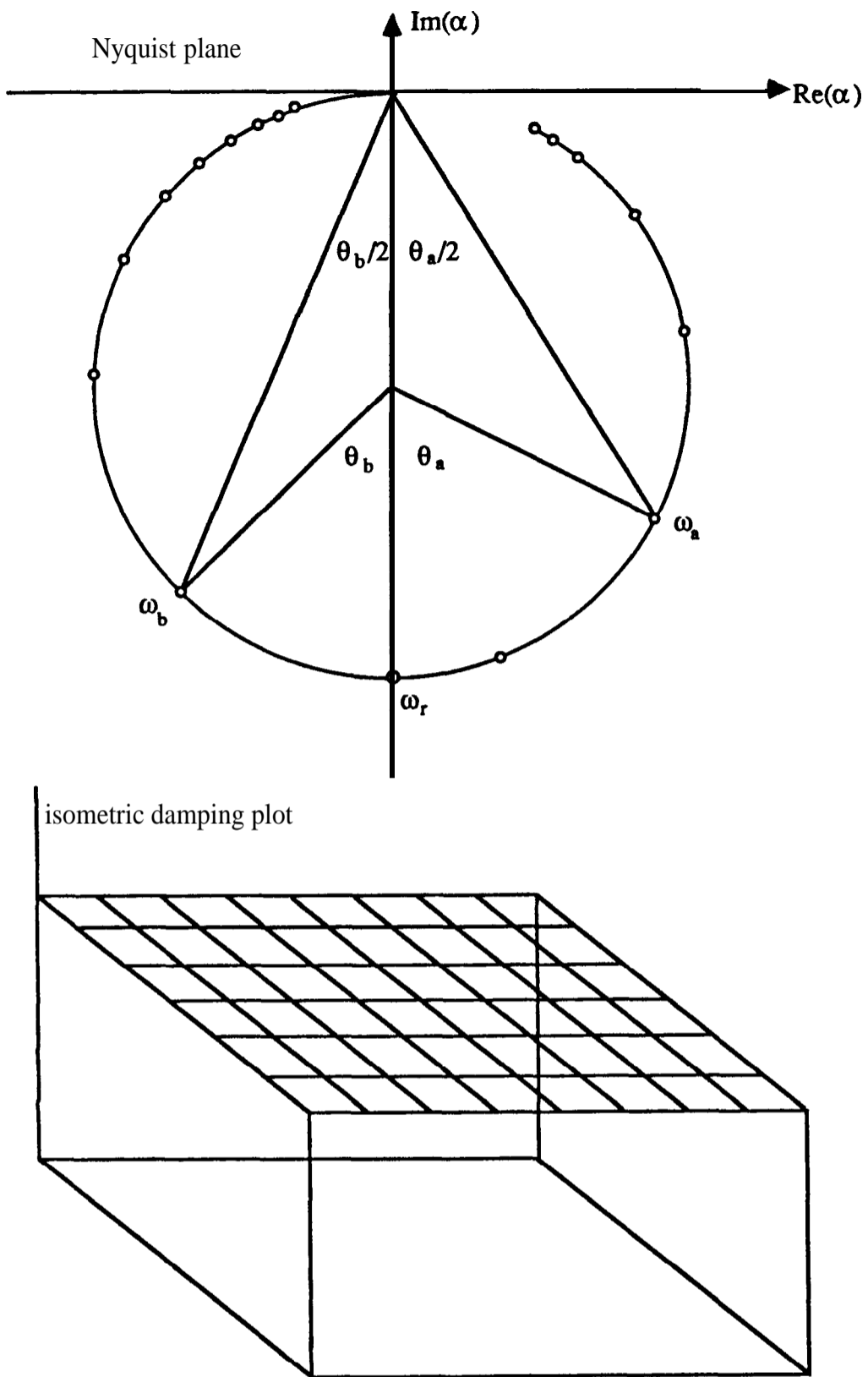


Figure 8-4 Isometric damping of a linear vibration mode

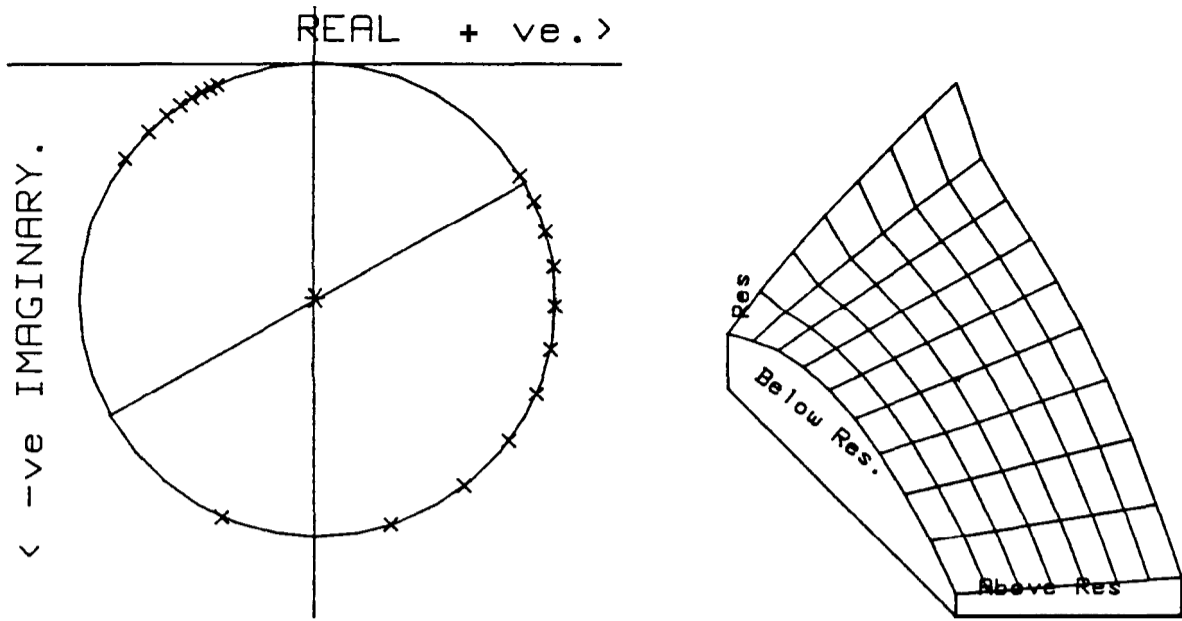


Figure 8-5 Modal analysis results of the FRF with hardening cubic stiffness

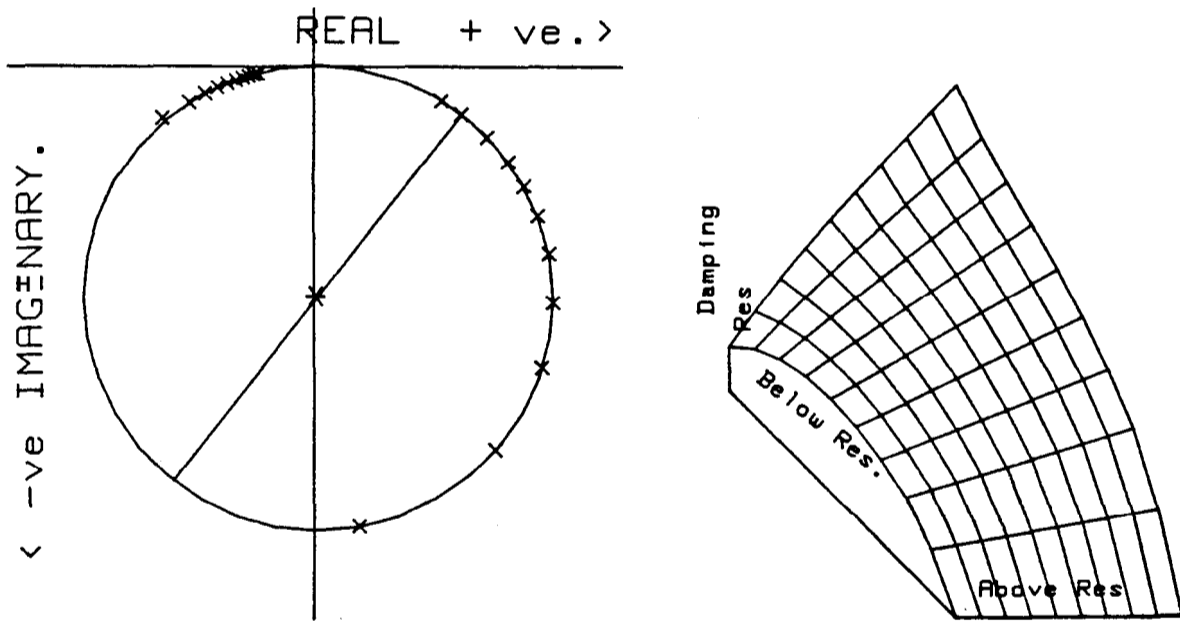


Figure 8-6 Modal analysis results of the FRF with hardening backlash stiffness

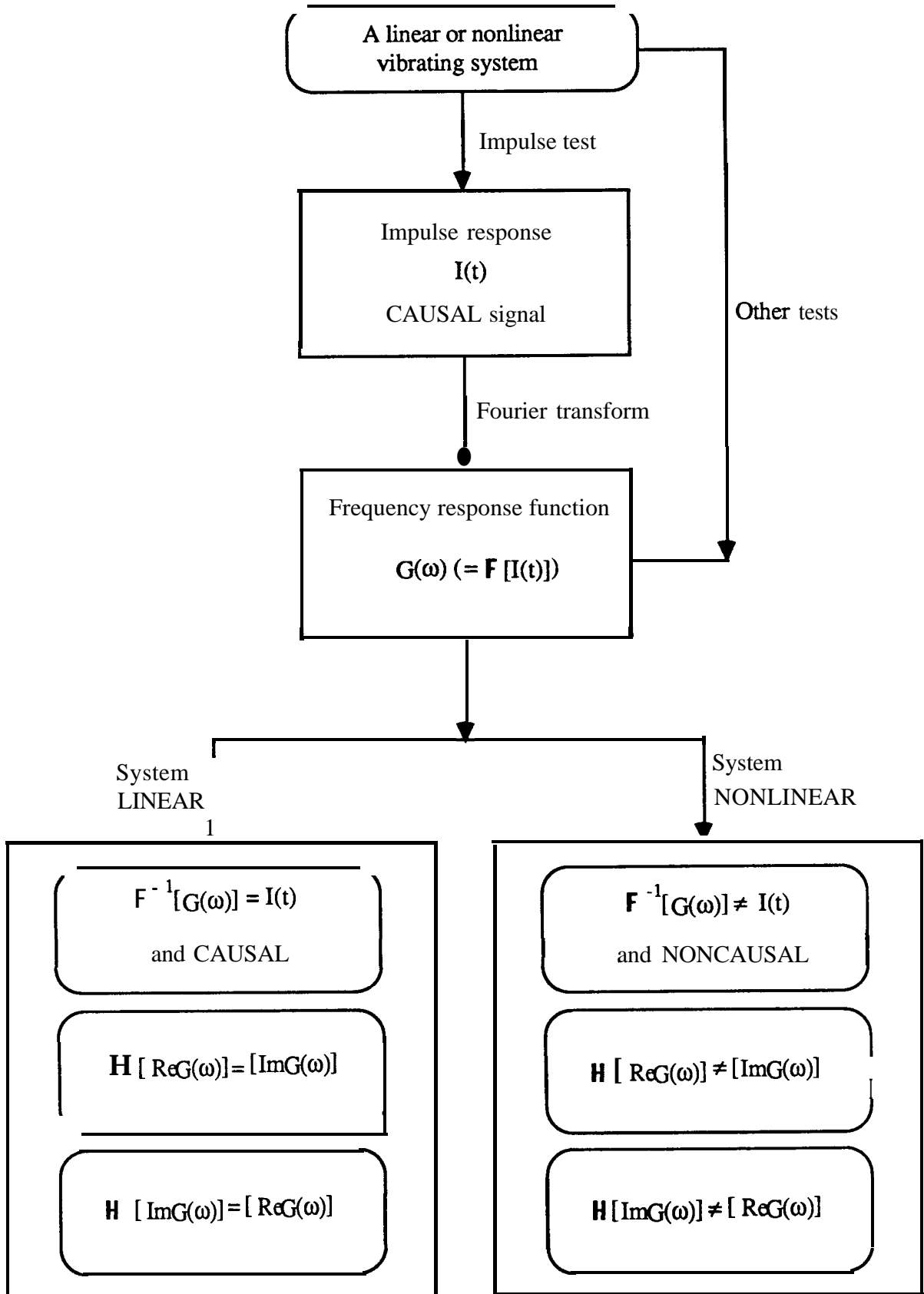


Figure 8-7 Basic idea of the Hilbert Transform

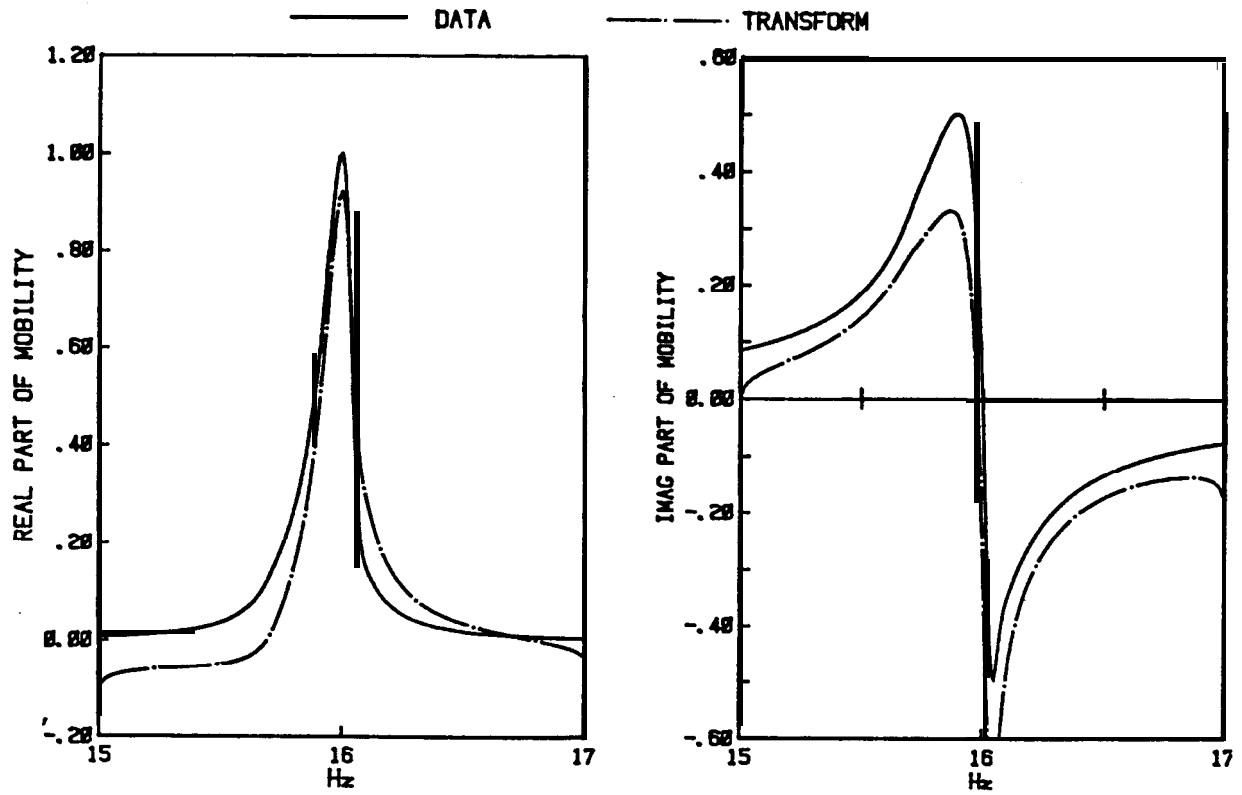


Figure 8-8 Real and imaginary parts of the FRF with hardening cubic stiffness and their Hilbert transform

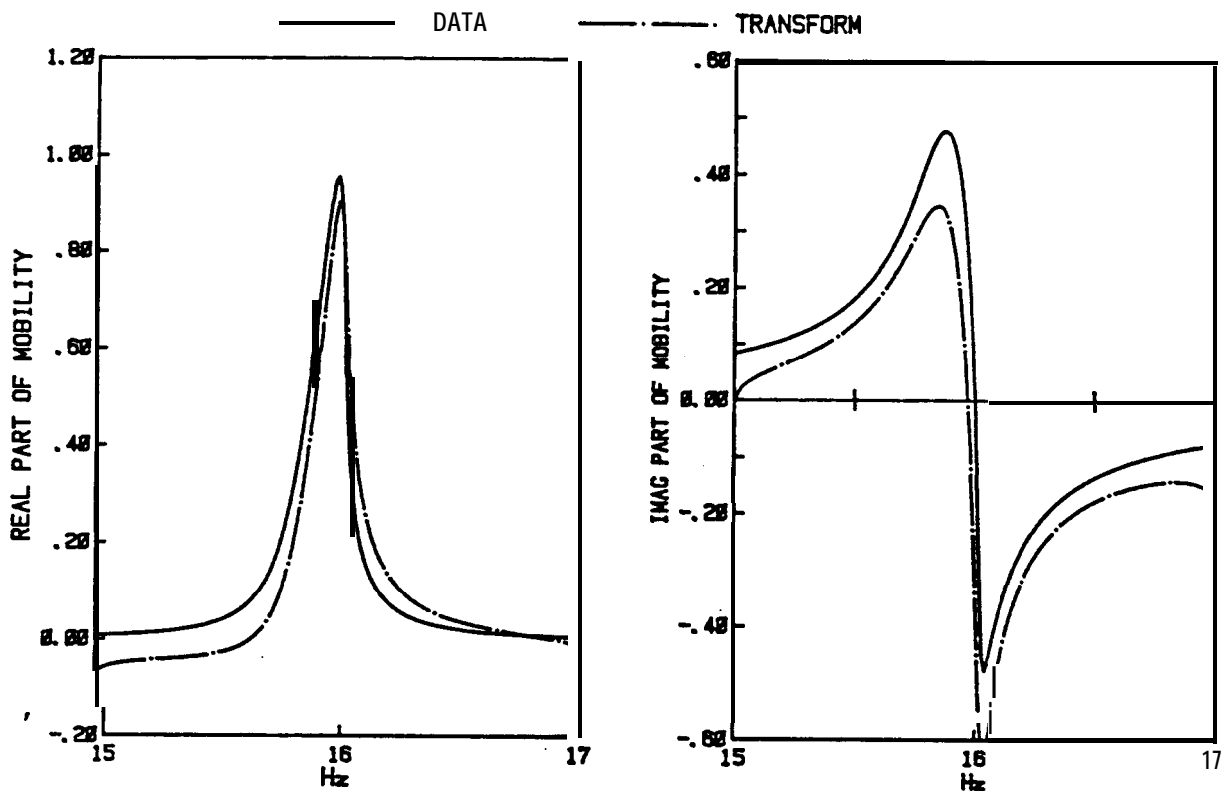


Figure 8-9 Real and imaginary parts of the FRF with hardening backlash stiffness and their Hilbert transform

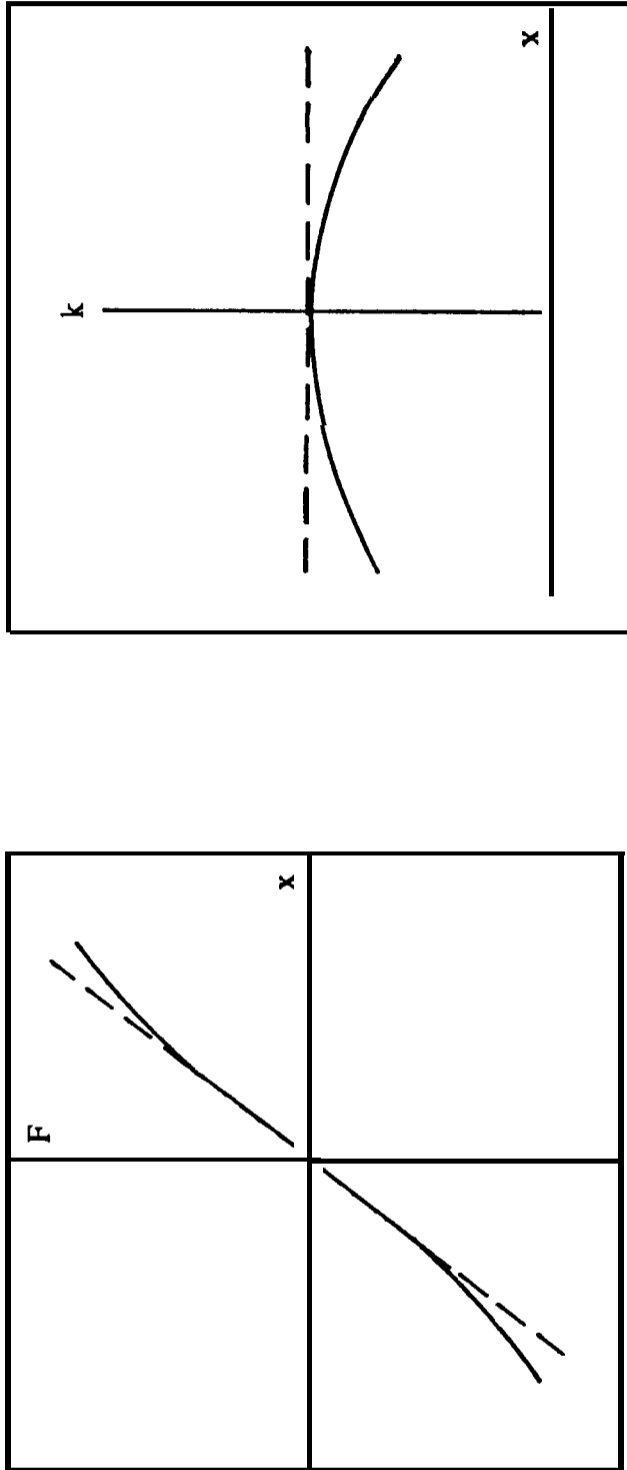


Figure 8-10 Characteristics of softening-cubic-type nonlinear stiffness

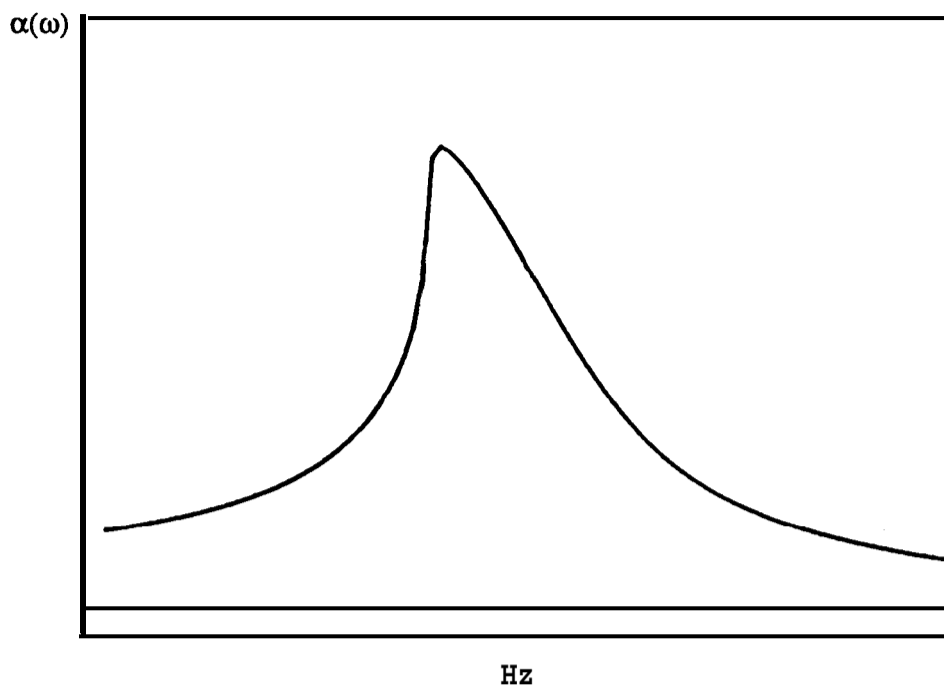


Figure 8- 11 Frequency response solution of the system subjected to a sinusoidal excitation ($f=Fe^{i\omega t}$), with stiffness characteristics shown in Figure 8-10

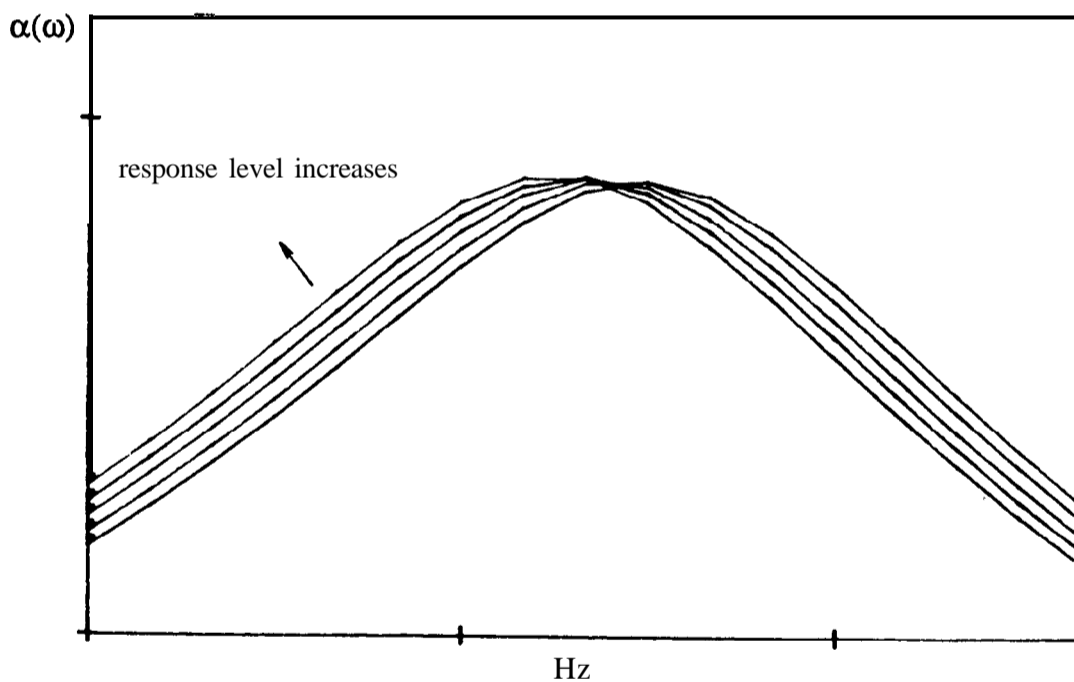


Figure 8- 12 Receptance **FRFs** of a SDOF system with softening cubic stiffness in the vicinity of the resonance using different response amplitude controls

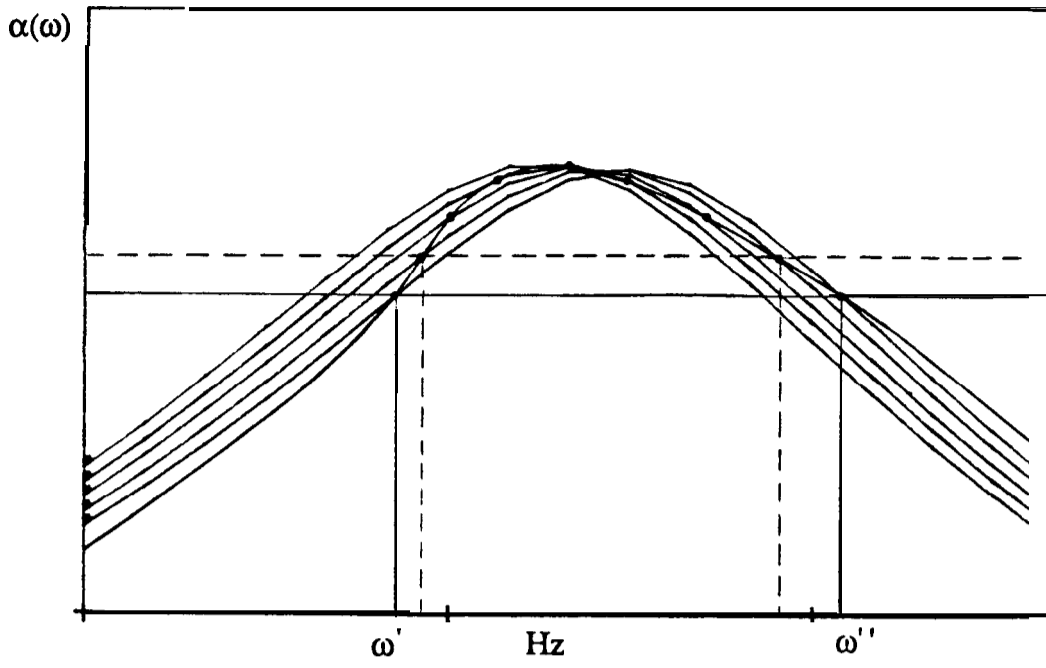


Figure 8-13 Composition of the FRF with constant force from the FRFs with different response amplitude controls using sinusoidal excitation

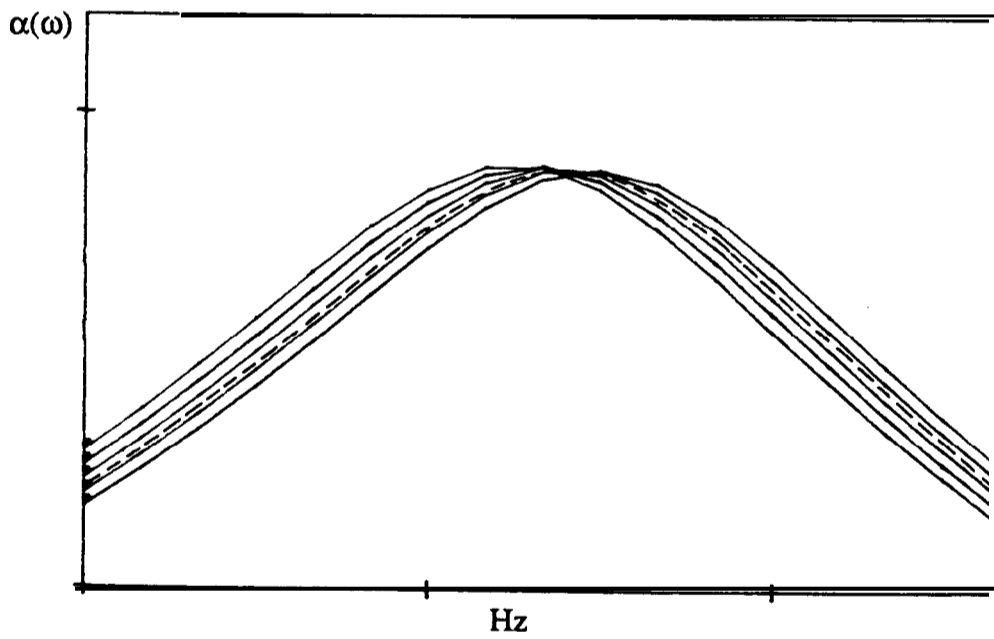


Figure 8-14 Illustration of the effect of random excitation on measured FRF

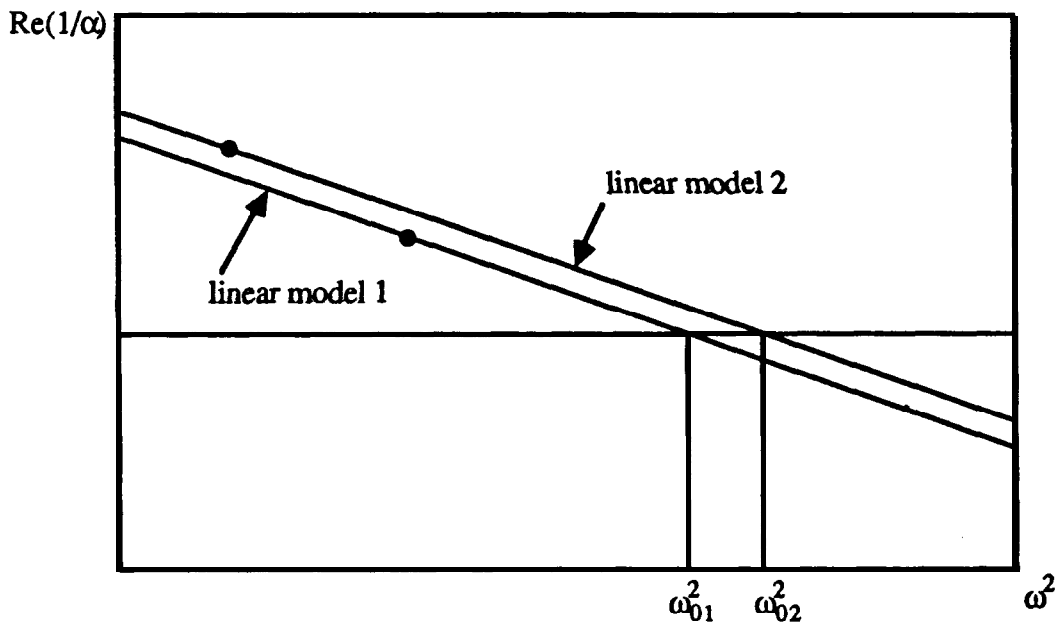


Figure 8-15 Each $\text{Re}(1/\alpha)$ corresponds to a linear system model represented by one straight line

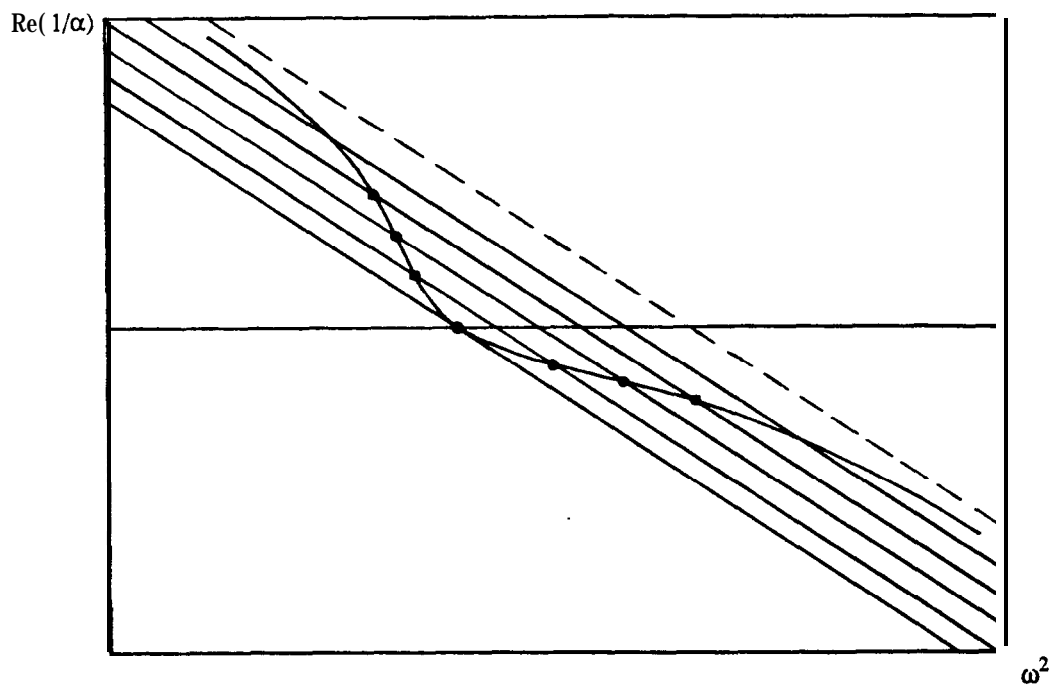


Figure 8-16 Principle of using $\text{Re}(1/\alpha)$ data to analyse nonlinear stiffness

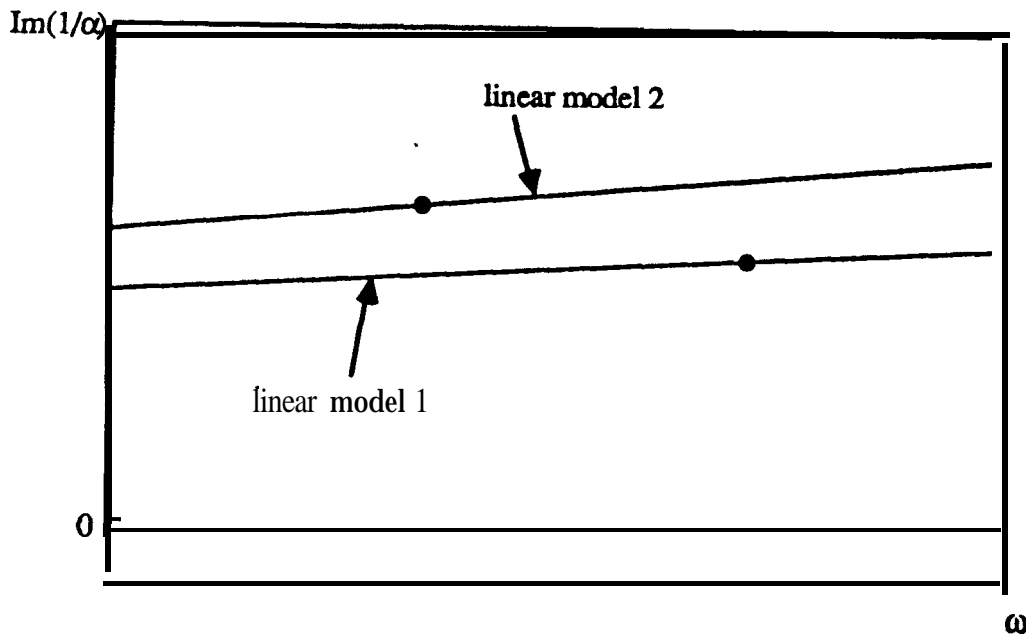


Figure 8-17 Each $\text{Im}(1/c)$ corresponds to a linear system model represented by one straight line

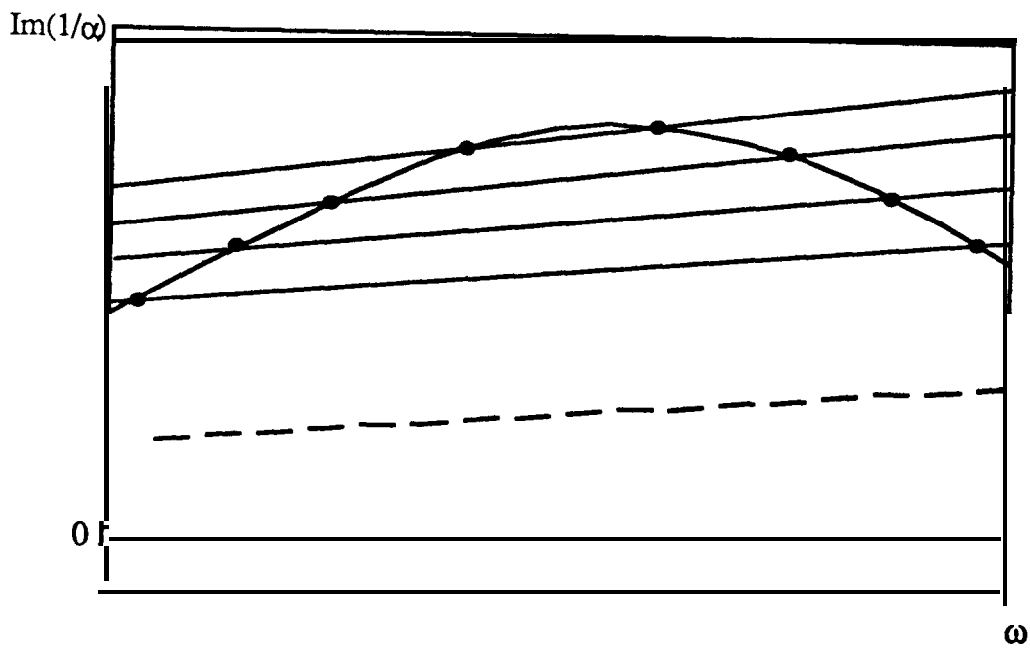


Figure 8-18 Principle of using the imaginary part of the **reciprocal** of receptance data to analyse nonlinear damping

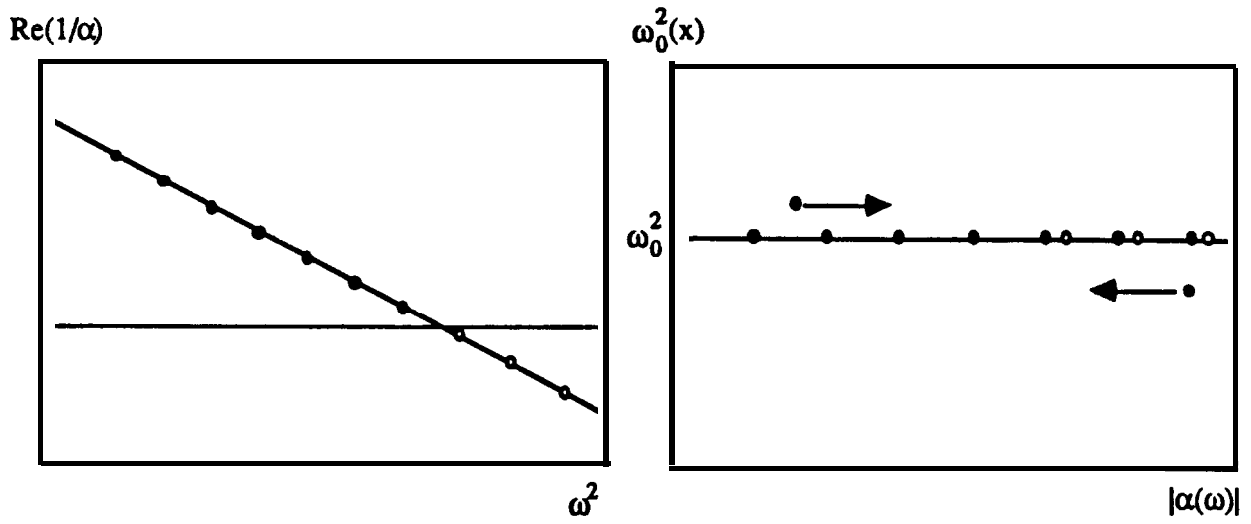


Figure 8-19 $\text{Re}(1/a)$ data of a linear system and the receptance amplitude against the natural frequencies estimated by equation (8-30)

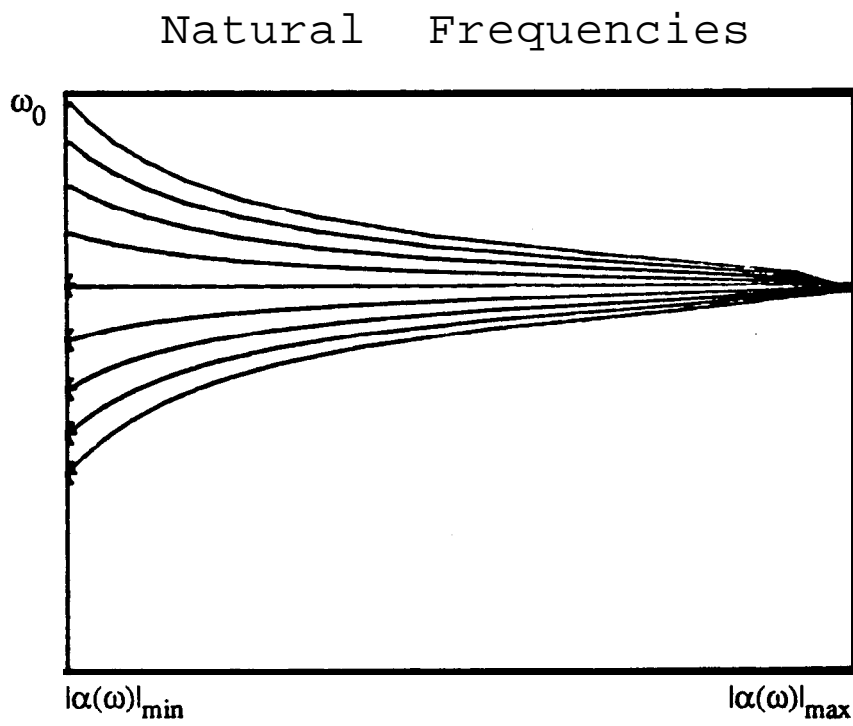


Figure 8-20 Effect of modal constant error AA on the natural frequency estimation using equation (8-3 1)

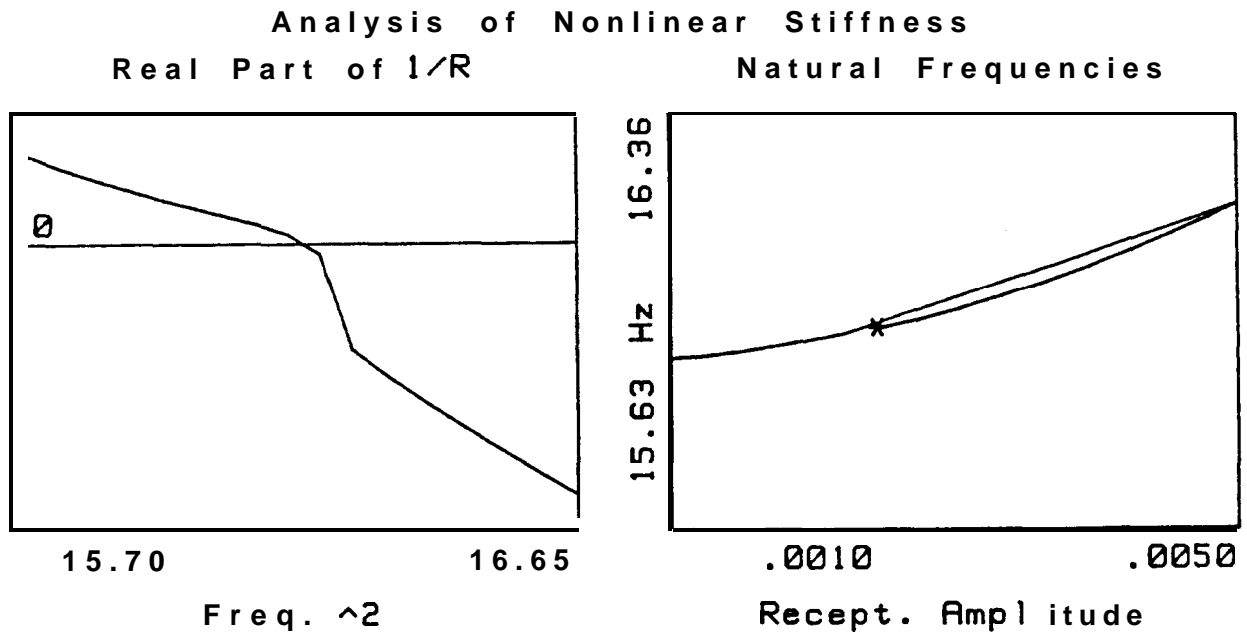


Figure 8-21 $Re(1/a)$ data with hardening cubic stiffness and the analysis results

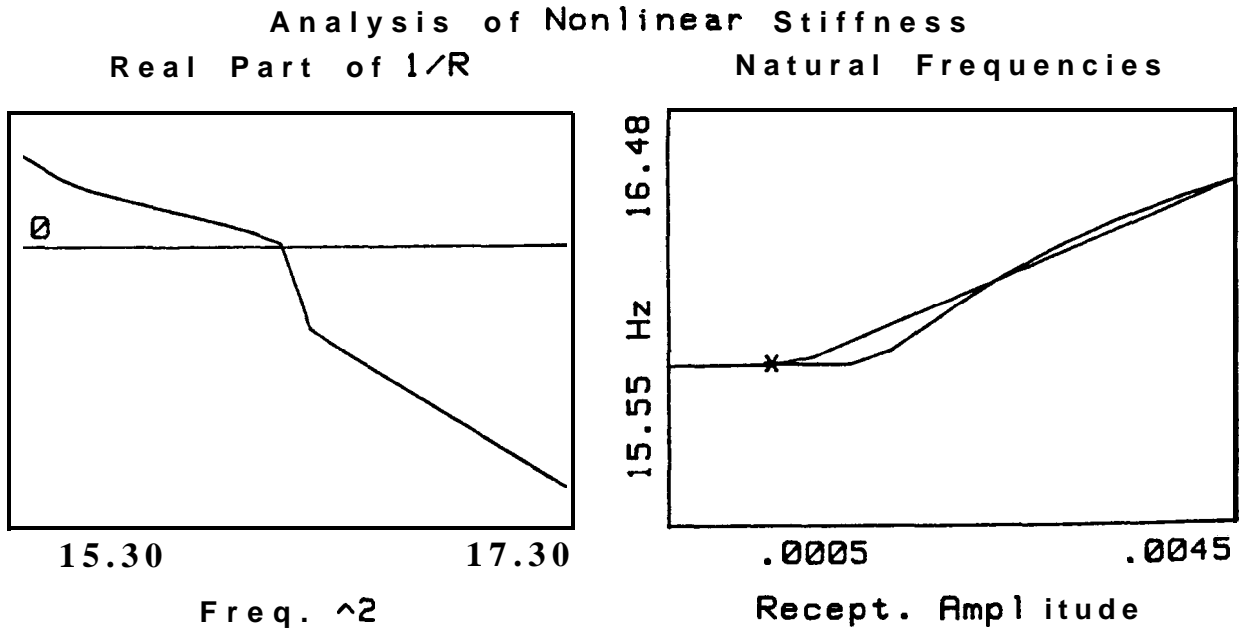


Figure 8-22 $Re(1/a)$ data with hardening backlash stiffness and the analysis results

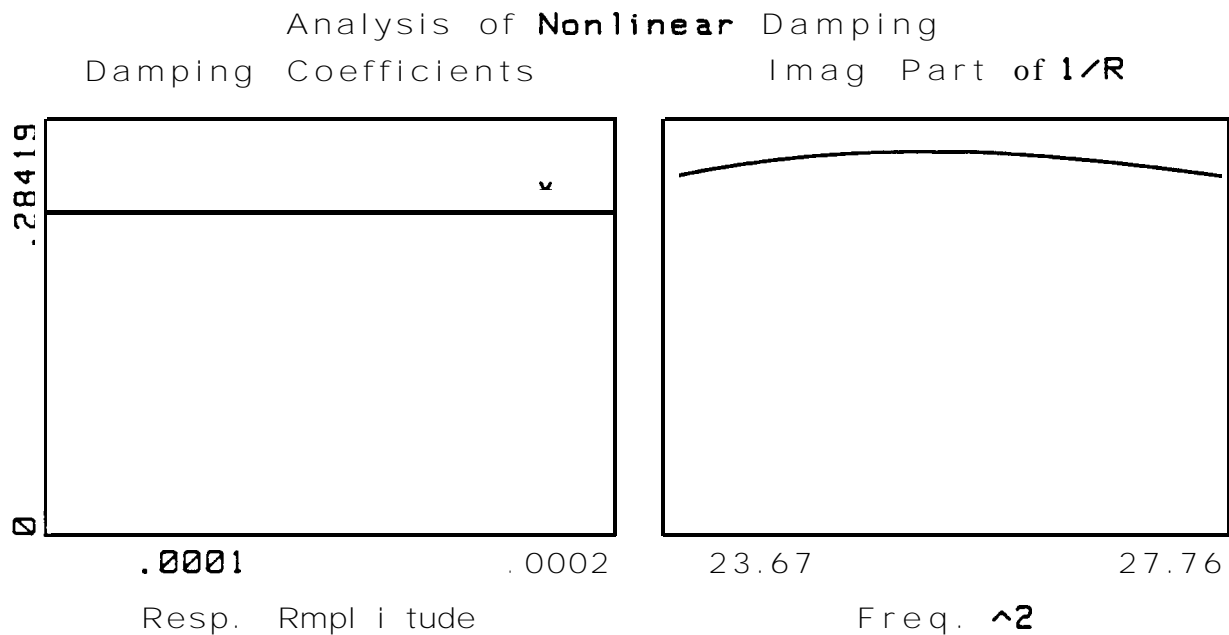


Figure 8-23 $\text{Im}(1/\alpha)$ data with quadratic damping and the analysis results

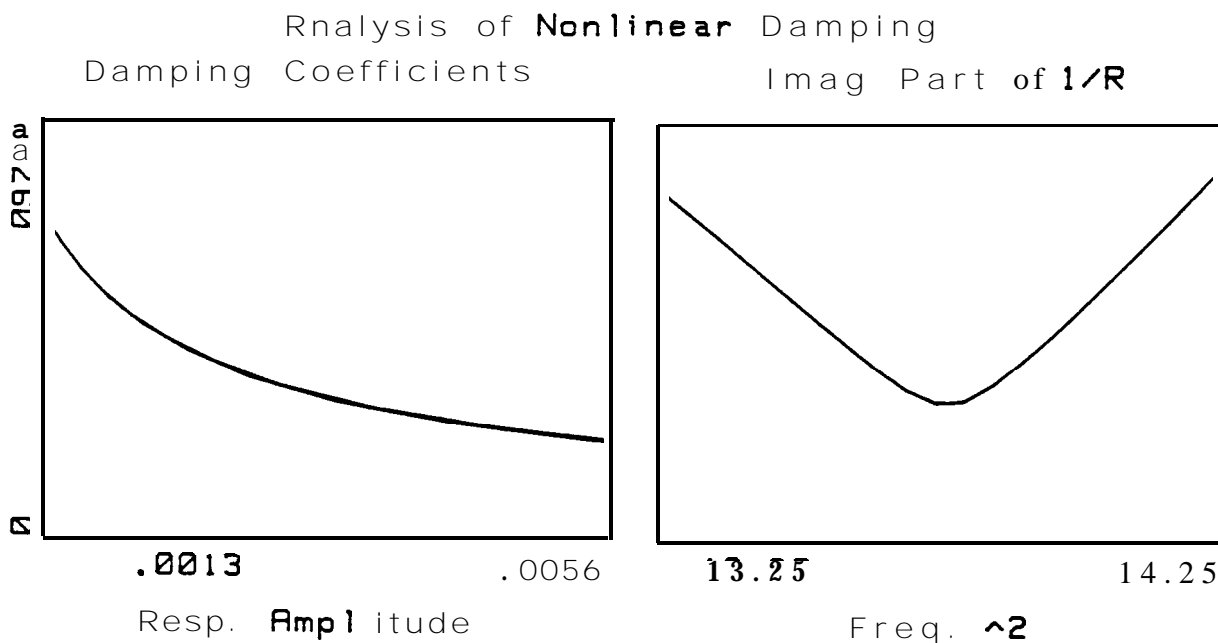


Figure 8-24 $\text{Im}(1/\alpha)$ data with dry friction damping and the analysis results

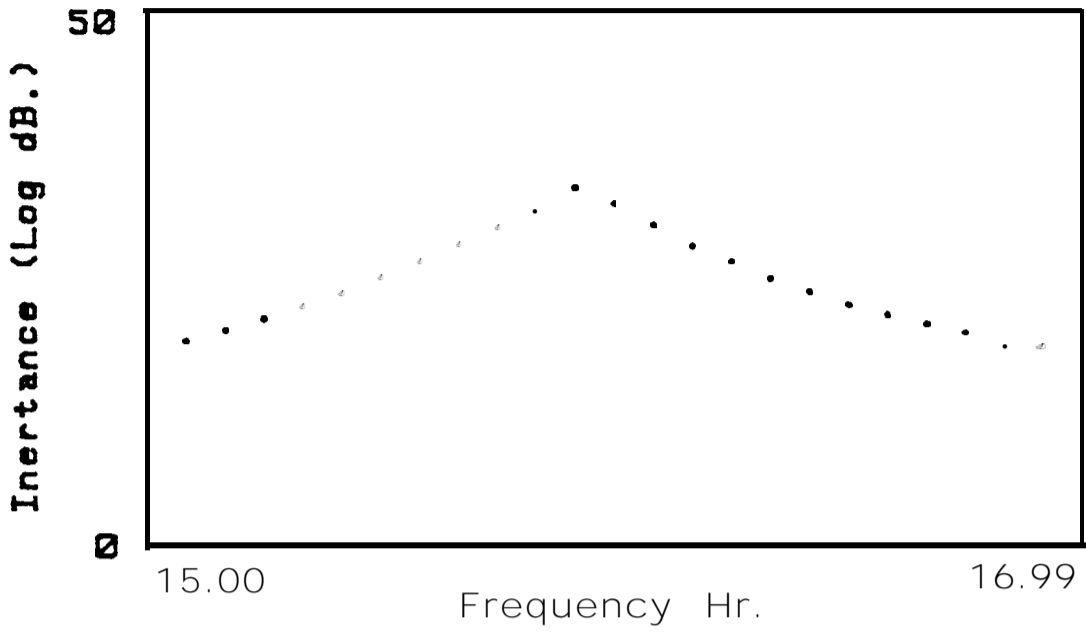


Figure 8-25 FRF data obtained from a SDOF system with cubic stiffness

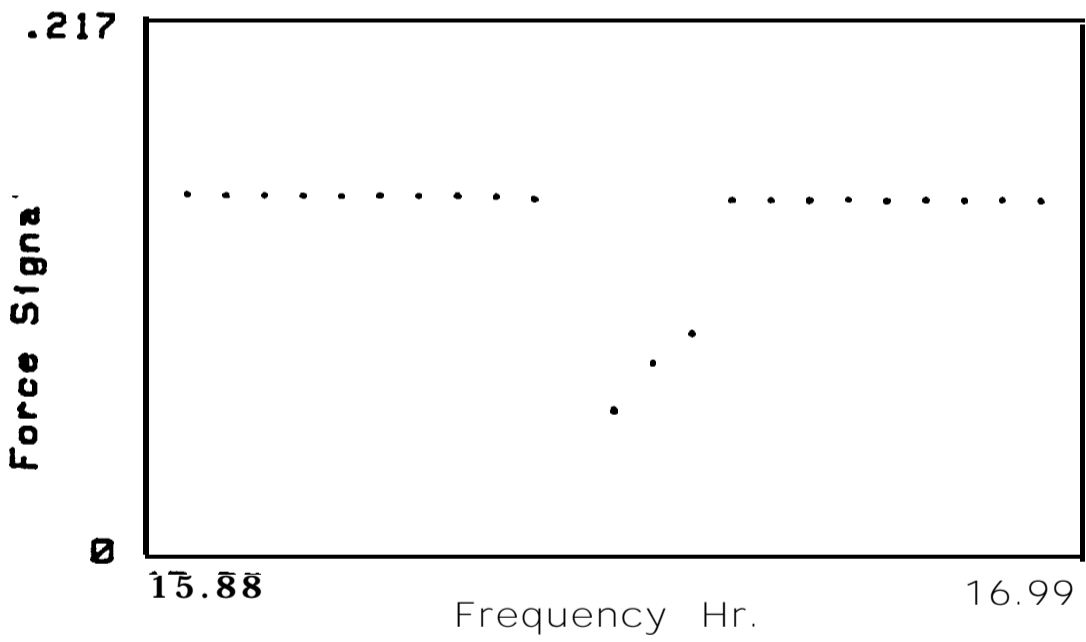


Figure 8-26 The force level used in the measurement

Reciprocal of Receptance.
Real Part Imaginary Part.

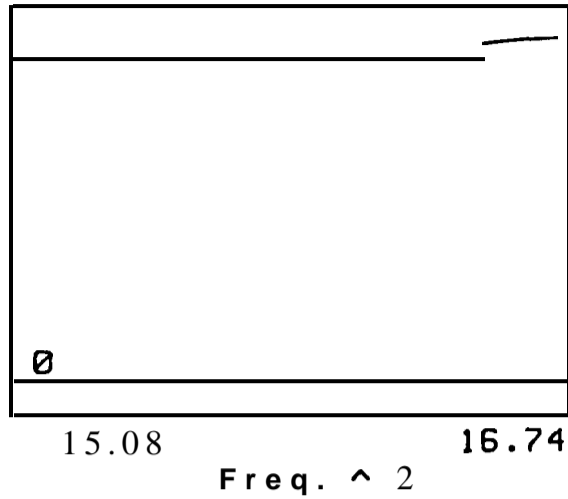
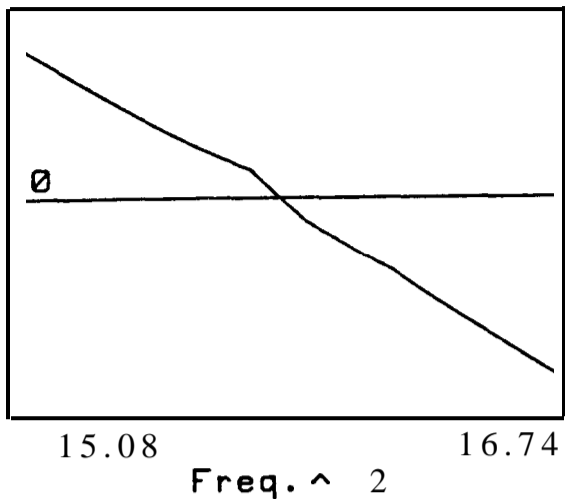


Figure 8-27 Reciprocal of receptance data of the FRF in Figure 8-25

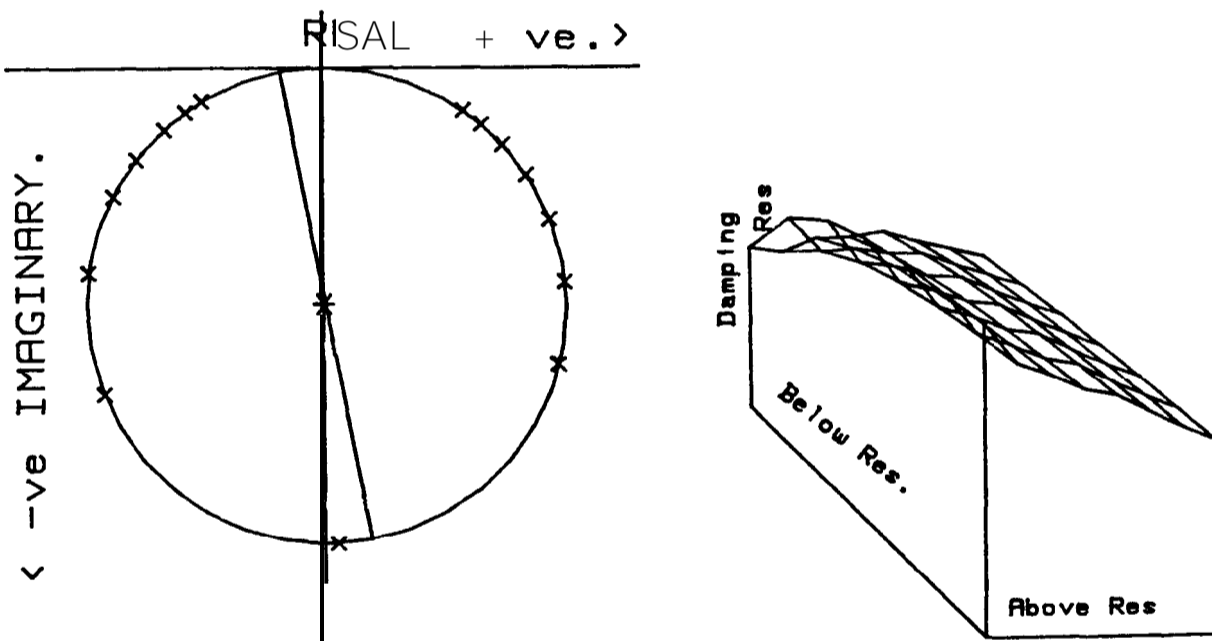


Figure 8-28 Modal analysis results of the FRF in Figure 8-25

Natural Frequencies

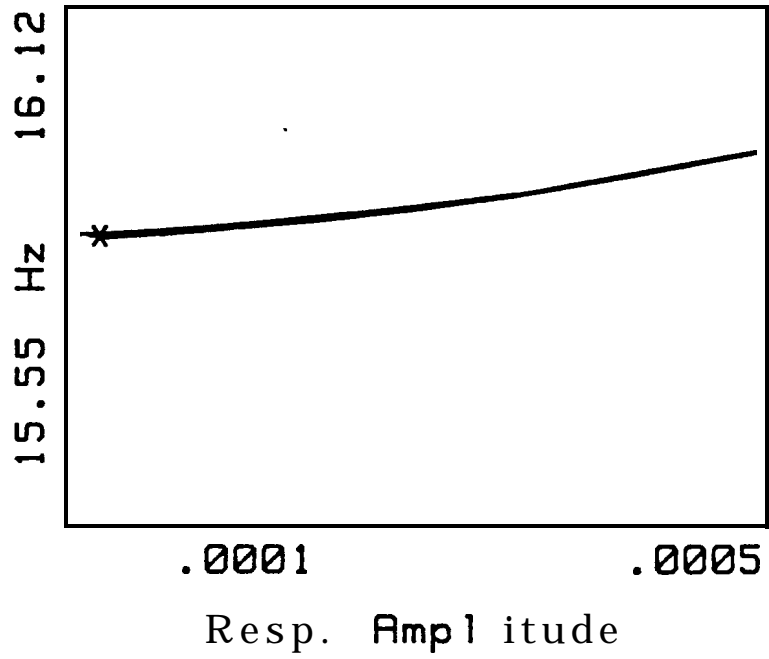


Figure 8-29 The analysis results

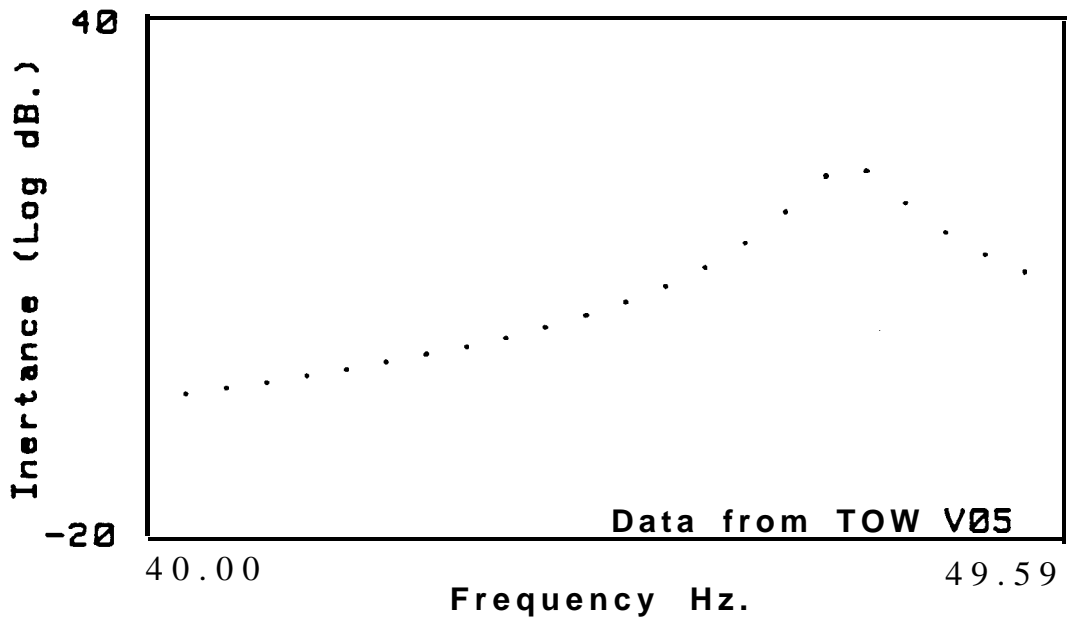


Figure 8-30 Inertance FRF data measured from a practical structure

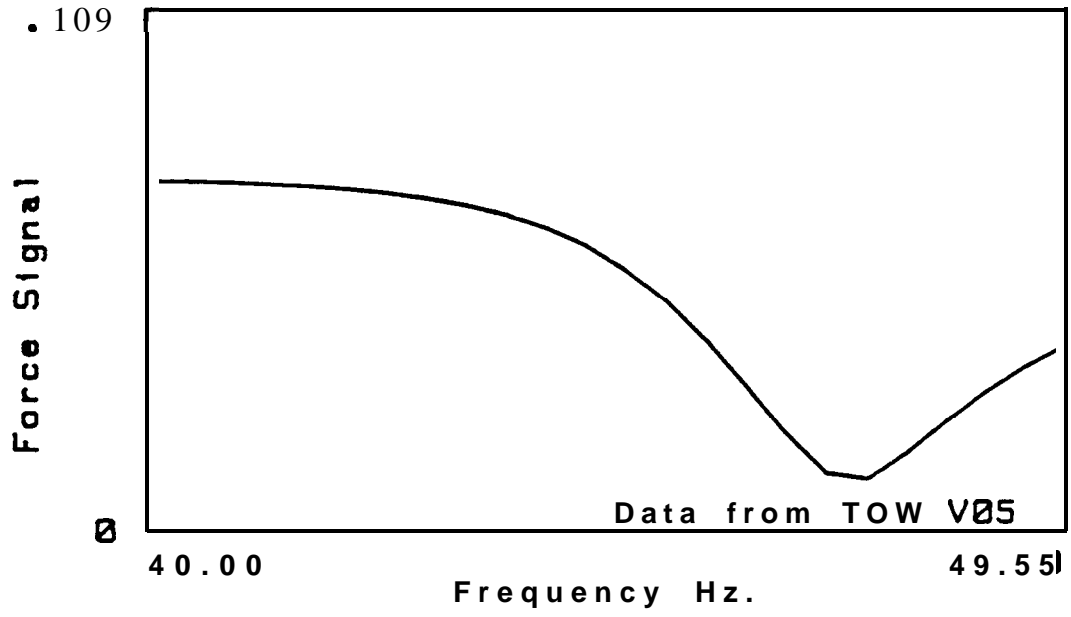


Figure 8-31 The force level generated by the shaker in the measurement

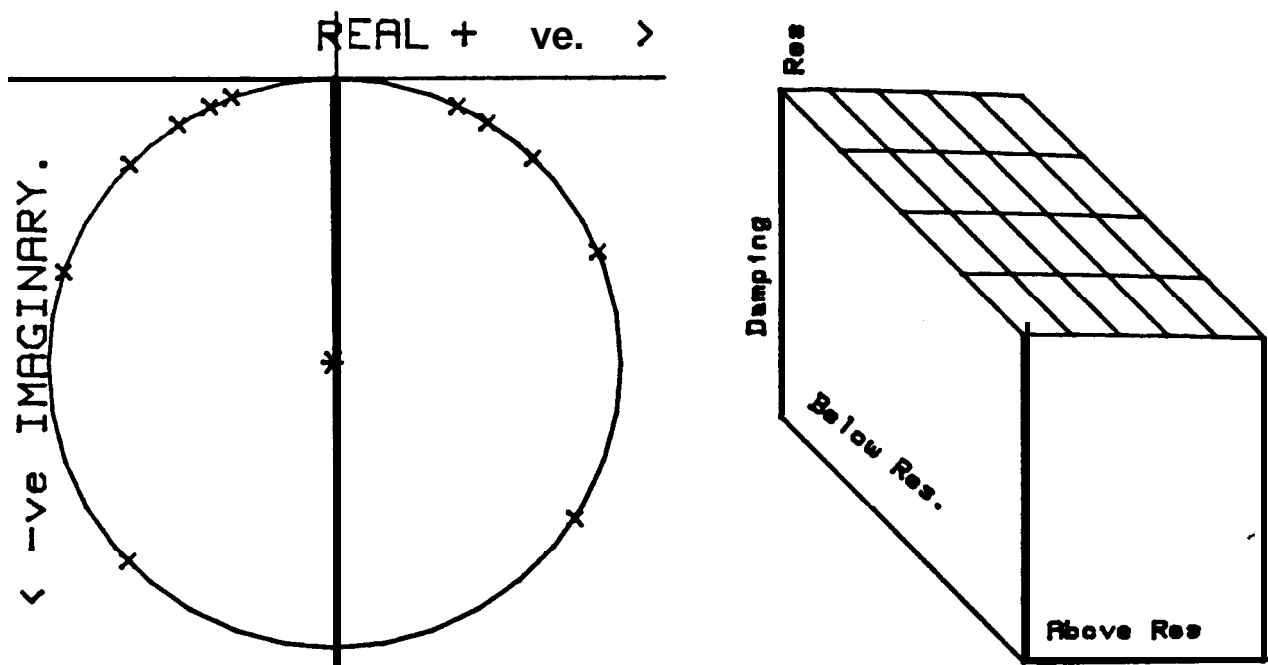


Figure 8-32 Modal analysis results of the FRF presented in Figure 8-30

Natural Frequencies

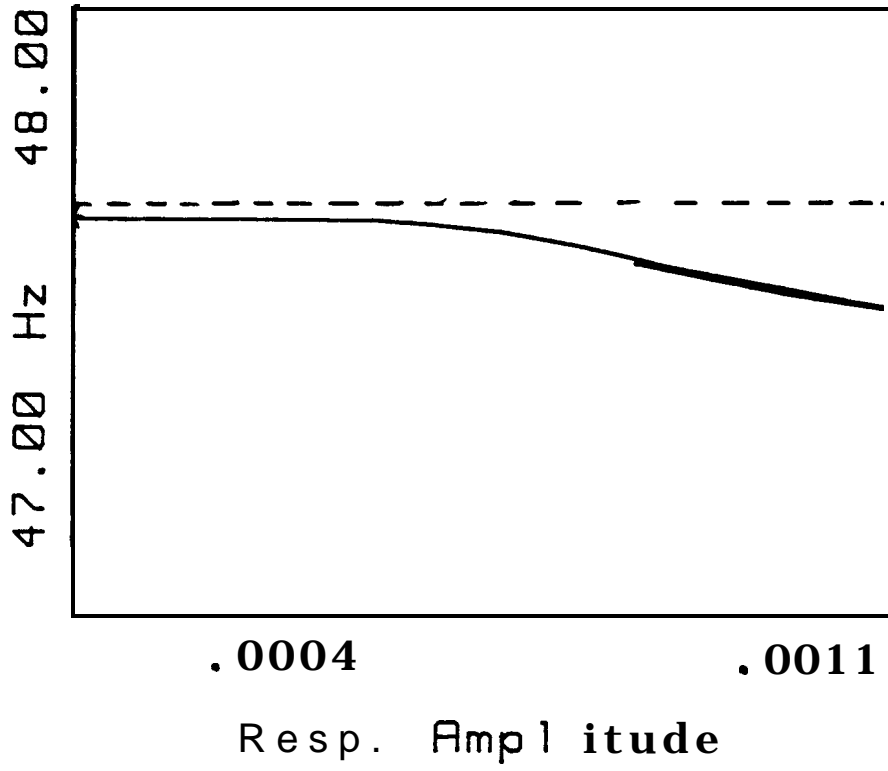


Figure 8-33 The analysis result using the new method

CHAPTER 9

CHAPTER 9

CONCLUSIONS AND SUGGESTION FOR FURTHER STUDIES

9-1 ANALYTICAL MODEL IMPROVEMENT USING MODAL TESTING

RESULTS

As current vibration practice demands more and more realistic mathematical models for vibrating structures, the study of analytical model improvement using modal testing results becomes increasingly important. This is because in the identification of dynamic characteristics of practical structures, both the analytical prediction and the modal testing have their own advantages and shortcomings. Using modal testing results to improve an analytical model effectively makes use of the advantages of both while at the same time overcoming their disadvantages and, it is by doing so that the most reliable mathematical model can be achieved.

It is understood from numerical studies that the major pitfall for most methods currently used, such as the constraint minimization method (CMM) or the error matrix method (EMM), to improve an analytical model using measured modes is to tackle it from a purely mathematical viewpoint, such as an optimization one, rather than to consider the structural characteristics as well, such as connectivity. As a consequence, the modified model could often be optimal in a mathematical sense, but physically unrealistic. For instance, the modified analytical stiffness matrix could suggest a stiffness component between coordinates i and j which are entirely unconnected on the real structure. Repeatedly using these methods rarely shows a convergence to correct answers. This is mainly because of the failure to preserve the physical connectivity and, furthermore,

because of the attempt to 'correct' the **correct** parts in the analytical model in the model improvement process.

Before and during this research for better methods of analytical model improvement, one important concept is always borne in mind, i.e. what kind of model is a **good** model and therefore is our target. It is believed that a good model is one which satisfies the following conditions; (1) it represents correct physical connectivity; (2) the corresponding vibration modes derived from it should agree with those observed in measurement and (3) it should predict correctly those modes which we are unable to measure or which are not yet measured. It is thought that condition (1) is a necessity for the model to be achieved - this is actually ignored by many current efforts to improve an analytical model - and condition (3) is the sufficiency for a good model. Philosophically, a successful model improvement practice should aim at achieving a model which satisfies condition (3), by imposing condition (2), based upon condition (1).

It is believed that the major errors will, in most cases, simply occur in a few localised regions in the analytical model. The key issue for a model improvement study is thus to be able to locate precisely where these major errors exist in the analytical model, using the measured modes as input. This is because it provides a useful guide either for possible further analytical modelling or for model improvement using measured vibration modes - or both. As far as model improvement is concerned, the improvement can be directed towards correcting those located errors in the model and the analytical model could thus be improved much more realistically and effectively if these erroneous regions in the model are somehow successfully located. In Chapter 3, a new method is proposed which uses as few as just one measured vibration mode to locate the major errors in the analytical model. Numerical case studies consistently suggest the correct error location achieved by this method. In addition, a new iteration procedure - to apply current methods such as the CMM or the EMM to improve an analytical model by correcting the located errors in the model - is suggested for analytical model improvement. This new iteration procedure has demonstrated marked advantages in achieving the correct model.

Nevertheless, it should be stressed that the error location process does not confine itself only for small error cases.

9-2 DAMPING PROPERTIES FOR PRACTICAL STRUCTURES

When the actual damping in a structure becomes significant and must be included in a dynamic analysis, the conventional approach is often to assume proportional damping for the analytical model. This assumption has been regarded as arbitrary since most practical damping is not distributed in the same way as stiffness and/or mass. In fact, for many practical structures, the major damping sources come from some restricted area(s), such as the joints between components. Since the measured vibration data contain information of the spatial damping distribution - although this information is neither complete nor explicit - Chapter 4 describes an investigation of the damping properties by first locating the major damping elements using the measured damped vibration modes. A more accurate damping model can then be introduced based on the damping element location results. It is also shown from numerical study that a correct damping matrix could be obtained, even quantitatively, if an iteration with reference to the introduced damping model is applied.

It is further understood that errors in an analytical model (error matrices $[AM]$ and $[AK]$) and the damping matrix can all be regarded as a kind of local properties of a vibrating structure - either local errors or local uncertainties. The best way of investigating such local properties is perhaps to localise them first and then, to seek their possible quantification. It has been found from this study that the mass and stiffness errors in an analytical model, and the damping elements, can be localised using a relatively small number of modes from modal testing results and these specified local properties can also be approximated or even correctly quantified.

9-3 COMPATIBILITY OF ANALYTICAL MODEL AND MEASURED VIBRATION MODES

A practical difficulty for some cases of model improvement is that the analytical model and the measured vibration modes are incompatible in the sense of the coordinates adopted. Usually, the analytical model uses a far greater number of coordinates than the measured modes can to describe the vibration properties. For such cases, the methods available for model improvement will not be directly applicable, unless this incompatibility is resolved first.

There are basically two methods currently used to cope with this incompatibility and these have been reviewed in Chapter 5, being: (1) to reduce the analytical model to the same coordinates as the measured modes by **Guyan** (or similar) reduction methods and (2) to expand the measured modes to the full set of coordinates as used by the analytical model itself. It is found that, as far as the location of the errors in the analytical model is concerned, method (2) is preferred because it preserves the physical connectivity of the analytical model - and therefore the error location as well. Numerical study based on a 21 DOF system has shown that the errors existing in the analytical model can be correctly located using the location technique developed in Chapter 3, after the 'measured modes' are expanded.

Since these two methods assume both the analytical and the experimental data to be real, they are not applicable to study the damping properties and to improve the analytical model when a structure is sufficiently damped that the measured vibration modes become complex. However, a new method has been proposed in this thesis to expand the damped measured modes to full coordinates using the analytical model including only mass and stiffness matrices. Thus, these expanded complex measured modes can be used, in a similar way to the expanded real modes, to locate the damping elements and, at the same time, to locate errors in the analytical mass and stiffness matrices.

The location of errors in an analytical model using measured vibration modes has been demonstrated by a practical application. The object used is a beam structure with two straight beams jointed together by nut and bolt. It is supposed that this joint is unknown so that the FE analysis predicts the stiffness properties of the structure as a continuous beam, while the mass properties are the same with or without the joint. Although the analysis covers the vibration characteristics of the structure in the frequency range up to some 3000 Hz, only three vibration modes are actually measured, and only half the coordinates are included. These measured modes are **firstly** expanded using the FE model and are then used, individually and collectively, to locate the errors in the analytical stiffness matrix. The location process successfully indicate the major errors corresponding to the joint in the structure.

9-4 NONLINEARITY IN MODAL TESTING

All the previous studies assume the vibration of the structure or system investigated to behave in a linear way, or that the nonlinearity could be ignored due to its small extent. This assumption can be too optimistic for some cases where nonlinearity becomes significant in the vibration characteristics.

Unlike theoretical studies, where the vibration characteristics of nonlinear systems can be described by differential equations, the major problem in the realm of modal testing of nonlinear systems is to study unknown types of nonlinearity. The key issue therefore becomes identifying the *types* of nonlinearity, after their existence is detected. The review and discussion of those methods currently used to investigate nonlinearity - all aiming basically to identify nonlinearity from their effects on the measured data - have suggested their practical applicability. However, conclusive identification of the types of nonlinearity is still problematic, because some types of nonlinearity can well produce quite similar effects on the measured data.

With the help of closer examination of the vibration data on nonlinear systems measured using stepped-sine excitation, a new interpretation is proposed to offer a better understanding of the effect of nonlinearity on the frequency response function data measured in conventional ways. It is found that one FRF curve measured with constant force level contains all the information of a series of FRF data with different constant response controls. Therefore, a nonlinearity study can be carried out using a single FRF curve obtained using sinusoidal excitation with constant force. Based upon this interpretation, and a SDOF assumption for the subsequent modal analysis, a new method is proposed to study nonlinearity. Instead of seeking the effects of nonlinearity on certain aspects such as the Hilbert transform or damping plot, as other methods do, this method aims at modelling the nonlinearity directly with respect to response amplitude. Thus, the identification of the type of nonlinearity becomes more conclusive and the quantification of its extent becomes possible. It is also found that this method does not even require the condition of using constant force to measure FRF data - which other methods necessarily require. Rather, the FRF data can be measured in most conventional way of sinusoidal excitation with neither force nor response control, as long as the force level is large enough to expose nonlinearity.

9-5 SUGGESTIONS FOR FURTHER STUDY

One obvious aspect for further study is to apply the technique developed for locating errors in an analytical model and/or locating damping elements in more sophisticated structures. In this study, the application is made only to a numerical study and a comparatively simple structure due to the limited period of time available and, success has already been demonstrated in satisfactorily locating analytical errors and damping elements.

When an incompatibility exists between the analytical model and the measured modes, it has been found that the location of errors in the analytical model and/or damping elements relies on expanding the measured vibration modes, damped or not, to the full coordinate

sets as the analytical model has by using the erroneous model itself. It has also been seen that by doing so, the error and/or damping element location can still be achieved successfully. However, further usage of these expanded measured modes, such as in an iteration procedure to correct analytical model, needs to be investigated fully. Although directly using these expanded measured modes to improve an analytical model has been suggested in the literature, the expanded modes are erroneous after all in those expanded coordinates (the measured coordinates are unchanged).

For nonlinearity investigation, it has been discovered that analogue simulation can play a significantly important role. Due to the limited capacity of the analogue computer used in this study, only SDOF nonlinear systems are simulated and studied. However, the principle of constructing MDOF nonlinear systems on an analogue computer has been demonstrated and it would be appropriate that MDOF systems with one and several types of nonlinearity should now be investigated,

The new method proposed to identify the type of nonlinearity and to quantify it is based upon the assumption that the mode to be analysed has little complexity. For those vibration modes in which ignoring complexity becomes unrealistic, this new method is not directly applicable. Further research can be oriented towards either removing the complexity first so that the new method can be used, or, developing the method further for cases of a high degree of complexity.

APPENDICES

APPENDIX 1

MATRIX PERTURBATION RESULTS

Basic perturbation theory studies the behaviour of a system subject to small perturbations in its variables. If the system is represented by a set of linear simultaneous equations of the following form:

$$[\mathbf{X}]\{\mathbf{a}\} = \{\mathbf{b}\} \quad (\text{A1-1})$$

the problem becomes that of determining $\{\mathbf{a}\}_1$ when matrix $[\mathbf{X}]$ exhibits a perturbation of the form $[\mathbf{X}] + \epsilon[\mathbf{X}]_1$, and vector $\{\mathbf{b}\}$ has a perturbation of the form $\{\mathbf{b}\} + \epsilon\{\mathbf{b}\}_1$. The constant ϵ is a scalar quantity which is much less than unity and is called the perturbation factor. Sometimes ϵ is included in $[\mathbf{X}]_1$ to mean that $[\mathbf{X}]_1$ contains small elements relative to those of $[\mathbf{X}]$.

The matrix perturbation theory relevant to vibration research is to study the relationship between the perturbation $[\mathbf{A}]$, of an $n \times n$ matrix $[\mathbf{A}]$ and the changes happening in its eigenvalues and eigenvectors. Since the matrices dealt with in vibration research such as mass, stiffness and damping matrices are usually symmetric, it is assumed here that matrix $[\mathbf{A}]$ and its perturbation $[\mathbf{A}]$, are symmetric, for the sake of simplicity. If the symmetric matrix $[\mathbf{A}]$ has the **eigenvalues**:

$$\lambda_1, \lambda_2, \lambda_3, \dots, \lambda_n$$

and corresponding eigenvectors:

$$\{\alpha\}_1, \{\alpha\}_2, \{\alpha\}_3, \dots, \{\alpha\}_n,$$

then the eigen-equation for matrix [A] is:

$$[A]\{\alpha\} = \lambda\{\alpha\}. \quad (A1-2)$$

The eigen-equation for the perturbed matrix $[A]+\epsilon[A]_1$ will become:

$$([A] + \epsilon[A]_1)\{\alpha\} = \lambda\{\alpha\} \quad (A1-3)$$

Theory shows that the eigenvalues λ_i and eigenvectors $\{\alpha\}_i$ ($i=1,2,\dots n$) of the perturbed matrix $[A]+\epsilon[A]_1$ can be approximated by the eigenvalues λ_i and eigenvectors $\{\alpha\}_i$ ($i=1,2, \dots n$) of the unperturbed matrix [A] together with the perturbation [A], such that:

$$\lambda_i \cong \lambda_i + \{\alpha\}_i^T [A]_1 \{\alpha\}_i \quad (A1-4)$$

and

$$\{\alpha\}_i \cong \{\alpha\}_i + \sum_{j=1, j \neq i}^n \frac{\{\alpha\}_j^T [A]_1 \{\alpha\}_i}{\lambda_i - \lambda_j} \{\alpha\}_j \quad (A1-5)$$

If its damping matrix [H] for a vibrating system is small compared with its stiffness matrix [K], then it can be regarded as a complex perturbation of [K]. The complex stiffness matrix $[K_c] (= [K_x] + i[H])$ is then regarded as the perturbed matrix.

According to the perturbation theory described above, the consequence of the perturbation $i[H]$ on stiffness matrix [K] is that each damped complex (mass normalized) mode shape of the system after the perturbation $\{\phi_x\}_r$ ($r=1,2 \dots n$) can be expressed as a combination of the corresponding undamped (mass-normalized) mode shapes before perturbation $\{\phi\}_r$ plus a contribution of all other undamped mode shapes, namely:

$$\{\phi_x\}_r = \{\phi\}_r + \sum_{s=1, s \neq r}^N (\omega_r^2 - \omega_s^2)^{-1} [\{\phi\}_s^T \mathbf{i}[\mathbf{H}] \{\phi\}_r] \{\phi\}_s \quad (\text{A1-6})$$

where N is the dimension of matrices $[\mathbf{K}]$ and $[\mathbf{H}]$;

ω_s^2 ($s=1, 2, \dots, N$) are the eigenvalues of the system before the perturbation;

$\{\phi\}_s$ ($s=1, 2, \dots, N$) are the eigenvectors of the system before the perturbation.

APPENDIX 2

INVERSE OF A COMPLEX MATRIX

Supposing that there is a non-singular complex matrix $[P]$ and it can be written by its real and imaginary parts as:

$$[P] = [A] + [B]i \quad (A2-1)$$

then the inverse of matrix $[P]$ is generally another complex matrix $[Q]$ which again can be written in the form of its real and imaginary parts:

$$[Q] = [X] + [Y]i \quad (A2-2)$$

Here, matrices $[A]$, $[B]$, $[X]$ and $[Y]$ are all real matrices and the inverse of the complex matrix $[P]$ can be obtained by deriving the two real matrices $[X]$ and $[Y]$.

According to the definition of matrix inversion,

$$[P][Q] = [I] + [0]i \quad (A2-3)$$

Or

$$([A] + [B]i)([X] + [Y]i) = [I] + [0]i \quad (A2-4)$$

Equation (A2-4) can be written as its real and imaginary counterparts, yielding:

$$[A][X] - [B][Y] = [I] \quad (A2-5)$$

$$[A][Y] + [B][X] = [0] \quad (A2-6)$$

Combining equations (A2-5) and (A2-6) into one matrix equation leads to:

$$\begin{bmatrix} [A] & -[B] \\ [B] & [A] \end{bmatrix} \begin{bmatrix} [X] \\ [Y] \end{bmatrix} = \begin{bmatrix} [I] \\ [0] \end{bmatrix} \quad (\text{A2-7})$$

Equation (A2-7) can be rearranged so that:

$$\begin{bmatrix} [X] \\ [Y] \end{bmatrix} = \begin{bmatrix} [I] & -[B] \\ [B] & [A] \end{bmatrix}^{-1} \begin{bmatrix} [I] \\ [0] \end{bmatrix} \quad (\text{A2-8})$$

The substitution of matrices [X] and [Y] into equation (A2-2) yields: the complex inverse matrix [Q] of matrix [P].

The same conclusion can be drawn if equation (A2-3) becomes:

$$[Q][P] = [I] + [0]i \quad \text{W-9)}$$

APPENDIX 3

FE ANALYSIS OF A BEAM ELEMENT

A beam element is as shown in Figure 6-3. In this case both ends of the element can undergo translational and rotational displacements. The mass and stiffness matrices of this beam element will then be:

$$[m] = \frac{mL}{420} \begin{bmatrix} 156 & 22L & 54 & -13L \\ 22L & 4L^2 & 13L & -3L^2 \\ 54 & 13L & 156 & -22L \\ -13L & -3L^2 & -22L & 4L^2 \end{bmatrix}$$

and

$$[k] = \frac{EI}{L^3} \begin{bmatrix} 12 & 6L & -12 & 6L \\ 6L & 4L^2 & -6L & 2L^2 \\ -12 & -6L & 12 & -6L \\ 6L & 2L^2 & -6L & 4L^2 \end{bmatrix}$$

Where: m - mass per unit length;

L - length of the element;

E - elasticity of the element;

I - moment of inertia.

REFERENCES

REF'ERENCES

- [1] Ewins, D J and **Gleeson**, P T
A method for modal identification of lightly damped structures
J of Sound and Vibration, **84(1)**, 1982, pp 57-79
- [2] Goyder, H G D
Methods and application of structural modelling from measured structural frequency response data
J of Sound and Vibration, **68(2)**, 1980, pp 209-230
- [3] Dobson, B J
Modal parameter estimation using difference equations
Proc of IMAC IV, 1986
- [4] Berman, A
Comment on "Optimal weighted orthogonalization of measured modes"
AIAA J, **Vol 17**, 1979, pp 927-928
- [5] Berman, A and **Flannelly**, W G
Theory of incomplete models of dynamic structures
AIAA J, **Vol 9**, 1971, pp 1481-1487
- [6] Collins, J D et al
Statistical identification of structures
AIAA J, **Vol 12**, 1974, pp 1851-190
- [7] Chen, J C and **Garba**, J A
Analytical model improvement using modal test results
AIAA J, **Vol 8**, 1980, pp 684-690
- [8] **Chen, J C et al**
Direct structural parameter identification by modal test results
AIAA paper 83-08 12
- [9] Baruch, M and Bar **Itzhack**, I Y
Optimal weighted orthogonalization of measured modes
AIAA J, **Vol 16**, 1978, pp 346-351
- [10] Baruch, M
Optimization procedure to correct stiffness and flexibility matrices using vibration tests
AIAA J, **Vol 16**, 1978, pp 1208-1210
- [11] Berman, A
Mass matrix correction using an incomplete set of measured modes
AIAA J, **Vol 17**, 1979, pp 1147-1148

- [12] Caesar, B
Update and identification of dynamic mathematical models
Proc of IMAC IV, 1986, pp 384401
- [13] Sandstrom, R E and Anderson, W J
Modal perturbation methods for marine structures
SNAME transactions, **Vol 90, 1982, pp 41-54**
- [14] Berman, A and **Wei, F S**
Automated Dynamic Analytical model improvement
NASA contract report **3452, 1981**
- [15] Berman, A and Nagy, E J
Improvement of a large analytical model using test data
AIAA J, **Vol 21, 1983, pp 1168-1173**
- [16] Sidhu, J and Ewins D J
Correlation of finite element and modal test studies of a practical structure
Proc of IMAC II, 1984
- [17] Dobson, B J
Modification of finite-element models using experimental modal analysis
Proc of IMAC II, 1984
- [18] Brown, T A
A unified approach to the identification of dynamic behaviour using the theory of vector spaces
PhD Thesis, Dept of Eng Math, Univ of Bristol, 1986
- [19] Gysin, H P
Critical application of the error matrix method for **localization of finite** modelling inaccuracies
Proc of IMAC IV, 1986
- [20] **Kabe, A M**
Stiffness matrix adjustment using mode data
AIAA J, **Vol 23, 1985, pp 1431-1436**
- [21] **Guyan, R J**
Reduction of stiffness and mass matrices
AIAA J, **Vol 3, 1965, pp 380-380**
- [22] Kidder, R L
Reduction of structural frequency equations
AIAA J, **Vol 11, 1973, pp 892-892**
- [23] **Brock, J E**
Optimal matrices describing linear systems
AIAA J, **Vol 6, 1968, pp 1292-1296**

- [24] Gravitz, S I
An analytical procedure for orthogonalization of experimentally measured modes
J of the **Aero/Space Sciences**, 1958, pp 721-722
- [25] He, J
Analytical model improvement
Internal report No 86001, Dynamics Section, Dept of **Mech Eng**, Imperial College
- [26] He, J and Ewins, D J
Analytical stiffness matrix correction using measured vibration modes
The **Intl J of Analytical and Experimental Modal Analysis**, **Vol 1**, No 3, July 1986
- [27] Chen, **Shyi-Yaung** and Fuh, Jon-Shen
Application of the generalized inverse in structural system identification
AIAA J, **Vol 22**, 1984, pp 1827-1828
- [28] Caughey, T K and Kelley, M E J
Classical normal modes in damped linear systems
Appl Mech, **Trans ASME**, **Vol 32**, 1965, pp 583-588
- [29] Ibrahim, S R
Computation of normal modes from identified complex modes
AIAA J, **Vol 21**, 1983, pp 446-451
- [30] Ibrahim, S R
Dynamic modelling of structures from measured complex modes
AIAA J, **Vol 21**, 1983, pp 898-901
- [31] Qiang Zhang and Lallement, G
New method of determining the eigensolutions of the associated conservative structure from the identified eigensolutions
Proc of IMAC III, 1985
- [32] Natke, H G and Robert, D
Determination of normal modes from the identified complex modes
Z. Flugwiss. Weltraumforsch. **9(1985)**, Heft 2
- [33] Ewins, D J
Whys and wherefores of modal testing
SEE J, September 1979
- [34] Potter, R and Richardson M
Mass, stiffness, and damping matrices from measured parameters
Proc of Intl. Instrumentation-Automation Conf., N.Y., **Oct 1974**
- [35] Thoren, A R
Derivation of mass and stiffness matrices from dynamic test data
AIAA paper 72-346

- [36] **Fretzen**, Claus-Peter
Identification of mass, damping, and stiffness matrices of mechanical systems
ASME J of Vibration, Acoustics, stress, and Reliability in Design, Vol **108**, **1986**,
pp 9-16
- [37] Luk, Y W and Mitchell, L D
System identification via modal analysis
AMD Vol 59, ASME, 1983
- [38] Berman, A
Determining structural parameters from dynamic testing
The Sound and Vibration Bulletin, Vo17, No **1**, **1985**
- [39] Fabunmi, J A
Extended damping models for vibration data analysis
Proc of 2nd Intl Con of recent Advances in Structural Dynamics, Southampton,1983
- [40] Goyder, H G D
Foolproof frequency response testing methods
Proc of 2nd Intl. Con. on Recent Advances in Structural Dynamics, April 1984,
ISVR
- [41] Dobson, B J
Modal analysis using dynamic stiffness data
Proc of IMAC III, 1985
- [42] Beards, C F
Damping in structural joints
Sound and Vibration Digest, Vol 11, No **9**, **1979**, pp 35-41
- [43] Beards, C F
Damping in structural joints
Sound and Vibration Digest, Vol 14, No 6, 1982, pp 9-1 1
- [44] Lin, D X and Adams, R D
Determination of the damping properties of structures by transient testing using
zoom-FFT
J of Physics E, Vol18, 1985, pp 161-165
- [45] He, J and Ewins, D J
Location of damping elements in a vibrating structure
Proc of 1 lth Intl Modal Analysis Seminar, **Leuven**, Belgium, 1986
- [46] Deif, A **S**
Advanced matrix theory for scientists and engineers
Abacus Press, 1982
- [47] Ewins, D J
Measurement and application of mechanical impedance data (3 parts)
JSEE, Vol 14.3, 15.1, 15.2, 1975-1976

- [48] Prater Jr, G and Singh, R
Quantification of the extent of non-proportional viscous damping in discrete vibratory systems
J of Sound and Vibration, **104(1)**, 1986, pp 109-125
- [49] Nicholson, D W
Stable response of damped linear systems
Sound and Vibration Digest, Vol 12, No **6**, **1980**, pp 3-4
- [50] Timoshenko, S
Vibration problems in engineering
Wiley
- [51] Cawley, P and Adams, R D
Improved frequency resolution from transient tests with short record lengths
J of Sound and Vibration, **64(1)**, 1979, pp 123-132
- [52] Hatter, D J
Matrix computer methods of vibration analysis
Butterworths London
- [53] Meinovitch, L
Elements of vibration analysis
McGraw Hill, 1975
- [54] Nayfeh, A H and Mook, D T
Nonlinear oscillations
A Wiley-Interscience Publication, John Wiley & Sons, New York, 1981
- [55] Caughey, T K
Equivalent linearization techniques
The Journal of **ASA**, 1963, **Vol 35(11)**, pp 1706-1711
- [56] Iwan, D W
A generalization of the concept of equivalent linearization
International Journal of Nonlinear Mechanics, **Vol 8**, 1973, pp 279-287
- [57] Den Hartog, J P and Stanley, J M
Forced vibrations with nonlinear spring contents
Transactions of **ASME**, **Vol 54**, **1932**
- [58] Maymon, G
Experimental determination of linear damping coefficients in elastic structures with geometric nonlinearity
Israel Journal of Technology, **Vol 16**, **1978**, pp 64-69
- [59] Tomlinson, G R and Hibbert, J H
Identification of the dynamics characteristics of a structure with **columb** friction
Journal of Sound and Vibration, **vol 64(2)**, 1979

- [60] White, R G and Pintington, R J
Practical application of the rapid frequency sweep technique for structural frequency response measurement
Aeronautical Journal of the Royal Aero Society, May, 1982, pp 179-199
- [61] Sidhu, J
Reconciliation of predicted and measured modal properties of structures
PhD thesis, 1983, Imperial College
- [62] Ewins, D J and Sidhu, J
Modal testing and the linearity of structures
Mecanique Materiaux Electicite, No 389-390-391, **Mai-Juin-Juillet**, 1982
- [63] J He
Simulation of nonlinearity on an analogue computer
Internal report No 84004, Dynamic Section, Dept **Mech Eng**, Imperial College.
- [64] Crandall, S H
Perturbation techniques for random vibration of nonlinear systems
The Journal of **ASA**, 1963, **Vol 35(11)**, pp 1700-1705
- [65] Tomlinson, G R
Modal analysis of nonlinear structures
Short course note, Simon Engineering Laboratory, Univ of Manchester
- [66] Charlesworth, A S and Fletcher, J R
Systematic analogue computer programming
Pitman Publishing
- [67] Cawley, P
The accuracy of frequency response function measurements using **FFT-based** analysers with transient excitation
ASME J of Vibration, Acoustics, stress, and Reliability in Design, Vol 108, 1986, pp 45-49
- [68] Dinca, F and Teodosiu, C
Nonlinear and random vibrations
- [69] Ewins, D J and He, J
Critical assessment of the extraction of modal data
10th International Modal Analysis Seminar, Leuven, Belgium, 1985
- [70] Cawley, P and Rigner, L G
Rapid measurement of modal properties using FFT analysers with random excitation
ASME J of Vibration, Acoustics, stress, and Reliability in Design, **Vol 108, 1986**, pp 394-398
- [71] Ewins, D J
Modal testing - theory and practice
Research Studies Press, 1984

- [72] He, J and Ewins, D J
A simple method of interpretation for the modal analysis of nonlinear systems
Proc of IMAC V, 1987
- [73] Goyder, H G D
Foolproof frequency response testing methods
Proc of 2nd Intl. Con. on Recent Advances in Structural Dynamics, April 1984,
ISVR
- [74] Simon, M and Tomlinson, G R
Application of the Hilbert transform in the modal analysis of non-linear systems
Journal of Sound and Vibration, 96 (3), 1984
- [75] Vinh, T and Haoui, A and Chevalier, Y
Extension of modal analysis to nonlinear structures by using Hilbert transform
Proc of IMAC II, 1984
- [76] Bracewell, R
The Fourier transform and its applications
Ma&raw-Hill Book Company
- [77] Rodden, W P
A method for deriving structural influence coefficients from ground vibration tests
AIAA J, Vol 5, 1967, pp 991-1000